





EX LIBRIS
UNIVERSITATIS
ALBERTENSIS

The Bruce Peel
Special Collections
Library



Digitized by the Internet Archive
in 2025 with funding from
University of Alberta Library

<https://archive.org/details/0162014920621>

University of Alberta

Library Release Form

Name of Author: Javed Afsar

Title of Thesis: Flexural Response of Masonry Walls Reinforced
With GFRP Sheets.

Degree: Master of Science

Year This Degree Granted: 2001

Permission is hereby granted to the University of Alberta Library to reproduce single copies of this thesis and to lend or sell such copies for private, scholarly, or scientific research purposes only.

The author reserves all other publication and other rights in association with the copyright in the thesis, and except as hereinbefore provided, neither the thesis nor any substantial portion thereof may be printed or otherwise reproduced in any material form whatever without the author's prior written permission.

University of Alberta

Flexural Response of Masonry Walls Reinforced with GFRP Sheets

by

Javed Afsar



A thesis submitted to the Faculty of Graduate Studies and Research in partial fulfillment
of the requirements for the degree of Master of Science

in

Structural Engineering

Department of Civil and Environmental Engineering

Edmonton, Alberta

Fall 2001

University of Alberta

Faculty of Graduate Studies and Research

The undersigned certify that they have read, and recommended to the Faculty of Graduate Studies and Research for acceptance, a thesis entitled Flexural Response of Masonry Walls Reinforced with GFRP Sheets submitted by Javed Afsar in partial fulfillment of the requirements for the degree of Master of Science in Structural Engineering.

To my family and friends

ABSTRACT

Traditional masonry walls have been designed as unreinforced or lightly reinforced to resist mainly the axial load. The risk associated with the seismic activity was therefore underestimated. Fiber reinforced polymer (FRP) composite materials can be used to strengthen these existing masonry elements, which are normally under-designed when evaluated according to modern codes for out-of-plane loading. Two series of reinforced masonry walls with externally bonded glass fiber reinforced polymer (GFPR) strips were tested in this study. The first series consisted of four 200 mm thick masonry walls and the second series consisted of four 150 mm masonry walls, both with externally bonded GFRP strips of various widths. Each specimen was 4 meters high and 1.2 meters wide. The primary objective was to study the behavior of reinforced masonry walls under out-of-plane lateral load. Response of the specimens under out-of-plane loading was extremely ductile and high mid-span deflection values were recorded. Three different modes of failure were observed: flexure-shear of masonry, delamination of FRP and tensile fracture of fibers. An analytical model to predict the out-of-plane behavior of reinforced masonry walls proposed by Kuzik *et al.* (1999) was modified to incorporate results obtained from the present study. Results obtained from the modified analytical model are in good agreement with the experimental results. A parametric study was conducted using the modified model to assist in the development of a design tool. Among the various parameters studied, amount of externally bonded GFRP strips has a clear and decisive effect in increasing the ultimate moment of the specimens. However, magnitude of constant axial load has insignificant effect.

ACKNOWLEDGEMENTS

The author thanks Dr. A. E. Elwi and Dr. J. J. Cheng for the support throughout. The author also acknowledges financial support from the Natural Sciences and Engineering Research Council of Canada (NSERC), the Canadian Masonry Research Institute (CMRI) and ISIS Canada.

TABLE OF CONTENTS

1. INTRODUCTION AND LITERATURE REVIEW	1
1.1 Background	1
1.2 Literature Review	2
1.3 Research Objectives and Scope	4
1.4 Organization of Thesis	5
2. EXPERIMENTAL PROGRAM	6
2.1 Introduction	6
2.2 Ancillary Tests	6
2.2.1 Concrete Masonry Units	6
2.2.2 Mortar Cubes	7
2.2.3 Grout Specimens	7
2.2.4 Masonry Prisms	7
2.2.5 Steel Reinforcement	8
2.2.6 Glass Fiber Reinforced Polymer (GFRP)	8
2.3 Test Specimens	9
2.3.1 Description	9
2.3.2 Selection of Various GFRP Layouts	9
2.3.3 Application of GFRP	10
2.4 Test Setup	11
2.4.1 Test Equipment Description	11
2.4.2 Lateral Load System	12
2.4.3 Axial Load System	12
2.4.4 Instrumentation	13
3. TEST OBSERVATIONS AND DISCUSSION OF RESULTS	29
3.1 Introduction	29
3.2 Testing Procedure	29
3.3 Test Observations	31

3.3.1	Wall-1 (200 mm)	31
3.3.2	Wall-2 (200 mm)	32
3.3.3	Wall-3 (200 mm)	33
3.3.4	Wall-4 (200 mm)	34
3.3.5	Wall-5 (150 mm)	35
3.3.6	Wall-6 (150 mm)	37
3.3.7	Wall-7 (150 mm)	37
3.3.8	Wall-8 (150 mm)	38
3.4	General Behavior of the Specimens	40
3.4.1	Moment versus Mid-Span Deflection Response	40
3.4.2	Load versus Strain Response	41
3.4.3	Modes of Failure	41
4.	ANALYTICAL MODEL	79
4.1	Introduction	79
4.2	GFRP Material and Section Properties	80
4.3	Section Properties Calculation	80
4.4	Components of Analytical Model	81
4.5	Flexural Model (Out of Plane Bending)	85
4.6	Comparison of Theoretical and Experimental Results	88
4.7	Comparison between the Two Models	89
5.	PARAMETRIC STUDY	103
5.1	Introduction	103
5.2	Selection of Various Parameters	104
5.3	Results of Parametric Study	105
5.3.1	Ultimate Moment versus Various Parameters	106
5.3.1.1	Amount of External GFRP Reinforcement	106
5.3.1.2	Amount of Vertical Steel Reinforcement	108
5.3.1.3	Masonry Unit Strength	109
5.3.1.4	Masonry Unit Thickness	109

5.3.1.5	Effect of Constant Axial Load	110
5.4	Flexural Stiffness versus Various Parameters	110
6. SUMMARY, CONCLUSIONS AND RECOMMENDATIONS		193
6.1	Introduction	193
6.2	Summary	193
6.3	Recommendations	194
REFERENCES		195

LIST OF TABLE

Table		Page
2.1	Individual Masonry Units Compression Test Results	15
2.2	Mortar Cubes Compression Test Results	16
2.3	Grout Specimen Compression Test Results	16
2.4	Steel Reinforcement Tension Test Results	16
2.5	GFRP Tension Coupons Test Results	16
2.6	Masonry Prisms Compression Test Results	17
2.7	Test Specimen Parameters	18
4.1	Parameters Associated with Test Specimens	91
4.2	Comparison of Experimental and Theoretical Results	91
4.3	Comparison of Results from the Two Models	92
5.1	Various Combinations of Parameters Used for Parametric Study	111
5.2	(a) 150mm Units, Unit Strength = 10 MPa	112
	(b) 150mm Units, Unit Strength = 15 MPa	113
	(c) 150mm Units, Unit Strength = 20 MPa	114
5.3	(a) 200mm Units, Unit Strength = 10 MPa	115
	(b) 200mm Units, Unit Strength = 15 MPa	116
	(c) 200mm Units, Unit Strength = 20 MPa	117
5.4	(a) 250mm Units, Unit Strength = 10 MPa	118
	(b) 250mm Units, Unit Strength = 15 MPa	119
	(c) 250mm Units, Unit Strength = 20 MPa	120
5.5	(a) Ultimate Moment Capacity and Percent Increase in Ultimate Moment Capacity for 150mm Walls.	121
	(b) Ultimate Moment Capacity and Percent Increase in Ultimate Moment Capacity for 200mm Walls.	122
	(c) Ultimate Moment Capacity and Percent Increase in Ultimate Moment Capacity for 250mm Walls.	123
5.6	(a) Percent Decrease in Ultimate Moment Capacity Due to Vertical Steel in 150mm Walls.	124
	(b) Percent Decrease in Ultimate Moment Capacity Due to Vertical Steel in 200mm Walls.	125
	(c) Percent Decrease in Ultimate Moment Capacity Due to Vertical Steel in 250mm Walls.	126
5.7	(a) Percent Increase in Ultimate Moment Capacity Due to Increase in Masonry Unit Strength (150mm Walls)	127
	(b) Percent Increase in Ultimate Moment Capacity Due to Increase in Masonry Unit Strength (200mm Walls)	128
	(c) Percent Increase in Ultimate Moment Capacity Due to Increase in Masonry Unit Strength (250mm Walls)	129
5.8	(a) Percent Increase in Ultimate Moment Capacity Due to Increase in Masonry Unit Thickness (15M@400)	130

5.8	(b) Percent Increase in Ultimate Moment Capacity Due to Increase in Masonry Unit Thickness (15M@800)	131
	(c) Percent Increase in Ultimate Moment Capacity Due to Increase in Masonry Unit Thickness (15M@1200)	132

LIST OF FIGURES

Figure	Page
2.1 Preparation of Grout Specimen	19
2.2 Testing of Grout Specimen in Compression	19
2.3 Typical Stress-Strain Plot of Steel Tension Test	20
2.4 Location of LVDT's during Compression Testing of Prism	20
2.5 Location of Grouted Cores and Bed Joint Reinforcement	21
2.6 Typical GFRP Layout Patterns	22
2.7 Modified Kuzik's Test Frame	23
2.8 Alternate Setup for Lateral Load	24
2.9 (a) Spring and Hydraulic Jack Arrangement	25
(b) Distributing Beam and Air Jacks	25
2.10 Instrumentation Layout	26
2.11 Typical Location of Strain Gages at Various GFRP Layouts	27
2.12 Strain Gage and Demec Points Pattern on Wall Surface	28
 3.1 Moment versus Deflection Response for Wall-1	44
3.2 Moment versus Deflection Response for Wall-2	45
3.3 Moment versus Deflection Hysterisis for Wall-3	46
3.4 Moment versus Deflection Hysterisis for Wall-4	47
3.5 Load versus Moment Response for Wall-5	48
3.6 Moment versus Deflection Hysterisis for Wall-6	49
3.7 Moment versus Deflection Hysterisis for Wall-7	50
3.8 Moment versus Deflection Hysterisis for Wall-8	51
3.8 (a) Superimposed response for Wall-5 and Wall-6	52
3.9 Load versus Strain for Wall-1	53
3.10 Load versus Strain for Wall-2	54
3.11 Load versus Strain for Wall-4	55
3.12 Load versus Strain for Wall-5	56
3.13 Load versus Strain for Wall-6	57
3.14 Load versus Strain for Wall-7	58
3.15 Load versus Strain for Wall-8	59
3.16 Failure of Wall-1	60
3.17 Failure of Wall-2	61
3.18 Failure of Wall-3	62
3.19 Failure of Wall-4	63
3.20 Failure of Wall-5	64
3.21 Rupture of GFRP Strips for Wall-7	65
3.22 Rupture of GFRP in Wall-8	66
3.23 Horizontal and diagonal Cracking in Wall-8	67
3.24 (a&b) Distribution of Strain Across the GFRP Strip for Wall-1	68,69
3.25 (a&b) Distribution of Strain Across the GFRP Strip for Wall-2	70,71
3.26 (a&b) Distribution of Strain Across the GFRP Strip for Wall-4	72,73
3.27 Distribution of Strain Across the GFRP Strip for Wall-5	74

3.28	Distribution of Strain Across the GFRP Strip for Wall-6	75
3.29	Distribution of Strain Across the GFRP Strip for Wall-7	76
3.30	(a&b) Distribution of Strain Across the GFRP Strip for Wall-8	77,78
4.1	Combined Regression for Maximum Strain	93
4.2	Combined Regression for Transition Moment	93
4.3	Typical Loading Envelope	94
4.4	Response of Wall-1 Test versus Predicted	95
4.5	Response of Wall-2 Test versus Predicted	95
4.6	(a) Response of Wall-3 Test versus Predicted (Pull)	96
	(b) Response of Wall-3 Test versus Predicted (Push)	96
4.7	(a) Response of Wall-4 Test versus Predicted (Push)	97
	(b) Response of Wall-4 Test versus Predicted (Pull)	97
4.8	Response of Wall-5 Test versus Predicted	98
4.9	Response of Wall-7 Test versus Predicted	98
4.10	(a) Response of Wall-6 Test versus Predicted (Pull)	99
	(b) Response of Wall-6 Test versus Predicted (Push)	99
4.11	(a) Response of Wall-8 Test versus Predicted (Push)	100
	(b) Response of Wall-8 Test versus Predicted (Pull)	100
4.12	(a) Response of Wall-3 (<i>Kuzik et al</i>) Test versus Predicted	101
	(b) Response of Wall-6 (<i>Kuzik et al</i>) Test versus Predicted	101
4.13	Moment(Test) versus Moment(Model)	102
5.1	Ultimate Moment versus Mid-Span Deflection for a Typical 150mm Wall	133
5.2	Ultimate Moment versus Mid-Span Deflection for a Typical 200mm Wall	134
5.3	Ultimate Moment versus Mid-Span Deflection for a Typical 250mm Wall	135
5.4	GFRP Area versus Ultimate Moment (15 MPa Masonry Units, Axial Load = 15 kN, 15M@400)	136
5.5	GFRP Area versus Ultimate Moment (15MPa Masonry Units, Axial Load = 15kN, 15M@800)	137
5.6	GFRP Area versus Ultimate Moment (15MPa Masonry Units, Axial Load = 15kN, 15M@1200)	138
5.7	GFRP Area versus Ultimate Moment (15MPa Masonry Units, Axial Load = 15kN, 15M@400 and 15M@800)	139
5.8	GFRP Area versus Ultimate Moment (15MPa Masonry Units, Axial Load = 15kN, 15M@400 and 15M@1200)	140
5.9	GFRP Area versus Ultimate Moment (15MPa Masonry Units, Axial Load = 15kN, 15M@800 and 15M@1200)	141
5.10	GFRP Area versus Ultimate Moment (15MPa Masonry Units, Axial Load = 30kN, 15M@400)	142
5.11	GFRP Area versus Ultimate Moment (15MPa Masonry Units, Axial Load = 30kN, 15M@800)	143
5.12	GFRP Area versus Ultimate Moment (15MPa Masonry Units, Axial Load = 30kN, 15M@1200)	144
5.13	GFRP Area versus Ultimate Moment (15MPa Masonry Units, Axial Load = 60kN, 15M@400)	145

5.14	GFRP Area versus Ultimate Moment (15MPa Masonry Units, Axial Load = 60kN, 15M@800)	146
5.15	GFRP Area versus Ultimate Moment (15MPa Masonry Units, Axial Load = 60kN, 15M@1200)	147
5.16	GFRP Area versus Ultimate Moment (15MPa, 150mm Masonry Units, Axial Load = 15kN, 15M@400, 15M@800, 15M@1200)	148
5.17	GFRP Area versus Ultimate Moment (15MPa, 150mm Masonry Units, Axial Load = 30kN, 15M@400, 15M@800, 15M@1200)	149
5.18	GFRP Area versus Ultimate Moment (15MPa, 150mm Masonry Units, Axial Load = 60kN, 15M@400, 15M@800, 15M@1200)	150
5.19	GFRP Area versus Ultimate Moment (15MPa, 200mm Masonry Units, Axial Load = 15kN, 15M@400, 15M@800, 15M@1200)	151
5.20	GFRP Area versus Ultimate Moment (15MPa, 200mm Masonry Units, Axial = 30kN, 15M@400, 15M@800, 15M@1200)	152
5.21	GFRP Area versus Ultimate Moment (15MPa, 200mm Masonry Units, Axial Load = 60kN, 15M@400, 15M@800, 15M@1200)	153
5.22	GFRP Area versus Ultimate Moment (15MPa, 250mm Masonry Units, (15M@400, 15M@800 and 15M@1200)	154
5.23	GFRP Area versus Ultimate Moment (15MPa, 250mm Masonry Units, Axial Load = 30kN, 15M@400, 15M@800, 15M@1200)	155
5.24	GFRP Area versus Ultimate Moment (15MPa, 250mm Masonry Units, Axial Load= 60kN,15M@400,15M@800,15M@1200)	156
5.25	Vertical Steel (15M@400) versus Ultimate Moment (15MPa Masonry Units, Axial Load = 15kN, Various Amount of GFRP)	157
5.26	Vertical Steel (15M@800) versus Ultimate Moment (15MPa Masonry Units, Axial Load = 15kN, Various Amounts of GFRP)	158
5.27	Vertical Steel (15M@1200) versus Ultimate Moment (15MPa Masonry Units, Axial Load = 15kN, Various Amounts of GFRP)	159
5.28	Vertical Steel (15M@400) versus Ultimate Moment (15MPa Masonry Units, Axial Load = 30kN, Various Amounts of GFRP)	160
5.29	Vertical Steel (15m@800) versus Ultimate Moment (15MPa Masonry Units, Axial Load = 30kN, Various Amounts of GFRP)	161
5.30	Vertical Steel (15M@1200) versus Ultimate Moment (15MPa Masonry Units, Axial Load = 30kN, Various Amounts of GFRP)	162
5.31	Vertical Steel (15M@400) versus Ultimate Moment (15MPa Masonry Units, Axial Load = 60kN, Various Amounts of GFRP)	163
5.32	Vertical Steel (15m@800) versus ultimate Moment (15MPa Masonry Units, Axial Load = 60kN), Various Amounts of GFRP)	164
5.33	Vertical Steel (15m@1200) versus Ultimate Moment (15MPa Masonry Units, Axial Load = 60kN, Various Amounts of GFRP)	165
5.34	Vertical Steel (15M@400, 800, 1200mm) versus Ultimate Moment (15MPa, 150mm Masonry Units, 2-65mm GFRP, Various Amounts of Axial Load)	166
5.35	Vertical Steel (15M@400, 800, 1200mm) versus Ultimate Moment (15MPa, 150mm Masonry Units, 2-125mm GFRP, Various Amounts of Axial Load)	167

5.36	Vertical Steel (15M@400, 800, 1200mm) versus Ultimate Moment (15MPa, 150mm Masonry Units, 2-250mm GFRP, Various Amounts of Axial Load)	168
5.37	Vertical Steel (15M@400, 800, 1200mm) versus Ultimate Moment (15MPa, 200mm Masonry Units, 2-65mm GFRP, Various Amounts of Axial Load)	169
5.38	Vertical Steel (15M@400, 800, 1200mm) versus Ultimate Moment (15MPa, 200mm Masonry Units, 2-125mm GFRP, Various Amounts of Axial Load)	170
5.39	Vertical Steel (15M@400, 800, 1200mm) versus Ultimate Moment (15MPa, 200mm Masonry Units, 2-250mm GFRP, Various Amounts of Axial Load)	171
5.40	Vertical Steel (15M@400, 800, 1200mm) versus Ultimate Moment (15MPa, 200mm Masonry Units, 2-65mm GFRP, Various Amounts of Axial Load)	172
5.41	Vertical Steel (15M@400, 800, 1200mm) versus Ultimate Moment (15MPa, 250mm Masonry Units, 2-125mm GFRP, Various Amounts of Axial Load)	173
5.42	Vertical Steel (15M@400, 800, 1200mm) versus Ultimate Moment (15MPa, 250mm Masonry Units, 2-250mm GFRP, Various Amounts of Axial Load)	174
5.43	Area of GFRP versus Flexural Rigidity (15MPa Units, Axial Load = 15kN) Various Unit Thicknesses, Vertical Steel 15M@400, and 800mm c/c	175
5.44	Area of GFRP versus Flexural Rigidity (15MPa Units, Axial Load = 15kN) Various Unit Thicknesses, Vertical Steel 15M@400, and 1200mm c/c	176
5.45	Area of GFRP versus Flexural Rigidity (15MPa Units, Axial Load = 15kN) Various Unit Thicknesses, Vertical Steel 15M@800, and 1200mm c/c	177
5.46	Area of GFRP versus Flexural Rigidity (15MPa Units, Axial Load = 30kN) Various Unit Thicknesses, Vertical Steel 15M@400, and 800mm c/c	178
5.47	Area of GFRP versus Flexural Rigidity (15MPa Units, Axial Load = 30kN) Various Unit Thicknesses, Vertical Steel 15M@400, and 1200mm c/c	179
5.48	Area of GFRP versus Flexural Rigidity (15MPa Units, Axial Load = 30kN) Various Unit Thicknesses, Vertical Steel 15M@800, and 1200mm c/c	180
5.49	Area of GFRP versus Flexural Rigidity (15MPa Units, Axial Load = 60kN) Various Unit Thicknesses, Vertical Steel 15M@400, and 800mm c/c	181
5.50	Area of GFRP versus Flexural Rigidity (15MPa Units, Axial Load = 60kN) Various Unit Thicknesses, Vertical Steel 15M@400, and 1200mm c/c	182

5.51	Area of GFRP versus Flexural Rigidity (15MPa Units, Axial Load = 60kN) Various Unit Thicknesses, Vertical Steel 15M@800, and 1200mm c/c	183
5.52	Area of Vertical Steel (15M@400c/c) versus Flexural Rigidity (15MPa Units, Axial Load = 15kN), Various Amounts of GFRP	184
5.53	Area of Vertical Steel (15M@800c/c) versus Flexural Rigidity (15MPa Units, Axial Load = 15kN), Various Amounts of GFRP	185
5.54	Area of Vertical Steel (15M@1200c/c) versus Flexural Rigidity (15MPa Units, Axial Load = 15kN), Various Amounts of GFRP	186
5.55	Area of Vertical Steel (15M@400c/c) versus Flexural Rigidity (15MPa Units, Axial Load = 30kN), Various Amounts of GFRP	187
5.56	Area of Vertical Steel (15M@800c/c) versus Flexural Rigidity (15MPa Units, Axial Load = 30kN), Various Amounts of GFRP	188
5.57	Area of Vertical Steel (15M@1200c/c) versus Flexural Rigidity (15MPa Units, Axial Load = 30kN), Various Amounts of GFRP	189
5.58	Area of Vertical Steel (15M@400c/c) versus Flexural Rigidity (15MPa Units, Axial Load = 60kN), Various Amounts of GFRP	190
5.59	Area of Vertical Steel (15M@800c/c) versus Flexural Rigidity (15MPa Units, Axial Load = 60kN), Various Amounts of GFRP	191
5.60	Area of Vertical Steel (15M@1200c/c) versus Flexural Rigidity (15MPa Units, Axial Load = 60kN), Various Amounts of GFRP	192

LIST OF ABBREVIATIONS

ASTM	American Society for Testing and Materials
ATC	Applied Technology Council
CFRP	Carbon Fiber Reinforced Polymer
GFRP	Glass Fiber Reinforced Polymer
HSS	Hollow Structural Section
kip	One Thousand Pound (Kilo pound)
kN	Kilo Newton
ksi	kips per square inch
LVDT	Linear Variable Differential Transducer
MPa	Mega Pascal
MTS	Material Testing System
URM	Unreinforced Masonry
W	Wide Flange Beam
WWF	Welded Wide Flange Beam

LIST OF SYMBOLS

A_e	Effective Area of Uncracked Cross-Section (mm^2)
A_{GFRP}	Area of GFRP on the Tension Face (mm^2)
A_s	Area of Tension Steel Reinforcement (mm^2)
a	Depth of Equivalent Rectangular Stress Block (mm)
b	Width of Compression Zone (mm)
d	Distance from the Extreme Compression Fiber to the Centroid of the Tension Steel (mm)
E	Modulus of Elasticity of Masonry (MPa)
E_{GFRP}	Modulus of Elasticity of Glass Fiber Reinforced Polymer (MPa)
E_m	Modulus of Elasticity of Masonry (MPa)
E_s	Modulus of Elasticity of the Reinforcing Steel (MPa)
f'_c	Compressive Strength of Concrete (MPa)
f_m	Compressive Strength of Masonry (MPa)
f_y	Yield Strength of the Steel Reinforcement (MPa)
f_t	Tensile Strength of Masonry (MPa)
h	Depth of Wall (mm)
I_{cr}	Cracked Moment of Inertia (mm^4)
I_g^f	Modified Moment of Inertia (mm^4)
I_o	Moment of Inertia of Uncracked Section (mm^4)
k	Constant used to Calculate Compressive Strength of Concrete
k_1	Factor used to Approximate the Depth of the Compressive Stress Block
k_2	Factor used to Locate the Centroid of the Compressive Stress Block
k_3	Factor used to Approximate the Height of the Compressive Stress Block
L	Wall Height (mm)
M	Bending Moment (kN-m)
M_a	Instantaneous Bending Moment (kN-m)
M_{cr}	Cracking Moment (kN-m)
M_{cr}^f	Modified Cracking Moment (kN-m)
M_f	Factored Moment (kN-m)
M_T	Transition Moment (kN-m)

M_T	Transition Moment (kN-m)
M_u	Ultimate Moment (kN-m)
P	Axial Load (kN)
R	Stiffness Interpolation Factor
R^2	Coefficient of Determination
S	Section Modulus (mm^3)
S_{cr}	Spacing of Horizontal Cracks (mm)
t_{GFRP}	Nominal GFRP Thickness (mm)
x	Length of Shear Span (mm)
y_t	Distance from Centroid to Extreme Fiber
A	Reduction Factor
B_1	Facto used to Approximate k_1
D_a	Mid-span Deflection at Service Moment (mm)
D_{cr}	Mid-span Deflection at Cracking Moment (mm)
D_{crf}	Mid-Span Deflection at Transition Moment (mm)
D_{max}	Maximum Mid-Span Deflection (mm)
D_t	Mid-Span Deflection at Transition Moment (mm)
D_u	Mid-Span Deflection at Ultimate Moment (mm)
D	Change in Length (mm)
$\epsilon_{u,GFRP}$	Maximum GFRP Strain at the Ultimate Moment (mm/mm)
T	Angle (Radians)
P	Resistance Factor for Reinforcing Bars (0.85)
P_m	Resistance Factor for Masonry (0.55)
R	Curvature
R_t	GFRP Reinforcement Ratio
P_u	Ultimate Tensile Strength (1/mm)
P_y	Yield Strength

Chapter 1

INTRODUCTION AND LITERATURE REVIEW

1.1 Background

Structurally and aesthetically, masonry is amongst the oldest construction materials still in use since the ancient times. Though masonry has been widely used in almost all types of structures, the research carried out on masonry has been behind steel and reinforced concrete. Due to its low tensile strength and lack of ductility, unreinforced masonry structures are unsuitable for use in seismic prone areas. Steel reinforcement is normally used in masonry structures to resist the probable lateral load. Unavailability of the design provisions in the past, lead to simple and empirical design methods for masonry structures. The reinforced masonry structures designed using these simple approaches are sometimes found deficient in steel reinforcement when evaluated in comparison to modern seismic design requirements. Normally, reinforced masonry walls in existing structures are designed to carry the vertical loads only. However, during a seismic event these walls are subjected to considerable in-plane and out-of-plane horizontal forces. When subjected to excessive lateral forces, such as wind load, earthquakes or blast load, these structures are susceptible to extensive damage or even catastrophic failure. Considerable loss of life and damage to infrastructure caused by recent earthquakes has intensified the needs to strengthen the existing masonry structures.

All components of masonry structures need in depth investigation as per strength requirements, but walls being one of the major component need particular attention. Recent research (Albert *et al.* 1998, Kuzik *et al.* 1999) has shown that the masonry walls that do not fulfill the current code requirements may be rehabilitated/strengthened by using fiber reinforced composite materials. The technique is very simple and easy to use with minimum disruptive to the use and occupancy of the structures.

1.2 Literature Review

After gaining a wide acceptance in aerospace, defense and marine sectors, the use of fiber-reinforced polymers (FRPs) in civil engineering has increased rapidly over the past few years. High strength to weight ratio, magnetic neutrality, high chemical and corrosion resistance, excellent fatigue performance and design flexibility are some of the characteristics behind the dramatic increase in acceptance of these materials. Despite all these advantageous characteristics, there are several shortcomings associated with FRPs, namely relatively small rupture strain, lack of plastic behavior, etc.

FRP composite materials are a blend of two materials: fibers and resin matrix. The reinforcement is in the form of fibers, sheets or fabric mats, whereas, the resin matrix is usually a relatively ductile material such as epoxy. The resin matrix helps in maintaining the orientation of fibers and to provide protection to fibers against environmental conditions. The orientation of the fibers has a substantial effect on the structural properties of the composites. The fibers that are continuous and aligned in one direction provide a high strength and high modulus in the fibers direction and low strength and low modulus in the perpendicular direction. The types of fiber commonly used in FRPs are carbon fibers, glass fibers and aramid fibers. The selection of the type depends mainly on the cost, environmental conditions and importance of the structure being used on.

Most of the work presented in this section is pertaining to masonry structures retrofitted with FRPs. The previous work in this area has demonstrated a considerable increase in the flexural strength of the reinforced masonry walls. Kuzik *et al.* (1999) published an extensive literature review related to application of FRPs in concrete and masonry structures and FRP-to-concrete bond behavior. Bruneau *et al.* (1993) did an extensive field survey of sites where masonry structures were subjected to severe earthquake loading. Performance of the masonry structures subjected to earthquakes specifically Northridge (Los Angeles) and Hyogo-ken Nanbu (Kobe, Japan) earthquakes have been discussed.

Ehsani (1995) tested six clay brick beams, externally reinforced with three different types of fibers. He reported that the specimens carried more than twenty times their own weight and withstood deflections in excess of 1/50 times the span. A field application has also been presented. The wall was constructed of 200 mm thick blocks with no reinforcing steel. The wall was severely damaged during the Northridge earthquake in January 1994. The wall was retrofitted using *QuakeWrap*TM. Field application consisted of applying the fibers on the entire surface of the wall. The authors concluded that significant increase in strength was achieved and the technique was very cost effective. Ehsani *et al.* (1999) tested three half-scale brick masonry walls retrofitted with vertical E-glass FRP strips. The specimens were 1.22 m long and 0.710 m high and were constructed by using reduced-scale clay bricks and type N mortar. The walls were subjected to a continuously repeating out-of-plane cyclic loading using an airbag system. No axial load was applied. Based on experimental results, it was concluded that the ultimate flexural capacity of the externally reinforced walls was significantly increased. Also tensile failure of GFRP strips is reported for specimens with lighter external reinforcement. It was concluded that GFRP composite strips is an excellent alternative to retrofit the un-reinforced masonry (URM) walls against lateral loads.

Albert *et al.* (1998) performed out-of-plane monotonic tests on 12 full-scale masonry walls. No vertical steel reinforcement was used. The specimens were reinforced externally using various types of FRP. The FRP was applied in various vertical and diagonal layouts. The types of FRP used were glass fiber sheet, carbon fiber strap and carbon fiber sheets supplied by various manufacturers. Three modes of failure were reported, namely mortar debonding or sliding failure, flexure-shear failure and rupture of fiber reinforcement. They reported a bilinear load versus mid-span deflection response. The first portion of the response was non linear and was dominated by the properties of masonry materials. The second portion was linear and was mainly controlled by the FRP properties. One cyclic test was also performed. The load versus mid-span deflection response for this specimen showed a bilinear response in the loading stage and a linear response in the unloading.

Kuzik *et al.* (1999) tested eight full-scale masonry walls under fully reversed cyclic loading. The GFRP used to reinforce the walls externally was SHE-51 with Tyfo®S epoxy supplied by FYFE CO. LLC. Kuzik *et al.* (1999) characterized the moment versus mid-span deflection response as bilinear for walls without vertical steel reinforcement. For walls containing vertical steel reinforcement, a trilinear response was characterized. However, the unloading path was linear, irrespective of the loading response. The governing mode of failure was characterized as the flexure-shear. An analytical model was presented to predict the displacement. More details about the model are discussed in Chapter 4.

1.3 Research Objectives and Scope

As mentioned above, the need for strengthening an existing masonry structure might arise when the strength and ductility is evaluated under the existing design standards. Research has been done in the past few years at the University of Alberta on the out-of-plane behavior of reinforced and unreinforced masonry walls subjected to monotonic and cyclic loading. As mentioned above, Kuzik *et al.* (1999) reported eight cyclic tests on 200 mm reinforced masonry walls strengthened with 250 mm and 125 mm wide FRP strips, respectively. Axial loads applied to the walls were 15, 30 and 60 kN. All strips were bonded against grouted cores.

This project is designed to further study the flexural behavior of reinforced masonry walls strengthened with glass fiber reinforced polymer (GFRP) strips. Additional narrower GFRP strips than the ones used by Kuzik *et al.* (1999) are used in the test program. Two wall thicknesses of 200 mm and 150 mm are used. The analytical models proposed by Kuzik *et al.* (1999) are used to evaluate the test results. The model is further modified based on the additional test results. The modified model is then used to perform a parametric study in order to provide a better understanding of the reinforced masonry walls under monotonic and cyclic out-of-plane bending with a constant axial force and varied GFRP reinforcements. A design guideline is proposed based on the

parametric studies. This research work is essentially an extension of the previous works by Albert *et al.* (1998) and Kuzik *et al.* (1999) at the University of Alberta.

1.4 Organization of Thesis

The thesis consists of six chapters. Chapter one comprises introduction to the FRP composite materials accompanied by a brief literature review and the objectives of the research. Chapter two presents the test setup. The instruments used to monitor the lateral deflection and the axial load are discussed. It contains information about the ancillary tests and the boundary conditions used in the load frame. The problems faced with the lateral load system and the alternate load systems are discussed. Also presented briefly are the parameters associated with the test specimens and the corresponding failure loads and deflections. Chapter three describes in detail the testing procedure and the test observations recorded during each test. Various modes of failures are discussed and photographs of the specimens at failure are presented. Plots showing the moment versus mid-span deflection and the load versus strain in GFRP are also presented. Chapter four briefly describes the analytical model used to predict the moment and mid-span deflection at failure for all walls. Calculation of sectional properties used in the analytical model is discussed. Chapter five contains the parametric study performed in this program. Various parameters including thickness of wall, width of GFRP strips and thickness of GFRP are discussed. Chapter six presents a summary of the research work and provides recommendations and suggestions for future research in this area. Conclusions derived from this study are presented.

Chapter 2

EXPERIMENTAL PROGRAM

2.1 Introduction

The testing program comprises two groups of walls. The first group consisted of four 150 mm walls, two were tested monotonically and two were tested cyclically. The second group consisted of four 200 mm walls, two were tested monotonically and two were tested cyclically. All walls were 1.2 m wide and 4.0 m high, built by professional masons. The load pattern was the same for both groups. Lateral out-of-plane load was applied at a distance of 1.2 m from the top and bottom respectively and a constant axial load was maintained. The parameters investigated were amount of GFRP, strain transfer, thickness of walls and spacing of GFRP strips. This chapter describes the test setup, ancillary tests and the test specimens.

2.2 Ancillary Tests

A series of ancillary tests were conducted on individual masonry blocks, masonry prisms, mortar cubes, grout specimens, steel bars and GFRP to determine the mechanical properties of these materials.

2.2.1 Concrete Masonry Units

Edcon from Edmonton supplied the concrete masonry units. Five masonry units were tested for each size of concrete masonry block to determine the compressive strength in accordance with CSA Standard A165.1-M94 (1994). A 10 mm fiberboard was placed at top and bottom of each unit as a capping to provide smooth surface. Results comprising the physical and mechanical properties are presented in Table 2.1.

2.2.2 Mortar Cubes

Type S mortar (Cement-Lime-Sand) was used. A total of six mortar cubes (50 mm) were tested in accordance with CSA Standard A369.1-M94 (1994). All the specimens were capped with melted sulfur capping material to provide a smooth surface. The specimens were tested in compression using MTS 1000 testing machine. Results are presented in Table 2.2.

2.2.3 Grout Specimens

Manstar Distributors Ltd supplied pre-mix grout. A total of six specimens were made in accordance with CSA Standard A179M to determine the compressive strength of the grout. Sufficient amount of water was added to the grout to make it more workable. All the specimens were capped with melted sulfur capping material. Figure 2.1 shows the preparation of grout specimens. The specimens were tested in compression using an MTS 1000 testing machine as shown in Figure 2.2. Results are presented in Table 2.3.

2.2.4 Masonry Prisms

The masonry prisms tested were assemblage of blocks and mortar with and without grout. Two series of masonry prisms were constructed during the construction of walls. The first series consisted of five grouted and five ungrouted prisms using 150 mm blocks and type S mortar. The second series consisted of five grouted and five ungrouted prisms using 200 mm blocks and type S mortar. Each prism was one and a half course wide and five courses in height. The joints were flushed with the face shells. Before testing, each prism was grounded manually using a sand stone to get rid of any bumps due to grouting or mortar. Each prism was capped with a 10 mm thick fiberboard at top and bottom to provide flat bearing surfaces and to facilitate application of uniform load. To measure vertical strains, linear variable differential transducers were mounted on each specimen on North and South face as shown in Figure 2.4. Gauge points were located at the top and bottom course so that the measured strain represents average values along the

height of the prism. Prisms were then subjected to axial compression using an MTS 6000 testing machine and the data was recorded using fluke. Rate of applied load was in accordance with CAN3-A369-M84. The typical failure mode was tension splitting and spalling of face shell. Stresses were calculated based on the net area of the block for ungrouted prisms and gross area for grouted prisms. The initial portion of the stress versus strain curve represents a crooked line due to seating of the specimen and was ignored. Remaining portion was reasonably linear and was used for the E_m calculations. CSA S304.1-94 (Clause 8.3.1.4) stipulates determination of E_m experimentally based on secant modulus measured over a stress range extending from 5% to 30%. The test results for both series of Prism tests are summarized in Table 2.6.

2.2.5 Steel Reinforcement

Tension tests were performed on two coupons cut from the same bars used for reinforcing walls. Testing was carried out using an MTS 1000 testing machine and the elongation was recorded by mounting an extensometer to the steel bar. A typical stress strain plot of a tension coupon test is shown in Figure 2.3. Test results are presented in Table 2.4.

2.2.6 Glass Fiber Reinforced Polymer (GFRP)

The GFRP used was MBraceTM EG 900 (E-glass Reinforcement System) produced by the Master Builders, Inc. The epoxy consisted of MBraceTM saturant and primer and was provided by same manufacturer. The unidirectional glass fiber sheet was provided in a 50 cm wide roll with continuous fibers assembled together in one direction. GFRP coupons were made and tested in accordance with ASTM D 3039-95a (1995). Test results are listed in Table 2.5. Based on the results obtained from the tension coupon tests and the physical characteristics of the fiber, throughout this study program, all results and discussions are based on the material properties provided by Sika Canada.

2.3 Test Specimens

2.3.1 Description

Two series of full-scale walls were constructed. The first series consisted of four 150 mm wide block walls and the second series consisted of four 200 mm wide block walls with various GFRP arrangements. Each specimen was 4 meters high and 1.2 meters wide with a constant thickness of bed and head joints of 10 mm. The walls were constructed using running bond and with the joints flushed with the face shells. All the specimens were reinforced horizontally and vertically. Horizontal joint reinforcement was provided at every third course. After laying three courses, the joint reinforcement was placed on top of fresh mortar and pressed by hand. The vertical steel reinforcement in each wall consisted of two 10M bars placed in the second core from each side thus leaving center-to-center distance of 600 mm. The steel reinforcement is consistent with a low ratio typically used in older masonry structures. The cores containing vertical steel reinforcement were then fully grouted as shown in Figure 2.5. The cores were grouted using a hopper lifted up by an overhead crane. Due to space restriction and safety reasons, no mechanical vibrators were used to consolidate the grout. All the specimens were built on movable steel plates to assist in moving them to the load frame. The parameters associated with each test specimen are listed in Table 2.7.

2.3.2 Selection of Various GFRP Layouts

Kuzik *et al.* (1999) tested a total of eight 200 mm thick full-scale specimens. Six out of eight walls were reinforced externally with 250 mm wide GFRP Strips on each face while two walls were reinforced with 65 mm and 125 mm wide GFRP strips respectively. Kuzik *et al.* (1999) also proposed a semi rational prediction model for the behavior. An excellent agreement was found between the experimental and analytical results. However, the model was based solely on the test results obtained from the testing of 200 mm walls with 2-250 mm GFRP strips on each face.

In order to investigate the agreement of Kuzik *et al.* (1999) analytical model for variable wall thickness and amount of GFRP, two series of walls were constructed for this experimental program. Various GFRP layouts consisting of 65 mm and 125 mm GFRP strips have been used. The GFRP was applied in the form of vertical strips against the grouted cores on both faces of the specimen for cyclic tests and on one face only for monotonic tests. However, a new layout scheme was used for Wall-4 by applying 125 mm GFRP strips at mid of the specimen (against ungrouted units). The applied axial load ranges between 15 kN and 60 kN and the resulting P- Δ effect due to large lateral deformations has been used in the moment calculations. Table 2.7 shows the various parameters associated with each test specimen.

2.3.3 Application of GFRP

In order to obtain a satisfactory bond between masonry and GFRP, preparation of the surface is of prime importance. Before application of GFRP on the surface of each wall, the surface was prepared. First the surface was marked with a felt pen and grounded manually with a sand stone to get rid of any mortar protrusions. Secondly the surface was grounded with an aluminum oxide sand paper (Fine 120 Grit) lightly to get rid of any loose material. Finally a brush was used to clean the surface.

A thin layer of primer coat was applied first to the areas already marked and smoothened and was allowed to cure for one day. The MBraceTM was made using a three to one ratio of part A and part B as recommended by the manufacturer. The MbraceTM saturant has the same mixing ratio as primer but with different components. The GFRP was then impregnated with epoxy and in the mean time a tack coat of epoxy was applied on top of dried primer. The soaked GFRP was then rolled and positioned against the surface of wall for vertical application. Finally a coat of epoxy was applied on top of the fiber to ensure good bond between wall surface and GFRP. A 3 mm foam roller was used for application of epoxy and primer. Though every effort was made to keep the density of the epoxy, uniform throughout the full length of the GFRP strip but due to the vertical surface, viscous nature and short pot life of epoxy, some regions might had different

density of epoxy. This inconsistency might have affected the bond between the masonry surface and GFRP. Figure 2.6 shows the typical GFRP layout patterns. For applications in the field, the surface of the wall can be covered with stucco or any other architectural coating.

2.4 Test Setup

2.4.1 Test Equipment Description

The loading frame was designed as a self-equilibrating, two point loading system. This scheme divided the vertical span into two constant shear regions at top and bottom with a constant moment region in the middle. The major benefit choosing this setup being easier identification of shear and flexural behavior. The test frame was modified from one originally built by Kuzik *et al.* (1999). Each wall was tested as an element supported on a knife-edge pinned at the bottom and fitted with a roller allowing vertical movement at top. Two line loads were applied at 1.2 m from top and bottom. The reaction frame consisted of two W310x129 columns approximately 1830 mm center-to-center and bolted to the strong floor. Two WWF350x137 crossbeams joining these columns were used to mount the hydraulic jacks. Two W150x22 beams joined together with a 19 mm thick steel plate at each end were used as “clamps” to apply lateral load to the specimen. The purpose of the clamps was to convert the point load from hydraulic jacks into a uniformly distributed line load along the width of the specimen and to avoid any premature crushing at the point of application. Each clamp was lifted up with an overhead crane and slipped down at a pre-specified height on the wall. A redi-rod arrangement was then used to snug the two sections against the wall. Boundary conditions at the bottom of the specimen consisted of a knife-edge and roller arrangement. Figure 2.7 shows the complete test setup.

2.4.2 Lateral Load System

The lateral load was applied using two double-acting hydraulic rams mounted on the crossbeams. Pull and push capacity of each ram was 20000 lbs (90 kN). Stroke control loading mechanism was used for all the specimens. Each Hydraulic ram was equipped with a Linear Variable Displacement Transducer (LVDT) to control its movement. An MTS pump supplied constant fluid pressure and Servo valves were used to control the flow. The wall was supported laterally by using two reaction links at top and bottom respectively. Each reaction link was made of an HSS 76 x 51 x 4.8 section and was pin-connected to the wall at the top and bottom clamp to allow out of plane deflection of the wall. The connections were also able to accommodate some lateral and angular movement.

Due to a malfunction in the lateral load system, a different setup was used for walls 4, 7 and 8. The alternate system consisted of four hydraulic jacks compressed by the MTS 1000 testing machine to supply constant fluid pressure to the hydraulic rams. Before mounting the jacks into MTS 1000 testing machine, a hand pump was used to force the oil into the hydraulic jacks before they reached their maximum limit. Pulling and pushing was accomplished by switching the hoses after every half cycle. The loading rate already programmed in the MTS machine was modified according to the needs. Figure 2.8 shows the plan of mechanism adopted for this setup.

2.4.3 Axial Load System

The setup used for application of axial load was different from that used by Kuzik *et al.* (1999). The modification was made to provide more lateral room to the specimen under excessive deflections. The axial load assembly consisted of a W150x22 beam positioned on top of the wall with a fiberboard located between the steel and top of the masonry surface. Two 920 mm high strength threaded rods were connected at both ends of the steel beam. A load distribution mechanism comprising of two HSS 127x51x6.4 joined together with high strength steel rods was then connected with

the hanging rods on each side. High strength steel rods were then connected to the bottom HSS sections and finally passed through the strong floor, thus making a *whiffle tree* arrangement. Spring coil and hydraulic jacks were then connected to the end of these steel rods underneath strong floor. The capacity of each of these jacks was 12 tons. Figure 2.9 (a) shows the spring and hydraulic jack setup underneath strong floor. However, for wall-2 (Axial load = 60 kN) a different setup was used. This setup consisted of ten air jacks, each having a capacity of 3000 lbs (13 kN). A distributing beam was used underneath strong floor to hold the jacks. Figure 2.9 (b) shows the setup.

2.4.4 Instrumentation

Measurements included the applied axial and lateral load, out-of-plane mid-span deflection and strains in the GFRP in the constant moment region. The vertical/axial loads were measured by mounting a load cell on each of the vertical rods carrying the axial load. Lateral load was measured by mounting a load cell on each of the jacks and the four rigid reaction links.

A total of five LVDT's and cable transducers were used to measure the out-of plane deflection of the wall specimens. An LVDT's was mounted on the load frame to measure the deflection between the top loading and reaction clamps and it was repeated at the bottom. Another LVDT was used to measure the mid-deflection of the wall. Two cable transducers were used to measure deflection at upper and lower quarter points between the two loading clamps. Figure 2.10 shows a detailed layout of all these instruments.

Kuzik *et al.* (1999) observed a particular pattern of behavior in which steel yield is implicated. Therefore, it was decided to re-examine the rebar strains in this program. Strain data was measured using 5 mm foil strain gauges with a nominal resistance of 120 Ohms. Three strain gages were applied on one of the two vertical steel reinforcing bars in each specimen. The locations of the gages were lower bed joint, middle of block and upper bed joint of the tenth course. An electrical grinder was used to smoothen the

area restricted for the foil strain gage and the gage was bonded with a strong adhesive. A layer of silicon was then applied on each gage to make it water resistant. After soldering of wires a thick layer of silicon was applied over each gage to protect it from any damage that can result during grouting.

Foil gages on GFRP were applied by first forming a thin layer of five minute epoxy on the surface to smoothen it. All the gages were located at 10 mm from the outer edge and the number of strain gages varies from specimen to specimen. A typical pattern of application of strain gages on GFRP is shown in Figure 2.11.

Albert *et al.* (1998) and Kuzik *et al.* (1999) reported a shear lag phenomenon on the face shell adjacent to GFRP locations. This phenomenon was expressed in the form of diagonal cracks in the face shell. An attempt to verify the strain field in this region was made in the current study, but applying the strain gages directly on the masonry surface is a tedious job and results in futile effort at the end. The surface was smoothened first using a floor leveler and then the protrusions were smoothened using a sand paper. The gages were then applied directly on the surface using Bond 200 Glue. Most of the strain gages at the time of test did not respond to the fluke data acquisition system. Figure 2.12 shows the set up used. It is clear from the figure that the space between the strain gages was too small and thus results in congestion of connecting wires, which might lead to the loss of bond between the gage and the masonry surface.

A Fluke 2400B data acquisition system was connected with the computer to record all measurements. Lab View was used to plot and view the real time load versus deflection behavior of each specimen.

Table 2.1 Individual Masonry Units Compression Test Results**(a) 200 mm Units**

	Ultimate Load (kN)	Ultimate Strength (MPa) ¹
1	609	13.76
2	640	14.46
3	598	13.51
4	555	12.54
5	684	15.45
6	602	13.60
Average		13.88 MPa
Standard Deviation		0.98 MPa
Coefficient of Variation		7.08 %

(b) 150 mm Units

	Ultimate Load (kN)	Ultimate Strength (MPa) ²
1	461	13.39
2	456	13.24
3	658	19.11
4	538	15.63
5	535	15.54
6	471	13.68
7	525	15.25
8	468	13.59
Average		14.93
Standard Deviation		1.96
Coefficient of Variation		13.16 %

¹ Based on net area = 44269 mm²² Based on net area = 34430 mm²

Table 2.2 Mortar Cubes Compression Test Results

Specimen Number	Max. Load (kN)	Strength (MPa)
1	46	18.4
2	48	19.2
3	49	19.6
4	46	18.4
5	36	14.4
6	39	15.6

Table 2.3 Grout Specimen Compression Test Results

Specimen Number	Max. Load (kN)	Strength (MPa) [†]
1	201	35.7
2	190	33.7
3	213	37.8
4	145	25.7
5	194	34.4
6	185	32.8

[†] Based on average area = 5636.5 mm²

Table 2.4 Steel Reinforcement Tension Test Results

Bar Size	Nominal Area (mm ²)	Yield Stress (MPa)	Ultimate Stress (MPa)	Modulus of Elasticity E* (MPa)
10 M	100	421	649	196400

* Only two tension coupons were tested

Table 2.5 GFRP Tension Coupons Test Results

GFRP Type	Thickness (mm)	Max. Stress (MPa)	E (MPa)
MBrace EG 900	0.353		69651 ^b 74867 ^c
Glass Sheet (SEH51) ^a	1.2954	309	27579 ^b 35651 ^c

^a Properties Used in the Model.

^b Modulus provided by the manufacturer.

^c Modulus obtained from the tension coupon tests.

Table 2.6 Masonry Prisms Compression Test Results**(a) 200 mm Prisms**

Specimen Number	UngROUTed ^a		Fully Grouted ^b	
	Max. Load (kN)	Stress (MPa)	Max. Load (kN)	Stress (MPa)
1	351	5.8	882	8.1
2	436	7.2	808	7.4
3	348	5.7	757	7
4	416	6.8	917	8.5
5	372	6.1	715	6.6
Average		6.3		7.5
STD		0.65		0.78
C.O.V		10		10.3

(b) 150 mm Prisms

Specimen Number	UngROUTed ^c		Fully Grouted ^d	
	Max. Load (kN)	Stress (MPa)	Max. Load (kN)	Stress (MPa)
1	522	11.56	806	10.9
2	394	8.73	870	11.7
3	409	9.06	746	10.1
4	519	11.50	782	10.5
5	467	10.34	689	9.3
Average		10.24		8.3
STD		1.32		1.62
C.O.V		12.94		19.48

^a based on average area = 60753 mm²^b based on average area = 108490 mm²^c based on average area = 45144 mm²^d based on average area = 74200 mm²

f'm = Average - 1.5 STDEV

Table 2.7 Test Specimen Parameters

Specimen	Thickness (mm)	Vertical Steel (mm)	GFRP [#]	Type of Lateral Loading	Axial Load (kN)	Cycles	Total load (kN)	Total Deflection (mm)	Type of Failure (Maximum Strain)
Wall-1	200	2-10M	2-125	Monotonic	30	-	35	119	A (1.8 %)
Wall-2	200	2-10M	2-125	Monotonic	60	-	39	140	B (1.4 %)
Wall-3	200	2-10M	2-65	Cyclic	30	12	34	135	A (-)
Wall-4	200	2-10M	1-125	Cyclic	30	9.5	32	165	A (1.5 %)
Wall-5	150	2-10M	2-125	Monotonic	30	-	32	235	B (2.26 %)
Wall-6	150	2-10M	2-125	Cyclic	15	3.0	26	149	*(1.0 %)
Wall-7	150	2-10M	2-65	Monotonic	30	-	15	190	C (2.4 %)
Wall-8	150	2-10M	2-65	Cyclic	15	10.5	18	205	C (1.5 %)

[#]Number of GFRP Strips on each Face. One Face for Monotonic and Both Faces for Cyclic.

A→Delamination of GFRP Strips

B→Delamination of GFRP Strips accompanied by Flexure-Shear failure

C→Delamination accompanied by Rupture of GFRP Strips

*→Not loaded to failure

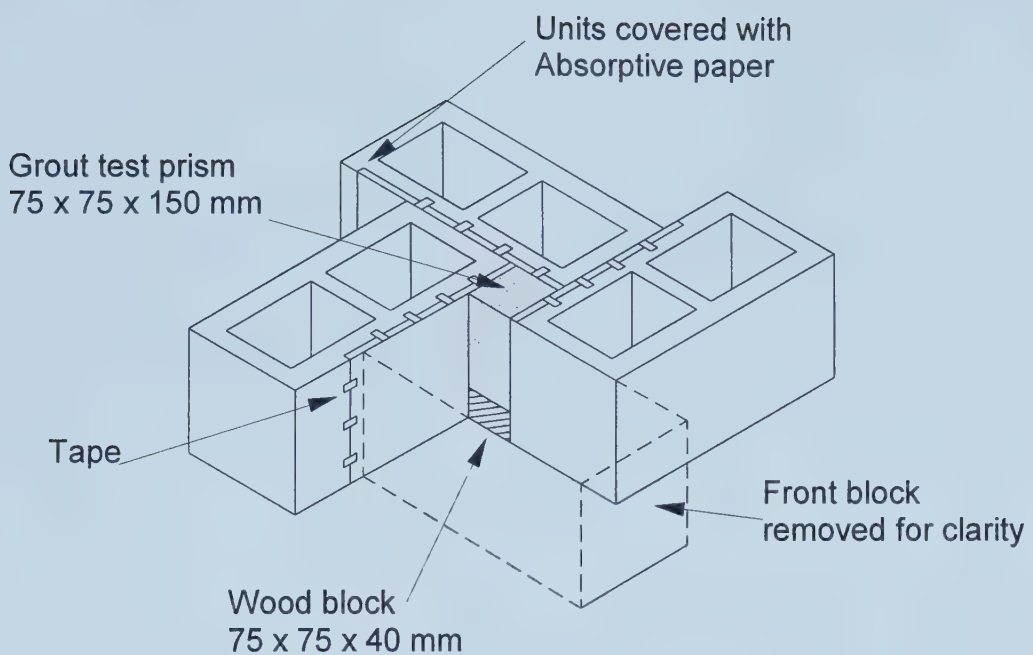


Figure 2.1 Preparation of Grout Test Specimen

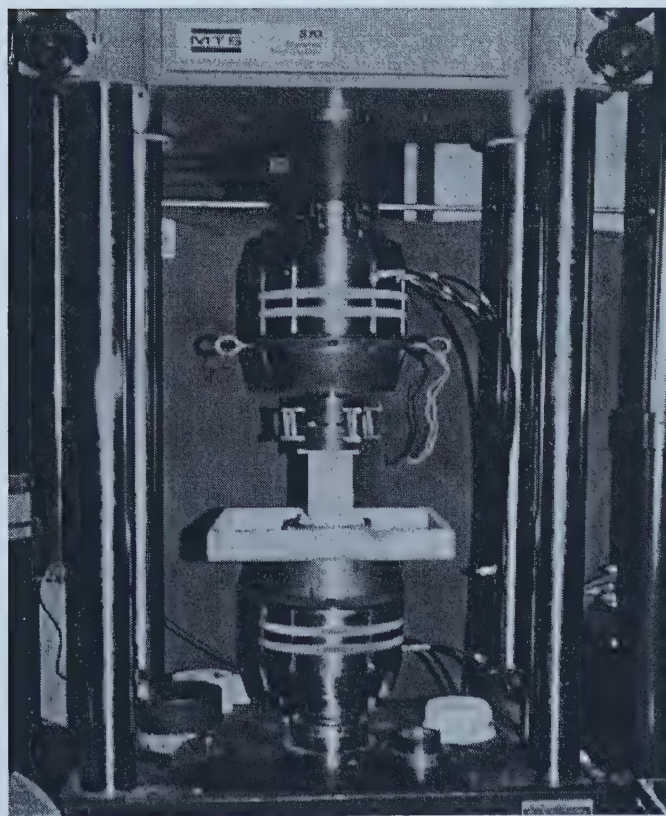


Figure 2.2 Testing of Grout Specimen in Compression

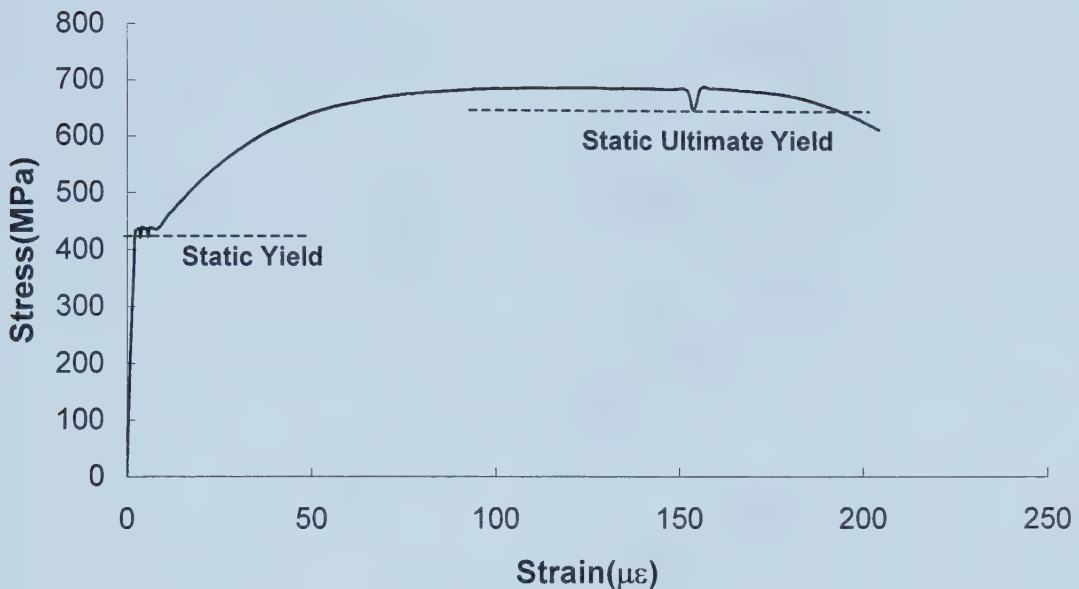


Figure 2.3 Typical Stress-Strain Plot of Steel Tension Test

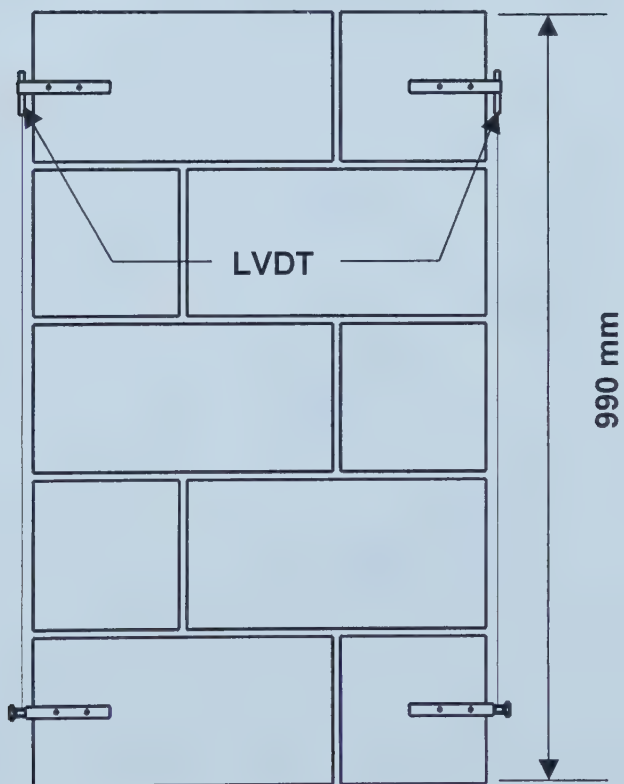


Figure 2.4 Location of LVDT's during Compression Testing of Prisms

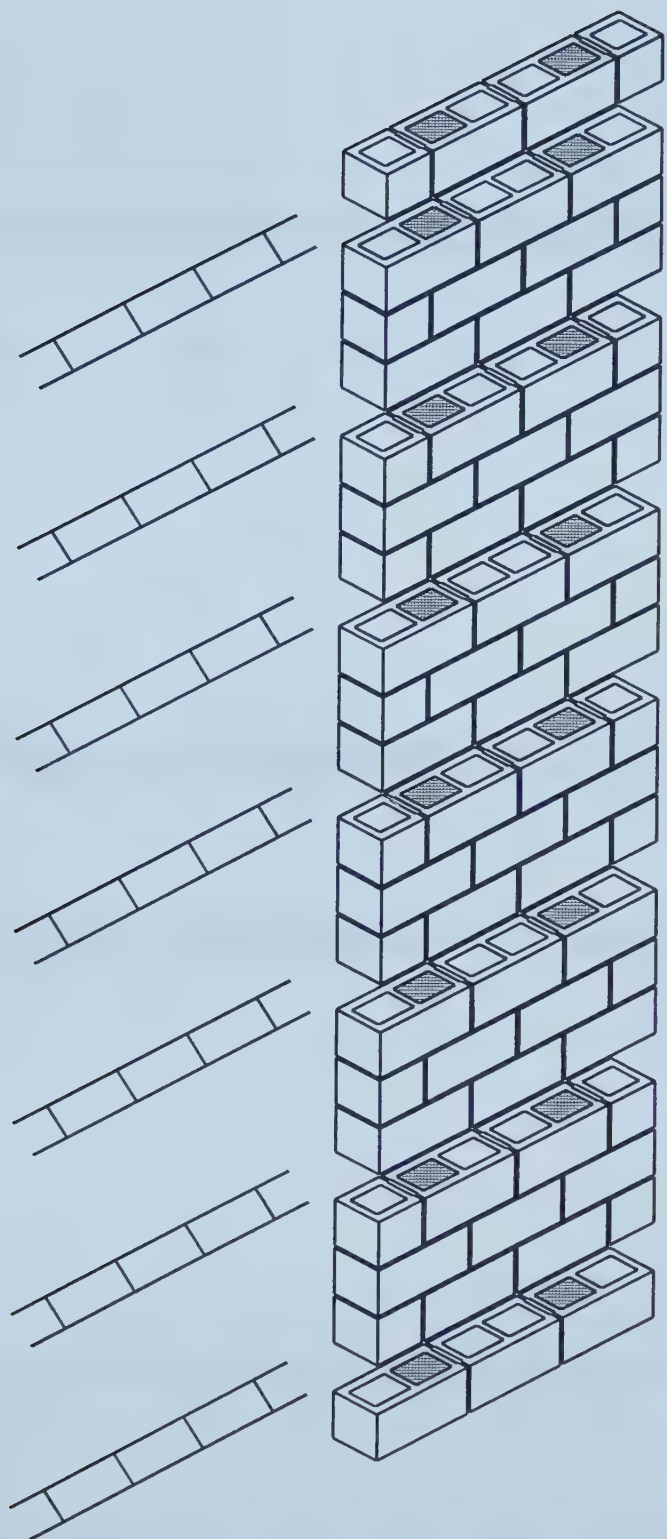
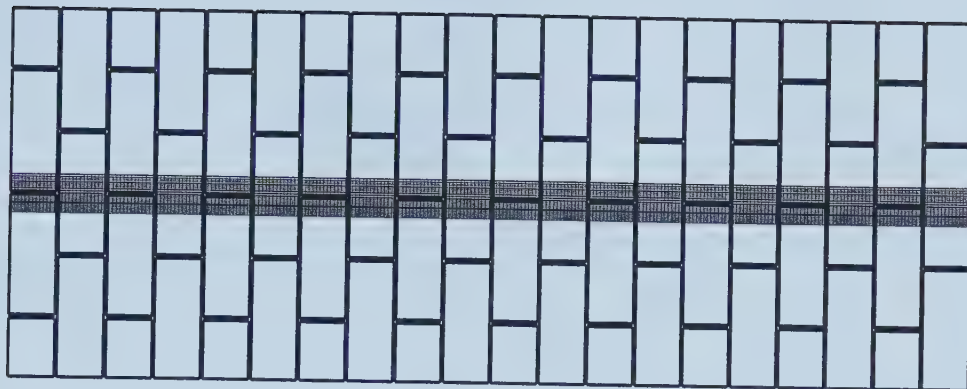
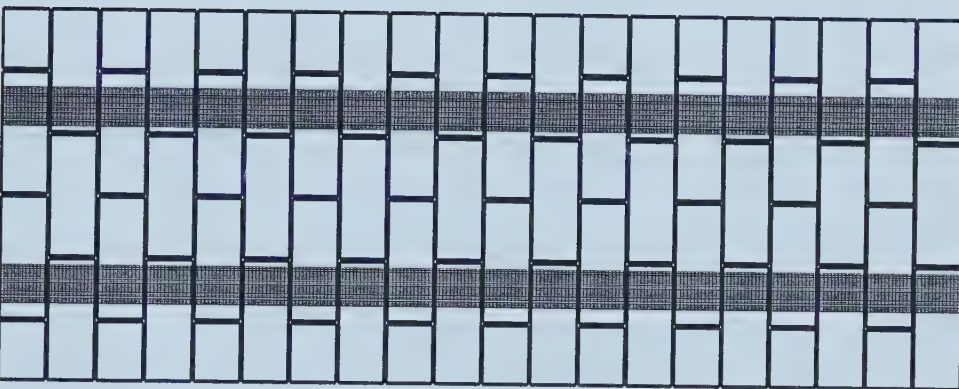


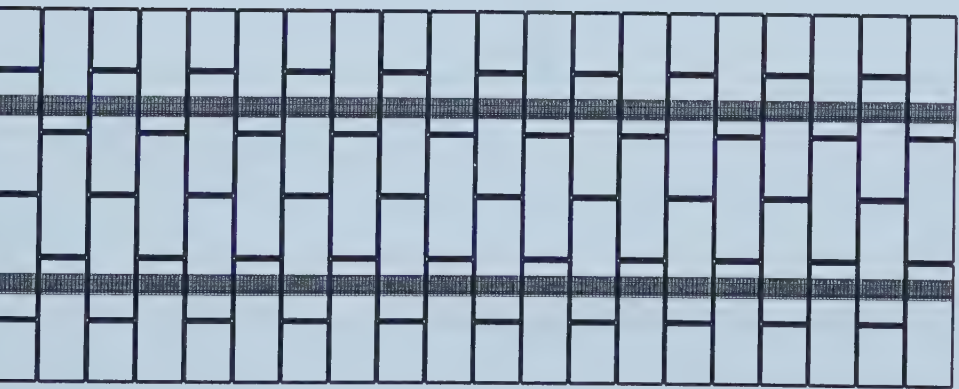
Figure 2.5 Location of Grouted Cores and Bed Joint Reinforcement



125 mm Strips @ Mid



125 mm Strips



65 mm Strips

Figure 2.6 Typical GFRP Layout Patterns

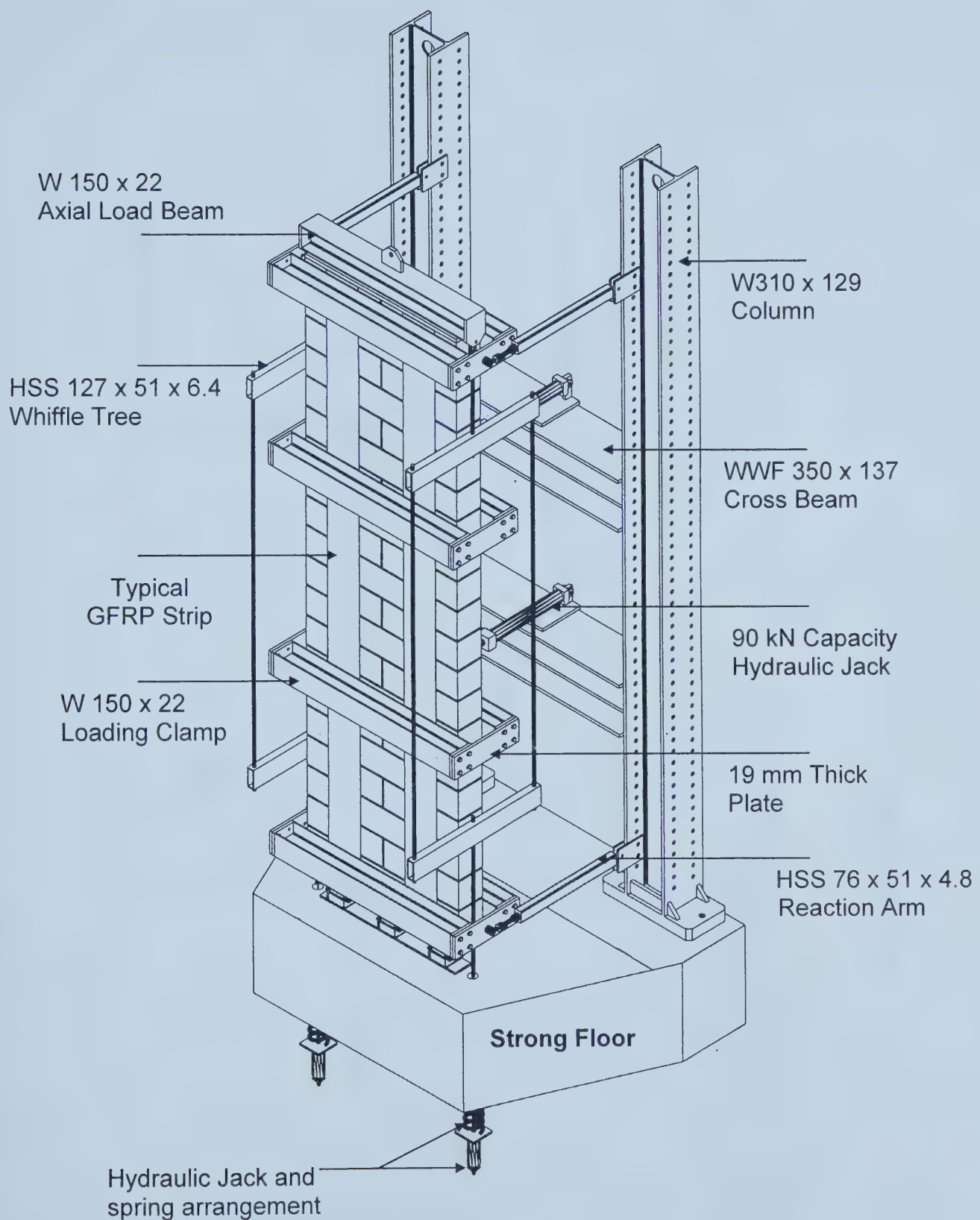
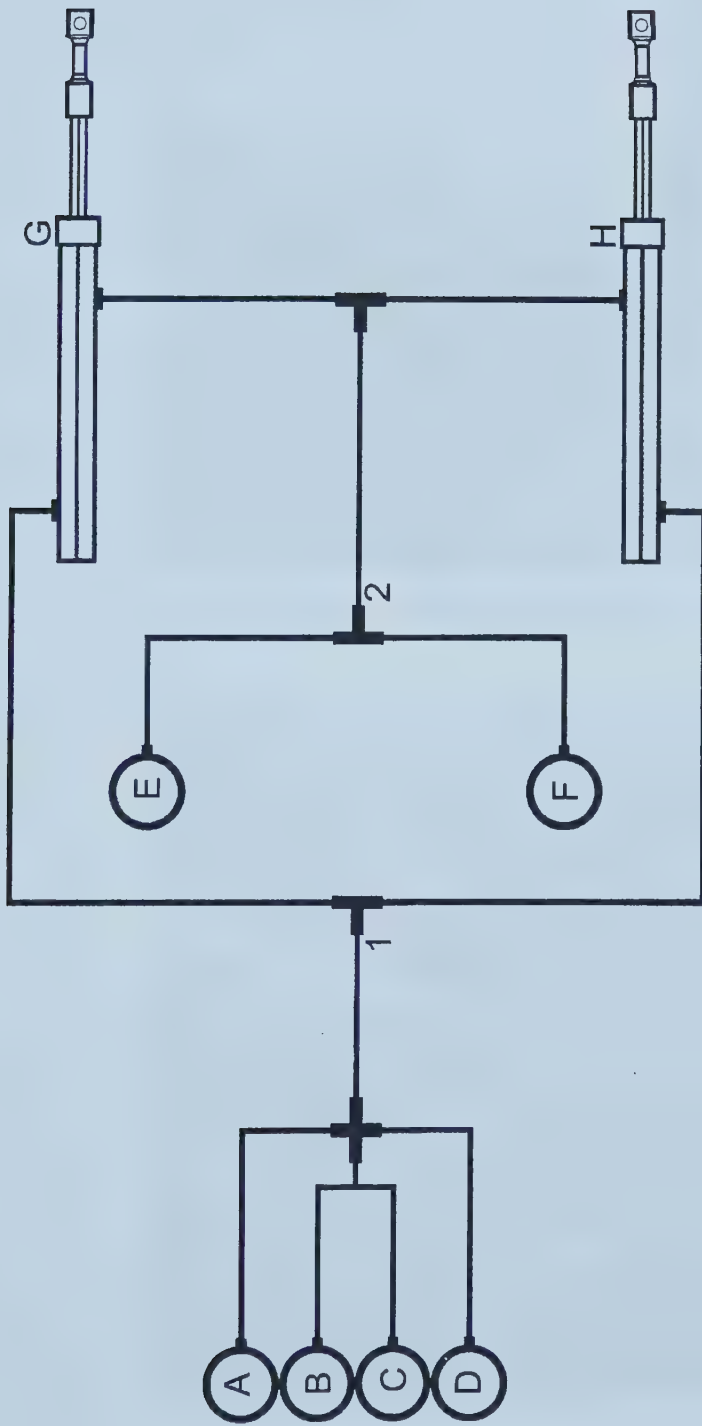


Figure 2.7 Modified Kuzik's Test Frame

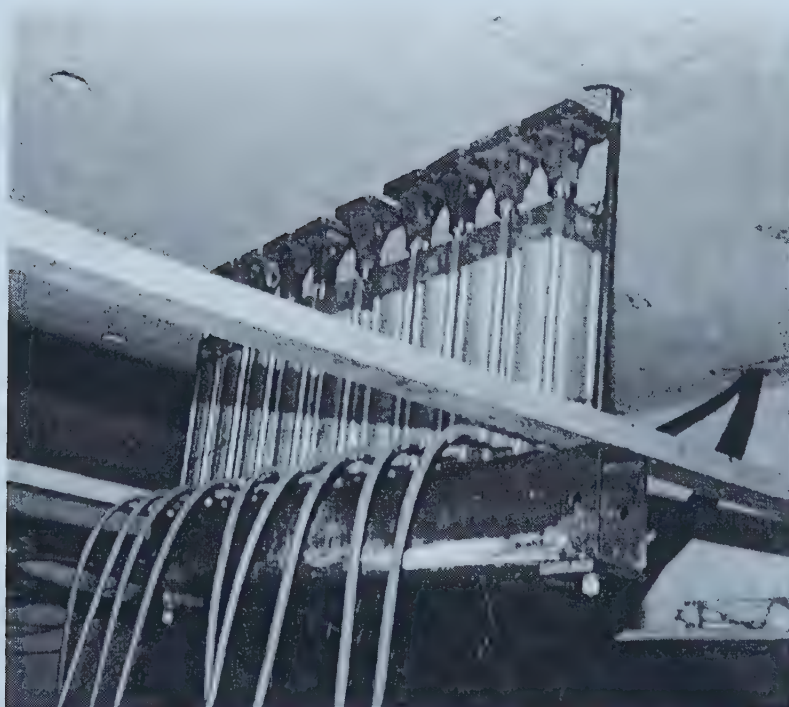


A, B, C, D \Rightarrow Hydraulic Jacks under Compression
 E, F \Rightarrow Hydraulic Jacks acting as Return Reservoirs
 G, H \Rightarrow Top and Bottom Hydraulic Jacks for Lateral Loads
 1, 2 \Rightarrow Hose connections to be switched

Figure 2.8 Alternate setup for Lateral Load



(a) Spring and Hydraulic Jack Arrangement



(b) Distributing Beam and Air Jacks

Figure 2.9 Two Different Arrangements used for Application of Axial Load

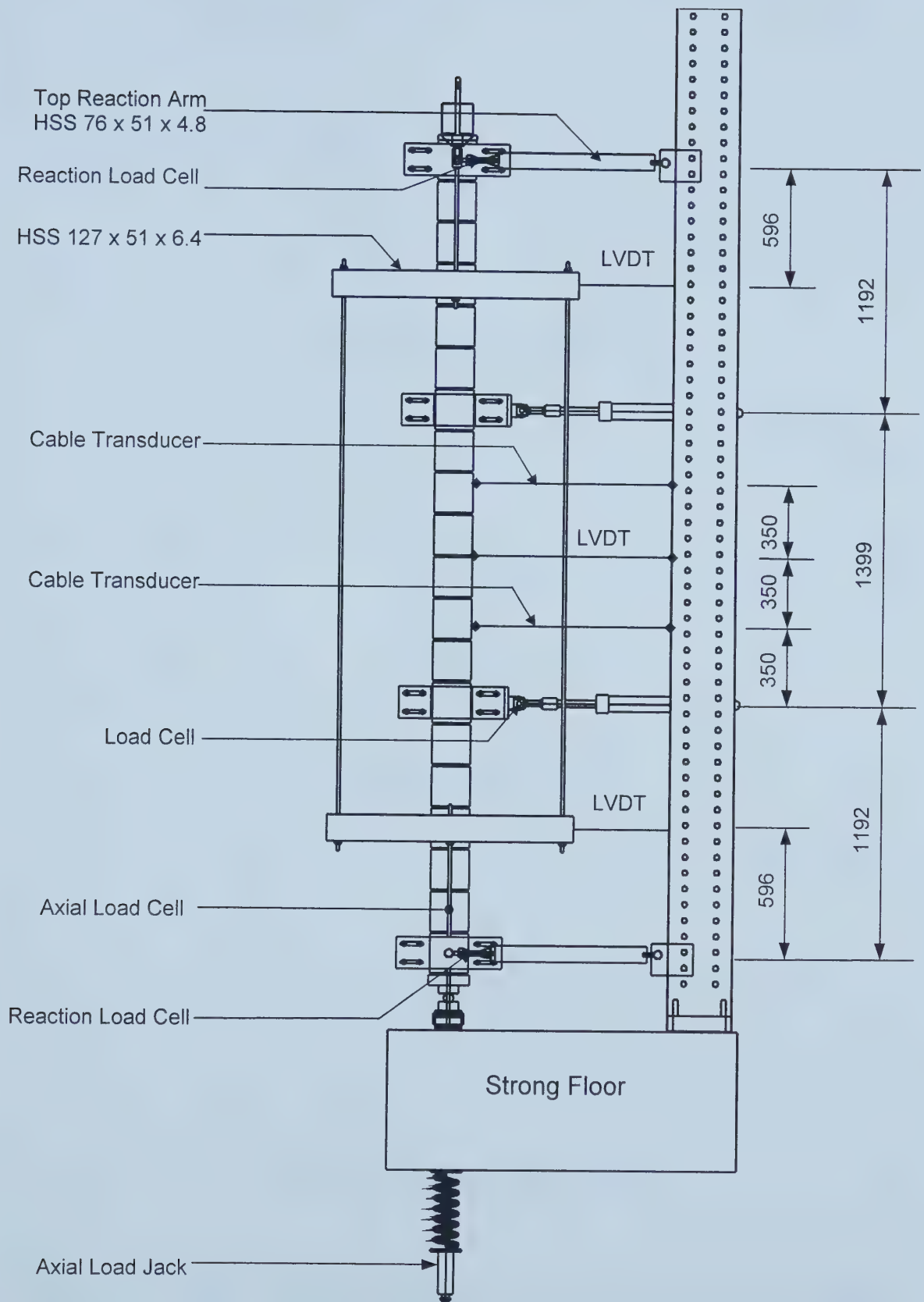
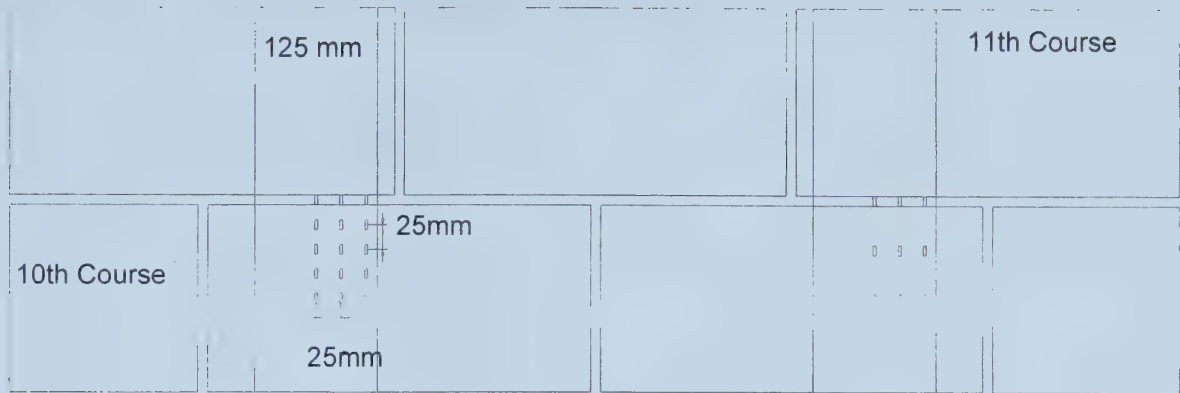
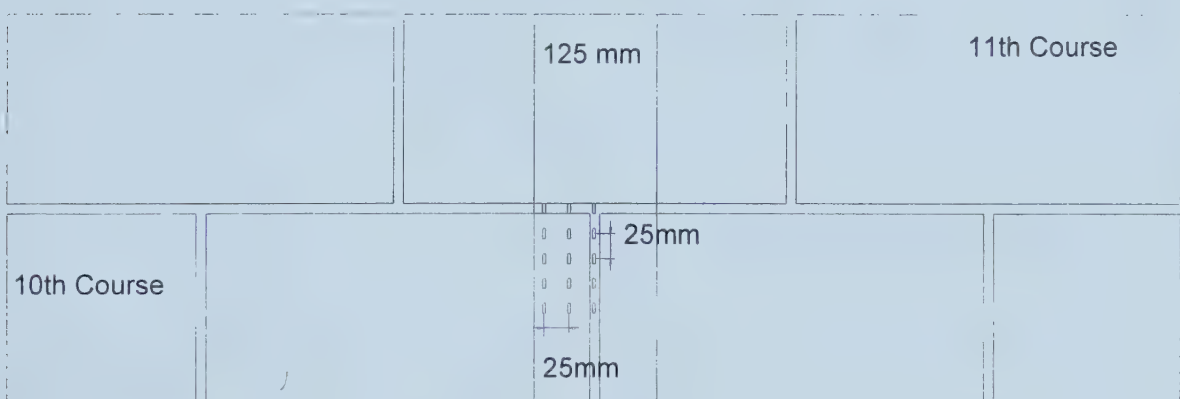


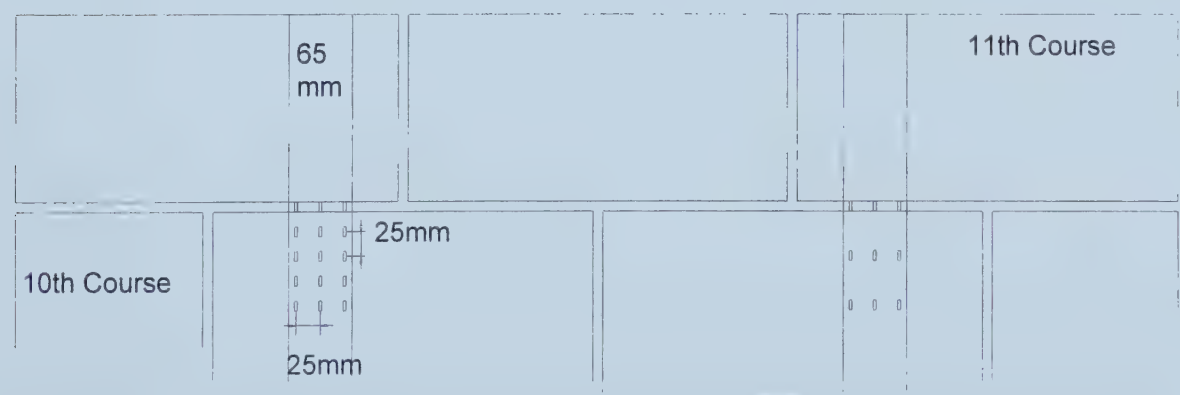
Figure 2.10 Instrumentation Layout



(a) Typical 125 mm GFRP Strip



(B) 125 mm GFRP at Mid



(C) Typical 65 mm GFRP Strip

Figure 2.11 Typical Location of Strain Gages at Various GFRP Layouts

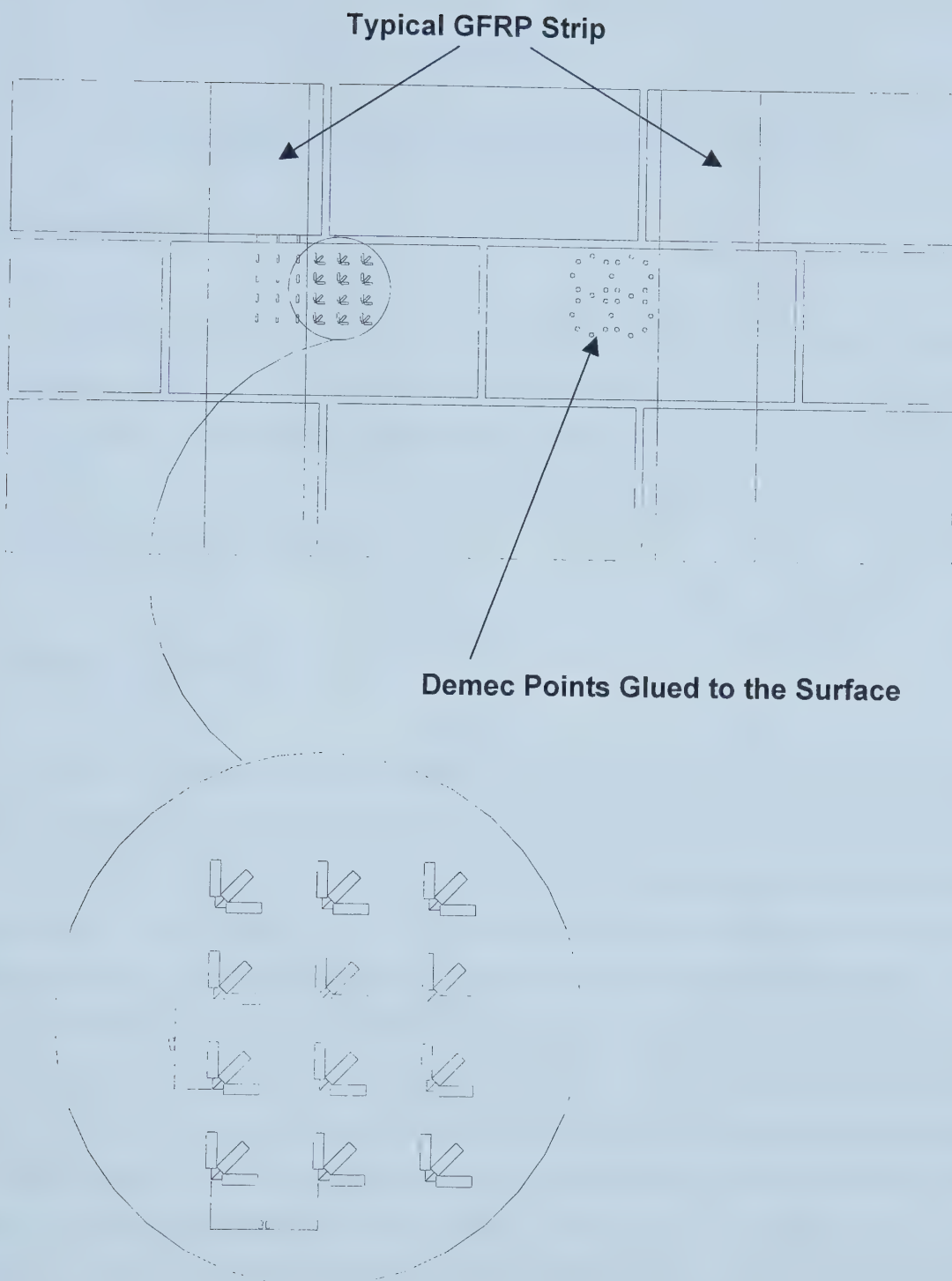


Figure 2.12 Strain Gage and Demec Points Pattern on Wall Surface

Chapter 3

TEST OBSERVATIONS AND DISCUSSION OF RESULTS

3.1 Introduction

This chapter describes the test procedure and the observations recorded during the test. In order to include the effect of axial load, mid-span deflection versus second order moment has been plotted instead of lateral load versus deflection. Plots showing variation of strain along and across the width of GFRP are presented. Photographs of the specimens at failure are presented.

3.2 Testing Procedure

The walls were constructed vertically and cured at various available spaces on the lab floor. Due to the intrinsic fragile nature of masonry, a slight out-of-plane load could cause cracks between the mortar and the blocks. To avoid any excessive stresses during transportation of the specimen into the load frame, a unique mechanism was used. As a first step, locations of the clamps along the height of the wall were marked using a felt pen. The (W150 x 22) axial load-distributing beam was then mounted on the top of the wall and high strength rods were connected to each end. Two specially fabricated adapter plates were then bolted on each side of the base plate. A turnbuckle was bolted with each of these adapter plates. The turnbuckle had left and right threads to accommodate elongation or shortening. Eyebolts were connected with each of the hanging rods using couplers. Finally, the eyebolts were joined with the turnbuckles using a bolt and cotter pin arrangement and were tightened. By using this mechanism, the specimen was subjected to some axial compression, thus permitting safe and uncracked transportation of the wall into the load frame. The wall was then ready to be lifted.

The bottommost clamp was leveled on the strong floor nearer to the load frame. The wall was then lifted using an overhead crane and slide along into the clamp. The clamp was then centered and finally constricted against the wall using the redi-rod arrangement. The other clamps were then positioned in a similar fashion. The wall was then lifted again using an overhead crane and positioned on the lower boundary steel plate. The reaction arms were then connected with the top and bottom clamps on each side. The hydraulic jacks were then connected with the clamps via yokes bolted to the clamps. Smaller rods then replaced eyebolts along with the longer rods on each side. The axial load apparatus consisted of two HSS 127 x 51 x 6.4(Whiffle Tree), joined together by two high strength threaded rods was connected with the smaller rods on each side using nuts and washers. Longer rods were connected to the bottom of the whiffle tree and inserted through holes in the lab strong floor. Finally, spring and hydraulic jack arrangement was mounted on these rods underneath the strong floor. Figure 2.9(a & b) shows the setup. The instrumentation described in Section 2.4.4 was then mounted and the wall was ready for testing. Figure 2.7 and 2.10 shows the complete setup.

After moving the specimen into the load frame, the bolts associated with the lateral load apparatus were adequately torqued. The instrumentation including strain gages, cable transducers and LVDT's were connected and checked. Before application of any load, the electronic instrumentation was allowed to warm up. First the axial load was applied gradually to the required level and an initial reading was taken. Secondly, the cyclic lateral load was applied at a rate of 1 mm per minute. For cyclic loading the real time plot of load versus mid-span deflection was carefully monitored and upon seeing a change in the slope of the curve, the loading was reversed. Loading rates up to 2 mm per minute have been used to load the specimen. Whereas, rates up to 6 mm have been used to unload the specimens. The specimens were subjected to three cycles at each maximum displacement level. Each subsequent displacement level was chosen as a multiple of the initial displacement. Once the specimen was failed in pulling or pushing, it was loaded in the opposite direction until failure occurred in that direction too. In the following discussion, failure is described as a load level where the lateral load dropped. Also the term cycle refers to a complete loading and unloading of specimen for a specific load.

The term “set” refers to a total of three cycles. Throughout the discussion the course elevation is referenced from the bottom of the wall. Various parameters and loadings associated with each specimen are summarized in Table 2.7.

3.3 Test Observations

3.3.1 Wall-1(200 mm)

The GFRP reinforcement for this wall consisted of 2-125 mm strips on one face only. The axial load applied was 30 kN. The moment versus mid-span deflection response is shown in Figure 3.1. The test was started by pushing the wall. Fine cracks at the interface of bed joints and masonry units were observed at a load of 15 kN in the constant moment region. Fine diagonal cracks were observed at a load of 23 kN at the elevation of the 9th and 10th courses. These cracks were accompanied by some horizontal cracks at the location of the 10th course. When the mid-span deflection of the wall reached 100 mm, it was realized that the horizontal clamps were actually pushing the vertical rods responsible for carrying axial load. The test was, therefore, stopped and a modification was made in the axial load setup. The modification in the axial load set-up consisted of the whiffle tree described in Section 2.4.3. The new set-up was capable of accommodating at least 250 mm of mid-span deflection, without running into the axial load carrying rods. This process postponed the test for approximately two weeks. The wall was then loaded again with the new setup in place and finally failed by delamination of the GFRP strips throughout most of the constant shear regions at the top and bottom of the wall. Figure 3.16 shows the failure of the specimen.

From the strain gages mounted on the GFRP strips a maximum of 1.8 % longitudinal tensile strain was measured. Figure 3.9 shows the load versus strain behavior for this specimen. Distribution of strain along the width of the fiber is shown in Figure 3.24.

3.3.2 Wall-2(200 mm)

The delamination failure observed at the top and bottom constant shear regions in the previous specimen is not desirable. In order to shift the failure to the flexural zone, the GFRP strips in Wall-2 were anchored at top and bottom. Bonding an extra 270 x 270 mm patch of GFRP on top and bottom of each GFRP strip provided the anchorage. The direction of the fibers in each patch was parallel to the bed joints. Moment versus mid-span deflection response for Wall-2 is shown in Figure 3.2.

This wall was reinforced externally with two 125 mm GFRP strips on one face. The axial load applied was 60 kN. A total of 15 strain gages were mounted on the GFRP strips. Test was started by pulling the wall. Cracking at the interface of bed joints and masonry units was observed at a load of 9 kN. These cracks started at the top and bottom of the 6th and 15th courses. At a load of 27 kN bed joint cracks were clearly visible in the constant moment region. Horizontal cracks were observed at a load of 30 kN in the middle of blocks located at 8th course. The cracks initiated from the edge of the GFRP strip and propagated towards the center of the wall. Diagonal cracks appeared at a load of 32 kN and propagated at an angle of 45 degrees towards the nearest bed joints. The GFRP strips started delaminating in the bottom constant shear region (6th course) at a load of 36 kN. At the same load, delamination also started at level of 12th and 13th course. A loud cracking sound accompanied the failure of the specimen by more delamination throughout the constant shear regions. A flexure shear crack was observed at an elevation of 15th course on the North side. Hence the failure can be categorized as delamination accompanied by flexure shear failure. Figure 3.17 shows more details related to the failure of the specimen.

From the gages located on the GFRP strip, a maximum longitudinal tensile strain of 1.4 % was measured. Figure 3.10 shows the plot of load versus strain for this specimen. Distribution of strain along the width of the fiber is shown in Figure 3.25.

3.3.3 Wall-3(200 mm)

After moving the wall into the load frame, the instrumentation was connected to the wall. During an adjustment of the lateral load apparatus, the top jack accidentally ran out of control and pierced through the wall at an elevation of 15th course. The damaged block was replaced with a half block using plaster of Paris instead of mortar. This postponed the test to the next day.

The wall was reinforced externally with Two 65 mm GFRP strips on each face. The axial load was 30 kN. A total of 24 strain gages were mounted on the GFRP strips with 15 gages mounted on the southeast strip and nine gages on the southwest strip. The test was started by pulling the wall. It was revealed that the signal conditioners were experiencing some noise from the Fluke data acquisition system. The test was stopped to adjust the problem. For the first set of cycles, a cyclic load of 12 kN (each jack) was applied. However, due to a malfunction in the load system, the hysteresis loop showed abrupt changes in stiffness (nonsymmetrical behavior) of the wall on different sides. The same level of mid-span deflection was achieved on the other side but at a lesser load (8.75 kN and 6.31 kN in the bottom and top jacks). Moment versus mid-span deflection hysteresis is shown in Figure 3.3. It was also noticed that the load in the top and bottom jack is more harmonized in pulling rather than pushing.

For the third set of cycles, lateral load of 35 kN was applied. At the peak of 1st loop, diagonal and horizontal cracks were observed. For the northeast strip, horizontal cracks at the middle of blocks appeared at the 8th, 9th, 10th and 12th courses. Whereas, on the southeast strip, horizontal cracks were observed at the elevation of 9th and 10th courses and diagonal cracks at the elevation of the 10th, 11th and 12th courses. During the last loop of the 3rd set of cycles, the horizontal cracks propagated towards the bottom of the course. Figure 3.18(a) shows the horizontal and diagonal cracks.

When the mid-span deflection reached 100 mm, the GFRP strips started delaminating in the constant moment region. The delamination was accompanied by a deep crack at both edges of the strip. For the last set of cycles, a load equal to 34 kN was applied leading to more delamination in the constant moment and constant shear regions. The penetration of cracks across the wall width in the constant moment region was measured as 82.6% of the total wall thickness. Figure 3.18(b) shows the cracking at the elevation of the 15th course and penetration of the crack. Finally the wall failed due to delamination of GFRP strips. Maximum mid-span deflection attained on the east face was 120 mm. The wall failed at a mid-span deflection of 130 mm to the west.

3.3.4 Wall-4 (200 mm)

Prior to the testing of Wall-4, the loading jacks were taken out from the load frame. The jacks were found deficient in oil. Oil was replaced and the jacks were mounted back into the load frame. In order to test the working condition of the jacks, Wall-4 was subjected to a series of small displacement tests. For each of these tests, cyclic load was applied to the wall to get a maximum deflection of 30 mm on each side. However, it was found that anomalies still existed in the jacks. Some irregularities in the servo valves were also found. The jacks were, therefore, sent for repair. Due to the time constraint, the second lateral load setup described in Section 2.4.2 was used.

This wall was externally reinforced with one 125 mm GFRP strip at mid-face on each face. The axial load applied was 30 kN. A total of 24 strain gages were mounted on the GFRP strips with 15 gages on the east face and nine gages on the west face. Moment versus deflection hysteresis response is shown in Figure 3.4. The test was started by pulling the wall, thus inducing tension on the east face. For the first set of cycles, the wall was pulled 36 mm of mid-span deflection. At the end of first cycle, fine cracks at the interface of mortar and blocks appeared. These cracks were associated with the 7th and 14th courses. For the second set of cycles, the wall was displaced 65 mm mid-span

deflection. At the start of second loop of second set of cycles, fine diagonal cracks emerged from the edges of the GFRP strips and propagated to join the bed joint cracks. For the third set of cycles, the wall was displaced 90 mm of mid-span deflection. At the end of the 1st loop of the 3rd set of cycles, horizontal cracks in the blocks in the constant moment region appeared. The test was stopped due to safety reasons. The test was resumed the next day and the wall was loaded to failure. The wall failed by delamination of the GFRP strips in the constant shear regions, along with severe cracking of blocks. This is shown in Figure 3.19. The wall failed at 119 mm of mid-span deflection to the east at a load of 25 kN. The wall was pushed back to the west and failed at mid-span deflection of 165 mm at a load of 32 kN.

From the strain gages mounted on the GFRP strips on both faces, a maximum of 1.5 % longitudinal tensile strain was measured. Figure 3.11 shows the plot of load versus strain. Distribution of strain along the width of the fiber is shown in Figure 3.26.

3.3.5 Wall-5(150 mm)

This specimen was reinforced externally with two 125 mm GFRP strips on one face only. Extra patches of GFRP (270 mm x 270 mm) were bonded at the top and bottom of each GFRP strip to provide an extra anchorage. The constant axial load applied was 30 kN. The moment versus mid-span deflection response is shown in Figure 3.5. A total of 24 strain gages were mounted on the GFRP strips with 15 gages on the southeast strip and nine gages on the northeast strip. The test started by pulling the specimen with GFRP strips located on the tension side. Debonding of bed joints from the adjacent masonry units in the constant moment region was observed at a lateral load of 10 kN. Fine horizontal cracks in blocks of 8th course were observed at a load of 17 kN. The cracks started from the edge of the GFRP strip and propagated horizontally in the opposite direction. Similar cracks were observed at the mid of the 6th, 11th and 12th courses at a load of 19 kN. Immediately after horizontal cracks appeared, diagonal cracks

also appeared in 11th and 13th course. At the same load, penetration of the debonding cracks across the wall width was measured approximately at 75% of the total wall thickness. Accidentally the emergency stop button of MTS testing machine was pressed and the specimen got unloaded. The wall was reloaded again and the test was continued until it reached a mid-span deflection of 180 mm. This was the maximum deflection attained so far in the load frame. The test was stopped for safety reasons, and postponed to the next day. However, at this stage, chunks of mortar fell off from the compression side in the constant moment region.

The test was started the next day with some safety arrangements in place. The failure was initiated by the delamination of GFRP strips in the constant shear regions. The failure was supplemented by a flexure shear failure at the 15th course on South side. Figure 3.20(a) shows the delamination of GFRP strips and Figure 3.20(b) shows the flexure shear crack at failure of the specimen. The shear crack split the block into two pieces and upon removal of these pieces it was observed that the adjacent grouted core was also severely cracked. Delamination of the GFRP strips might have initiated because of the flexure shear cracking in the block and grouted core. No tensile failure in the GFRP was observed. The ultimate load and mid-span deflection at failure were 32 kN and 235 mm respectively. Overall response of the specimen can be categorized as tri-linear as shown in Figure 3.5.

As mentioned earlier, longitudinal strains were measured by mounting foil strain gages on the GFRP strips. A maximum longitudinal tensile strain of 2.26 % was measured in a gage mounted on GFRP located at a joint. Figure 3.12 shows load versus strain for this specimen. From the figure it is clear that gages at joints have higher strain as compared to the gages on block. Figure 3.27 shows the distribution of strain along the width of the fiber. The stains increased linearly (assumption) from the edge of the wall and dropped to the original value near the center of the strip.

3.3.6 Wall-6(150 mm)

This wall was reinforced externally with 2-125 mm GFRP strips on each face with an extra anchorage at top and bottom on each side. The axial load level was 15 kN. The wall was tested only for three sets of displacements of 35 mm, 75 mm and 150 mm respectively. Unlike other walls, the wall was subjected to one cycle at each of these displacements. Moment versus mid-span deflection hysteresis response is shown in Figure 3.6. The specimen was loaded on the east face with a mid-span displacement of 150 mm and a load equal to 27 kN. On the other face, specimen was loaded to mid-span deflection of 140 mm with a load equal to 24 kN. The specimen was not loaded to failure.

From the gages mounted on the GFRP strips a maximum of 1 % longitudinal tensile strain was measured. Figure 3.13 shows the load versus strain plot for this specimen. Distribution of strain across the width of GFRP strip is shown in Figure 3.28.

3.3.7 Wall-7(150 mm)

This specimen was reinforced externally with 2-65 mm GFRP strips on one face only. The selection of 65 mm strips was decided after failure of wall-5 and wall-6 due to delamination of the GFRP in the constant shear regions. The axial load applied was 30 kN. A total of 24 strain gages were mounted on the GFRP strips with 15 on the northwest strip and 9 on the southwest strip. The moment versus mid-span deflection response is shown in figure 3.7. Pushing the wall, thus inducing tension on the west face, started the test. When the mid-span deflection reached 12 mm, a discrepancy was observed in the loading rate. The wall was unloaded and the rate was adjusted. The test was started again by pushing the wall. At a load of 10 kN, hairline cracks appeared at the interface of bed joints and masonry units in the constant moment region. No significant difference was observed except the widening of cracks till a load of 11.3 kN was reached. Small diagonal cracks were observed in the constant moment region at a load of 13.5 kN. Like

other tests, the cracks initiated from the edge of the strip and propagated towards the bed joints at approximately 45° . Horizontal cracks at the mid of blocks at 10th and 13th course were observed at a load of 14 kN. After reaching mid-span deflection of 70 mm and lateral load of 14 kN, the behavior of the wall became very ductile. Mid-span deflection increased without any considerable increase in the lateral load. At a mid-span deflection of 165 mm, a popping sound was heard with start of delamination of GFRP at the top of 9th course on the northwest strip and 10th course on the southwest strip in the constant moment region. Finally tension failure occurred due to sudden rupture of the northwest strip in the constant moment region. Figure 3.21(a) shows the rupture of GFRP. Though the loading was stopped at this stage, minor increase in deflection of the wall was still observed. This lead to a partial rupture of the southwest strip in the constant moment region. Figure 3.21(b) shows the partial rupture of GFRP strip and cracking of masonry units.

Moment versus mid-span deflection response for Wall-7 as shown in Figure 3.7 shows a trilinear behavior. A maximum of 2.4 % longitudinal tensile strain was measured at rupture of GFRP. Figure 3.14 shows the load versus strain plot for this specimen. The strain was measured by a gage located on the GFRP at a joint. Figure 3.29 shows the distribution of strain across the width of fiber.

3.3.8 Wall-8(150 mm)

This specimen was externally reinforced with two 65 mm GFRP on each face. The axial load was equal to 15 kN. A total of 33 strain gages were mounted on the GFRP strips with 24 gages on the east face and 9 gages on the west face. Out of 24 gages on the east face, 15 gages were mounted on the southeast strip and nine gages on the northeast strip. During application of the GFRP strips and while applying hand pressure to the impregnated GFRP against the surface of the wall, an imperfection occurred. This imperfection described by ISIS-M05-00 is called *Waviness*. In a localized region of

southwest GFRP strip, the fibers deviate from the general straight-fiber line in the form of kinks. The length of this localized region was approximately 60 mm. Moment versus mid-span deflection hysteresis response for this specimen is shown in Figure 3.8.

Testing was started by pulling the wall, thus inducing tension on the east face of the wall. At the end of 1st set of cycles (12 mm mid-span deflection), fine cracks appeared at the interface of bed joints and masonry units in the constant moment region. For the second set of cycles the wall was pushed to a maximum of 25 mm. At the start of 3rd set of cycles with tension on east face, fine horizontal cracks at mid of the blocks emerged from the edge of the GFRP strip at elevation of 11th and 12th course. At the start of third set of cycles some cracks were observed on the west face in the constant moment region. Whereas, at the same load, numerous bed joint and diagonal cracks were observed on the east face. At load equal to 16 kN with mid-span deflection of 100 mm the LVDTs ran out of travel and the wall was unloaded for adjustment of instruments. This postponed the test to next day. Test was started next day by pulling the wall. At a load of 15 kN and mid-span deflection of 94 mm, the southwest GFRP strip failed in tension exactly at the location of waviness. Figure 3.22(a) shows the failure in the southwest strip. The test was therefore restricted to end at this cycle and the wall was pulled till failure on the east face. At a load of 18 kN with mid-span deflection of 170 mm, southeast strip started delaminating in the constant moment region. At this stage it was anticipated that a tension failure would occur in the constant moment region. However, the wall failed due to delamination of the southeast GFRP strip in the top constant shear and constant moment region (See Figures 3.22 and 3.23). Also the northeast strip got ruptured in the constant shear region at an elevation of 14th course. Figure 3.22(b) shows the rupture of northeast GFRP strip.

Strain versus load response for wall-8 is shown in Figure 3.15. Maximum 1.5 % longitudinal tensile strain was measured through strain gages on GFRP strips. Figure 3.30 shows the distribution of strain across the width of GFRP.

3.4.1 General Behavior of the Specimens

The general behavior of the tested specimens can be described as ductile. The cracks started at the interface of bed joints and units and with the increase in load widened, especially in the constant moment region. However, the GFRP strips restrained the horizontal bed joint cracks from opening extensively up to a certain load level. Diagonal cracks emerged from the edges of the bonded GFRP strips and propagated toward the nearest bed joint. Crushing and spalling of mortar joints on the compression face were observed at high mid-span deflections. Crack spacing and pattern remained identical for both series of walls (150 mm and 200 mm thick) with various widths of GFRP strips. Delamination of GFRP was observed mostly in the constant shear region indicating a weak zone between masonry and GFRP. However, it was observed in many cases that the delaminated GFRP strip sheared off a considerable portion of the face shell with it, thus indicating a good bond between masonry and the GFRP.

3.4.1 Moment versus Mid-Span Deflection Response

The load deflection response associated with the walls subjected to monotonic loading is quite similar. The response is a straight line up to the cracking and then a gradual decrease in stiffness is observed. For the specimens subjected to cyclic loading the stiffness reduced considerably after each cycle leading to a stiffness degradation response. The 150 mm walls showed greater inelastic deformations as compared to the 200 mm walls. Figure 3.8(a) shows the superimposed results for typical 150 mm walls. The cyclic response of Wall-6 as shown in Figure 3.8(a) is well below that of Wall-5 which is likely because of variability in the construction of 150 mm walls and do not because of delamination in the cyclic behavior.

3.4.2 Load versus Strain Response

Load versus strain response has been plotted for each of the specimen. Being a flexible sheet, the GFRP strips showed negligible strength in compression. However, in tension the response is similar to the moment versus deflection plots. Figure 3.9 to 3.15 shows this response. In order to study the propagation of strain along and across the GFRP strip, distance versus strain graphs are plotted through Figures 3.24 to 3.30(b). From the plots, no specific trend is obtained related to the propagation of strain across or along the GFRP strip. Typical response can be categorized as linear, thus showing uniform strains across the width of the GFRP strip. Width of GFRP strips wider than the ones used, might give some different trend.

3.4.3 Modes of Failure

As mentioned earlier, two series of walls were tested. First series consisted of four 200 mm thick walls and the second series consisted of four 150 mm thick walls. As already explained in Section 2.4.1, the lateral load was transferred to the specimen via two rigid steel clamps. At large deflections, extensive damage of the face shells was observed in the masonry units adjacent to the edges of these clamps. This mechanism might had occurred due to two main reasons. Firstly due to the nature of the loading system where the specimens were restrained laterally at the supports with only rotation allowed. Secondly, due to the concentration of stresses due to axial and lateral loads in the deformed configuration of the specimen. Prior to failure the specimen acted like a two hinged arch with the hinges located at the points of application of lateral load. This permitted no further increase in load in the constant moment region but an increase in deflection. In eight specimens tested, three different modes of failure were observed.

(1) *Delamination of the GFRP Strips in the Constant Shear Regions*

This mode of failure was observed in Wall-1, Wall-3 and Wall-4. Though GFRP strips in several specimens were anchored at top and bottom, the strategy didn't work effectively. However, provision of this extra anchorage helped slippage and buckling out of GFRP strips. Slippage of GFRP strips is shown in Figure 3.16(b). This failure mode can be further divided into two different mechanisms. First mechanism of failure comprised of peeling-off of the GFRP strip at the masonry-GFRP interface. This resulted in a smooth surface under the peeled off strip. In the second type, the failure was comprised of delamination of some portion of the face shell. However, in most of the cases the delamination of the GFRP strip was accompanied by peeling off of a considerable portion of face shell. For simplicity, a single type was assigned to both mechanisms of failure.

(2) *Delamination of GFRP strips in the constant shear regions accompanied by flexure-shear failure*

This mode of failure was observed in Wall-2 and Wall-5. The flexure-shear cracks were accompanied by high mid-span deflection and debonding at the interface of bed joints and masonry units. Delamination as in the first mode of failure was observed in the constant shear regions at top and bottom of the specimen. Albert *et al.* (1998) and Kuzik *et al.* (1999) have reported the same mode of failure. Figure 3.17(b) and 3.20(b) shows the flexure-shear failure for Wall-2 and Wall-5 respectively.

(3) *Rupture of GFRP strips in the constant moment and constant shear regions*

This mode of failure was observed in Wall-7 and Wall-8. Both specimens were reinforced externally with 65 mm GFRP strips. Figures 3-21 and 3-22 show the rupture of GFRP strips. It can be seen clearly in Figure 3-21 that the GFRP strips took off some portion of the face shell with it. Hence, the failure didn't occur due to lack of epoxy bond strength between masonry and GFRP. Loud cracking and excessive mid-span deflection accompanied rupture of GFRP strips. This mode of failure can be categorized as a brittle failure as the rupture of the GFRP strips was sudden and without any significant warning. As mentioned earlier, due to excessive deflection the final deflected shape of the specimens resembled the bending moment diagram of a beam subjected to a two point loading at equal distance from the supports. This caused severe damage to the specimens at the location of maximum shear and moment and led to rupture of GFRP strips in the constant shear region.

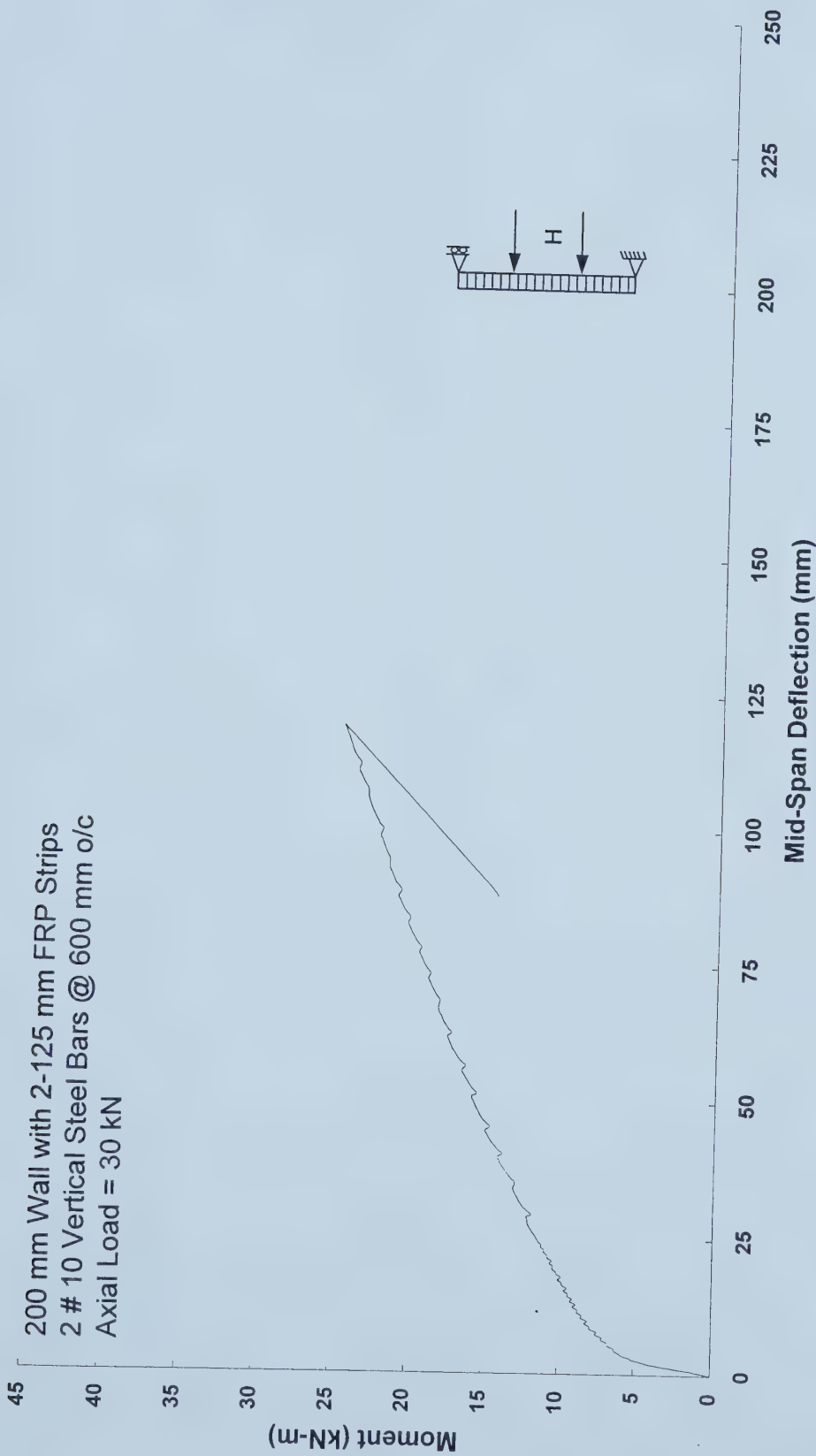


Figure 3.1 Moment versus Deflection Response for Wall-1

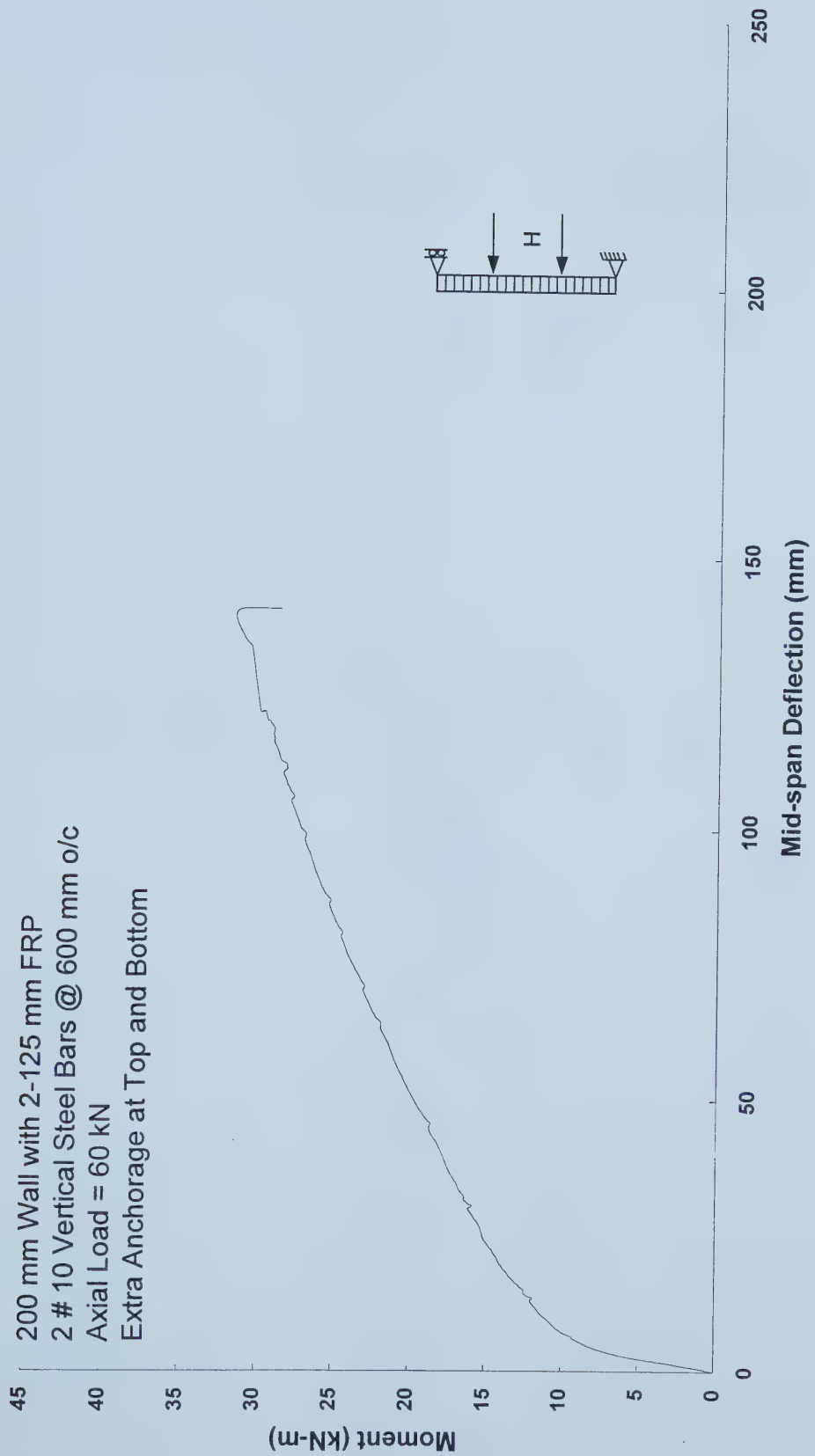


Figure 3.2 Moment versus Deflection Response for Wall-2

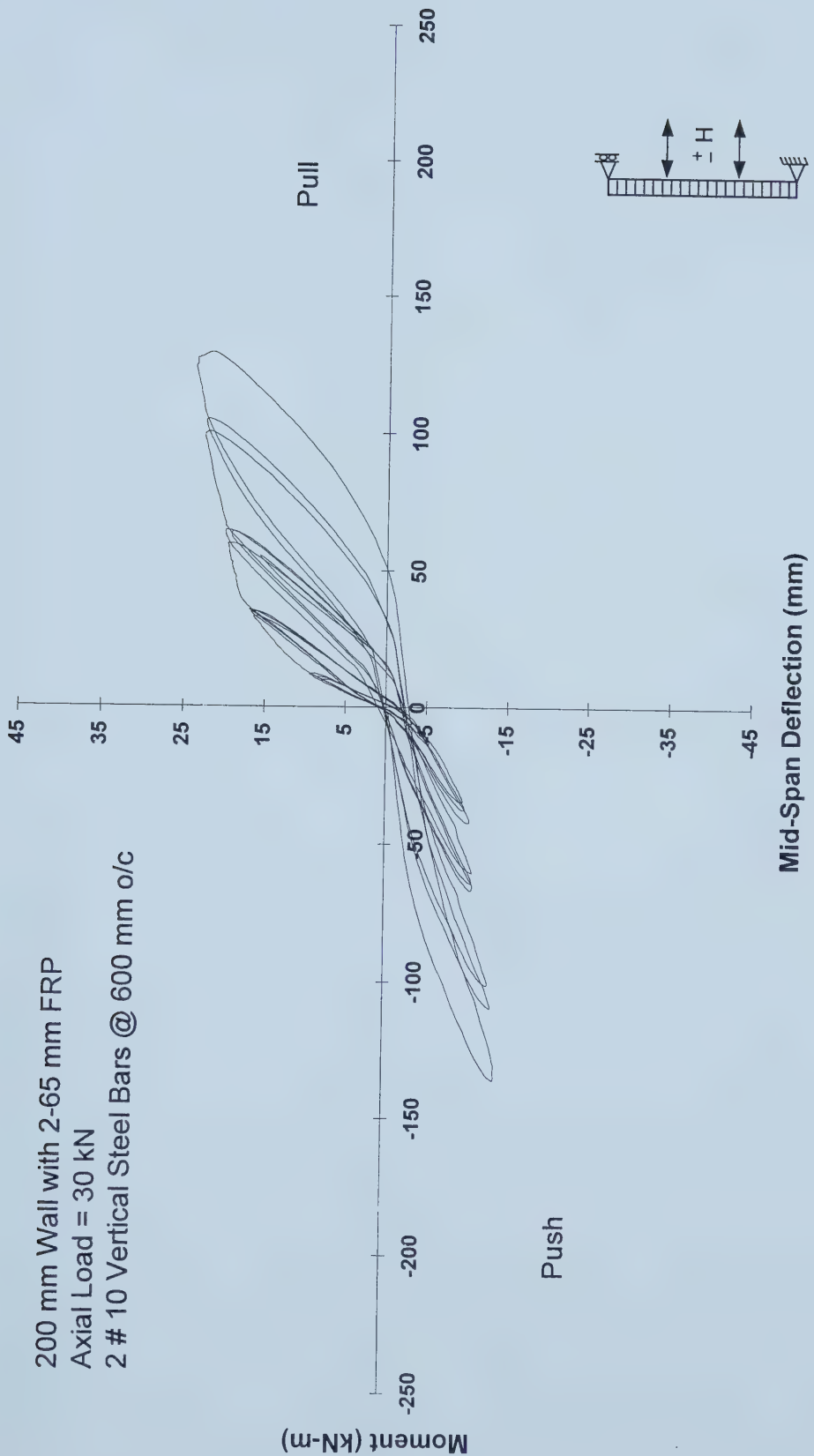


Figure 3.3 Moment versus Deflection Hysteresis for Wall-3

200 mm Wall with 1-125 mm FRP @ Mid
2 # 10 Vertical Steel Bars @ 600 mm o/c
Axial Load = 30 kN

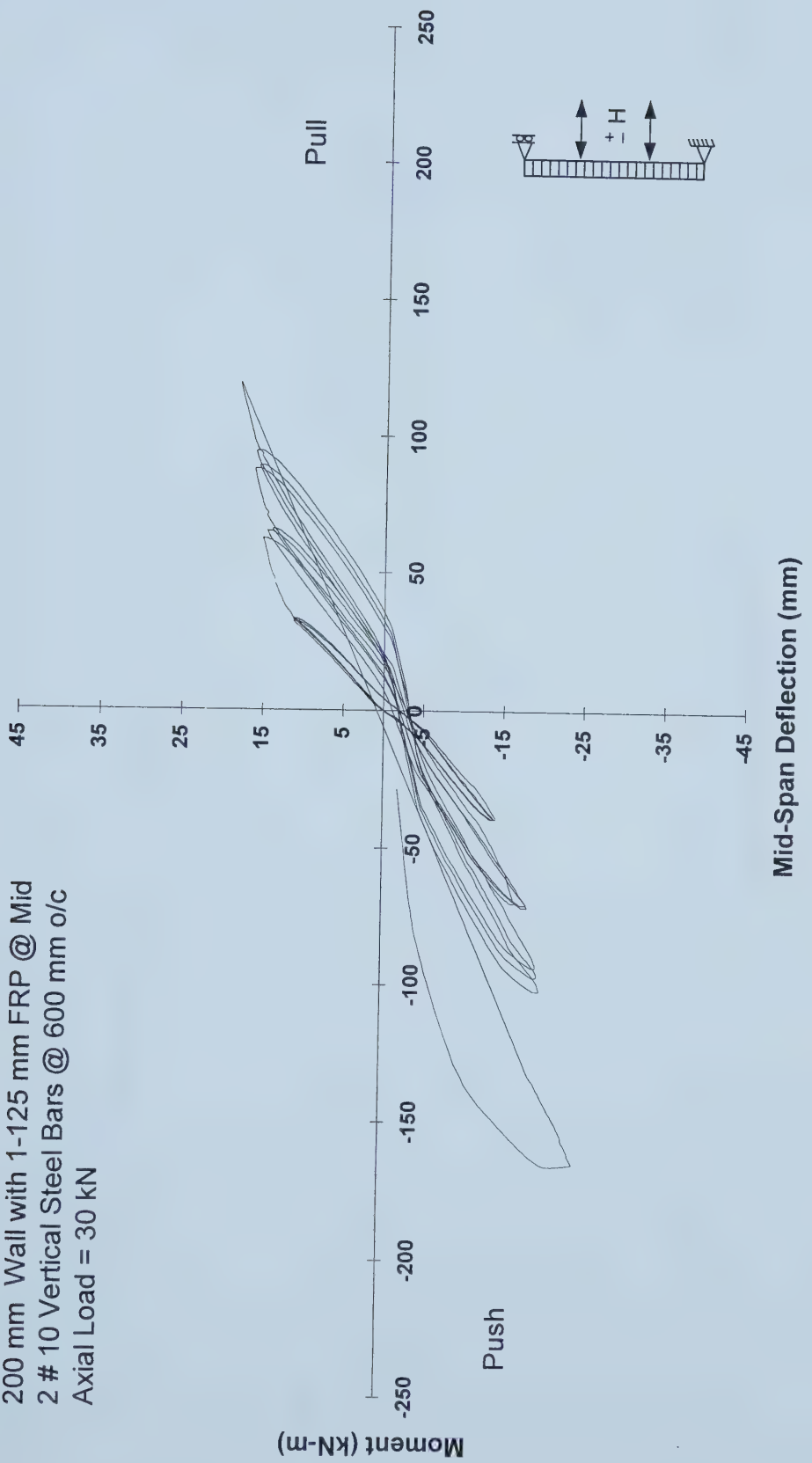


Figure 3.4 Moment versus Deflection Hysteresis for Wall-4

150 mm Wall with 2-125 mm FRP Strips
2 # 10 Vertical Steel Bars @ 600 mm o/c
Axial Load = 30 kN
Extra Anchorage of FRP Strips at Top and Bottom

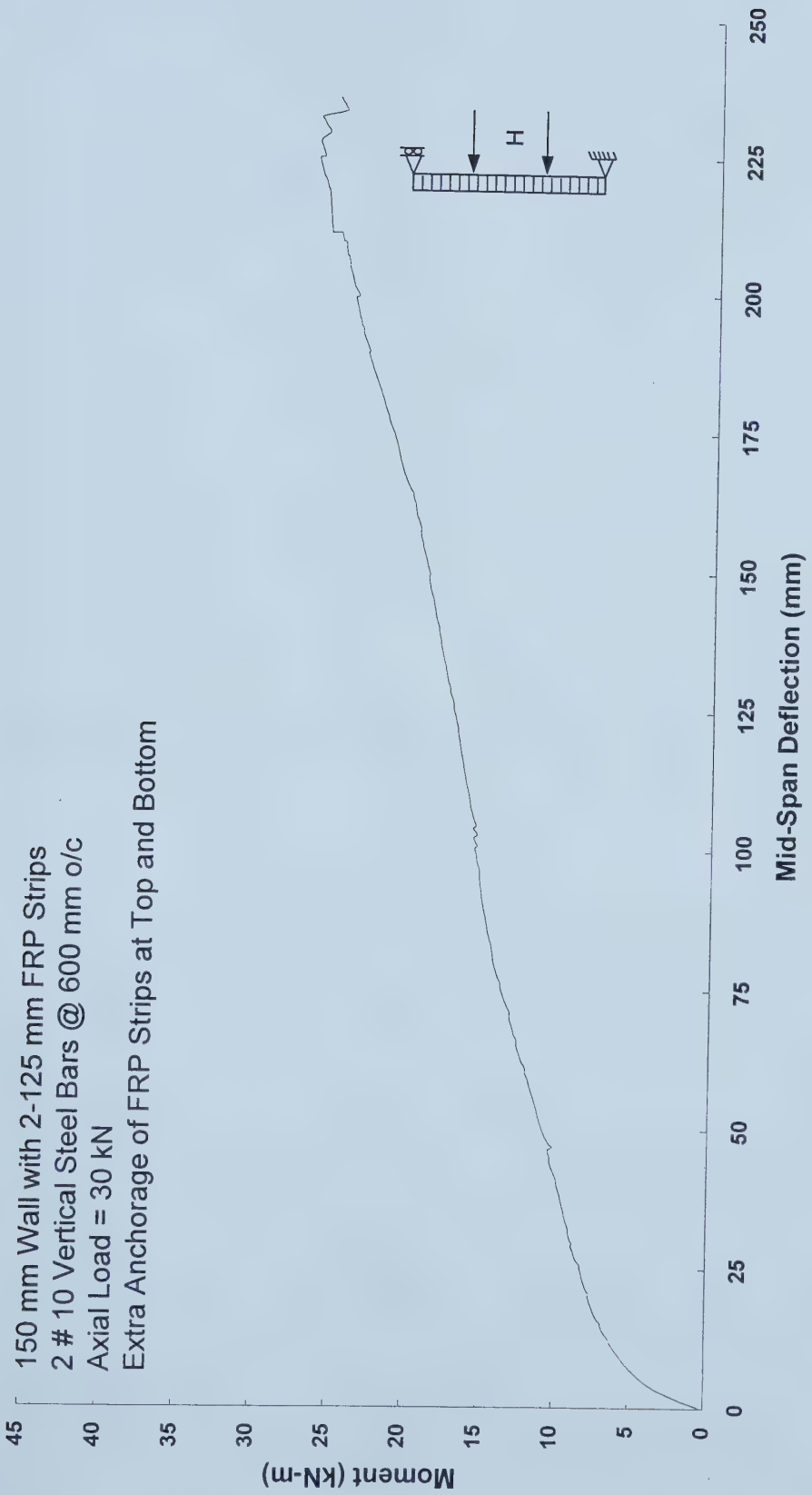


Figure 3.5 Load versus Moment Response for Wall-5

150 mm Wall with 2-125 mm FRP
2 # 10 Vertical Steel Bars @ 600 mm o/c
Axial Load = 15 kN
Extra Anchorage at Top and Bottom

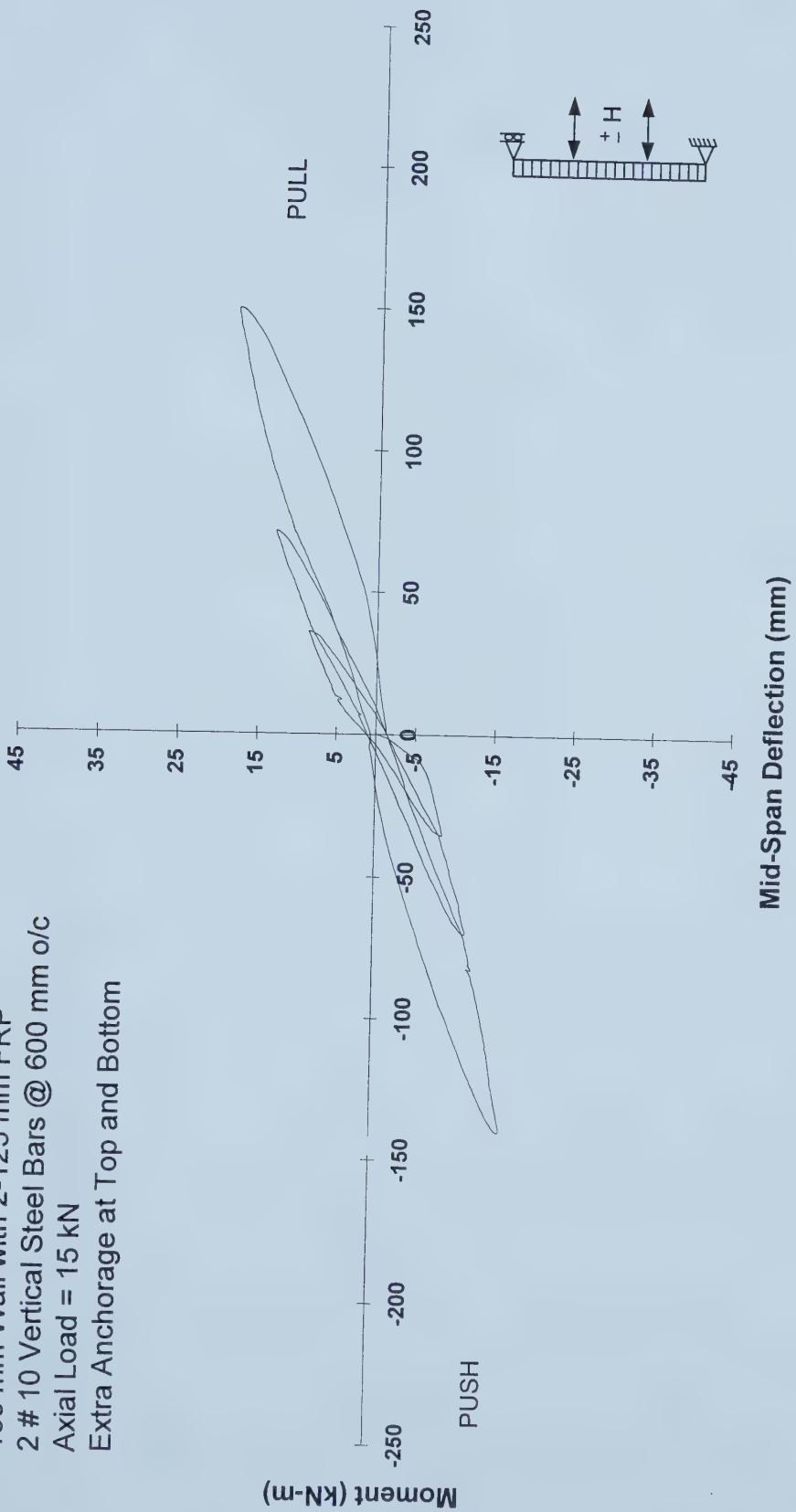


Figure 3.6 Moment versus Deflection Hysteresis for Wall-6

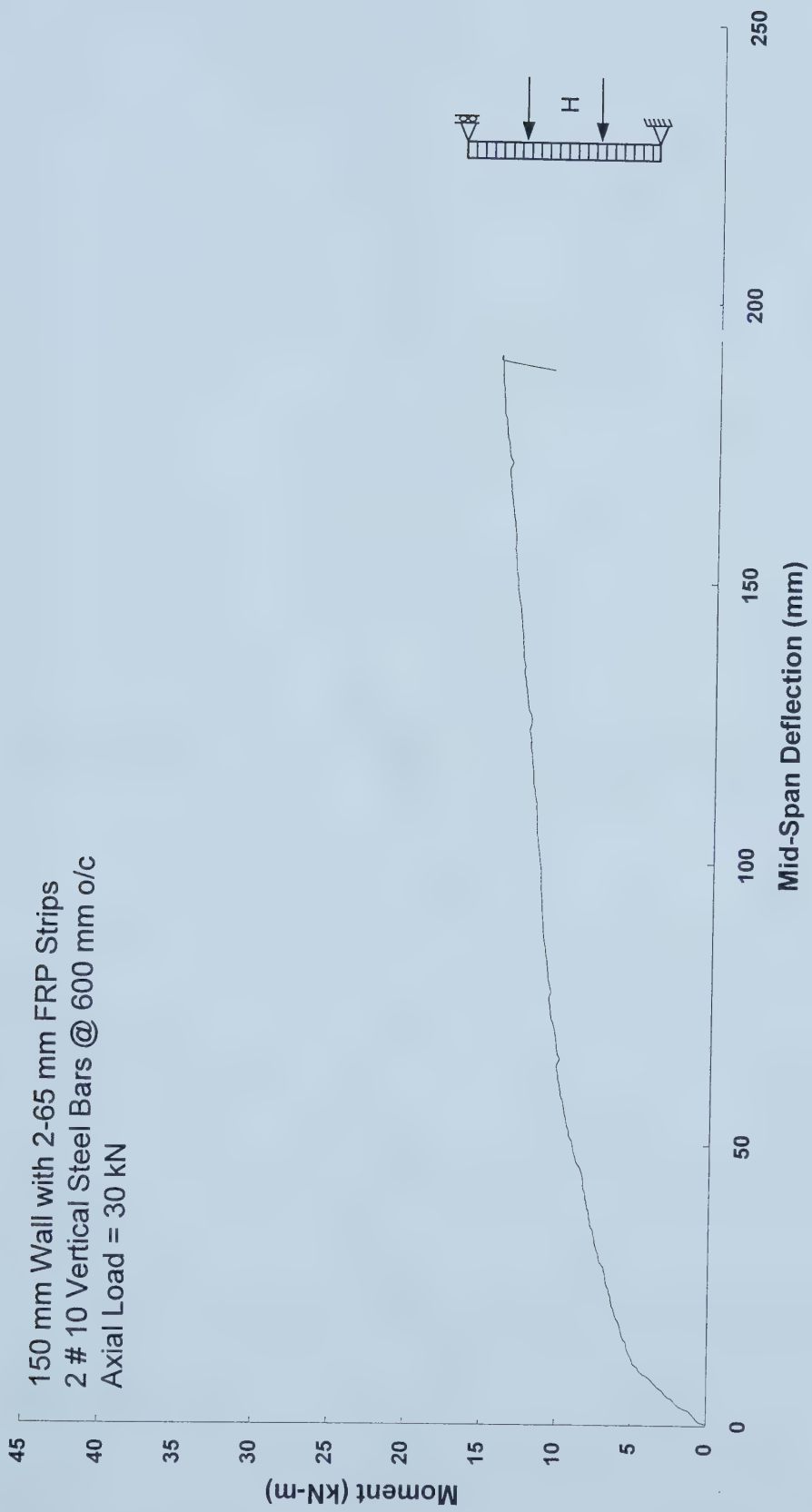


Figure 3.7 Moment versus Deflection Hysteresis for Wall-7

150 mm Wall with 2-65 mm FRP Strips
2 # 10 Vertical Steel Bars @ 600 mm o/c
Axial Load = 15 kN

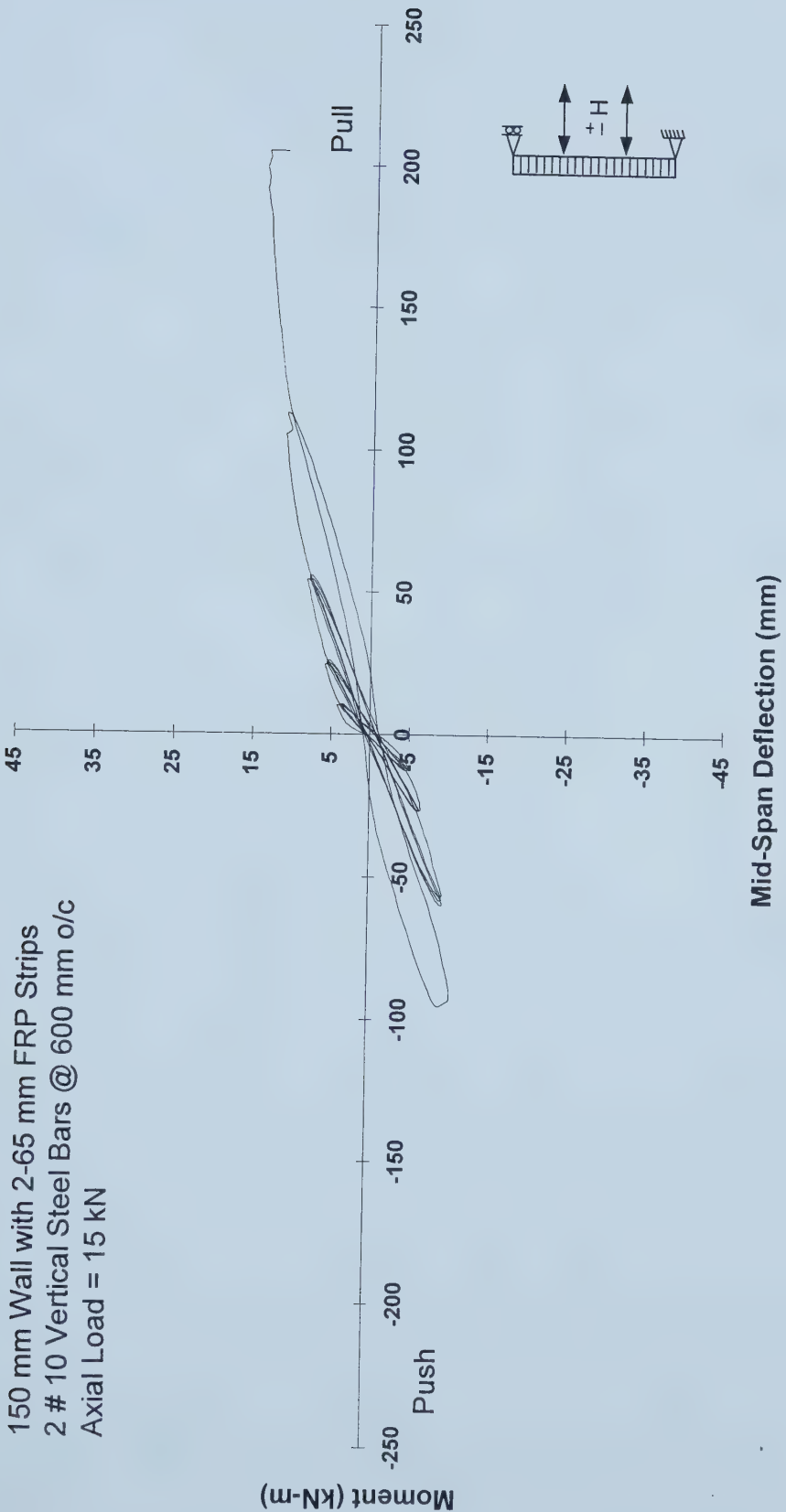


Figure 3.8 Moment versus Deflection Hysteresis for Wall-8

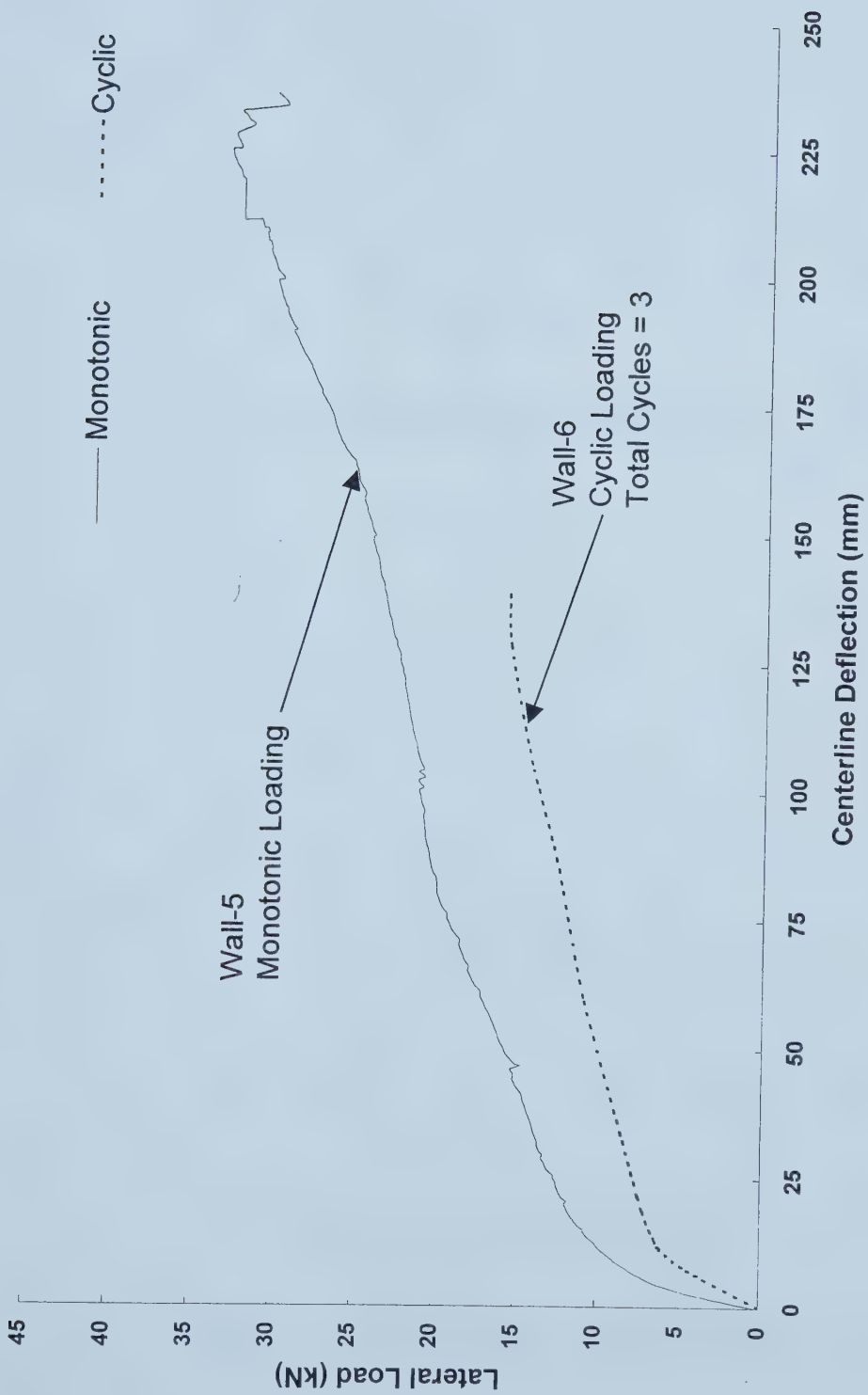
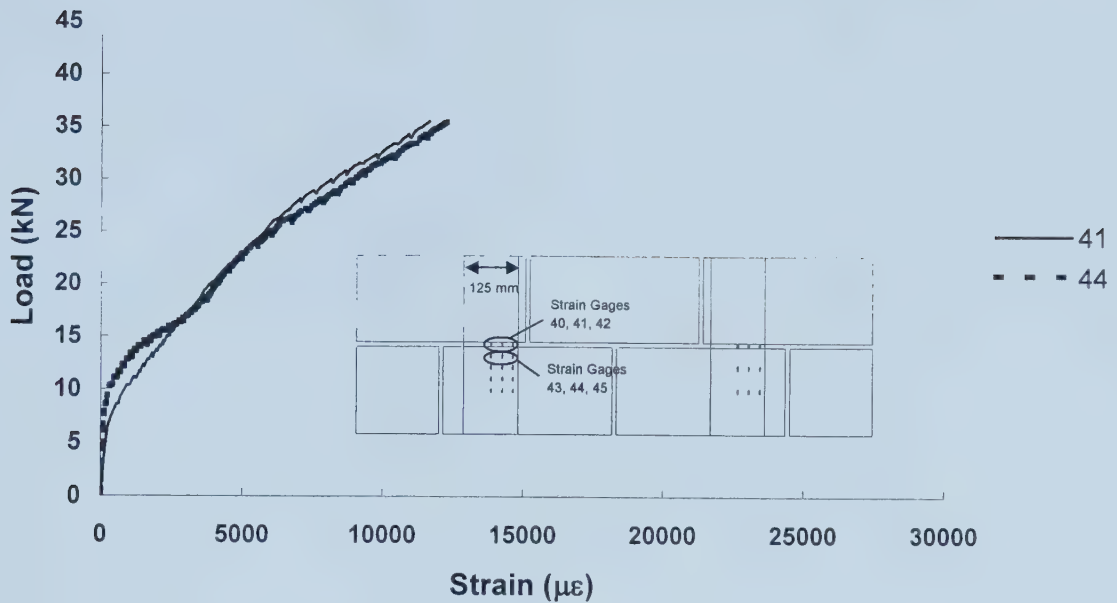
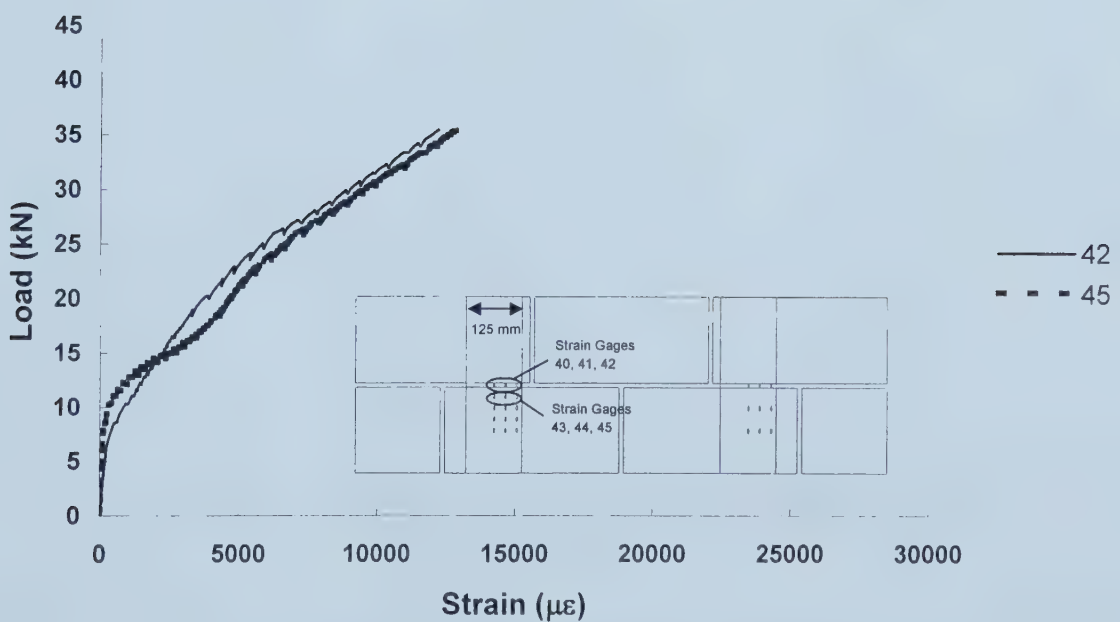


Figure 3.8(a) Superimposed Response for Wall-5(Monotonic) and Wall-6(Cyclic-Push)

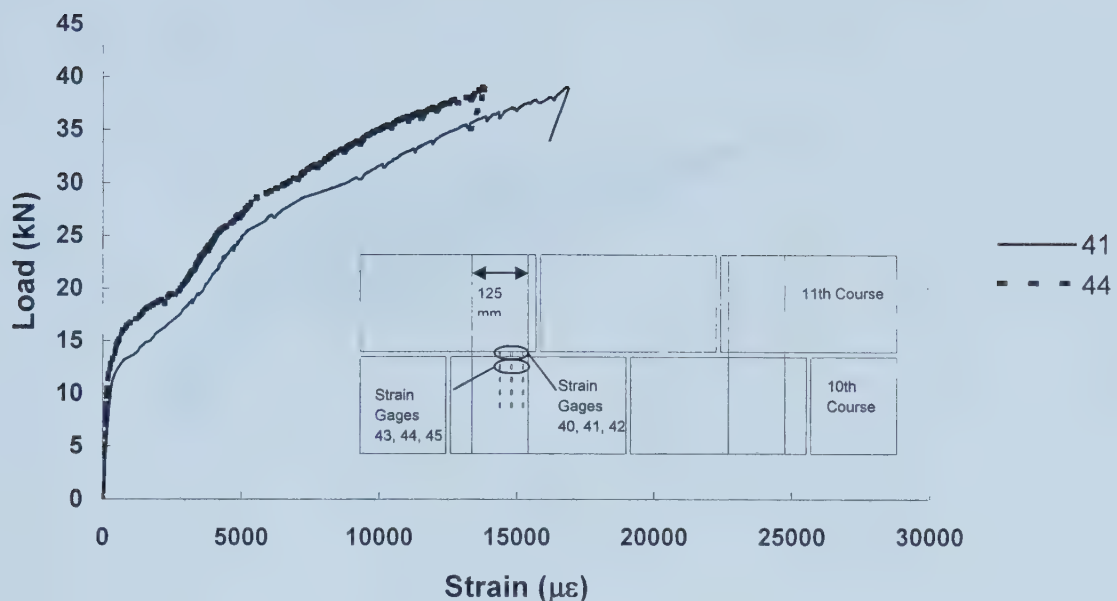


(a) Gages 41 & 44 on N-W Strip

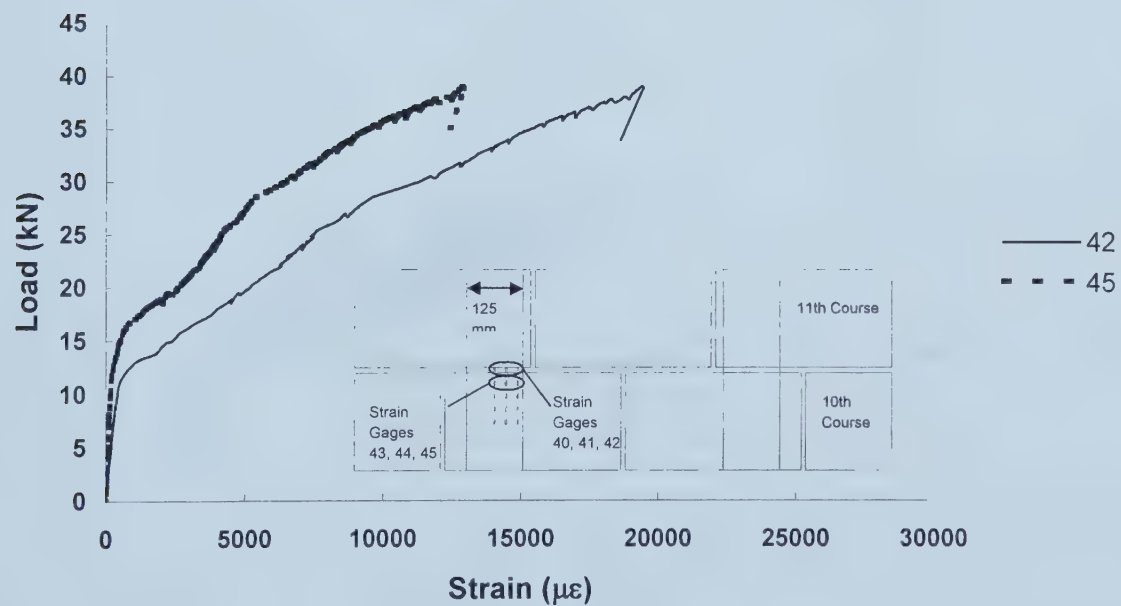


(b) Gages 42 & 45 on N-W Strip

Figure 3.9 Load versus Strain for Wall-1

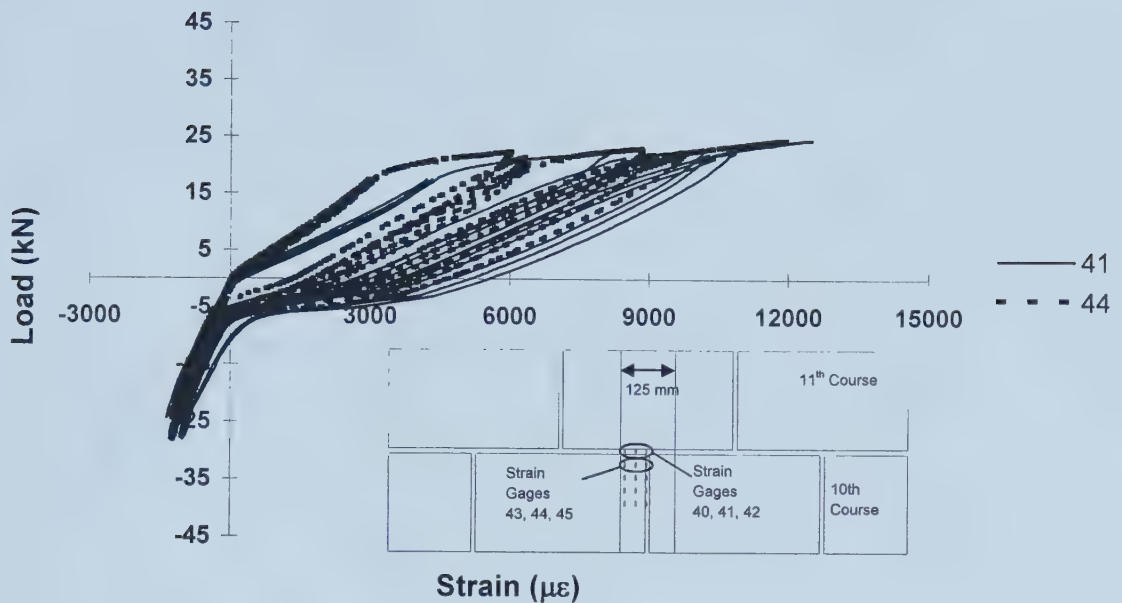


(a) Gages 41 & 44 on N-E Strip

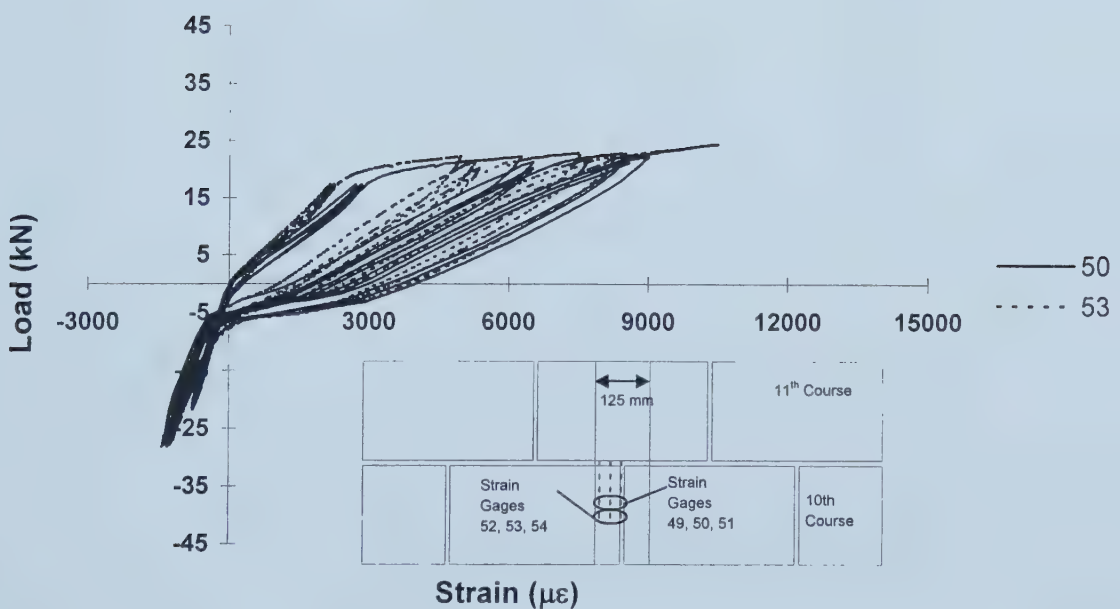


(b) Strain in Gage 42 & 45 on N-E Strip

Figure 3.10 Load versus Strain for Wall-2

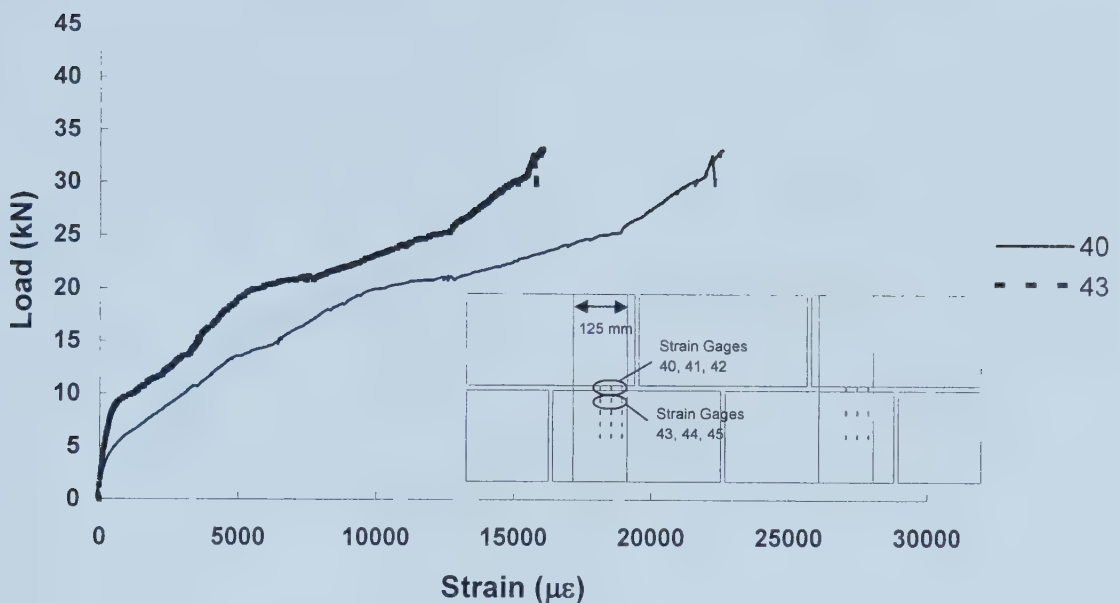


(a) Gages 41 & 44 on East Strip

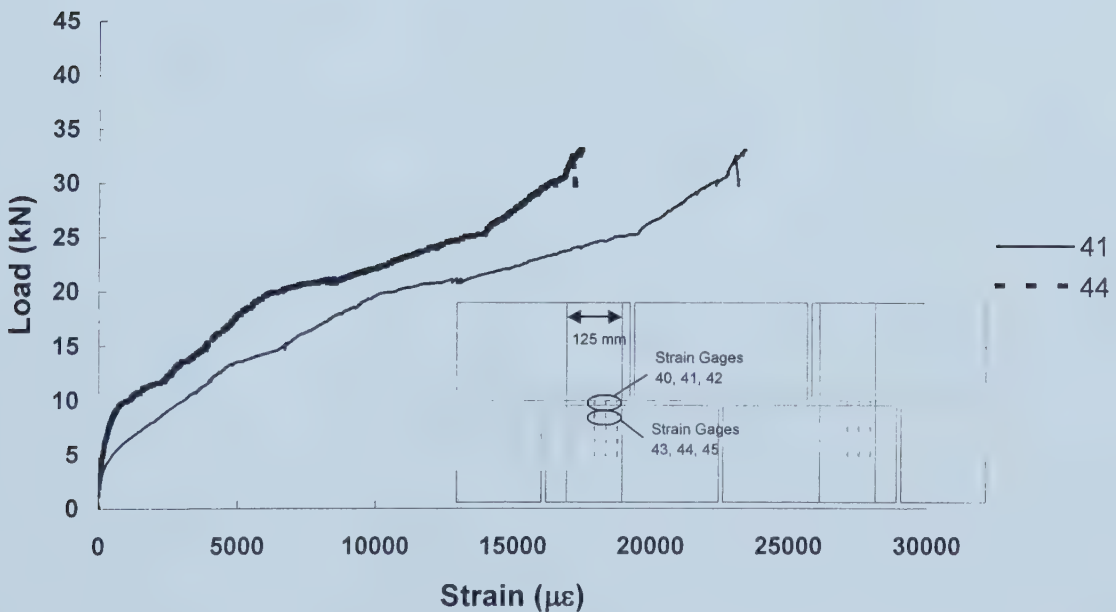


(b) Gages 50 & 53 on East Strip

Figure 3.11 Load versus Strain for Wall-4

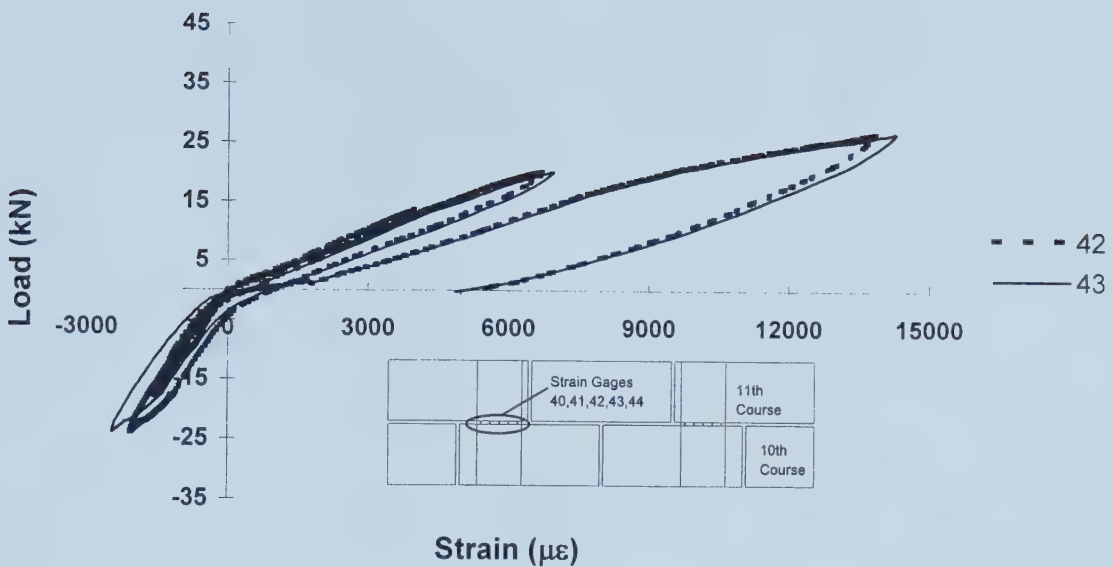


(a) Gages 40 & 43 on N-E Strip

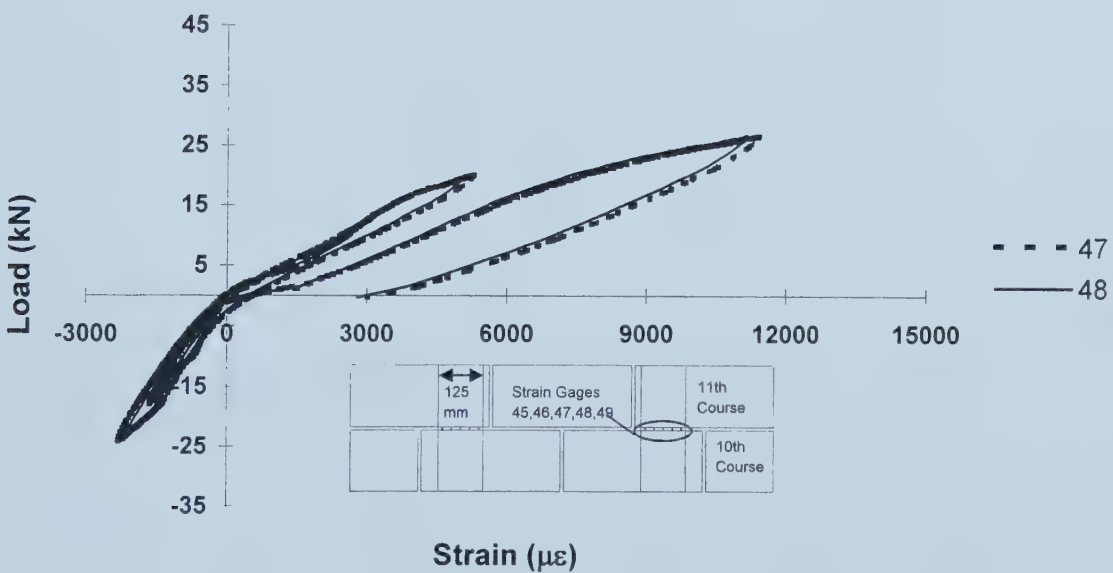


(b) Gages 41 & 44 on N-E Strip

Figure 3.12 Load versus Strain for Wall-5

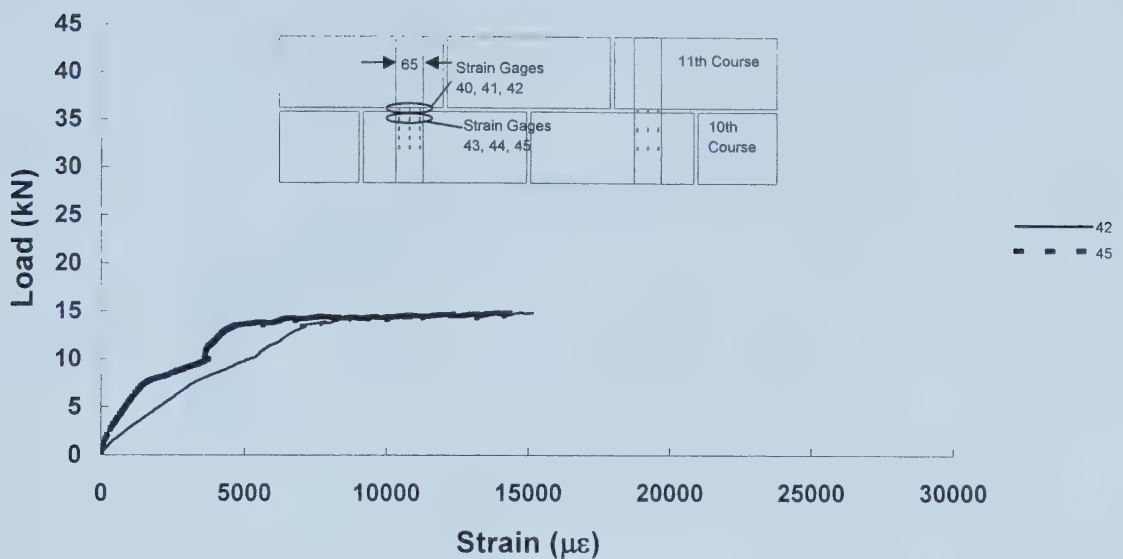


(a) Gages 42 & 43 on S-E Strip

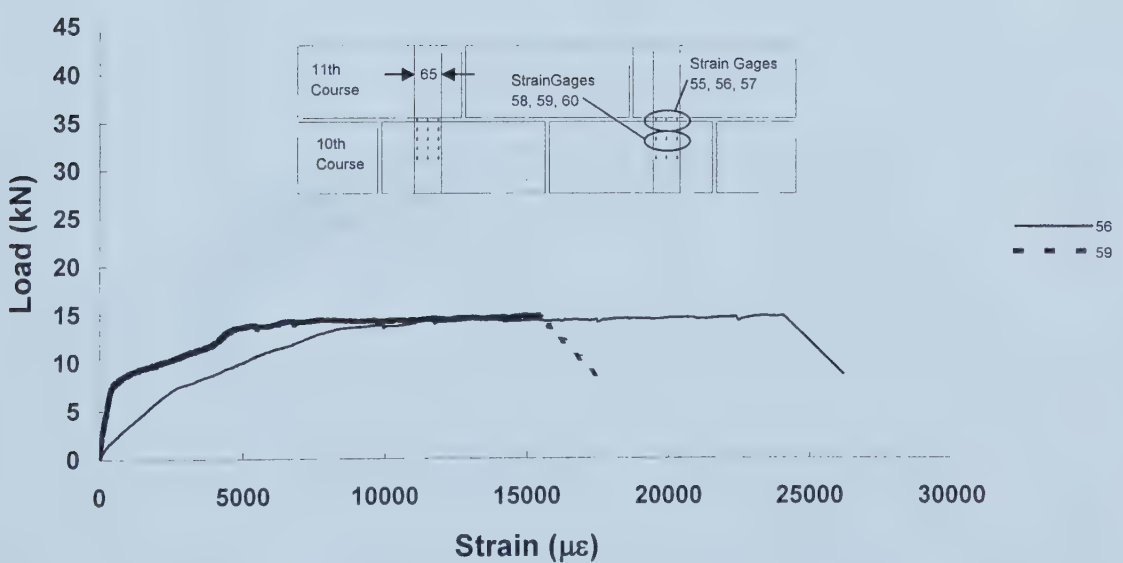


(b) Gages 47 & 48 on N-E Strip

Figure 3.13 Load versus Strain for Wall-6

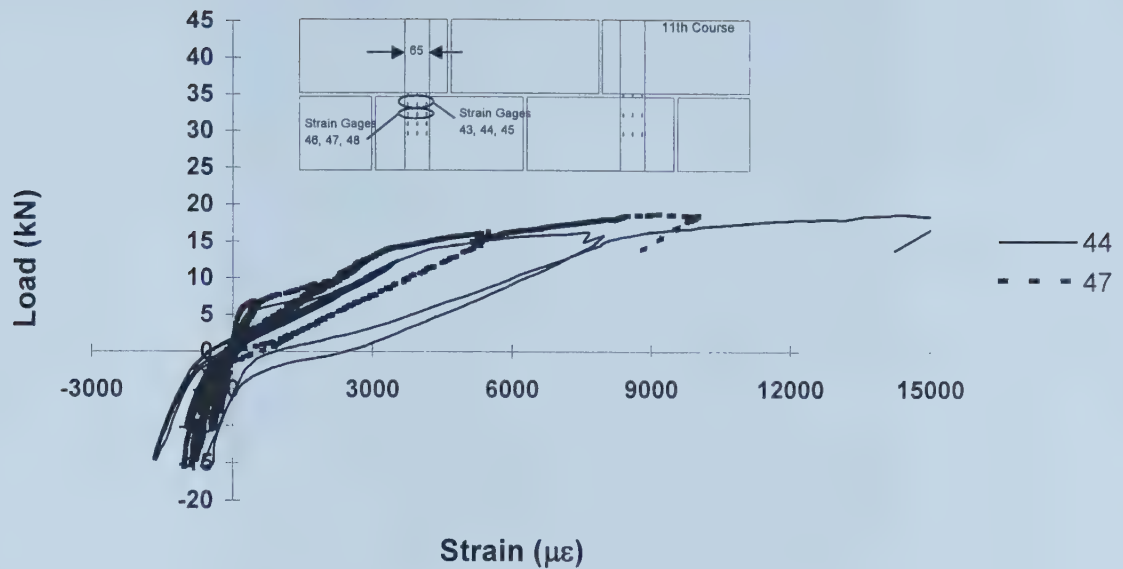


(a) Gages 42 & 45 on N-W Strip

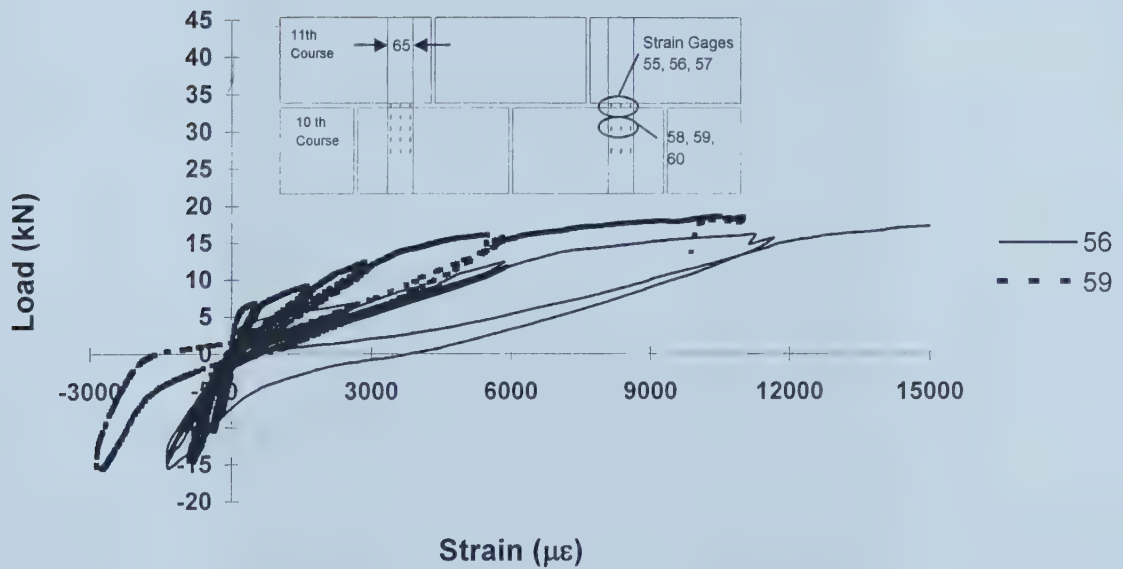


(b) Gages 56 & 59 on S-W Strip

Figure 3.14 Load versus Strain for Wall-7

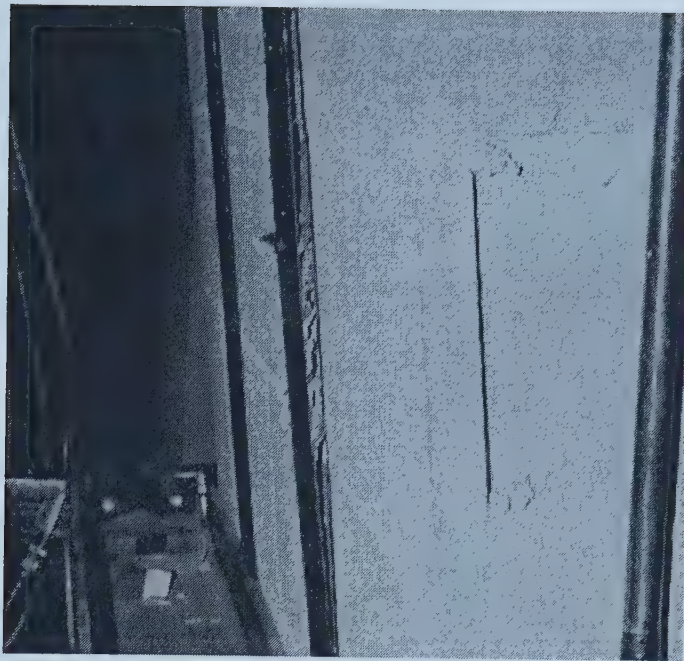


(a) Gages 44 & 47 on S-E Strip

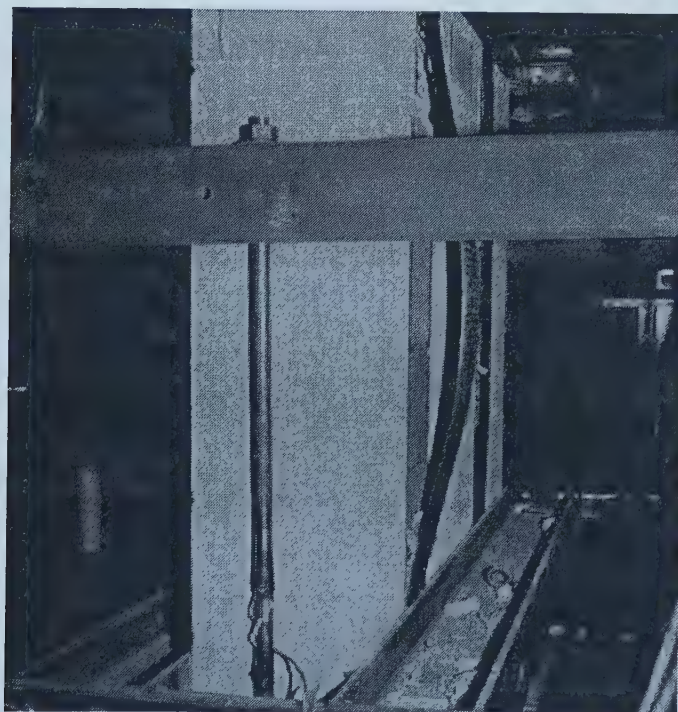


(b) Gages 56 & 59 on N-E Strip

Figure 3.15 Load versus Strain for Wall-8

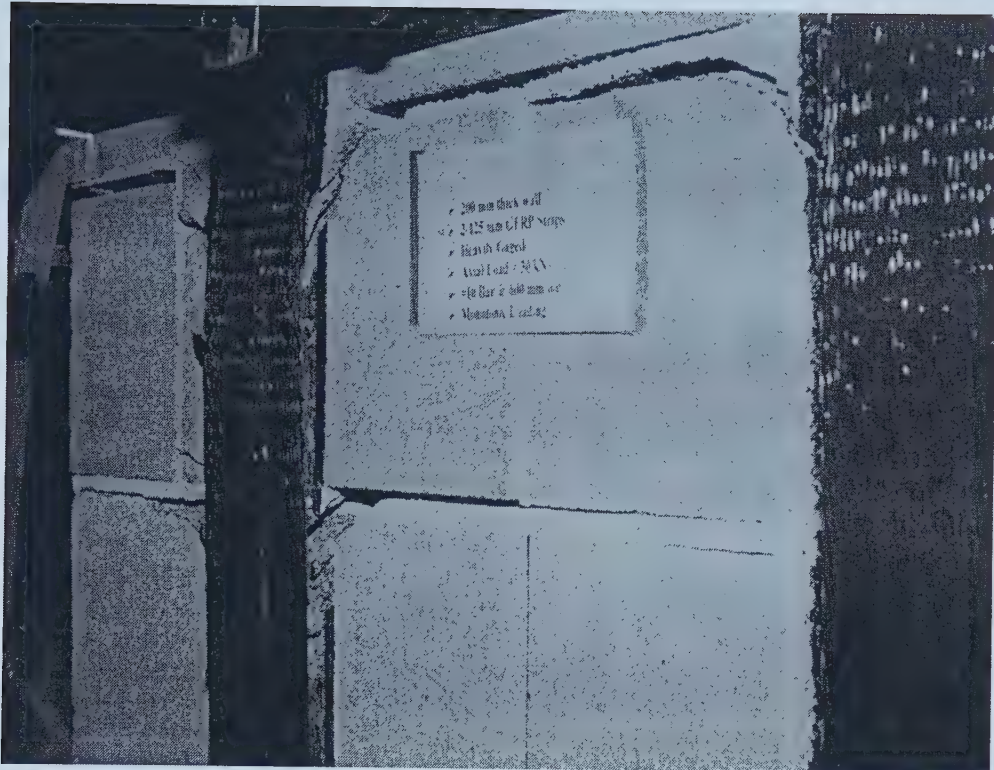


(a) Initiation of Delamination in the Constant Shear Region

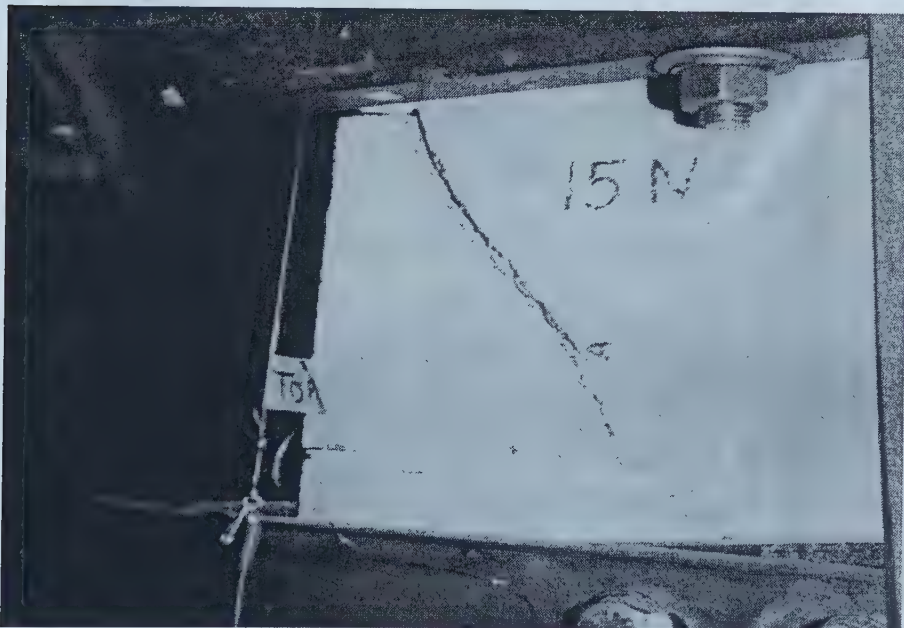


(b) Slipping and Buckling of Delaminated GRRP Strip

Figure 3.16 Failure of Wall-1

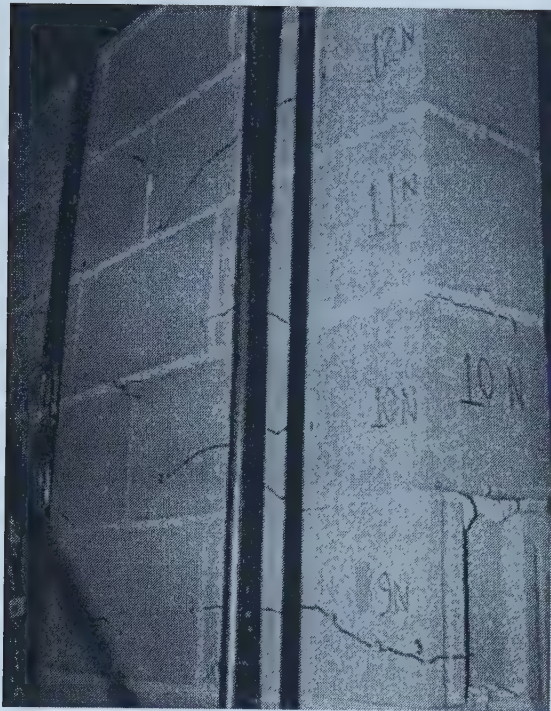


(a) Cracking in the lower constant shear region at failure

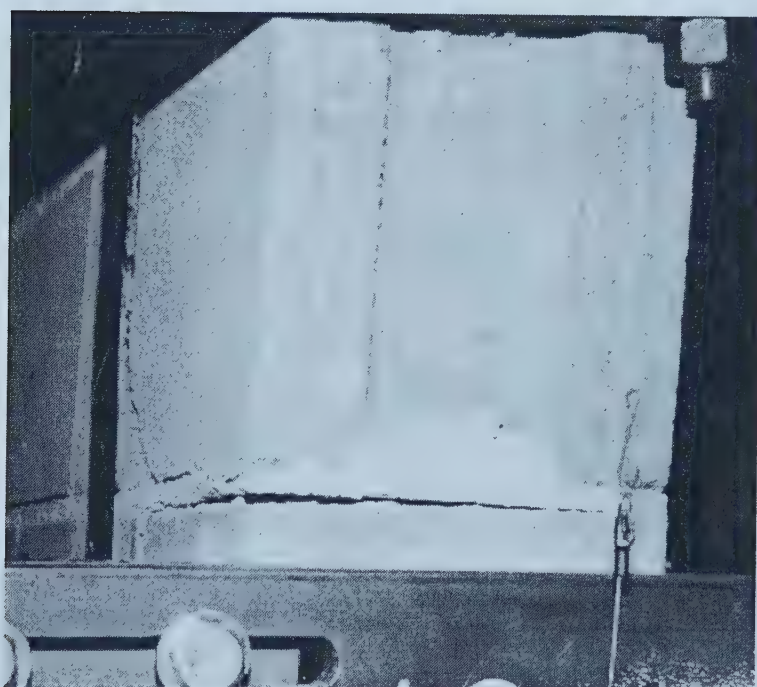


(b) Flexure shear Failure

Figure 3.17 Failure of Wall-2



(a) Horizontal and Diagonal Cracking



(b) Opening of Bed joints

Figure 3.18 Failure of Wall-3

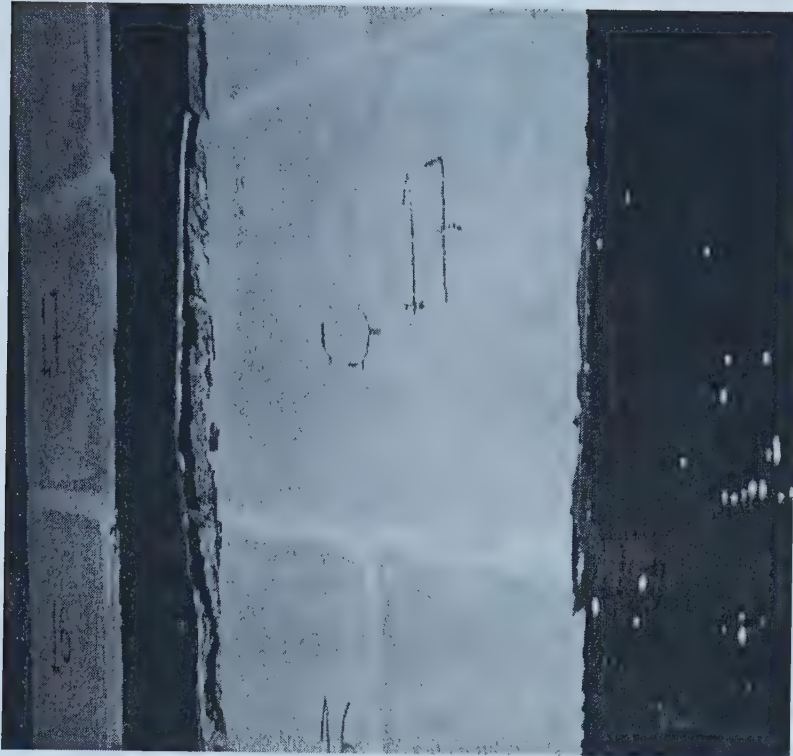


(a) Cracking in the Constant Shear Region on the East Face



(b) Delamination in the constant shear region on the West Face

Figure 3.19 Failure of Wall-4



(a) Delamination of GFRP in Constant Shear Region on East Face

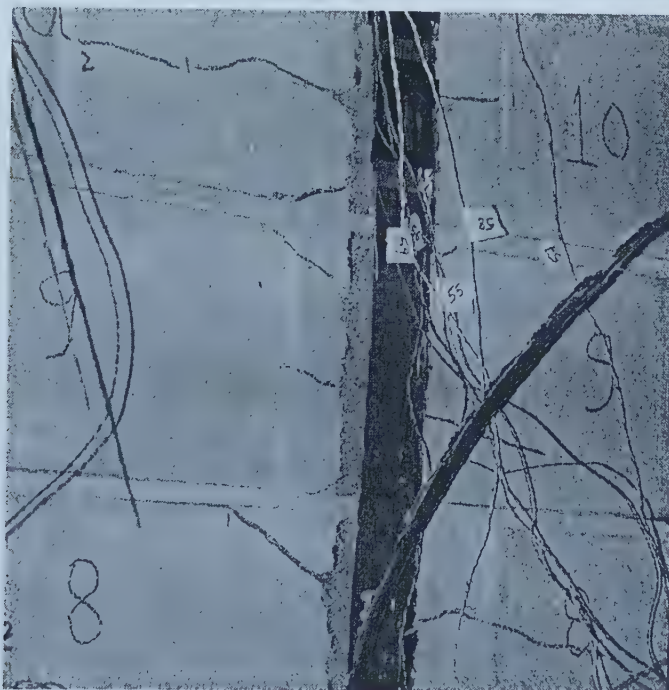


(b) Flexure Shear Failure on South Side

Figure 3.20 Failure of Wall-5

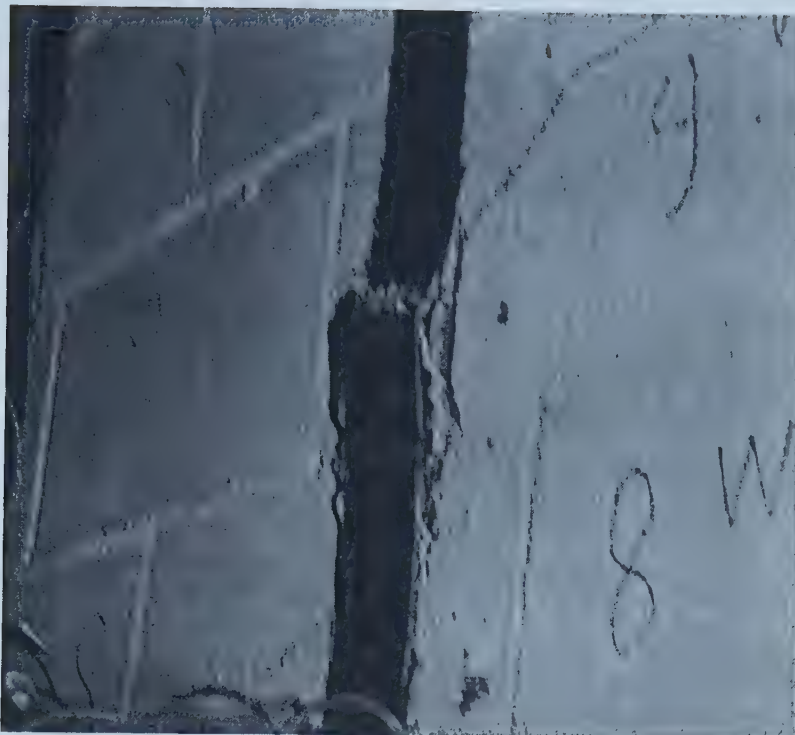


(a) Rupture of Northeast Strip in the Constant Moment Region

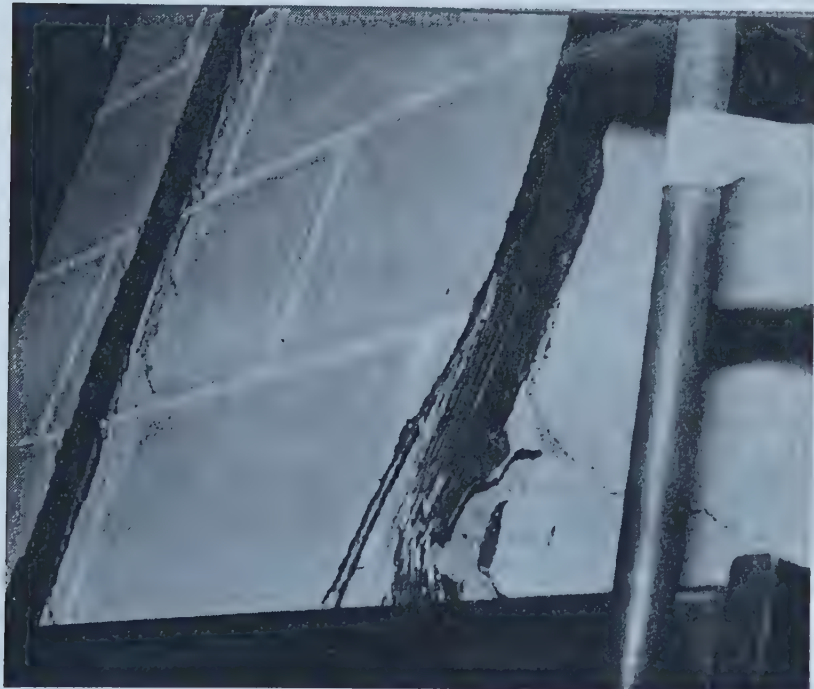


(b) Rupture of Southeast Strip in the Constant Moment Region

Figure 3.21 Rupture of GFRP Strips for Wall-7

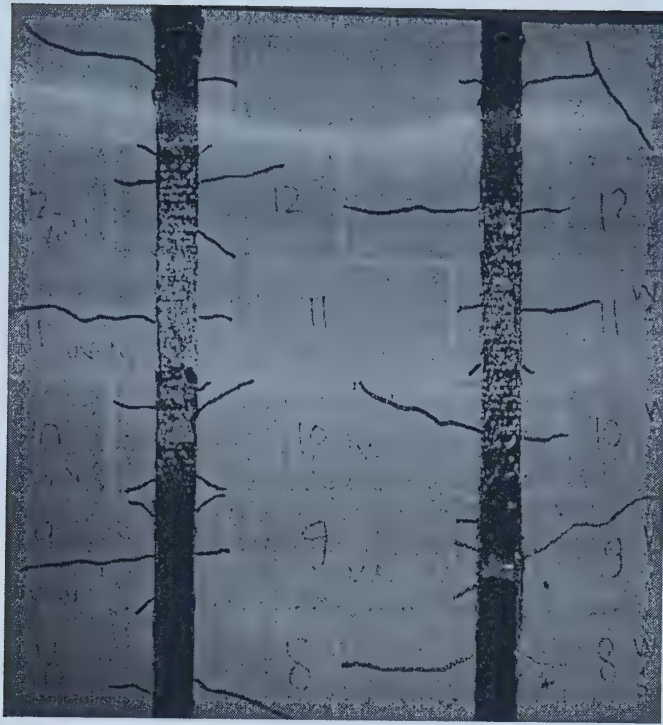


(a) Rupture of Southwest Strip at location of Waviness



(b) Rupture of Northeast Strip at 14th Course

Figure 3.22 Rupture of GFRP in Wall-8



(a) Cracking in the Constant Moment Region on the West Face

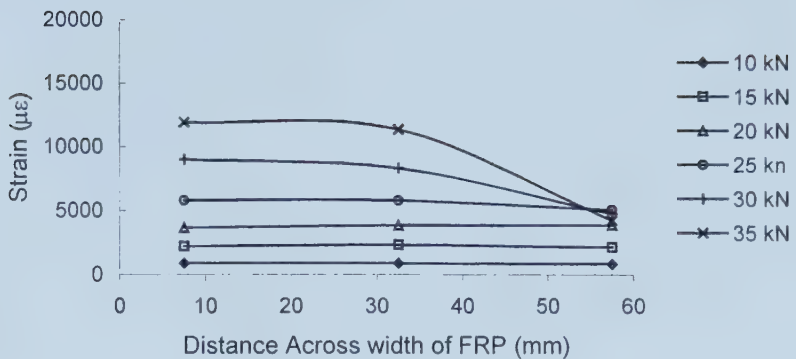


(b) Cracking in the constant Moment Region on the East Face

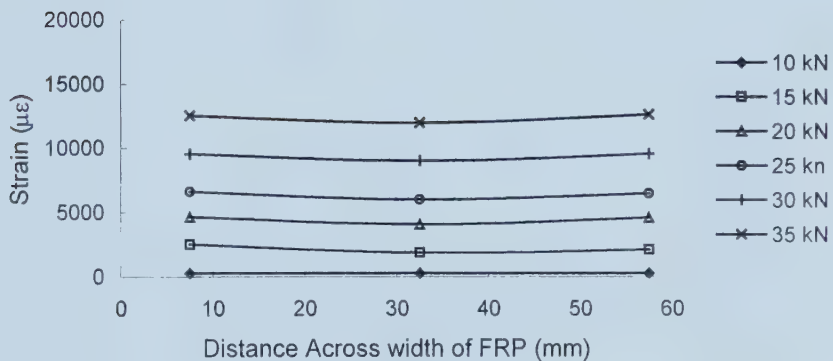
Figure 3.23 Horizontal and Diagonal Cracking in Wall-8

Note: Cracks have been highlighted

Gages 1, 2, 3



Gages 4, 5, 6



Gages 7, 8, 9

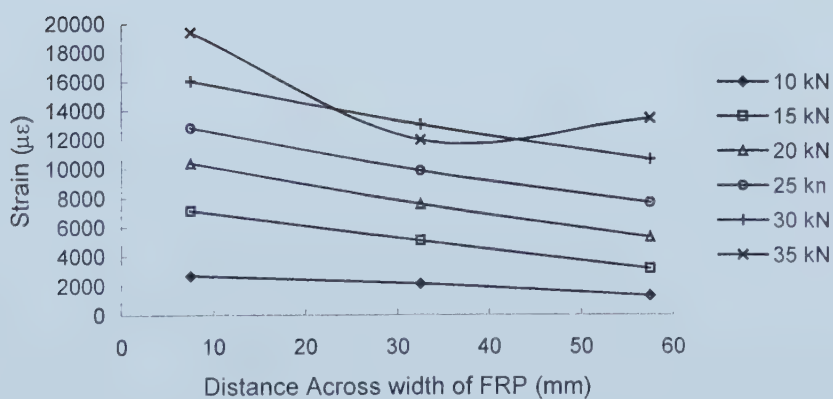
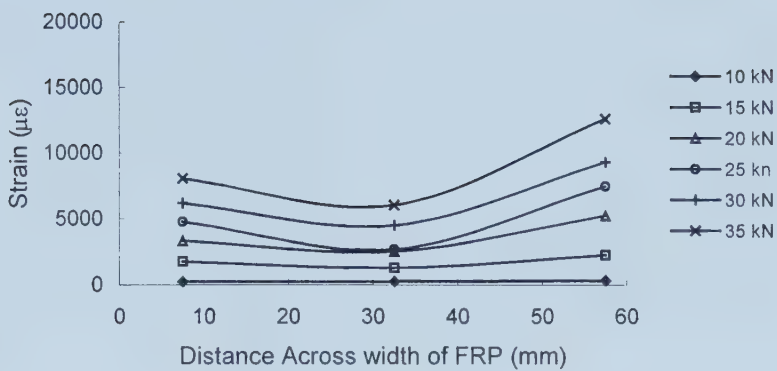
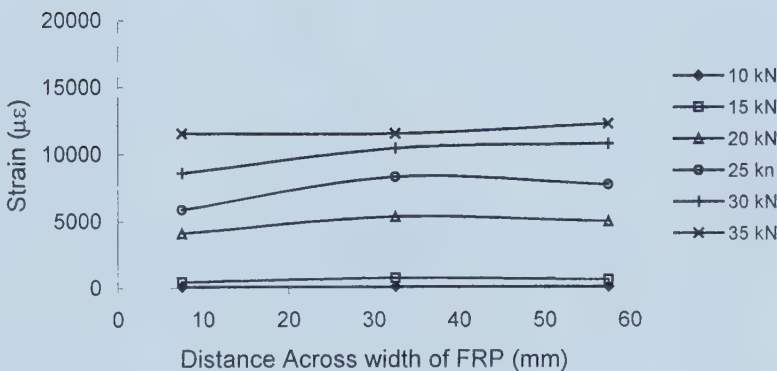


Figure 3.24(a) Distribution of Strain Across the FRP Strip for Wall-1

Gages 10, 11, 12



Gages 13, 14, 15



Gages 16, 17, 18

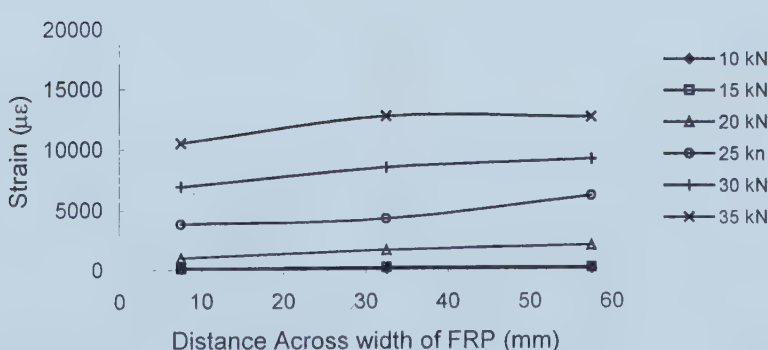
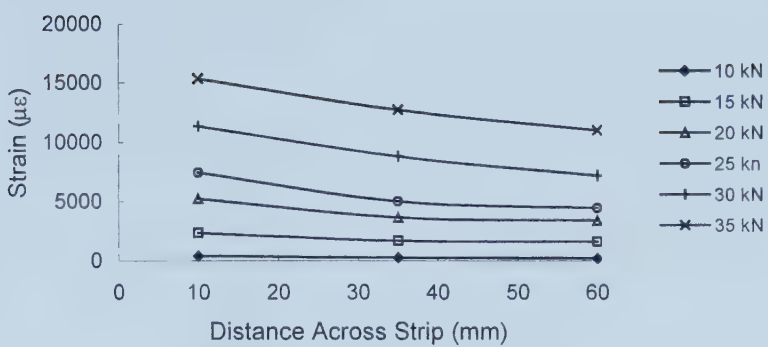
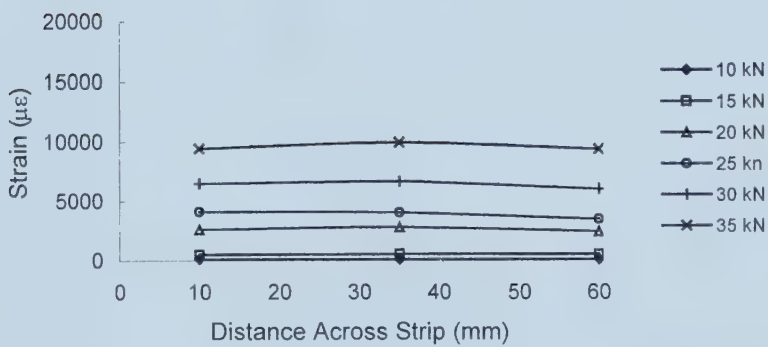


Figure 3.24(b) Distribution of Strain Across the GFRP Strip for Wall-1

Gages 40, 41, 42



Gages 43, 44, 45



Gages 46, 47, 48

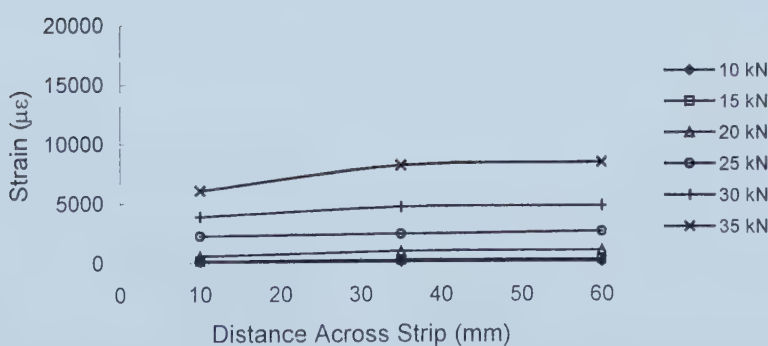
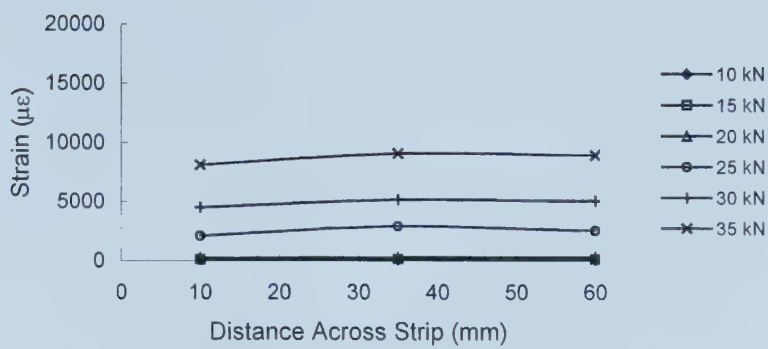


Figure 3.25(a) Distribution of Strain Across the GFRP Strip for Wall-2

Gages 49, 50, 51



Gages 52, 53, 54

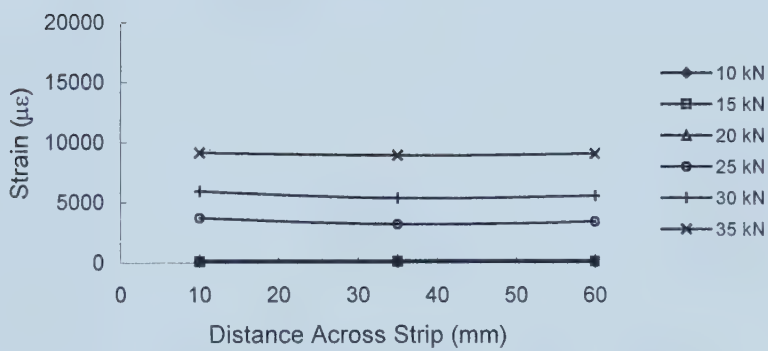
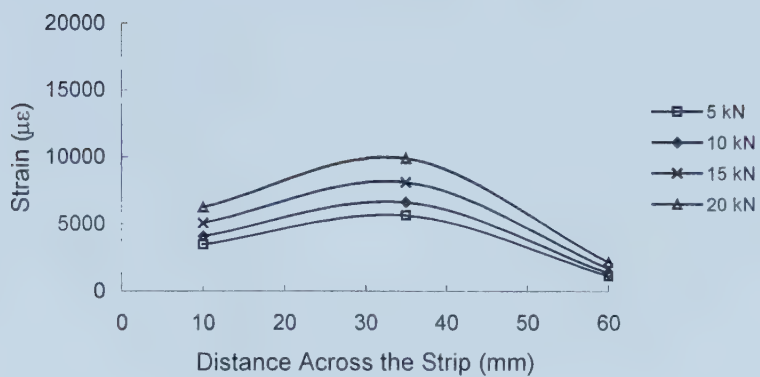
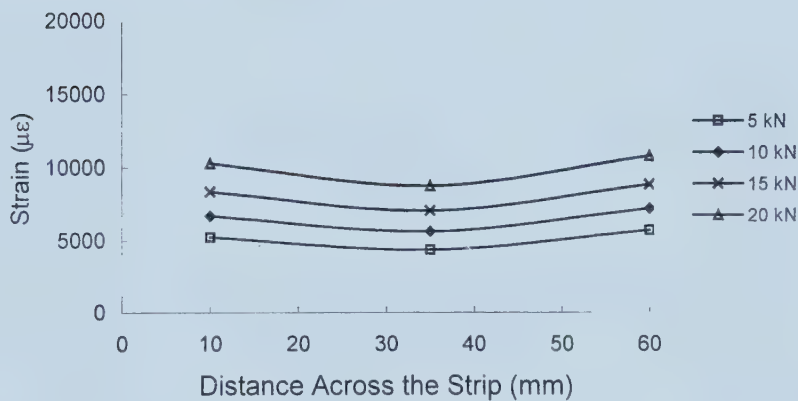


Figure 3.25(b) Distribution of Strain Across the GFRP Strip for Wall-2

Gages 40, 41 & 42 (Ascending)



Gages 43, 44 & 45 (Ascending)



Gages 46, 47 & 48 (Ascending)

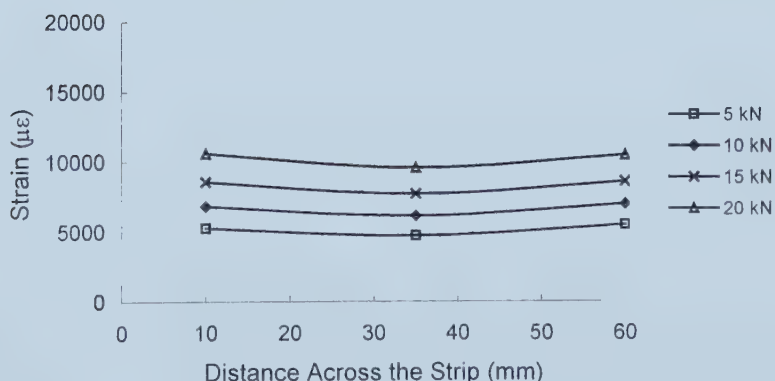
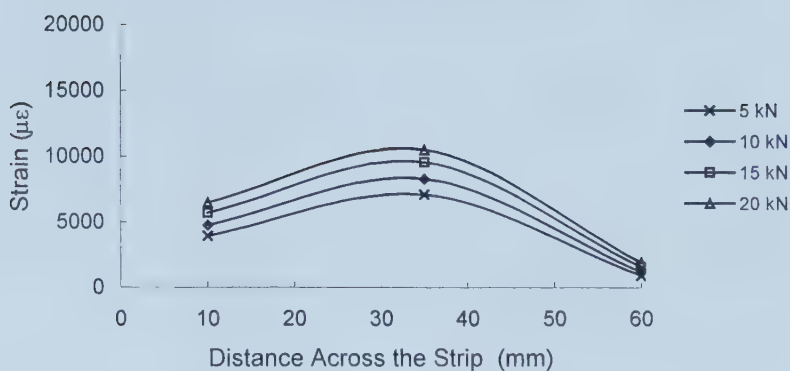
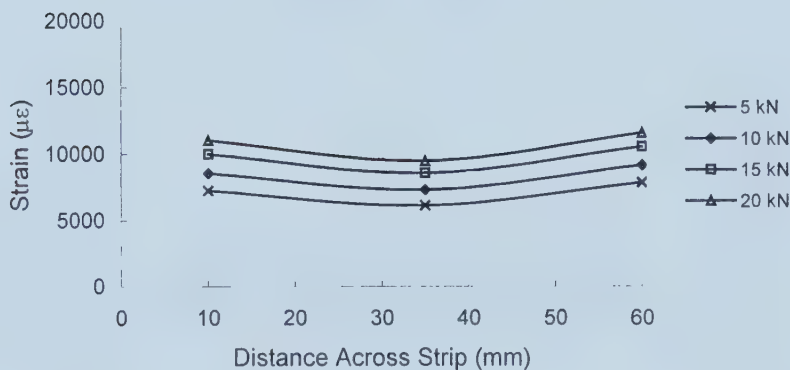


Figure 3.26(a) Distribution of Strain Across the GFRP Strip for Wall-4

Gages 40, 41 & 42(Descending)



Gages 43, 44 & 45 (Descending)



Gages 46, 47 & 48 (Descending)

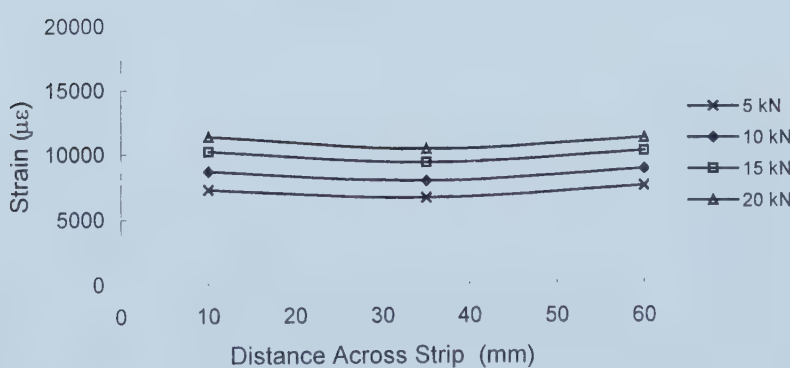
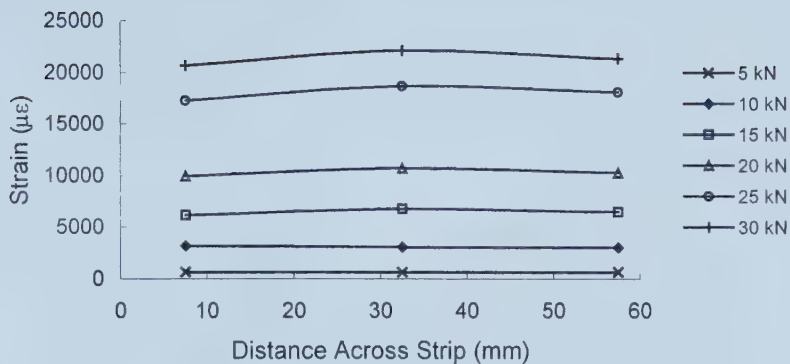
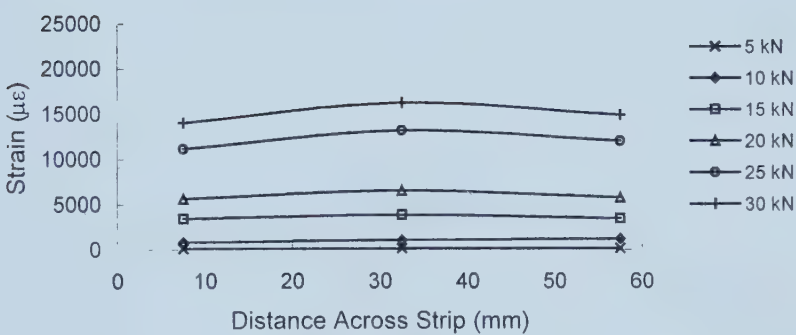


Figure 3.26(b) Distribution of Strain Across the GFRP Strip for Wall-4

Gages 40, 41, 42



Gages 43, 44, 45



Gages 46, 47, 48

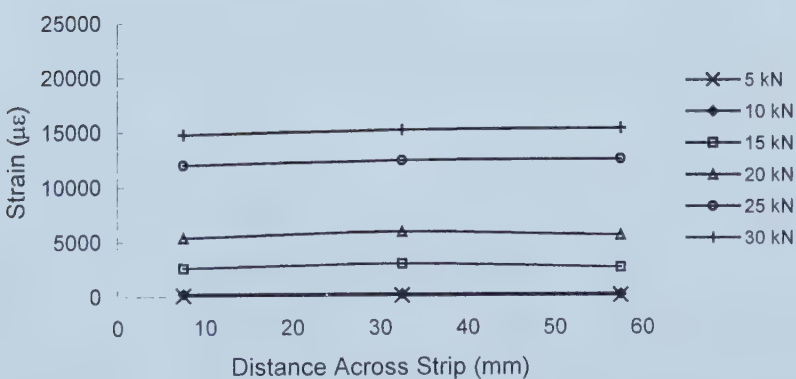
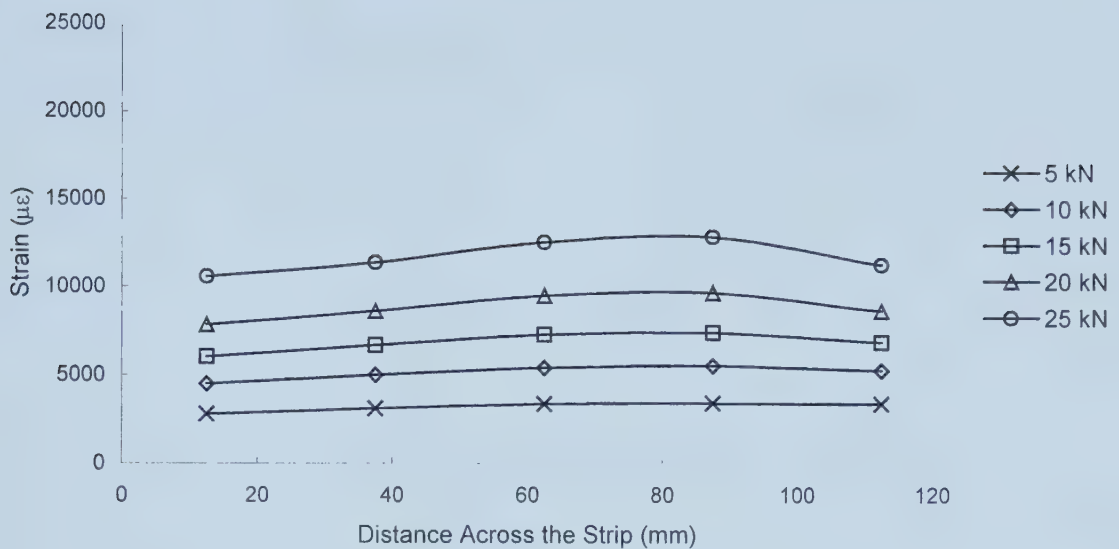


Figure 3.27 Distribution of Strain Across the GFRP Strip for Wall-5

Gages 40, 41, 42, 43, 44 (Ascending)



Gages 40, 41, 42, 43, 44 (Descending)

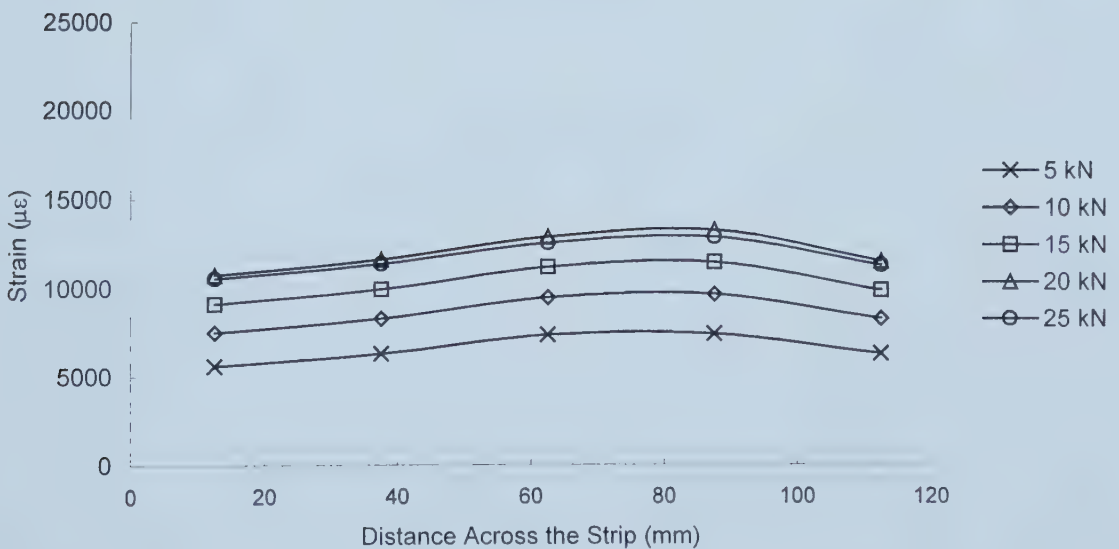
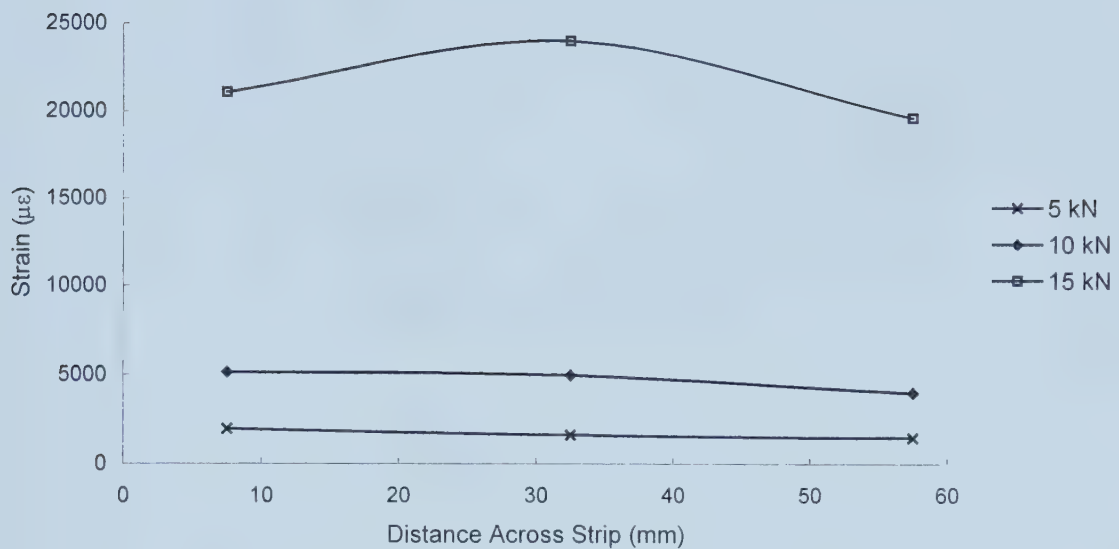


Figure 3.28 Distribution of Strain Across the GFRP Strip for Wall-6

Gages 55, 56, 57



Gages 61, 62, 63

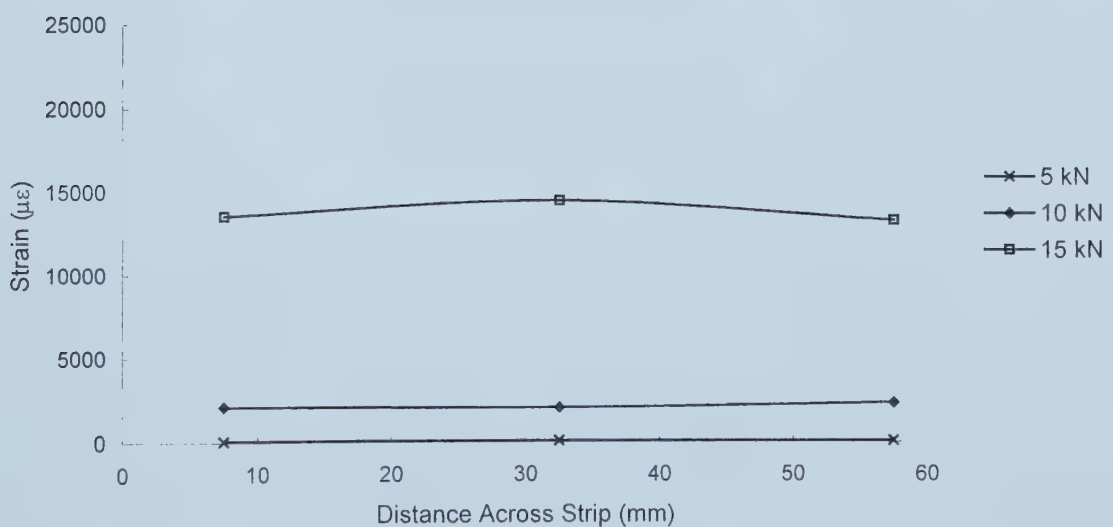
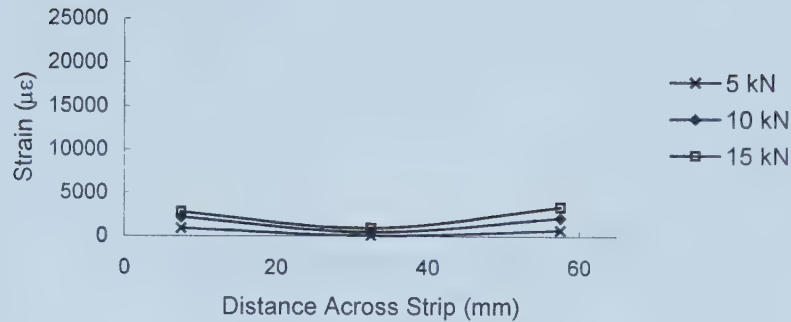
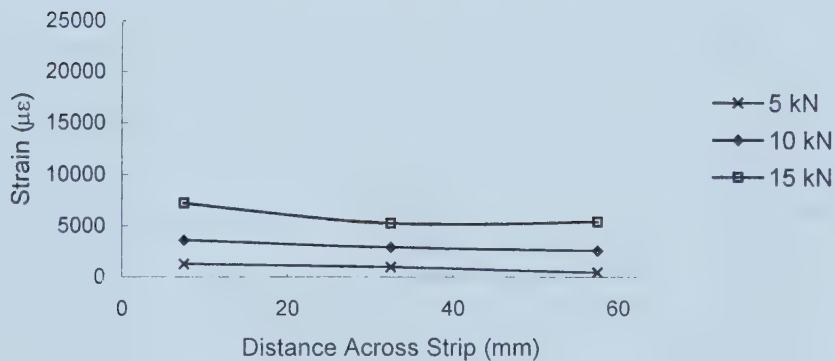


Figure 3.29 Distribution of Strain Across the GFRP Strip for Wall-7

Gages 40,41 & 42 (Ascending)



Gages 43, 44 & 45 (Ascending)



Gages 46,47 & 48 (Ascending)

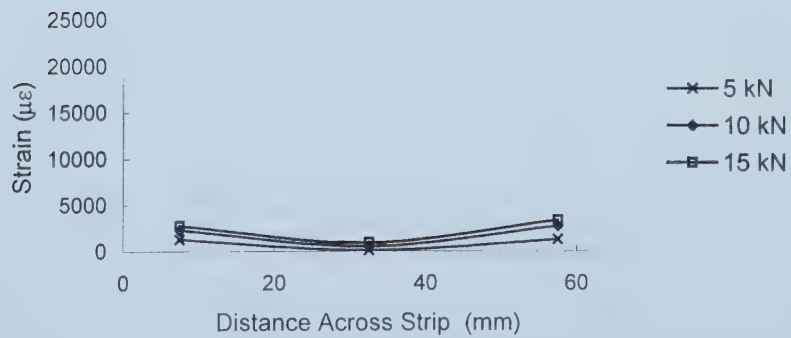
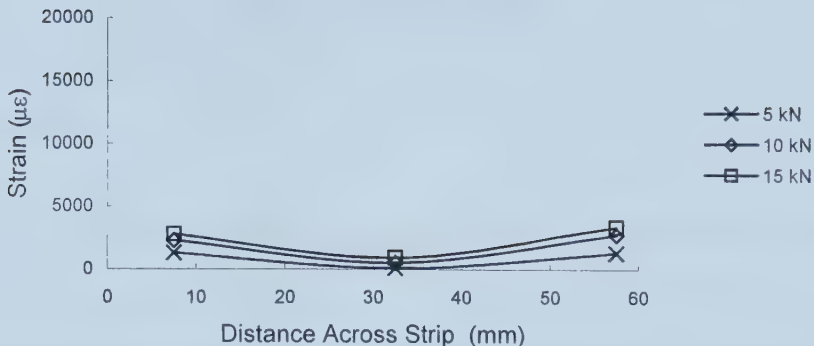
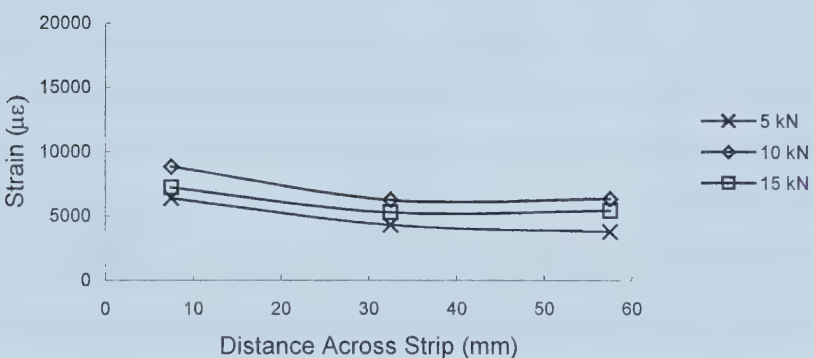


Figure 3.30(a) Distribution of Strain Across the GFRP Strip for Wall-8

Gages 40,41 & 42 (Descending)



Gages 43, 44 & 45 (Descending)



Gages 46,47,48 (Descending)

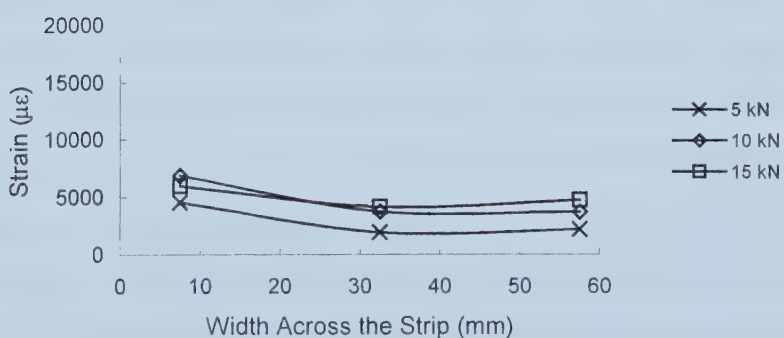


Figure 3.30(b) Distribution of Strain Across the GFRP Strip for Wall-8

Chapter 4

ANALYTICAL MODEL

4.1 Introduction

A numerical model capable of predicting the ultimate moment and deflection using a non-linear approach is presented. The model was initially assembled by Kuzik *et al.* (1999). It is based on a practical hysteresis loop developed by Saiidi and Sozen, which contain the characteristics of the hysteresis loops obtained from the tests. Another important constituent is a flexural stiffness model proposed by Aboud *et al.* (1995) to predict the stiffness degradation after the specimen has cracked. In order to make the model flexible, all the calculations have been performed in a spreadsheet. The model parameters assembled by Kuzik *et al.* (1999) were based solely on the test results obtained from 200 mm thick walls with somewhat constant width of GFRP strips. A linear regression was performed between area of the GFRP and the failure load of the specimen. Also the only mode of failure reported was flexure shear failure. In this study the Kuzik's model is modified to improve performance. Explanation of all equations in detail will come later in this chapter.

The work reported in chapters 2 and 3 has primarily extended the database available. As explained in detail earlier, two series of walls comprising 150 mm and 200 mm thick walls were tested. The external reinforcement in the walls consisted of variable widths of GFRP strips as shown in Table 2.7. Three different failure modes were observed as explained in Section 3.4.3. In order to achieve full advantage of the available data, the experimental results obtained by Kuzik *et al.* (1999) were combined with the present study results. A linear regression analysis (best-fit) was performed as shown in Figures 4.1 and. 4.2. The resulting expression is slightly different from the one reported by Kuzik *et al.* (1999). However, this difference is quite justifiable as different wall thickness and amount of GFRP were used in the present study. The resulting equation obtained from regression analysis was then used in the analytical model to predict the

behavior of 200 mm and 150 mm thick walls. No effort has been made to incorporate the various failure modes explicitly in the model.

4.2 GFRP Material and Section Properties

The analyses were performed using GFRP material and section properties provided by the manufacturer, Master-Builders. However, more rational results were obtained when material properties provided by Sika Canada for the same material were used. Kuzik *et al.* (1999) used similar properties in their model. As a simple check, a sample from each product with the same geometric properties was weighed carefully on an electronic scale and found that both materials have the same density. This urged the author to use the more rational material properties. However, more justification is required to prove the validity of this decision. Throughout this chapter, all results and discussions are based on the material properties provided by Sika Canada.

4.3 Section Properties Calculation

Before a detailed explanation of the analytical model, it is necessary to describe the assumptions underlying the calculation of various section properties. All section properties are calculated about the geometric centroid of the cross-section. The gross moment of inertia of a cross section is obtained by summing moment of Inertia about the centroid using parallel axis theorem. Previous research in this area has shown that cracking at the bed joint occurs at very initial stage of loading. Therefore, a better approximation of moment of inertia up to cracking moment is calculated using the gross area less the tension face shell. Aboud *et al.*(1995) defined this term as modified moment of inertia I_g^f . The cracked moment of inertia is obtained by considering one face shell and cross section of GFRP strips.

4.4 Components of Analytical Model

The general behavior observed during the testing of the specimens is shown in Figure 4.3. The behavior can be generalized as a tri-linear. The moment deflection model consisted of an initial zone, which represents the uncracked zone and it is assumed that the tensile stresses in masonry are less than the rupture strength of the masonry. Due to the reasons mentioned in Section 4.3, modified moment of inertia (I_g^f) is used in the calculation of the response for this section. Thus the following equation is used to calculate the cracking moment of the specimen.

$$M_{crf} = \left[f_t + \frac{P}{A_e} \right] \left[\frac{2I_g^f}{h} \right] \quad (4.1)$$

in which,

- f_t = tensile strength of masonry (MPa)
 P = factored axial compressive load (kN)
 A_e = effective cross section (mm^2)
 I_g^f = modified moment of inertia (mm^4)
 h = thickness of the wall (mm)

The above equation is obtained by slightly modifying the equation reported in CSA-S304.1-94. It is assumed that the neutral axis until cracking coincides with the centroidal axis leading to $y_t = h/2$. This explains the factor 2 used in the above equation. After the section is cracked the response is primarily influenced by the amount of external GFRP reinforcement expressed as a reinforcement ratio modified through the material moduli of elasticity. This allows the equation to be used for different types of FRP other than glass. In order to determine a relationship between the GFRP reinforcement ratio and the ratio of transition moment and the modified cracking moment (M_T/M_{crf}), a linear regression analysis is performed on the two sets of data, obtained by

Kuzik *et al.* (1999) and the present study, as shown in Figure 4.2. The resulting equation is then combined with Equation 4.1 to obtain an expression for the transition moment M_T .

$$M_T = \left[f_t + \frac{P}{A_e} \right] \left[\left(\frac{2I_g}{h} \right) (1 + 93.8\rho_{GFRP}) \right] \quad (4.2)$$

in which, ρ_{GFRP} is the ratio of the GFRP area transformed to preserve strain compatibility with the effective masonry area.

$$\rho_{GFRP} = \frac{A_{GFRP} \cdot E_{GFRP}}{A_e \cdot E_m} \quad (4.3)$$

in which,

A_{GFRP} =area of GFRP on the tension face (mm^2)

ρ_{GFRP} =GFRP reinforcement ratio

E_m =modulus of elasticity of masonry (MPa)

The regression equation incorporated in Equation (4.2) is almost the same that was used by Kuzik *et al.*(1999).

After the transition moment region, the wall behavior is primarily inelastic. The loading portion of the response is limited by an ultimate strain in the GFRP. The unloading/reloading behavior is secant elastic as shown in Figure 4.3. The ultimate strain is ideally a function of the mode of failure. For simplicity it is obtained here in an empirical manner. In order to be able to predict the strain in the GFRP at failure, a linear regression was performed using again the two sets of data. Kuzik *et al.*(1999) reported a linear regression equation based on the test results of 200 mm masonry walls. All the results were based on 250 mm wide GFRP strips and the only mode of failure was flexure shear. The regression equation was also based on only three data points, thus resulting in a value of coefficient of determination very close to unity. In the present study, walls of 200 mm and 150 mm are tested and different failure modes including delamination and

rupture of GFRP were observed. The Kuzik's data and the data obtained from the present study were combined and a linear regression was performed to obtain an equation for GFRP strains at failure. Figure 4.1 shows the resulting regression equation based on tests performed by Kuzik *et al.* (1999) and the present study. The regression equation reported by Kuzik *et al.* (1999) is also shown in Figure 4.1 for comparison. The constant term in the combined data equation is much higher than the Kuzik's term (13,233), because higher GFRP strains were recorded in the present study.

$$\epsilon_{uGFRP} = -12.26A_{GFRP} + 17,000 \quad (4.4)$$

This off course is a result of larger strains observed when the shear flexure mode is not an issue. Such walls should have less GFRP and small wall thickness. The calculation of the ultimate moment is similar to that for singly reinforced concrete sections. However, to incorporate the contribution of GFRP, a second term is added to the equation representing the moment of the force in the GFRP sheet about the neutral axis. The resulting equation can be expressed as

$$M_u = A_s f_s \left(d - \frac{a}{2} \right) + (A_{GFRP} \cdot E_{GFRP} \cdot \epsilon_{uGFRP}) \left[\left(h + \frac{t_{GFRP}}{2} \right) - \frac{a}{2} \right] \quad (4.5)$$

in which,

f_s = the yield stress in the reinforcement(MPa)

t_{GFRP} = nominal thickness of GFRP sheet reinforcement (mm)

a = distance from the extreme compression fiber to neutral axis (mm)

d = distance from the extreme compression fiber to the center of tension steel (mm)

The fundamental expression is again similar to that used for reinforced concrete sections except that a second term is added to take into account the effect of GFRP. The term $t_{GFRP}/2$ is very small relative to the wall thickness, h , and therefore can be neglected. The Equation 4.5 can therefore be rewritten as

$$M_u = A_s f_s \left(d - \frac{a}{2} \right) + (A_{GFRP} E_{GFRP} \epsilon_{u,GFRP}) \left(h - \frac{a}{2} \right) \quad (4.6)$$

The equation for the calculation of depth of compression block “a” can be expressed as

$$a = \frac{P + A_s f_s + A_{GFRP} E_{GFRP} \epsilon_{u,GFRP}}{0.85 f'_m b} \quad (4.7)$$

in which,

b = width of the wall-section in compression (mm)

f'_m = compressive strength of masonry (MPa)

A_s = area of vertical steel reinforcement (mm^2)

Kuzik *et al.* (1999) found that the use of general term of 0.85 in Equation 4.7 as stipulated by CSA S304.1 is highly conservative. Hognestad *et al.* (1955) conducted an investigation to develop the flexural compressive concrete stress block. The model used by Hognestad consisted of applying axial compressive loads at two different locations to create pure compression and moment. The location of application of loads was such that the entire cross section was in compression. Kaar *et al.* (1978) further carried the work done by Hognestad *et al.* (1955) and came up with a fourth order equation to determine the product $k_1 k_3$.

$$k_1 k_3 = 0.00003 f'_c^4 - 0.0013 f'_c^3 + 0.0214 f'_c^2 - 0.1672 f'_c + 1.1564 \quad (4.8)$$

In the above equation, k_1 and k_3 are the coefficients related to the magnitude and position of internal compressive force in masonry compression zone ($k_1 k_3 = \beta_1 * 0.85$, ksi) and f'_c is the concrete compressive strength in ksi units. Kuzik *et al.* (1999) obtained an average compressive strength of 10 MPa from masonry prism tests and therefore, by using the equation proposed by Kaar *et al.* (1978) obtained a factor of 0.96 in the denominator in Equation 4.7. However, the masonry strength obtained by the author is considerably less

than 10 MPa and, therefore, the factor of 0.96 cannot be used directly. More rational justification is required prior to adoption of the above-mentioned approach. CSA S304.1 stipulates a factor β_1 equal to 0.85 for masonry strength up to 20 MPa combined with a masonry strength factor of 0.55. Eliminating the masonry strength factor, the final equation is as shown in Equation 4.7.

4.5 Flexural Model (Out-Of-Plane Bending)

Reinforced masonry walls are built from highly non-homogenous materials with highly variable material properties. Therefore, it is difficult to assess the stiffness and deflection parameters. However, adequate information on material properties and placement of rebars were obtained from ancillary tests. In addition, boundary conditions were well defined and the wall aspect ratio was within that governed by material behavior ($h/t = 20$ and 27.5). Thus the flexural model for this test program can be reasonably predicted by ordinary beam theory. The test model is in accordance with ASTM E518. The behavior of a reinforced masonry wall when subjected to flexural loads is commonly described in terms of various limit states. These limit states are usually categorized as serviceability limit states and ultimate limit states. The moment versus deflection model used in this program is characterized into three limit states namely, cracking moment, yielding moment and ultimate moment.

To describe the deflection behavior of the wall, two values are needed. The transition deflection, Δ_T , and the ultimate deflection Δ_U corresponding to the failure. The transition deflection Δ_T corresponding to the transition moment M_T can be obtained as

$$\Delta_T = \frac{M_T}{E_m I_g} \frac{(3L^2 - 4x^2)}{24} \quad (4.9)$$

in which,

x = length of shear span (mm)

L = wall height (mm)

Equation 4.9 is analogous to the equation for a simply supported beam subjected to a two point loading system. However, the equation for flexural deflection is expressed in terms of moment and flexural rigidity. Past the transition moment the wall continuously degrades with the effective flexural stiffness EI_{eff} as a function of the achieved strain. The ultimate deflection can be obtained from a test result. In order to compute Δ_u , a rational approach was proposed by Kuzik *et al.* (1999). This approach is based on calculating the ultimate deflection from the curvature. The ultimate curvature elements M_u/EI can be replaced with an expression based on the ultimate strain previously obtained from Equation 4.4 and introducing a deflection correction factor, the Equation 4.9 can be rewritten in a general form to estimate the ultimate deflection as

$$\Delta_u = \left[\frac{\varepsilon_{uGFRP}}{h - a} \right] \cdot \left[\frac{(3L^2 - 4x^2)}{24 \left(1 - 2 \cdot \frac{S_{cr}}{L} \right)} \right] \quad (4.10)$$

Where the bracket in the denominator containing the crack spacing S_{cr} was introduced to smear the joint strain ε_{uGFRP} over the full block height. The crack spacing is assumed to be 200 mm. Between (M_T, Δ_T) and (M_u, Δ_U) the behavior could be obtained by using a practical model proposed by Aboud *et al.* (1995) to predict the out of plane deflection of reinforced masonry walls. However, the stiffness model is applicable only in the post cracking range. The equation for the effective stiffness interpolating between the effective and the cracked stiffness is given as

$$(EI)_{eff} = E_m I_g^f R + \alpha E_m I_{cr} (1 - R) \quad (4.11)$$

Where,

R = stiffness interpolation factor

α = reduction factor

The factor R takes into account the tension stiffening effect in the cracked masonry and thus, results in a smooth transition from an uncracked section to a fully

cracked section. It is important to mention here that the value of R is 1 upto the transition moment M_T . Also the fourth order expression is used to increase the accuracy in estimating stiffness. The equation for R is represented as

$$R = 0.4 \left(\frac{M_u - M_a}{M_u - M_{cr}} \right) + 0.6 \left(\frac{M_u - M_a}{M_u - M_{cr}} \right)^4 \quad (4.12)$$

Where,

M_a = applied bending moment (kN-m)

M_{cr} = cracking moment (kN-m)

M_u = ultimate moment (kN-m)

Based on a regression analysis, Aboud *et al.* (1995) proposed the coefficients 0.4 and 0.6 as average values in Equation 4.12 to approximate the shape of the polynomial curve. The coefficient α described in Equation 4.11 is expressed as

$$\alpha = \frac{M_u I_g^f \Delta_{cr}}{M_{cr} I_{cr} \Delta_u} \quad (4.13)$$

Where,

Δ_{cr} = mid-span deflection at cracking moment (mm)

Δ_u = mid-span deflection at ultimate moment (mm)

To summarize, the moment versus deflection model is based on a model proposed by Aboud *et al.* (1995). However, the original equations have been modified to incorporate the effects of externally applied GFRP strips. All the calculations involved have been performed in a spreadsheet using Microsoft Excel. This flexible pattern will help later in the next chapter to perform parametric studies. In plotting the response, the initial portion of the curve corresponds to a loading condition where the load induced

tensile stress is less than the modulus of rupture for masonry. A straight line is, therefore, plotted from the origin to the point where the masonry is cracked. This point is defined as a transition point between the uncracked and cracked wall cross-section. In all these calculations the load-induced moment is used as a measurable variable and corresponding deflection is then obtained from the relative equation. The cracking moment and the transition moment are obtained from Equations 4.1 and 4.2. Deflection associated with the transition moment is obtained simply from Equation 4.9. The ultimate moment is obtained by using Equation 4.5 and the corresponding deflection is obtained from Equation 4.10. The instantaneous deflection values between the transition moment and the ultimate moment is obtained by using Equation 4.9 with a replacement of M_T with M_a i.e. applied moment and EI calculated from equation 4.11. This leads to a nonlinear region between the transition and ultimate moment. The unloading path is considered linear from any value of instantaneous moment back to origin.

4.6 Comparison of Theoretical and Experimental Results

The moment versus deflection hysteresis envelopes are plotted for each specimen. Figures 4.4 through 4.12 compare the total moment and deflection obtained in the tests with the theoretical deflections obtained from the analytical model. Though the intention was to plot the push and pull response for cyclic tests on a single graph, but due to dislocation of the vertical steel during grouting, the effective depth is different for push and pull. For this reason, push and pull responses are different and therefore, separate plots for push and pull are shown. It can be seen that except for Wall-1 and Wall-6, the predicted ultimate moment is less than the ultimate moment obtained from the test (Table 4.2). This can be attributed to the typical mode of failure due to the delamination of the GFRP strip. Also, the analytical model is based on a constantly increasing monotonic loading, whereas, some specimens in this test program were subjected to fully reversed out of plane cyclic loading. The strength of a specimen subjected to out of plane cyclic loading is expected to be less than the specimen subjected to monotonic loading due to stiffness degradation. However, this phenomenon can only be justified if the specimens under consideration have similar parameters.

The ultimate deflections predicted by the model are greater than the deflections obtained from the tests except in Wall-5. This discrepancy can be attributed to the method of measuring deflections in the test program. In certain cases, the LVDT used to measure out of plane deflection ran out of travel or the wire connecting the LVDT with the masonry surface lost the contact. These situations resulted in re-adjustment of the instrument and possible error.

Various parameters associated with the test specimens are summarized in Table 4.1. The test to predicted ratios for transition moment, ultimate moment and ultimate deflection for Wall-1 through Wall-8 are shown in Table 4.2. For 200 mm monotonically loaded specimens, the test to predicted ratios for ultimate moment ranges from 0.97 to 1.14. The predicted and the actual response are in good agreement with each other. For 200 mm walls subjected to cyclic loading, the test to predicted ratios for ultimate moment ranges from 1.15 to 1.27. As mentioned earlier, due to a malfunction in the loading system, the actual response obtained from the test for Wall-3 deviated drastically from the predicted. The test to predicted ratios for 150 mm walls subjected to monotonic loading ranges from 1.02 to 1.35 and for cyclic loading ranges from 0.99 to 1.04. The overall response is in good agreement with the predicted one.

4.7 Comparison between the Two Models

A control specimen was tested by Kuzik *et al.* (1999). This specimen was reported with the name Wall-8. The specimen consisted of a 200 mm thick wall with 2-10M vertical steel rebars at 600 mm c/c. No external reinforcement was applied and the test was conducted in two stages. First, the specimen was loaded until no increase in the lateral loading was observed. Secondly, the cracked specimen obtained from stage one was reinforced externally with 2-250 mm wide GFRP strips on each face.

The major difference between the current model and the model reported by Kuzik *et al.* (1999) is that the Kuzik's model is based only on the results obtained from 200 mm thick walls with the constant amount of GFRP and a single mode of failure.

However, the current model is based on the test results obtained from 150 mm and 200 mm thick walls with varying amount of GFRP and axial load as well as different failure modes. In order to compare the validity of present model, the data obtained by Kuzik *et al.* (1999) for Wall-3 and Wall-6 was plotted using the current model. The results are presented in Table 4.3. Figure 4.13 shows a plot between the predicted moment and the ultimate moment calculated from the experiment. For the present study the ratio between the experimental moment and predicted moment ranges from 0.97 to 1.35. Whereas, this ratio ranges between 1.01 and 1.38 for the results reported by Kuzik *et al.* (1999). From the results it is clear that the present model shows good agreement with the previous model in terms of ultimate moment.

Table 4.1 Parameters Associated with Test Specimens

Specimen	Thickness (mm)	Axial Load (kN)	E_{GFRP}^1 (MPa)	E_m^2 (MPa)	Area (GFRP) ³ (mm ²)	I_{gross} (mm ⁴)	$I_{cracked}$ (mm ⁴)	$I_{modified}$ (mm ⁴)	E_{gross} (N-mm ²)	E_{crack} (N-mm ²)	$E_{modified}$ (N-mm ²)
Wall-1	200	30	27521	5100	323.85	6.35E8	2.83E8	3.68E8	3.24E12	1.44E12	1.88E12
Wall-2	200	60	27521	5100	323.85	6.35E8	2.83E8	3.68E8	3.24E12	1.44E12	1.88E12
Wall-3	200	30	27521	5100	336.8	6.36E8	2.83E8	3.69E8	3.24E12	1.44E12	1.88E12
Wall-4	200	30	27521	5100	323.85	6.27E8	2.75E8	3.61E8	3.24E12	1.4E12	1.84E12
Wall-5	150	30	27521	7650	323.85	2.57E8	1.2E8	1.43E8	1.97E12	0.92E12	1.09E12
Wall-6	150	15	27521	7650	647.7	2.63E8	1.26E8	1.48E8	2.01E12	0.96E12	1.13E12
Wall-7	150	30	27521	7650	168.4	2.54E8	1.17E8	1.4E8	1.94E12	0.9E12	1.07E12
Wall-8	150	15	27521	7650	336.8	2.57E8	1.2E8	1.43E8	1.97E12	0.92E12	1.09E12

¹ Provided by Manufacturer

² Based on $E_m = 850 f_m$

³ Based on GFRP Thickness = 1.295 mm (Provided by Manufacturer)

Table 4.2 Comparison of Experimental and Theoretical Results

Specimen	Transition Moment (kN-m)			Ultimate Moment (kN-m)			Ultimate Deflection (mm)		
	$M_{(Test)}$ (kN-m)	M_{Model} (kN-m)	M_{Test}/M_{Model}	M_{Test} (kN-m)	M_{Model} (kN-m)	M_{Test}/M_{Model}	Δ_{Test} (mm)	Δ_{Model} (mm)	$\Delta_{Test}/\Delta_{Model}$ (mm)
Wall-1	6.7	6.7	1.0	25	25.7	0.97	119	152.9	0.78
Wall-2	10.6	8.1	1.3	32	28.1	1.14	140	157.3	0.89
Wall-3	3.7	3.9	0.95	24	20.9	1.15	125	156	0.80
Wall-4	4.6	3.9	1.18	24	18.9	1.27	165	165.1	0.99
Wall-5	5.7	3.5	1.63	25	18.5	1.35	236	185.6	1.27
Wall-6	3.8	3.2	1.19	18	18.2	0.99	150	189	0.79
Wall-7	5.0	2.78	1.8	14	13.7	1.02	189	235.7	0.8
Wall-8	4.0	2.4	1.67	14	13.9	1.04	205	242	0.85

Table 4.3 Comparison of Results from the Two Models

Specimen	Axial Load (kN)	GFRP (Both Faces)	Ultimate Moment ♦		Ultimate Deflection ♦		Predicted▲ (Ultimate)
			Test	Predicted	Test	Predicted	
Wall-3	115	2-125 mm	26.5	26.3	122.2	111.5	27.9
Wall-6	30	2-250 mm	40.9	37.4	113.5	93.7	35.65

♦ Kuzik *et al.*(1999)

▲ Present Study (2001)

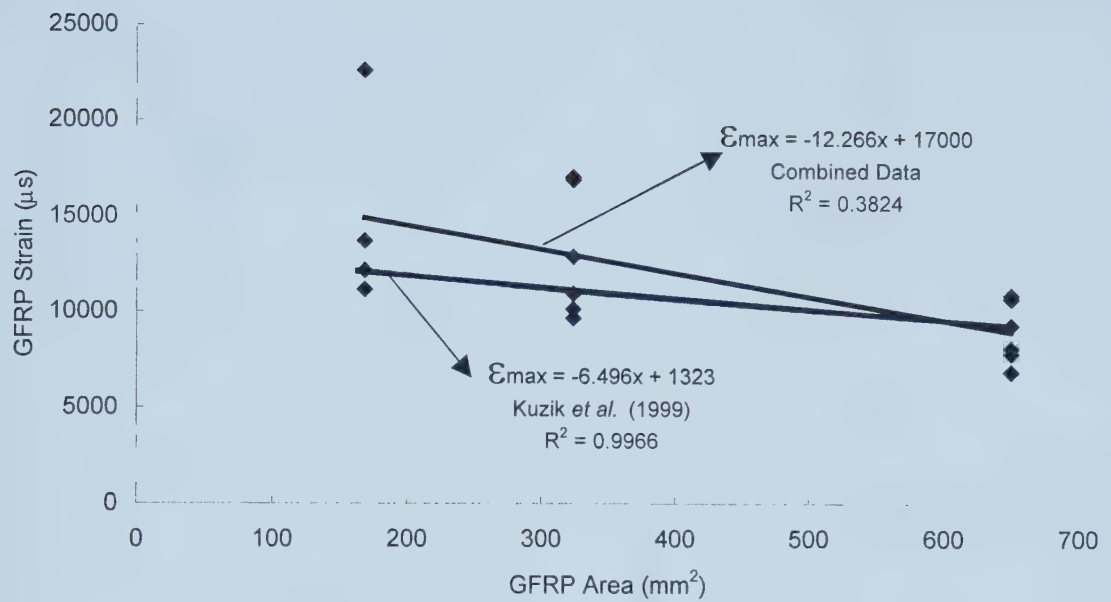


Figure 4.1 Combined Regression for Maximum Strain

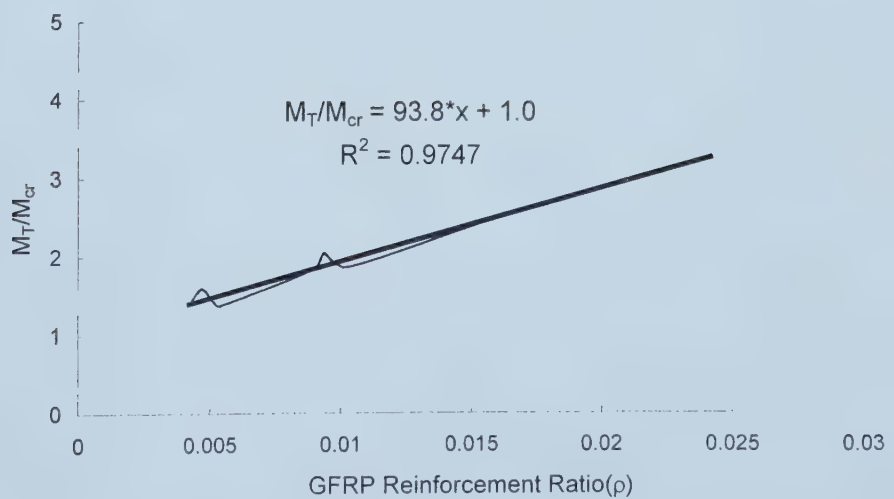


Figure 4.2 Combined Regression Analysis for Transition Moment

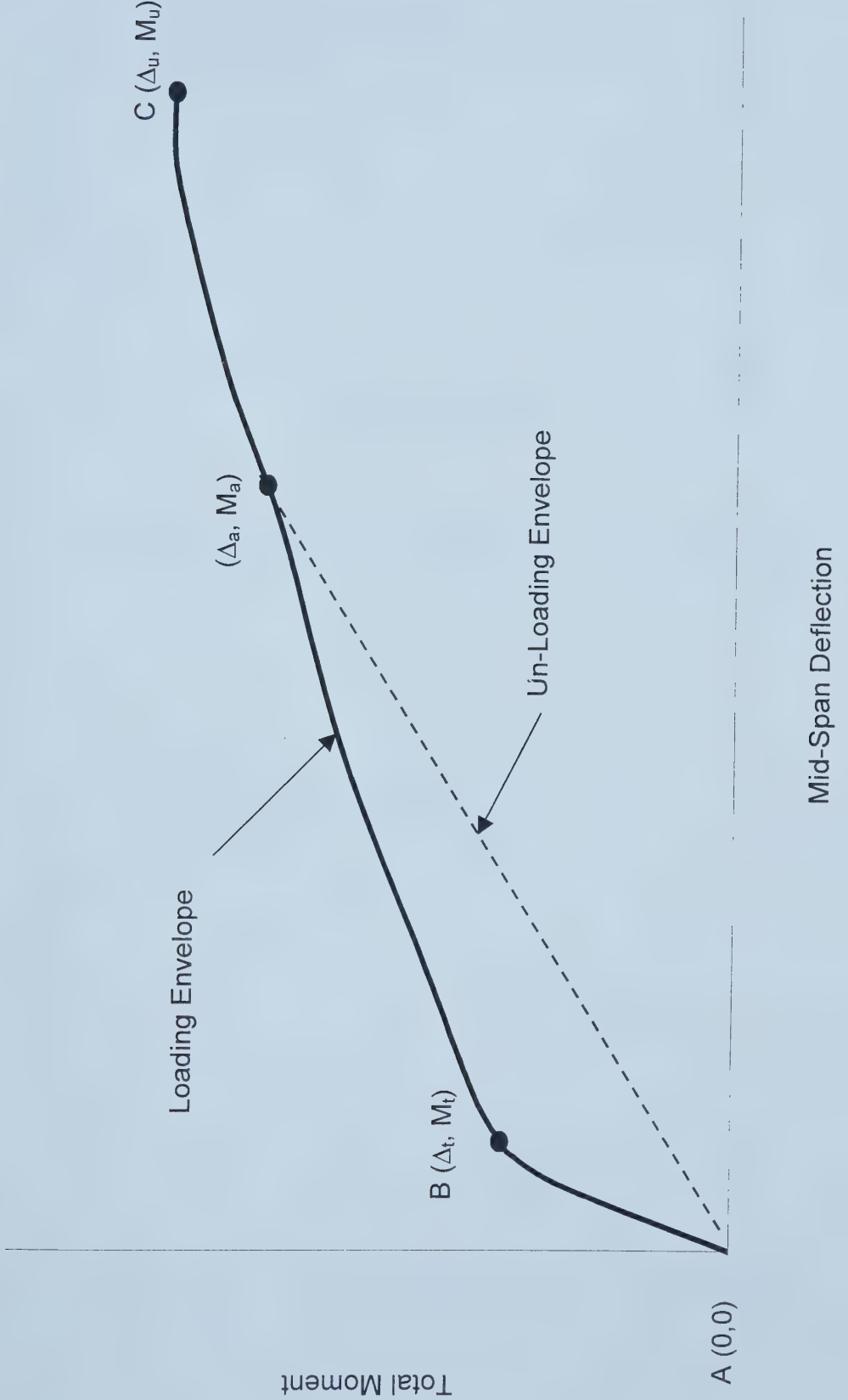


Figure 4.3 Typical Loading Envelope

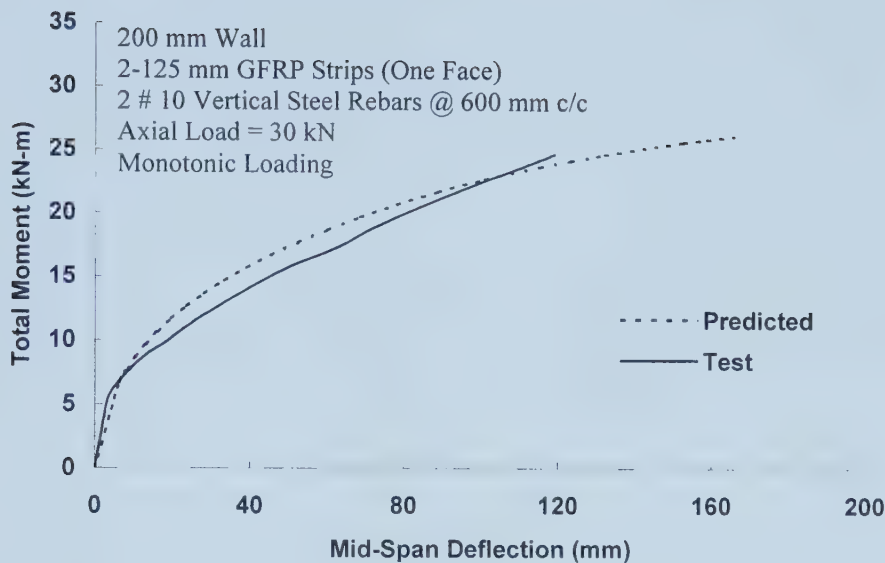


Figure 4.4 Response of Wall-1 Test versus Predicted

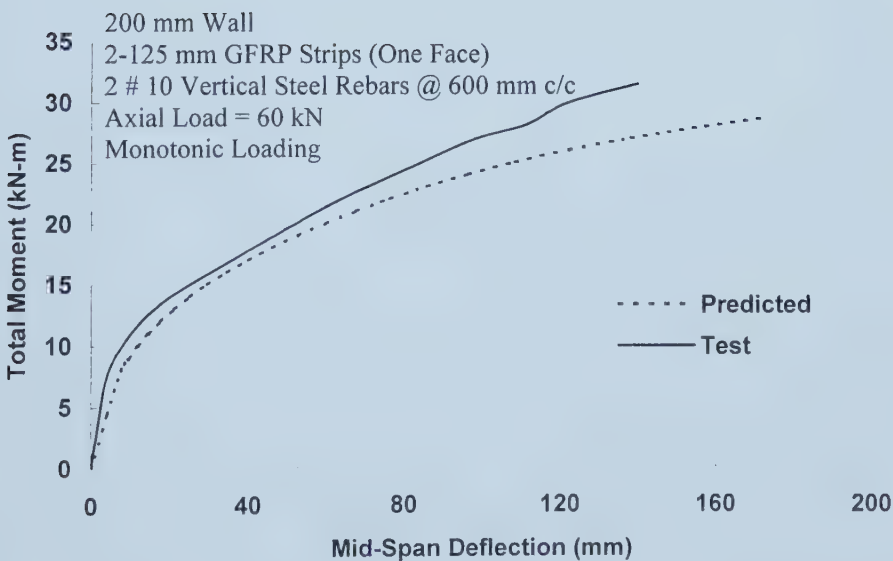


Figure 4.5 Response of Wall-2 Test versus Predicted

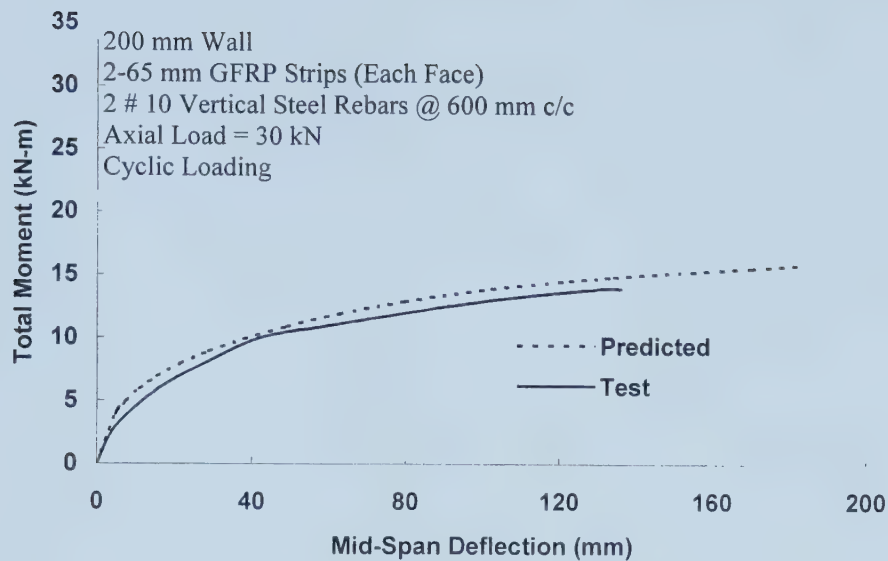


Figure 4.6a Response of Wall-3 Test versus Predicted (Pull)

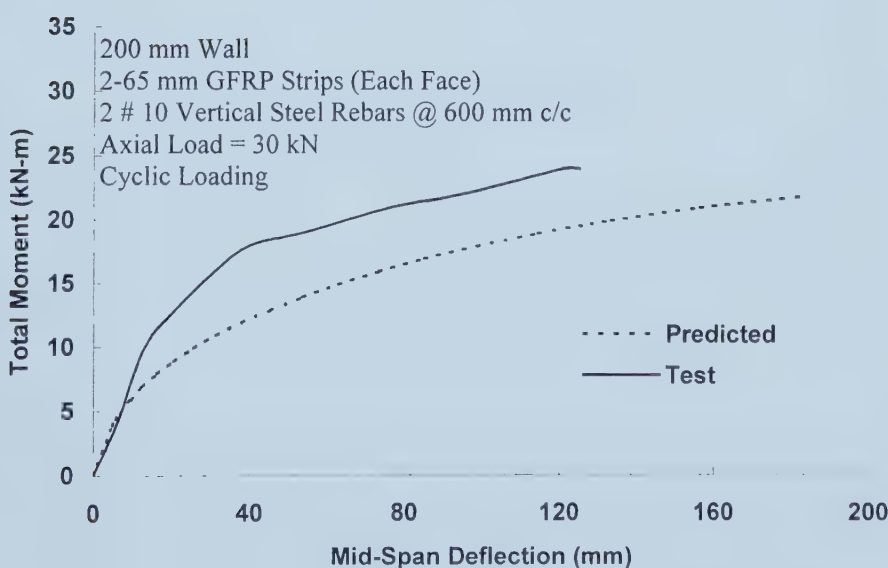


Figure 4.6b Response of Wall-3 Test versus Predicted (Push)

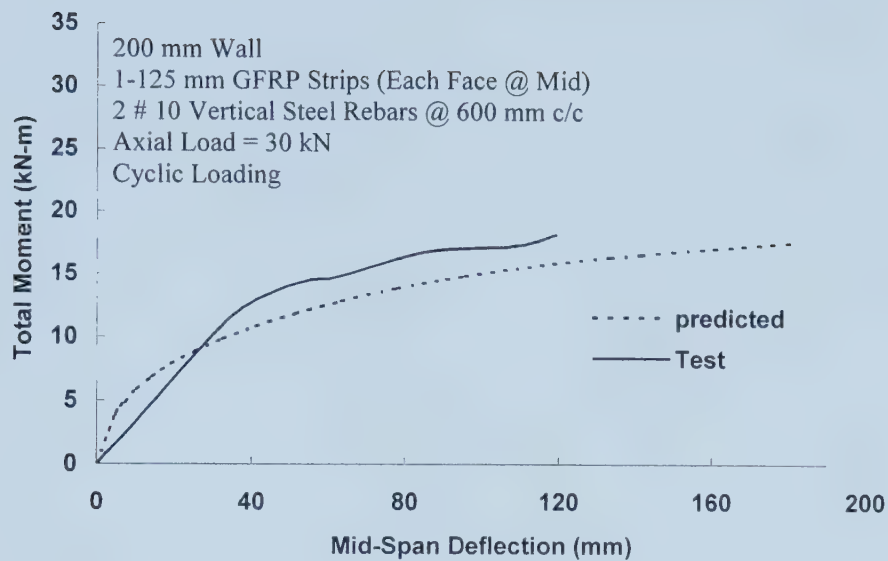


Figure 4.7a Response of Wall-4 Test versus Predicted (Push)

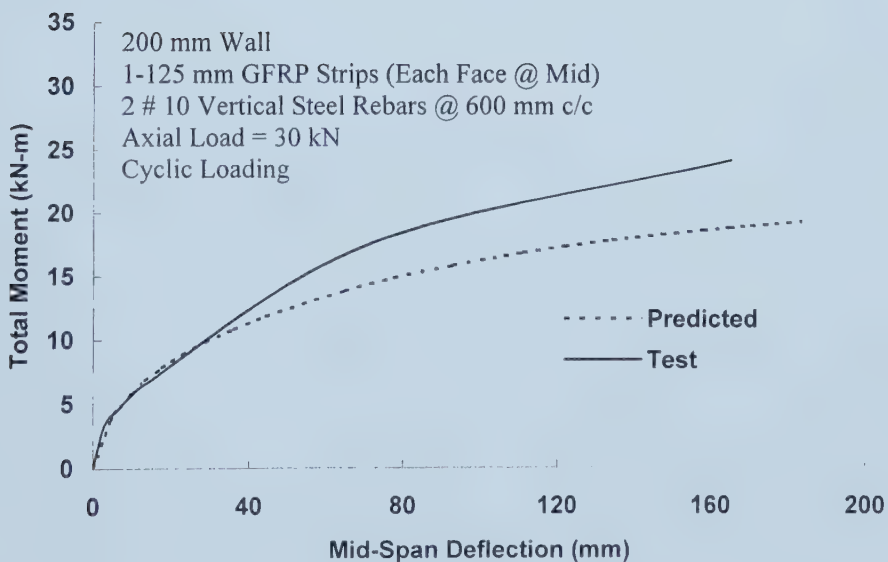


Figure 4.7b Response of Wall-4 Test versus Predicted (Pull)

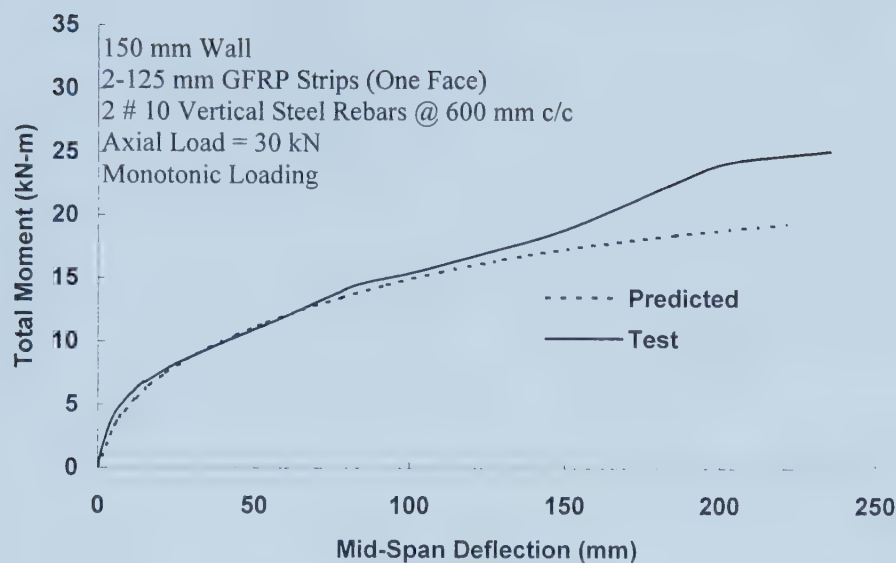


Figure 4.8 Response of Wall-5 Test versus Predicted

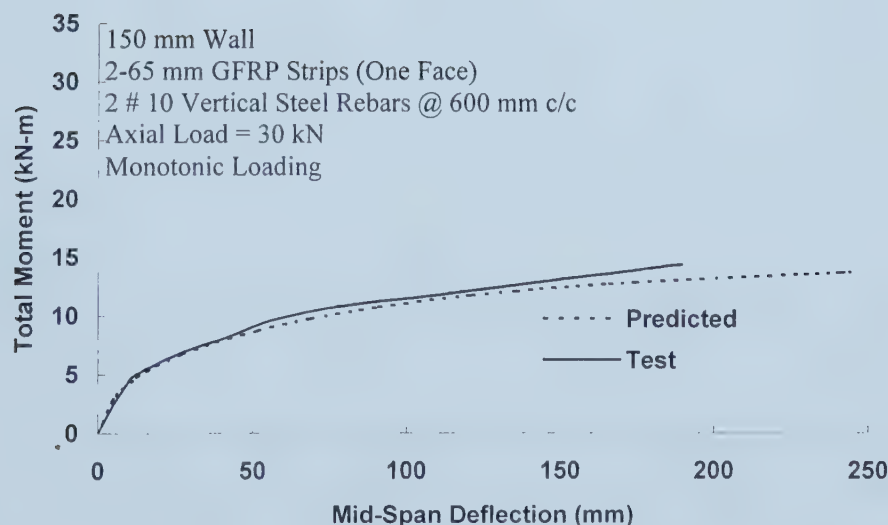


Figure 4.9 Response of Wall-7 Test versus Predicted

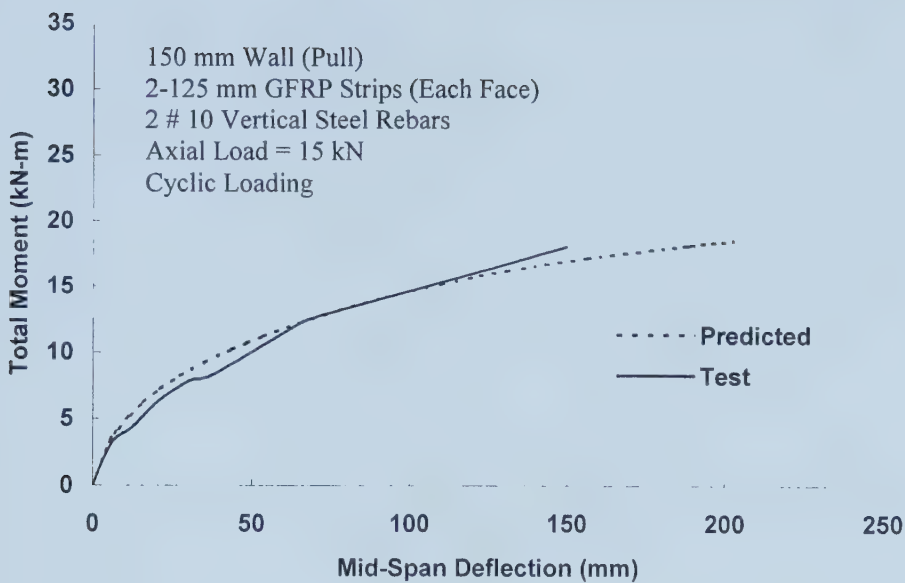


Figure 4.10a Response of Wall-6 Test versus Predicted (Pull)

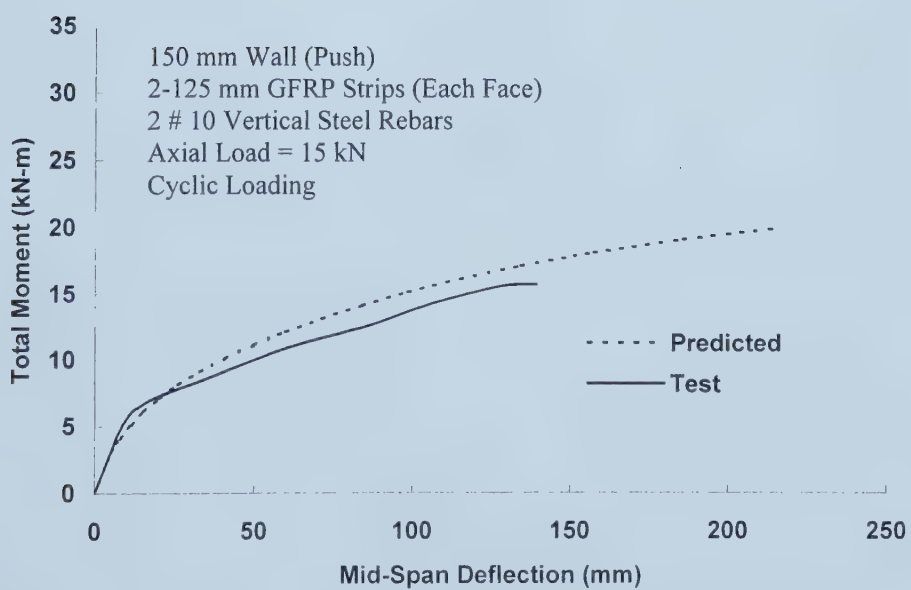


Figure 4.10b Response of Wall-6 Test versus Predicted (Push)

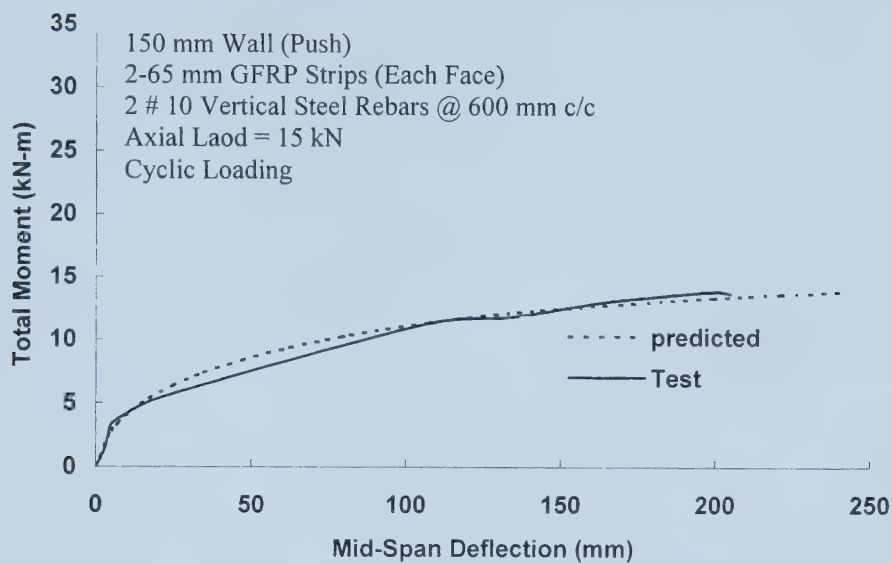


Figure 4.11a Response of Wall-8 Test versus Predicted (Push)

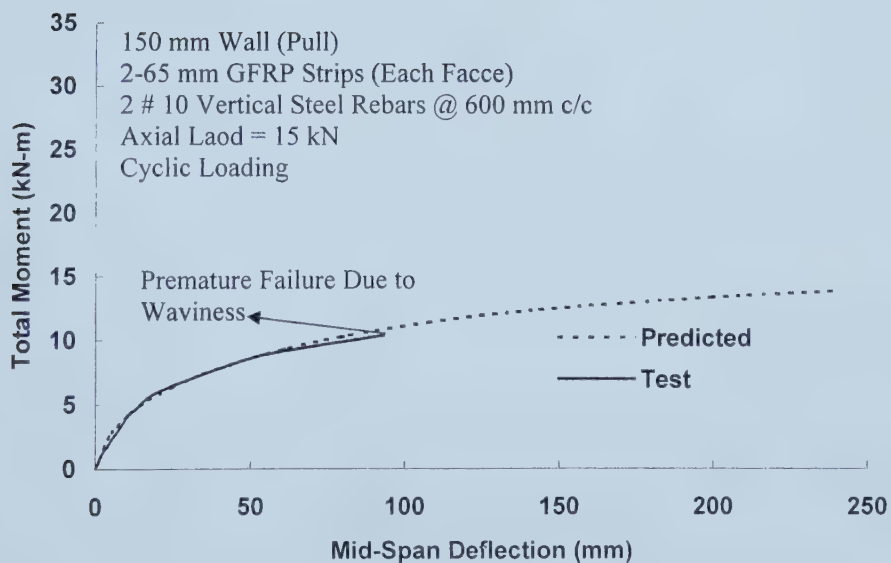


Figure 4.11b Response of Wall-8 Test versus Predicted (Pull)

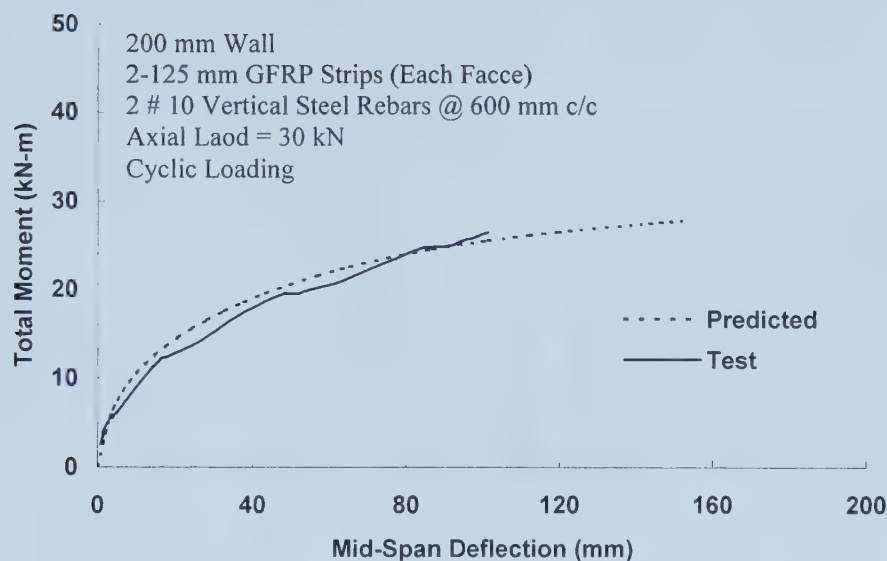


Figure 4.12a Response of Wall-3(Kuzik et al) Test versus Predicted

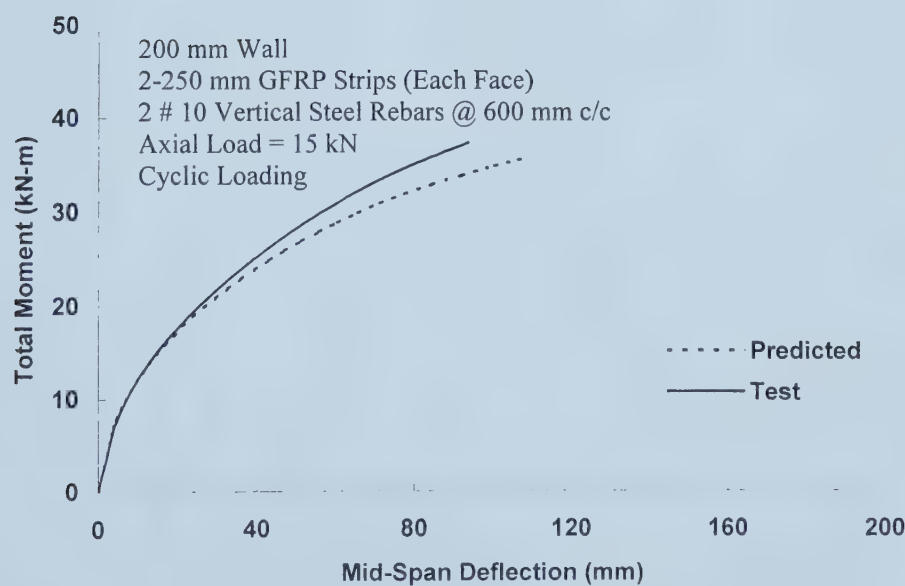


Figure 4.12b Response of Wall-6(Kuzik et al) Test versus Predicted

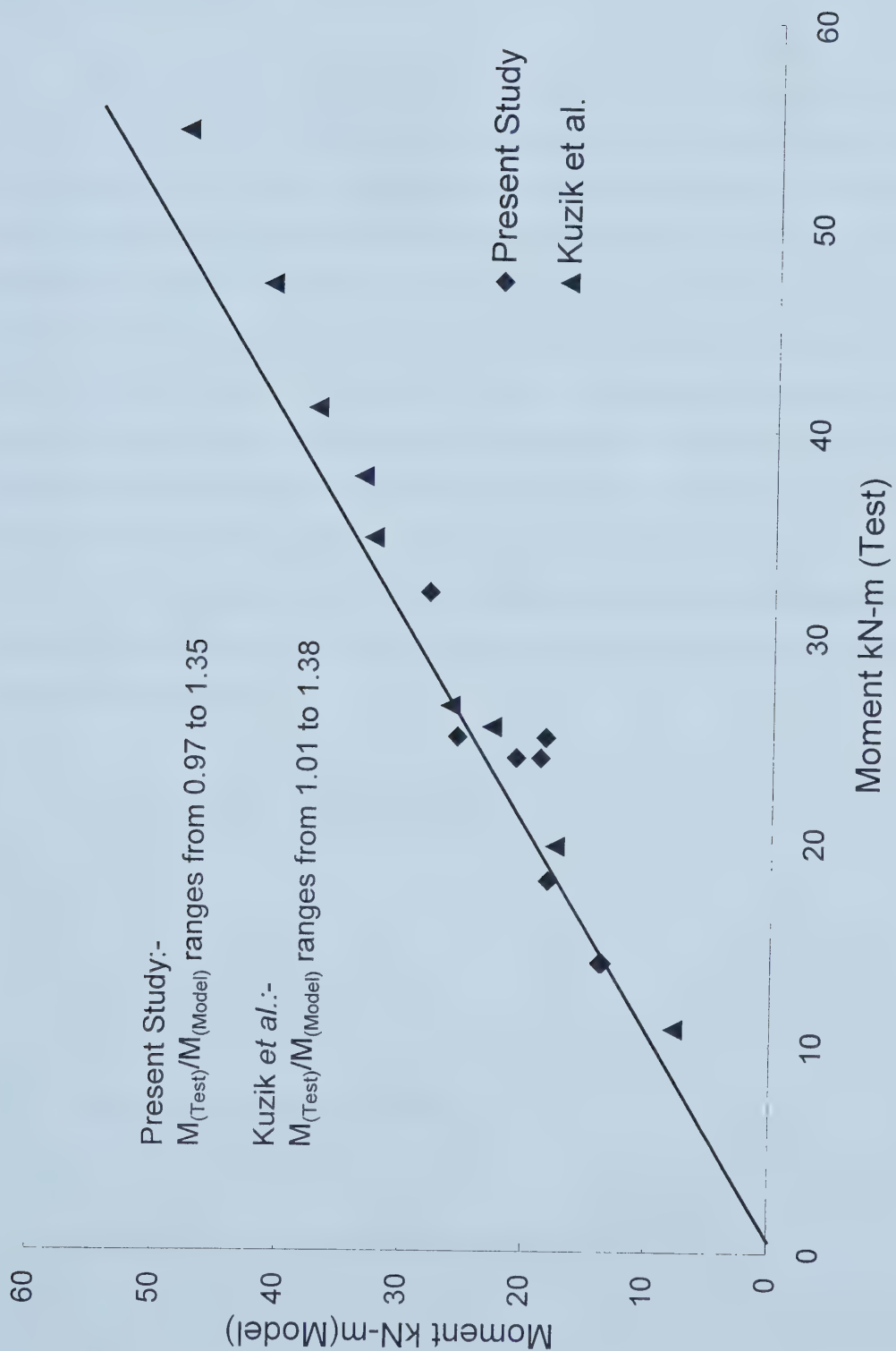


Figure 4.13 Moment(Test) versus Moment(Model)

Chapter 5

PARAMETRIC STUDY

5.1 Introduction

The analytical model assembled in Chapter 4 was used to perform a parametric study. However, a brief summary of the analytical model is given here. The analytical model proposed in Chapter 4 predicts the out-of-plane behavior of reinforced masonry walls strengthened externally with composite material sheets. The model basically predicts two points of bending moments and associated deflections for a given wall height. The first point is defined as the “Transition moment” and represents the end of linear behavior. Up to this point the masonry is assumed uncracked, although the cracking moment might have a smaller value than the transition moment. Beyond the transition moment the flexural cracks in the masonry bed joints engage the externally bonded GFRP and then spread along the height of a block between two joints. This portion of the response is predicted by using a non-linear stiffness degradation model proposed by Abboud *et al.* (1995). The equations used to assemble the analytical model are summarized below.

$$M_T = \left[f_t + \frac{P}{A_e} \right] \left[\left(\frac{2I_g'}{h} \right) (1 + 93.8\rho_{GFRP}) \right] \quad 4.2$$

$$\rho_{GFRP} = \frac{A_{GFRP}.E_{GFRP}}{A_e.E_m} \quad 4.3$$

$$\varepsilon_{uGFRP} = -12.26.A_{GFRP} + 17000 \quad 4.4$$

$$M_u = A_s f_s \left(d - \frac{a}{2} \right) + (A_{GFRP}.E_{GFRP}.\varepsilon_{uGFRP}) \left[\left(h + \frac{t_{GFRP}}{2} \right) - \frac{a}{2} \right] \quad 4.5$$

$$a = \frac{P + A_s f_s + A_{GFRP} E_{GFRP} \epsilon_{u,GFRP}}{0.85 f' m b} \quad 4.7$$

$$\Delta_T = \frac{M_T}{E_m I_g^f} \frac{(3L^2 - 4x^2)}{24} \quad 4.9$$

$$\Delta_u = \left[\frac{\epsilon_{u,GFRP}}{h-a} \right] \cdot \left[\frac{(3L^2 - 4x^2)}{24 \left(1 - 2 \cdot \frac{S_{cr}}{L} \right)} \right] \quad 4.10$$

In the parametric study various wall thicknesses, widths of GFRP strips, axial loads and steel reinforcement ratios were considered. Table 5.1 shows the various parameters considered.

5.2 Selection of various parameters

As discussed in previous chapters, Kuzik *et al.* (1999) tested eight full-scale masonry wall specimens constructed with 200 mm hollow concrete blocks. These walls were lightly reinforced with vertical steel rebars. GFRP strips of 250 mm width were used as external reinforcement for most of the specimens. Previous work on reinforced masonry walls strengthened with GFRP did not address any parametric study involving various thickness of masonry units, spacing of vertical steel and various levels of axial loads. In the present study, two groups of walls comprising 200 mm and 150 mm thickness were tested with varying amount of GFRP and axial load. Various parameters associated with the specimens are described in Table 2.7. The results were shown and described in Chapter 3. The results obtained from the analytical model developed in Chapter 4 show good confidence in predicting the ultimate moment and deflection.

In order to assist in the development of a design tool using the analytical model assembled in Chapter 4, a parametric study was performed. Walls comprising 250 mm unit thickness were included in the parametric study as the analytical model successfully

predicted the response of 150 mm and 200 mm thick walls. In the tests carried out to date, the vertical steel was kept constant as 10M rebars at 600 mm c/c. This steel ratio is consistent with a low ratio typically used in older masonry structures. For the parametric study, spacing of 800 mm and 1200 mm were considered with 15M rebars. All the specimens tested in the present study were partially grouted, cores with vertical steel rebars being the only grouted cores. This trend of partially grouted walls is commonly used by the construction industry and is perceived as more economical and efficient than fully grouted walls. Masonry units with compressive strength of 10 MPa, 15 MPa and 20 MPa were considered, as these are the commonly available units in the masonry market. The masonry strength ($f'm$) was calculated by using linear interpolation in the values given in Table 5 of S304.1-94. A brief summary of the various parameters considered is given in Table 5.1.

5.3 Results of Parametric Study

As mentioned earlier, each parameter was varied while keeping others as constant to study the parametric effect. Results obtained from the parametric study are presented in the form of plots and tables and discussed in the rest of this chapter. Among the graphs, which show a similar behavior only few will be discussed in detail to avoid duplication. Among the various parameters, the glass fiber axial stiffness was calculated simply by multiplying the area of the GFRP with the modulus of elasticity of the GFRP. Deflections corresponding to transition moment were obtained from the graphs and flexural stiffness EI_T is calculated using Equation 4.9. Since all the variables in Equation 4.9 are known except E and I, therefore, equation can be solved for the product EI_T . Tables 5.2(a, b, c,), 5.3(a, b, c) and 5.4(a, b, c) list the results of the study for the 150 mm, 200 mm and 250 mm walls respectively. These tables represent a summary of values obtained for the transition moment, ultimate moment and the corresponding deflections. Figures 5.1 to 5.3 show typical graphs plotted between moment and mid-span deflection values obtained from the analytical model for various parametric values. The plots obtained show expected behavior so that the 150 mm thick masonry walls exhibit a more ductile behavior as compared to 200 mm and 250 mm walls. In other words,

200 mm and 250 mm thick walls attracted greater loads and less deformation. The model thus behaves regularly with no anomalies.

For the purpose of this study, the most important parameter is the amount of FRP bonded to the walls. The effects of all other parameters will be measured against the amount of GFRP. Four quantities are of primary importance namely M_T , Δ_T , M_U and Δ_U . The quantities M_T and Δ_T will be combined in a single quantity, M_T/Δ_T , which is proportional to EI/l^2 and will be called flexural stiffness. This quantity is important for serviceability requirements. For simplicity l^2 will be dropped as a geometric parameter. The ultimate deflection, Δ_U is important because it relates to the ductility of the system. It will however be related to Δ_T in a non-dimensional quantity Δ_U/Δ_T . In the following each quantity will be discussed separately. Throughout this chapter the discussion can be generalized as quantitative and qualitative.

5.3.1 Ultimate Moment versus Various Parameters

A very large number of graphs could be obtained from the data generated. To illustrate the important points of the study only a small number of graphs have been plotted. As mentioned earlier the results are summarized in the form of tables and graphs. However, through the rest of this chapter, the comparisons will concentrate primarily on the results of the 15 MPa units.

5.3.1.1 Amount of External GFRP Reinforcement

The ultimate moment capacity obtained for various wall thicknesses with varying amount of vertical steel, masonry strength and block thickness is shown in Table 5.5(a) through 5.5(c). These tables represent the comparison of the ultimate moment capacities of the walls without external GFRP reinforcement with the walls reinforced with 2-65mm GFRP strips. For these units the ultimate moment results versus the area of GFRP for the different unit thicknesses for ordinary reinforcement patterns of 15M @ 400 mm,

800 mm and 1200 mm presented in Figures 5.4 through 5.6 respectively; all for an applied axial load of 15 kN. The first figures are combined in Figures 5.7 through 5.9. These plots are repeated for an axial load of 30 kN in Figure 5.10 through 5.12 and for 60 kN axial load in Figures 5.13 through 5.15.

The results obtained clearly shows that amount of GFRP reinforcement has a decided and regular influence on the ultimate moment capacity. For example if one considers the 150 mm block wall subjected to 15 kN load with 15M rebars @ 1200 mm c/c as shown in Figure 5.6, the increase in ultimate moment capacity is 415% due to the provision of 2-65 mm GFRP strips. Therefore, even the provision of minimal amounts of GFRP reinforcement, 2-65 mm for this study, has a significant effect on the ultimate moment capacity. The maximum increase (592 %) in ultimate moment capacity due to minimum GFRP reinforcement was observed in 150 mm walls with 10 MPa unit strength and vertical steel at maximum spacing (15M @ 1200 mm c/c). Similarly the minimum gain (113 %) in ultimate moment capacity was observed in 250 mm walls with 20 MPa unit strength and minimum vertical steel spacing (15M @ 400 mm c/c).

The influence of GFRP reinforcement increases dramatically as the amount of steel reinforcement decreases. Figures 5.16 through 5.24 show this behavior. For example if one considers 200 mm walls with 15 MPa of masonry unit strength and reinforced with 15M @ 1200 mm c/c, the increase in moment capacity is 296 % when one increases the amount of GFRP from none to 2-65 mm (168 mm^2). The maximum increase in ultimate moment capacity by using 2-65 mm GFRP reinforcement is 592% and this is attributed to 150 mm wall with 10 MPa unit strength with vertical steel at 1200 mm c/c. Similarly minimum increase in ultimate moment capacity is 113% and is associated with 250 mm wall with 20 MPa units and vertical steel reinforcement at 400 mm c/c. Similarly in 200 mm walls the maximum increase is 342 % and the minimum is 136 %. For 250 mm walls the maximum increase is 277 % and the minimum increase is 113 %. The numerical values mentioned in the discussion above are summarized in Tables 5.5(a) through 5.5(c).

5.3.1.2 Amount of vertical Steel Reinforcement

The compressive strength of reinforced masonry $f'm$ is based on the amount of vertical steel reinforcement and therefore depends on the number of grouted cores in the specimen. Figures 5.25 through 5.33 show the plots associated with various spacings of vertical steel reinforcement for different thicknesses of walls and external GFRP reinforcement. The plots are presented for 15 kN, 30 kN and 60 kN axial loads. Numerical results are shown in Tables 5.6(a) through 5.6(c). In general decreasing the amount of vertical steel reinforcement i.e. increasing the spacing of vertical steel, reduces the ultimate capacity. However, in some cases especially with masonry unit strength of 10 MPa and 20 MPa, the ultimate capacity slightly increases due to an increase in the $f'm$ value. The graphs presented in Figures 5.25 through 5.33 are representative of 15 MPa units only and therefore, this behavior cannot be seen in the plots.

The maximum decrease in the ultimate moment capacity as observed in 250 mm walls with 20MPa units is 31% when the spacing of vertical steel reinforcement is increased from 800 mm to 1200 mm c/c. For 150 mm and 200 mm walls the decrease in ultimate moment capacity is 28% and 30% respectively. The values mentioned above are associated with the specimens in which the amount of GFRP is minimum i.e. 2 -65 mm strips and when the spacing of vertical steel is increased from 800 mm to 1200 mm c/c. As mentioned earlier, in some instances the decrease in amount of vertical steel increases the ultimate moment capacity. This behavior is associated with 10 MPa masonry units only for the 150 mm, 200 mm and 250 mm wall thicknesses. Also this behavior is more obvious in 150 mm thick walls and negligible in 250 mm walls. The general behavior of decrease in ultimate moment capacity due to decrease in amount of vertical steel reinforcement is more obvious in 250 mm walls.

5.3.1.3 Masonry Unit Strength

Increasing the area of GFRP while increasing the masonry unit strength considerable increase the ultimate moment capacity. Figures 5.25 through 5.33 show the plots for 15 MPa unit strength only with various amounts of GFRP reinforcement and axial loads. Numerical results are presented in Tables 5.7(a) through 5.7(c). For example Table 5.7(a) shows the maximum percent increase in ultimate moment capacity (61.8 %) for 150 mm thick walls with 15M @ 400 mm c/c and 2-250 mm GFRP strips. This increase is obtained when the unit strength is increased from 15 MPa to 20 MPa. The minimum increase as shown in Table 5.7(c) is 2.6 %. This is attributed to 250 mm Walls with 15M @ 1200 mm c/c and 2-65 mm (161 mm^2) GFRP strips. The increase is obtained if masonry unit strength is increased from 15 MPa to 20 MPa. As shown in Table 5.7(a) through 5.7(c), the maximum increase in ultimate moment capacity is obtained for walls with maximum GFRP strips, 2-250 mm for this study, while the minimum increase in ultimate moment capacity is obtained for walls with minimum GFRP and low vertical reinforcement ratio.

5.3.1.4 Masonry Unit Thickness

Increase in masonry unit thickness always results in an increase of ultimate moment capacity due to increase in the flexural stiffness of the wall. However, increasing the masonry unit thickness increases the efficiency of external GFRP reinforcement. Figures 5.4 through 5.6 show the ultimate moment capacity plotted against various wall thicknesses and amount of GFRP. Numerical results are presented in Tables 5.8(a) through 5.8(c). The increase in ultimate moment capacity due to increase in masonry unit thickness is more for walls with high vertical steel reinforcement ratio and higher amount of GFRP. However, for low vertical steel reinforcement ratios, the increase in ultimate moment capacity due to change in masonry unit thickness is almost negligible.

The maximum increase in ultimate moment capacity due to increase in masonry unit thickness as presented in Table 5.8(a) is 62.6%. This is associated with

200 mm wall reinforced with 10M @ 400 mm c/c and 2-250 mm GFRP reinforcement and by changing masonry unit thickness from 150 to 200 mm. The minimum increase in ultimate moment capacity is 27.6 %. In general the weakest walls, the 150 mm walls with 10 MPa unit strength and with vertical steel reinforcement at 400 mm c/c appears to have gained maximum increase in ultimate moment capacity, when the unit thickness is changed from 150 mm to 200 mm.

5.3.1.5 Effect of Constant Axial Load

Amount of constant axial load has little effect on ultimate moment capacity. Figures 5.34 through 5.42 show the relationship between axial load and ultimate moment capacity for various wall thicknesses and amount of GFRP reinforcement and vertical steel reinforcement.

5.4 Flexural Stiffness versus Various Parameters

Figures 5.43 through 5.60 show various graphs plotted for flexural Stiffness (EI_T) versus various parameters. From the graphs it is clear that amount of external GFRP reinforcement has very little effect on the flexural stiffness EI_T .

Unit Strength (MPa)	Unit Thickness (mm)	Vertical Steel	Area GFRP (mm) ²	Axial Load (kN)
10, 15, 20	150	15 M @ 400mm c/c	2-65 mm = 168.4	15, 30, 60
10, 15, 20	150	15 M @ 400mm c/c	2-125 mm = 323.85	15, 30, 60
10, 15, 20	150	15 M @ 400mm c/c	2-250 mm = 647.7	15, 30, 60
10, 15, 20	200	15 M @ 400mm c/c	2-65 mm = 168.4	15, 30, 60
10, 15, 20	200	15 M @ 400mm c/c	2-125 mm = 323.85	15, 30, 60
10, 15, 20	200	15 M @ 400mm c/c	2-250 mm = 647.7	15, 30, 60
10, 15, 20	250	15 M @ 400mm c/c	2-65 mm = 168.4	15, 30, 60
10, 15, 20	250	15 M @ 400mm c/c	2-125 mm = 323.85	15, 30, 60
10, 15, 20	250	15 M @ 400mm c/c	2-250 mm = 647.7	15, 30, 60
10, 15, 20	150	15 M @ 800mm c/c	2-65 mm = 168.4	15, 30, 60
10, 15, 20	150	15 M @ 800mm c/c	2-125 mm = 323.85	15, 30, 60
10, 15, 20	150	15 M @ 800mm c/c	2-250 mm = 647.7	15, 30, 60
10, 15, 20	200	15 M @ 800mm c/c	2-65 mm = 168.4	15, 30, 60
10, 15, 20	200	15 M @ 800mm c/c	2-125 mm = 323.85	15, 30, 60
10, 15, 20	200	15 M @ 800mm c/c	2-250 mm = 647.7	15, 30, 60
10, 15, 20	250	15 M @ 800mm c/c	2-65 mm = 168.4	15, 30, 60
10, 15, 20	250	15 M @ 800mm c/c	2-125 mm = 323.85	15, 30, 60
10, 15, 20	250	15 M @ 800mm c/c	2-250 mm = 647.7	15, 30, 60
10, 15, 20	150	15 M @ 1200mm c/c	2-65 mm = 168.4	15, 30, 60
10, 15, 20	150	15 M @ 1200mm c/c	2-125 mm = 323.85	15, 30, 60
10, 15, 20	150	15 M @ 1200mm c/c	2-250 mm = 647.7	15, 30, 60
10, 15, 20	200	15 M @ 1200mm c/c	2-65 mm = 168.4	15, 30, 60
10, 15, 20	200	15 M @ 1200mm c/c	2-125 mm = 323.85	15, 30, 60
10, 15, 20	200	15 M @ 1200mm c/c	2-250 mm = 647.7	15, 30, 60
10, 15, 20	250	15 M @ 1200mm c/c	2-65 mm = 168.4	15, 30, 60
10, 15, 20	250	15 M @ 1200mm c/c	2-125 mm = 323.85	15, 30, 60
10, 15, 20	250	15 M @ 1200mm c/c	2-250 mm = 647.7	15, 30, 60

Table 5.1 Various Combinations of Parameters Used for Parametric Study

Area of Vertical Steel (mm ²)	Area of GFRP (mm ²)	Axial Load kN	Transition Moment (kN-m)	Transition Deflection Δ _T	Ultimate Moment kN-m	Ultimate Deflection (mm)	Moment @ L/360 kN-m
600 ^a	168.4 ^d	15	2.9	8.1	16.97	359	3.5
600	323.85 ^e	15	4.2	11.3	20.29	340	4.1
600	647.7 ^f	15	7.2	18.0	22.31	232	5.7
400 ^b	168.4	15	2.8	6.7	16.31	291	3.9
400	323.85	15	3.9	9.1	20.87	275	4.4
400	647.7	15	6.5	14.2	24.85	206	5.6
200 ^c	168.4	15	2.7	6.3	13.43	256	3.8
200	323.85	15	3.8	8.6	18.77	241	4.4
200	647.7	15	6.4	13.3	23.82	183	5.7
600	168.4	30	3.3	9.2	16.54	373	3.6
600	323.85	30	4.8	12.9	19.8	354	4.4
600	647.7	30	8.2	20.5	21.77	242	6.5
400	168.4	30	3.1	7.6	16.03	299	3.9
400	323.85	30	4.5	10.4	20.53	282	4.6
400	647.7	30	7.5	16.3	24.45	212	6.1
200	168.4	30	3.1	7.2	13.25	262	3.9
200	323.85	30	4.4	9.8	18.53	246	4.7
200	647.7	30	7.3	15.2	23.53	188	6.1
600	168.4	60	4.2	11.5	15.7	402	4.2
600	323.85	60	6.0	16.1	18.8	386	5.1
600	647.7	60	10.3	25.6	20.7	266	8.5
400	168.4	60	3.9	9.5	15.5	315	4.2
400	323.85	60	5.6	13.0	19.85	299	5.1
400	647.7	60	9.3	20.3	23.66	226	7.4
200	168.4	60	3.9	9.0	12.9	273	4.2
200	323.85	60	5.4	12.2	18.06	258	5.1
200	647.7	60	9.1	19.0	22.94	197	7.4

^a 15M @ 400 c/c ^d 2-65mm GFRP Strips
^b 15M @ 800 c/c ^e 2-125mm GFRP Strips
^c 15 M @ 1200 c/c ^f 2-250mm GFRP Strips

Table 5.2(a) 150 mm Units, Unit Strength = 10 MPa

Area of Vertical Steel (mm ²)	Area of GFRP (mm ²)	Axial Load kN	Transition Moment (kN-m)	Transition Deflection Δ _T	Ultimate Moment kN-m	Ultimate Deflection (mm)	Moment @ L/360 kN-m
600 ^a	168.4 ^d	15	2.4	3.9	21.31	293	4.9
600	323.85 ^e	15	3.1	5.0	26.95	285	5.5
600	647.7 ^f	15	4.8	7.3	34.46	254	6.5
400 ^b	168.4	15	2.4	3.8	18.2	269	4.8
400	323.85	15	3.1	4.9	24.39	261	5.4
400	647.7	15	4.7	7.2	32.72	232	6.4
200 ^c	168.4	15	2.3	3.6	14.47	249	4.5
200	323.85	15	3.0	4.6	21.24	241	5.3
200	647.7	15	4.6	6.7	30.66	215	6.5
600	168.4	30	2.7	4.4	21.05	298	5.0
600	323.85	30	3.6	5.7	26.6	290	5.7
600	647.7	30	5.5	8.4	34.09	259	6.7
400	168.4	30	2.7	4.4	18.04	273	4.8
400	323.85	30	3.5	5.6	24.16	265	5.5
400	647.7	30	5.4	8.2	32.42	236	6.7
200	168.4	30	2.7	4.2	14.3	253	4.7
200	323.85	30	3.5	5.3	21.08	245	5.6
200	647.7	30	5.3	7.7	30.43	218	6.8
600	168.4	60	3.4	5.6	20.53	308	5.2
600	323.85	60	4.5	7.1	26.03	301	6.0
600	647.7	60	6.8	10.4	33.35	269	7.0
400	168.4	60	3.4	5.5	17.66	282	5.1
400	323.85	60	4.4	7.0	23.69	274	5.8
400	647.7	60	6.8	10.3	31.82	244	7.1
200	168.4	60	3.3	5.2	14.11	259	4.9
200	323.85	60	4.3	6.6	20.75	252	5.8
200	647.7	60	6.6	9.6	29.97	224	7.2

^a 15M @ 400 c/c ^d 2-65mm GFRP Strips
^b 15M @ 800 c/c ^e 2-125mm GFRP Strips
^c 15 M @ 1200 c/c ^f 2-250mm GFRP Strips

Table 5.2(b) 150 mm Units, Unit Strength = 15 MPa

Area of Vertical Steel (mm ²)	Area of GFRP (mm ²)	Axial Load kN	Transition Moment (kN-m)	Transition Deflection Δ _T	Ultimate Moment kN-m	Ultimate Deflection (mm)	Moment @ L/360 kN-m
600 ^a	168.4 ^d	15	2.2	2.8	22.74	277	5.7
600	323.85 ^e	15	2.8	3.5	29.27	272	6.4
600	647.7 ^f	15	4.0	4.9	39.2	253	7.4
400 ^b	168.4	15	2.2	2.7	19.2	260	5.5
400	323.85	15	2.7	3.3	26.26	255	6.3
400	647.7	15	3.9	4.6	37.19	237	7.5
200 ^c	168.4	15	2.2	2.5	15.0	246	5.2
200	323.85	15	2.7	3.1	22.55	241	6.2
200	647.7	15	3.8	4.3	34.46	225	7.5
600	168.4	30	2.5	3.2	22.54	281	5.8
600	323.85	30	3.2	4.0	29.03	276	6.5
600	647.7	30	4.6	5.6	38.88	257	7.6
400	168.4	30	2.5	3.0	19.06	263	5.7
400	323.85	30	3.1	3.8	26.08	258	6.5
400	647.7	30	4.5	5.2	36.95	240	7.7
200	168.4	30	2.5	2.9	14.91	248	5.3
200	323.85	30	3.1	3.5	22.42	243	6.4
200	647.7	30	4.4	4.9	34.27	227	7.7
600	168.4	60	3.1	4.0	22.13	287	6.0
600	323.85	60	3.9	5.0	28.55	283	6.7
600	647.7	60	5.7	7.0	38.27	264	7.1
400	168.4	60	3.1	3.8	18.77	269	5.8
400	323.85	60	3.9	4.7	25.71	263	6.7
400	647.7	60	5.6	6.5	36.72	246	8.0
200	168.4	60	3.1	3.6	14.72	253	5.5
200	323.85	60	3.8	4.4	22.17	248	6.6
200	647.7	60	5.4	6.1	33.90	232	8.0

^a 15M @ 400 c/c ^d 2-65mm GFRP Strips
^b 15M @ 800 c/c ^e 2-125mm GFRP Strips
^c 15 M @ 1200 c/c ^f 2-250mm GFRP Strips

Table 5.2(c) 150 mm Units, Unit Strength = 20 MPa

Area of Vertical Steel (mm ²)	Area of GFRP (mm ²)	Axial Load kN	Transition Moment (kN-m)	Transition Deflection Δ _T		Ultimate Moment kN-m	Ultimate Deflection (mm)	Moment @ L/360 kN-m
				Deflection	Δ _T			
600 ^a	168.4 ^d	15	4.8	5.1	26.36	220	7.6	
600	323.85 ^e	15	6.5	6.9	31.81	200	8.7	
600	647.7 ^f	15	10.5	10.5	35.27	132	10.7	
400 ^b	168.4	15	4.5	4.3	23.77	194	7.8	
400	323.85	15	6.1	5.6	30.65	178	9.1	
400	647.7	15	9.6	8.4	36.84	129	11.2	
200 ^c	168.4	15	4.5	4.1	18.9	178	7.4	
200	323.85	15	6.0	5.3	26.62	164	9.0	
200	647.7	15	9.3	7.9	34.09	122	11.2	
600	168.4	30	5.3	5.7	25.93	225	7.7	
600	323.85	30	7.2	7.7	31.32	204	9.0	
600	647.7	30	11.6	11.7	34.74	135	11.1	
400	168.4	30	5.0	4.8	23.48	197	8.0	
400	323.85	30	6.8	6.3	30.31	181	9.4	
400	647.7	30	10.6	9.3	36.44	132	11.7	
200	168.4	30	5.0	4.5	18.73	181	7.6	
200	323.85	30	6.6	5.9	26.39	166	9.2	
200	647.7	30	10.3	8.7	33.80	124	11.6	
600	168.4	60	6.4	6.9	25.06	236	8.2	
600	323.85	60	8.7	9.2	30.33	215	9.6	
600	647.7	60	14.0	14.0	33.66	142	12.5	
400	168.4	60	6.1	5.7	22.92	204	8.4	
400	323.85	60	8.1	7.5	29.63	188	9.9	
400	647.7	60	12.8	11.2	36.55	137	12.5	
200	168.4	60	6.0	5.4	18.37	186	8.0	
200	323.85	60	8.0	7.1	25.92	171	9.8	
200	647.7	60	12.4	10.5	33.0	128	12.6	

^a 15M @ 400 c/c ^d 2-65mm GFRP Strips
^b 15M @ 800 c/c ^e 2-125mm GFRP Strips
^c 15 M @ 1200 c/c ^f 2-250mm GFRP Strips

Table 5.3(a) 200 mm Units, Unit Strength = 10 MPa

Area of Vertical Steel (mm ²)	Area of GFRP (mm ²)	Axial load kN	Transition Moment (kN-m)	Transition Deflection Δ _T	Ultimate Moment kN-m	Ultimate Deflection (mm)	Moment @ L/360 kN-m
600 ^a	168.4 ^d	15	4.0	2.6	30.92	198	10
600	323.85 ^e	15	5.0	3.2	39.32	189	11.3
600	647.7 ^f	15	7.2	4.4	50.8	163	13.4
400 ^b	168.4	15	4.0	2.5	25.85	187	9.4
400	323.85	15	5.0	3.1	34.78	178	11.0
400	647.7	15	7.2	4.3	47.11	153	13.2
200 ^c	168.4	15	3.9	2.4	20.1	177	8.6
200	323.85	15	4.9	3.0	29.67	169	10.6
200	647.7	15	7.0	4.1	43.23	147	13.1
600	168.4	30	4.4	2.9	30.66	200	10.1
600	323.85	30	5.6	3.5	39.01	191	11.5
600	647.7	30	8.0	4.9	50.43	165	13.6
400	168.4	30	4.4	2.8	25.66	189	9.5
400	323.85	30	5.5	3.5	34.54	180	11.2
400	647.7	30	8.0	4.8	46.81	155	13.5
200	168.4	30	4.4	2.7	19.98	179	8.8
200	323.85	30	5.5	3.3	29.51	171	10.8
200	647.7	30	7.8	4.5	43.0	148	13.4
600	168.4	60	5.3	3.4	30.14	204	10.4
600	323.85	60	6.7	4.2	38.4	195	12.1
600	647.7	60	9.7	5.9	49.68	169	14.2
400	168.4	60	5.3	3.4	25.28	193	9.8
400	323.85	60	6.7	4.2	34.07	184	11.6
400	647.7	60	9.6	5.8	46.21	159	14.0
200	168.4	60	5.3	3.2	19.74	182	9.1
200	323.85	60	6.6	3.9	29.18	174	11.2
200	647.7	60	9.4	5.5	42.54	151	14.0

^a 15M @ 400 c/c ^d 2-65mm GFRP Strips
^b 15M @ 800 c/c ^e 2-125mm GFRP Strips
^c 15 M @ 1200 c/c ^f 2-250mm GFRP Strips

Table 5.3(b) 200 mm Units, Unit Strength = 15 MPa

Area of Vertical Steel (mm ²)	Area of GFRP (mm ²)	Axial Load kN	Transition Moment (kN-m)	Transition Deflection Δ _T	Ultimate Moment kN-m	Ultimate Deflection (mm)	Moment @ L/360 kN-m
600 ^a	168.4 ^d	15	3.7	1.9	32.42	192	11.3
600	323.85 ^e	15	4.5	2.2	41.91	185	13.0
600	647.7 ^f	15	6.2	3.0	56.59	168	15.3
400 ^b	168.4	15	3.7	1.8	26.9	183	10.7
400	323.85	15	4.5	2.1	36.94	177	12.6
400	647.7	15	6.1	2.8	52.76	162	15.3
200 ^c	168.4	15	3.7	1.7	20.70	176	9.6
200	323.85	15	3.4	2.0	31.26	171	10.2
200	647.7	15	4.6	2.6	48.17	156	12.7
600	168.4	30	4.2	2.1	32.22	193	11.5
600	323.85	30	5.0	2.5	41.67	187	13.1
600	647.7	30	6.9	3.3	56.29	170	15.5
400	168.4	30	4.1	2.0	26.75	185	10.8
400	323.85	30	5.0	2.4	36.76	179	12.8
400	647.7	30	6.8	3.1	52.52	163	15.5
200	168.4	30	4.1	1.9	20.61	178	10.1
200	323.85	30	4.9	2.2	31.14	172	12.1
200	647.7	30	6.6	2.9	47.98	157	15.3
600	168.4	60	5.0	2.5	31.82	196	11.7
600	323.85	60	6.1	3.0	41.19	190	13.4
600	647.7	60	8.3	4.0	55.69	173	15.9
400	168.4	60	5.0	2.4	26.46	188	11.1
400	323.85	60	6.0	2.8	36.39	182	13.1
400	647.7	60	8.1	3.8	52.04	166	15.9
200	168.4	60	4.9	2.3	20.43	180	10.0
200	323.85	60	5.9	2.7	30.88	174	12.5
200	647.7	60	8.0	3.5	47.61	160	15.8

^a 15M @ 400 c/c ^d 2-65mm GFRP Strips
^b 15M @ 800 c/c ^e 2-125mm GFRP Strips
^c 15 M @ 1200 c/c ^f 2-250mm GFRP Strips

Table 5.3(c) 200 mm Units, Unit Strength = 20 MPa

Area of Vertical Steel (mm ²)	Area of GFRP (mm ²)	Axial Load kN	Transition Moment (kN-m)	Transition Deflection Δ _T	Ultimate Moment kN-m	Ultimate Deflection (mm)	Moment @ L/360 kN-m
							159.0
600 ^a	168.4 ^d	15	6.4	3.4	35.75	159.0	12.8
600	323.85 ^e	15	8.1	4.2	43.34	141.0	14.3
600	647.7 ^f	15	11.9	6.0	48.23	92.0	16.9
400 ^b	168.4	15	6.1	2.9	31.22	145.0	12.6
400	323.85	15	7.7	3.5	40.44	132.0	14.7
400	647.7	15	11.0	4.8	48.82	94.0	17.6
200 ^c	168.4	15	6.1	2.7	24.38	137.0	11.6
200	323.85	15	7.6	3.3	34.48	124.0	14.1
200	647.7	15	10.8	4.6	44.36	91.0	17.4
600	168.4	30	6.8	3.6	35.31	161.0	12.7
600	323.85	30	8.7	4.5	42.85	144.0	14.5
600	647.7	30	12.8	6.4	47.7	93.0	17.2
400	168.4	30	6.6	3.1	30.94	147.0	12.8
400	323.85	30	8.3	3.8	40.10	133.0	14.9
400	647.7	30	11.9	5.2	48.43	96.0	17.9
200	168.4	30	6.5	2.9	24.2	138.0	11.7
200	323.85	30	8.1	3.6	34.24	125.0	14.3
200	647.7	30	11.6	4.9	44.07	92.0	17.7
600	168.4	60	7.8	4.1	34.44	167.0	13.0
600	323.85	60	9.9	5.2	41.86	149.0	14.9
600	647.7	60	14.6	7.3	46.63	97.0	17.9
400	168.4	60	7.5	3.5	30.37	151.0	13.1
400	323.85	60	9.4	4.3	39.42	137.0	15.3
400	647.7	60	13.5	5.9	47.64	98.0	18.5
200	168.4	60	7.4	3.3	23.85	141.0	12.1
200	323.85	60	9.3	4.7	33.78	128.0	14.7
200	647.7	60	13.2	5.6	43.48	94.0	18.3

^a 15M @ 400 c/c ^d 2-65mm GFRP Strips
^b 15M @ 800 c/c ^e 2-125mm GFRP Strips
^c 15 M @ 1200 c/c ^f 2-250mm GFRP Strips

Table 5.4(a) 250 mm Units, Unit Strength = 10 MPa

Area of Vertical Steel (mm ²)	Area of GFRP (mm ²)	Axial Load kN	Transition Moment (kN-m)	Transition Deflection Δ _T		Ultimate Moment kN-m	Ultimate Deflection (mm)	Moment @ L/360 kN-m
				Deflection	Δ _T			
600 ^a	168.4 ^d	15	5.6	1.8	40.54	149.0	16.3	
600	323.85 ^e	15	6.6	2.1	51.69	141.0	18.7	
600	647.7 ^f	15	8.8	2.7	67.14	120.0	22.1	
400 ^b	168.4	15	5.6	1.7	33.47	143.0	15.0	
400	323.85	15	6.6	2.0	45.17	135.0	17.8	
400	647.7	15	8.8	2.6	61.50	115.0	21.5	
200 ^c	168.4	15	5.6	1.7	25.73	137.0	13.4	
200	323.85	15	6.5	1.9	38.11	130.0	16.7	
200	647.7	15	8.6	2.5	55.81	111.0	21.2	
600	168.4	30	6.0	1.9	40.28	150.0	16.4	
600	323.85	30	7.1	2.2	51.39	142.0	18.8	
600	647.7	30	9.5	2.9	66.76	121.0	22.3	
400	168.4	30	6.0	1.9	33.27	144.0	15.2	
400	323.85	30	7.1	2.2	44.93	136.0	17.9	
400	647.7	30	9.4	1.8	61.2	116.0	21.7	
200	168.4	30	6.0	2.1	25.61	138.0	13.5	
200	323.85	30	7.0	2.7	37.94	131.0	16.9	
200	647.7	30	9.3	3.0	55.58	112.0	21.3	
600	168.4	60	6.9	2.2	39.76	153.0	16.7	
600	323.85	60	8.1	2.5	50.78	145.0	19.1	
600	647.7	60	10.8	3.3	66.02	123.0	22.6	
400	168.4	60	6.9	2.1	32.89	146.0	15.4	
400	323.85	60	8.1	2.5	44.46	138.0	18.2	
400	647.7	60	10.7	3.2	60.60	118.0	22.1	
200	168.4	60	6.8	2.0	25.37	140.0	13.8	
200	323.85	60	8.0	2.4	37.61	133.0	17.2	
200	647.7	60	10.5	3.0	55.12	114.0	21.7	

^a 15M @ 400 c/c ^d 2-65mm GFRP Strips
^b 15M @ 800 c/c ^e 2-125mm GFRP Strips
^c 15 M @ 1200 c/c ^f 2-250mm GFRP Strips

Table 5.4(b) 250 mm Units, Unit Strength = 15 MPa

Area of Vertical Steel (mm ²)	Area of GFRP (mm ²)	Axial Load kN	Transition Moment (kN-m)	Transition Deflection Δ_T		Ultimate Moment kN-m	Ultimate Deflection (mm)	Moment @ L/360 kN-m
				Deflection	Transition			
600 ^a	168.4 ^d	15	5.4	1.3	42.11	146.0	18.4	
600	323.85 ^e	15	6.1	1.5	54.55	141.0	21.2	
600	647.7 ^f	15	7.8	1.9	74.0	126.0	25.3	
400 ^b	168.4	15	5.3	1.3	34.60	142.0	16.9	
400	323.85	15	6.1	1.4	47.62	136.0	20.2	
400	647.7	15	7.7	1.8	68.33	122.0	24.9	
200 ^c	168.4	15	5.3	1.2	26.41	138.0	14.8	
200	323.85	15	6.0	1.3	39.98	132.0	18.9	
200	647.7	15	7.6	1.7	61.88	120.0	24.3	
600	168.4	30	5.8	1.4	41.91	147.0	18.4	
600	323.85	30	6.6	1.6	54.31	141.0	21.3	
600	647.7	30	8.4	2.0	73.7	127.0	25.5	
400	168.4	30	5.7	1.4	34.45	142.0	17.0	
400	323.85	30	6.5	1.5	47.44	137.0	20.4	
400	647.7	30	8.3	1.9	68.09	123.0	25.1	
200	168.4	30	5.7	1.3	26.32	138.0	14.9	
200	323.85	30	6.5	1.4	39.85	133.0	19.0	
200	647.7	30	8.1	1.8	61.69	120.0	24.4	
600	168.4	60	6.6	1.6	41.5	149.0	18.6	
600	323.85	60	7.5	1.8	53.83	143.0	21.5	
600	647.7	60	9.6	2.3	73.10	128.0	25.8	
400	168.4	60	6.5	1.5	34.16	144.0	17.2	
400	323.85	60	7.4	1.7	47.07	139.0	20.6	
400	647.7	60	9.4	2.1	67.6	125.0	25.4	
200	168.4	60	6.5	1.5	26.14	140.0	15.2	
200	323.85	60	7.4	1.7	39.6	135.0	19.3	
200	647.7	60	9.2	2.0	61.32	122.0	24.8	

^d 2-65mm GFRP Strips
^e 2-125mm GFRP Strips
^f 2-250mm GFRP Strips

^a 15M @ 400 c/c
^b 15M @ 800 c/c
^c 15 M @ 1200 c/c

Table 5.4(c) 250 mm Units, Unit Strength = 20 MPa

AXIAL LOAD	15 kN				30 kN				60 kN			
	WITHOUT GFRP	2-65mm GFRP STRIPS		% Difference	WITHOUT GFRP	2-65mm GFRP STRIPS		% Difference	WITHOUT GFRP	2-65mm GFRP STRIPS		% Difference
		KN-m	KN-m	KN-m		KN-m	KN-m	KN-m		KN-m	KN-m	KN-m
10 MPa												
15M @ 400	3.72	16.97	356	3.84	16.54	331	3.89	15.7	304			
15M @ 800	2.77	16.31	489	2.84	16.03	464	2.96	15.5	424			
15M @ 1200	1.94	13.43	592	2.01	13.25	559	2.07	12.9	523			
15 MPa												
15M @ 400	6.02	21.31	254	6.11	21.05	245	6.29	20.53	226			
15M @ 800	4.02	18.2	353	4.11	18.04	339	4.29	17.66	312			
15M @ 1200	2.81	14.47	415	2.9	14.3	393	3.08	14.11	358			
20 MPa												
15M @ 400	7.52	22.74	202	7.62	22.54	196	7.84	22.13	182			
15M @ 800	4.89	19.2	293	5.37	19.06	255	5.49	18.77	242			
15M @ 1200	3.5	15.0	329	3.72	14.91	301	3.94	14.72	274			

Table 5.5(a) Ultimate Moment Capacity and Percent Increase in Ultimate Moment Capacity for 150 mm Walls.

AXIAL LOAD	15 kN				30 kN				60 kN			
	WITHOUT GFRP STRIPS		2-65mm GFRP STRIPS		WITHOUT GFRP		2-65mm GFRP STRIPS		WITHOUT GFRP		2-65mm GFRP STRIPS	
	KN-m	% Difference	KN-m	% Difference	KN-m	% Difference	KN-m	% Difference	KN-m	% Difference	KN-m	% Difference
10 MPa												
15M @ 400	6.51	26.36	30.5	6.61	25.93	292	6.82	25.06	267			
15M @ 800	6.13	23.77	28.8	6.24	23.48	276	6.47	22.92	254			
15M @ 1200	4.28	18.9	34.2	4.4	18.73	326	4.63	18.37	297			
15 MPa												
15M @ 400	10.42	30.92	19.7	10.57	30.66	190	10.88	30.14	177			
15M @ 800	7.05	25.85	26.7	8.06	25.66	218	9.29	25.28	172			
15M @ 1200	5.08	20.1	29.6	6.06	19.98	230	6.61	19.74	199			
20 MPa												
15M @ 400	12.13	32.42	16.7	12.95	32.22	149	13.46	31.82	136			
15M @ 800	7.32	26.9	26.7	8.44	26.75	217	10.51	26.46	152			
15M @ 1200	5.28	20.7	29.2	6.38	20.61	223	8.35	20.43	145			

Table 5.5(b) Ultimate Moment Capacities and Percent Increase in Ultimate Moment Capacity for 200 mm Walls.

AXIAL LOAD	15 kN				30 kN				60 kN			
	WITHOUT GFRP STRIPS		2-65mm GFRP STRIPS		WITHOUT GFRP		2-65mm GFRP STRIPS		WITHOUT GFRP		2-65mm GFRP STRIPS	
	KN-m	% Difference	KN-m	% Difference	KN-m	% Difference	KN-m	% Difference	KN-m	% Difference	KN-m	% Difference
10 MPa												
15M @ 400	9.79		35.75		205		9.95		35.31		255	
15M @ 800	8.72		31.22		258		9.69		30.94		219	
15M @ 1200	6.47		24.38		277		7.68		24.2		215	
15 MPa												
15M @ 400	15.13		40.54		168		15.8		40.28		155	
15M @ 800	9.25		33.47		262		10.65		33.27		212	
15M @ 1200	6.81		25.73		278		8.25		25.61		210	
20 MPa												
15M @ 400	16.06		42.11		162		17.3		41.91		142	
15M @ 800	9.51		34.6		264		11.02		34.45		213	
15M @ 1200	6.97		26.41		279		8.5		26.32		210	

Table 5.5(c) Ultimate Moment Capacities and Percent Increase in Ultimate Moment Capacity for 250 mm Walls.

AXIAL LOAD	15 kN*	30 kN			60 kN	
		400 mm to 800 mm	800 mm to 1200 mm	400mm to 800mm	800 mm to 1200 mm	400mm to 800mm
10 MPa						
2-65 mm (168.4 mm ²)	4.0	21.4	3.2	21	1.3	20.2
2-125 mm (323.85 mm ²)	-2.9	11.2	-3.7	10.8	-5.6	9.9
2-250 mm (647.7 mm ²)	-11.4	4.3	-12.3	3.9	-13.9	3.1
15 MPa						
2-65 mm (168.4 mm ²)	17.1	25.8	16.7	26.2	16.3	25.2
2-125 mm (323.85 mm ²)	10.5	14.8	10.1	14.6	9.9	14.2
2-250 mm (647.7 mm ²)	5.3	6.7	5.2	6.6	4.8	6.2
20 MPa						
2-65 mm (168.4 mm ²)	18.4	28.0	18.3	27.8	17.9	27.5
2-125 mm (323.85 mm ²)	11.5	16.5	11.3	16.3	11.0	16.0
2-250 mm (647.7 mm ²)	5.4	7.9	5.2	7.8	4.9	7.6

* -ve sign shows increase

Table 5.6(a) Percent Decrease in Ultimate Moment Capacity Due to Vertical Steel in 150 mm Walls.

AXIAL LOAD	15 kN*			30 kN			60 kN		
	400 mm to 800 mm	800 mm to 1200 mm	400mm to 800mm	800 mm to 1200 mm	400mm to 800mm	800 mm to 1200 mm	400 mm to 800mm	800 mm to 1200 mm	
10 MPa									
2-65 mm (168.4 mm ²)	10.9	25.8	10.4	25.4	9.3	24.8			
2-125 mm (323.85 mm ²)	3.8	15.1	3.3	14.9	2.4	14.3			
2-250 mm (647.7 mm ²)	-4.5	8.1	-4.9	7.8	-8.6	10.8			
15 MPa									
2-65 mm (168.4 mm ²)	19.6	28.6	19.5	28.4	19.2	28.1			
2-125 mm (323.85 mm ²)	13.1	17.2	12.9	17.0	12.7	16.8			
2-250 mm (647.7 mm ²)	7.8	9.0	7.7	8.9	7.5	8.6			
20 MPa									
2-65 mm (168.4 mm ²)	20.5	30.0	20.4	29.8	20.3	29.4			
2-125 mm (323.85 mm ²)	13.5	18.2	13.4	18.0	13.2	17.8			
2-250 mm (647.7 mm ²)	7.3	9.5	7.2	9.5	7.0	9.3			

Table 5.6(b) Percent Decrease in Ultimate Moment Capacity Due to Vertical Steel for 200 mm Walls

-ve sign shows increase

AXIAL LOAD	30 kN			60 kN		
	400 mm to 800 mm	800 mm to 1200 mm	400 mm to 800 mm	800 mm to 1200 mm	400 mm to 800 mm	800 mm to 1200 mm
10 MPa						
2-65 mm (168.4 mm ²)	14.5	28.1	14.1	27.9	13.4	27.3
2-125 mm (323.85 mm ²)	7.2	17.3	6.9-	17.2	6.2	16.7
2-250 mm (647.7 mm ²)	-1.2	10.1	-1.5	9.9	-2.2	9.5
15 MPa						
2-65 mm (168.4 mm ²)	21.1	30.1	21.1	29.9	20.9	29.6
2-125 mm (323.85 mm ²)	14.4	18.5	14.4	18.4	14.2	18.2
2-250 mm (647.7 mm ²)	9.2	10.2	9.1	10.1	8.9	9.9
20 MPa						
2-65 mm (168.4 mm ²)	21.7	31.0	21.7	30.9	21.5	30.7
2-125 mm (323.85 mm ²)	14.6	19.1	14.5	19.0	14.4	18.9
2-250 mm (647.7 mm ²)	8.3	10.4	8.2	10.4	8.1	10.2

-ve sign shows increase

Table 5.6(c) Percent Decrease in Ultimate Moment Capacity Due to Vertical Steel for 250 mm Walls

AXIAL LOAD	15 kN			30 kN			60 kN		
	10 MPa to 15 MPa	15 MPa to 20 MPa	10 MPa to 15 MPa	15 MPa to 20 MPa	10 MPa to 15 MPa	15 MPa to 20 MPa	10 MPa to 15 MPa	15 MPa to 20 MPa	15 MPa to 20 MPa
(15M @ 400 mm c/c)									
2-65 mm (168.4 mm ²)	25.6	6.7	27.3	7.1	30.8	7.8			
2-125 mm (323.85 mm ²)	32.9	8.6	34.3	9.1	38.5	9.7			
2-250 mm (647.7 mm ²)	36.5	13.8	56.6	14.1	61.8	14.8			
(15M @ 800 mm c/c)									
2-65 mm (168.4 mm ²)	11.6	5.5	12.5	5.7	13.9	6.3			
2-125 mm (323.85 mm ²)	16.9	7.7	17.7	7.9	19.3	8.5			
2-250 mm (647.7 mm ²)	31.7	13.7	34.8	14.0	34.5	14.6			
(15M @ 1200 mm c/c)									
2-65 mm (168.4 mm ²)	7.7	3.7	7.9	4.3	9.4	4.3			
2-125 mm (323.85 mm ²)	13.2	6.2	13.8	6.4	14.9	6.8			
2-250 mm (647.7 mm ²)	28.7	12.4	29.3	12.6	30.6	13.1			

Table 5.7(a) Percent Increase in Ultimate Moment Capacity Due to Increase in Masonry Unit Strength (150 mm Walls)

AXIAL LOAD	15 kN	30 kN			60 kN		
		10 MPa to 15 MPa	15 MPa to 20 MPa	10 MPa to 15 MPa	15 MPa to 20 MPa	10 MPa to 15 MPa	15 MPa to 20 MPa
(15M @ 400 mm c/c)							
2-65 mm (168.4 mm ²)	17.3	4.9	18.2	5.1	20.3	5.6	
2-125 mm (323.85 mm ²)	23.6	6.6	24.6	6.8	26.6	7.3	
2-250 mm (647.7 mm ²)	44.0	11.4	45.2	11.6	47.6	12.1	
(15M @ 800 mm c/c)							
2-65 mm (168.4 mm ²)	8.8	4.1	9.3	4.2	10.3	4.7	
2-125 mm (323.85 mm ²)	13.5	6.2	14.0	6.4	15.0	6.8	
2-250 mm (647.7 mm ²)	27.9	12.0	28.5	12.2	26.4	12.6	
(15M @ 1200 mm c/c)							
2-65 mm (168.4 mm ²)	6.3	3.1	6.7	3.2	7.5	3.5	
2-125 mm (323.85 mm ²)	11.5	5.4	11.8	5.5	12.6	5.8	
2-250 mm (647.7 mm ²)	26.8	11.4	27.2	11.6	28.9	11.9	

Table 5.7(b) Percent Increase in Ultimate Moment Capacity Due to Increase in Masonry Unit Strength (200 mm Walls)

AXIAL LOAD	15 kN			30 kN			60 kN		
	10 MPa to 15 MPa	15 MPa to 20 MPa	10 MPa to 15 MPa	15 MPa to 20 MPa	10 MPa to 15 MPa	15 MPa to 20 MPa	10 MPa to 15 MPa	15 MPa to 20 MPa	10 MPa to 15 MPa
(15M @ 400 mm c/c)									
2-65 mm (168.4 mm ²)	13.4	3.9	14.1	4.0	15.4	4.4			
2-125 mm (323.85 mm ²)	19.3	5.5	19.1	5.7	21.3	6.0			
2-250 mm (647.7 mm ²)	39.2	10.2	40.0	10.4	41.6	10.7			
(15M @ 800 mm c/c)									
2-65 mm (168.4 mm ²)	7.2	3.4	7.5	3.5	8.3	3.9			
2-125 mm (323.85 mm ²)	11.7	5.4	12.0	5.6	12.8	5.9			
2-250 mm (647.7 mm ²)	26.0	11.1	26.4	11.3	27.2	11.5			
(15M @ 1200 mm c/c)									
2-65 mm (168.4 mm ²)	5.5	2.6	5.8	2.8	6.4	3.0			
2-125 mm (323.85 mm ²)	10.5	4.9	10.8	5.0	11.3	5.3			
2-250 mm (647.7 mm ²)	25.8	10.9	26.1	11.0	26.7	11.2			

Table 5.7(c) Percent Increase in Ultimate Moment Capacity Due to Increase in Masonry Unit Strength (250 mm Walls)

AXIAL LOAD	15 kN	(15M @ 400 mm c/c)	30 kN			(15M @ 400 mm c/c)		60 kN			(15M @ 400 mm c/c)
			150 mm to 200 mm	200 mm to 250 mm	150 mm to 200 mm	200 mm to 250 mm	150 mm to 200 mm	200 mm to 250 mm	150 mm to 200 mm	200 mm to 250 mm	150 mm to 200 mm
10 MPa											
2-65 mm (168.4 mm ²)	55.3	35.6	56.8	59.6	36.2	56.8	59.6	36.2	59.6	37.4	59.6
2-125 mm (323.85 mm ²)	56.8	36.2	58.2	58.8	36.8	58.2	61.3	36.8	61.3	38.0	61.3
2-250 mm (647.7 mm ²)	58.1	36.7	59.6	59.6	37.3	59.6	62.6	37.3	62.6	38.5	62.6
15 MPa											
2-65 mm (168.4 mm ²)	45.1	31.1	45.7	45.7	31.4	45.7	46.8	31.4	46.8	31.9	46.8
2-125 mm (323.85 mm ²)	45.9	31.5	46.7	46.7	31.7	46.7	47.5	31.7	47.5	32.2	47.5
2-250 mm (647.7 mm ²)	47.4	32.2	47.9	47.9	32.4	47.9	49.0	32.4	49.0	32.9	49.0
20 MPa											
2-65 mm (168.4 mm ²)	42.6	29.9	42.9	42.9	30.1	42.9	43.8	30.1	43.8	30.4	43.8
2-125 mm (323.85 mm ²)	43.2	30.2	43.5	43.5	30.3	43.5	44.3	30.3	44.3	30.7	44.3
2-250 mm (647.7 mm ²)	44.4	30.8	44.8	44.8	30.9	44.8	45.5	30.9	45.5	31.3	45.5

Table 5.8(a) Percent Increase in Ultimate Moment Capacity Due to Increase in Masonry Unit Thickness (15M@400)

AXIAL LOAD	15 kN (15M @ 800 mm c/c)			30 kN (15M @ 800 mm c/c)			60 kN (15M @ 800 mm c/c)		
	150 mm to 200 mm	200 mm to 250 mm	150 mm to 200 mm	200 mm to 250 mm	150 mm to 200 mm	200 mm to 250 mm	150 mm to 200 mm	200 mm to 250 mm	
10 MPa									
2-65 mm (168.4 mm ²)	45.7	31.3	46.5		31.8		47.9		32.5
2-125 mm (323.85 mm ²)	46.9	31.9	47.6		32.3		49.3		33.0
2-250 mm (647.7 mm ²)	48.2	32.5	49.0		32.9		54.5		30.3
15 MPa									
2-65 mm (168.4 mm ²)	42.0	29.5	42.2		29.7		43.1		30.1
2-125 mm (323.85 mm ²)	42.6	29.9	43.0		30.1		43.8		30.5
2-250 mm (647.7 mm ²)	44.0	30.5	44.4		30.7		45.2		31.2
20 MPa									
2-65 mm (168.4 mm ²)	40.1	29.5	40.3		28.8		41.0		29.1
2-125 mm (323.85 mm ²)	40.7	28.9	41.0		29.1		41.5		29.3
2-250 mm (647.7 mm ²)	41.9	28.6	42.1		29.6		42.7		29.9

Table 5.8(b) Percent Increase in Ultimate Moment Capacity Due to Increase in Masonry Unit Thickness (15M@800)

AXIAL LOAD	15 kN (15M @ 1200 mm c/c)	30 kN (15M @ 1200 mm c/c)			60 kN (15M @ 1200 mm c/c)		
		150 mm to 200 mm	200 mm to 250 mm	150 mm to 200 mm	200 mm to 250 mm	150 mm to 200 mm	200 mm to 250 mm
10 MPa							
2-65 mm (168.4 mm ²)	40.7	29.0	41.4	29.2	42.4	29.8	
2-125 mm (323.85 mm ²)	41.8	29.5	42.4	29.7	43.5	30.3	
2-250 mm (647.7 mm ²)	43.1	30.1	43.6	30.4	43.9	31.8	
15 MPa							
2-65 mm (168.4 mm ²)	38.9	29.1	39.7	28.2	39.9	28.5	
2-125 mm (323.85 mm ²)	39.7	28.4	40.0	28.6	40.6	28.9	
2-250 mm (647.7 mm ²)	41.0	28.0	41.3	29.3	41.9	29.6	
20 MPa							
2-65 mm (168.4 mm ²)	38.0	27.6	38.2	27.7	38.8	27.9	
2-125 mm (323.85 mm ²)	38.6	27.9	38.9	28.0	39.3	28.2	
2-250 mm (647.7 mm ²)	39.9	28.5	40.0	28.6	40.4	28.8	

Table 5.8(c) Percent Increase in Ultimate Moment Capacity Due to Increase in Masonry Unit Thickness (15M@1200)

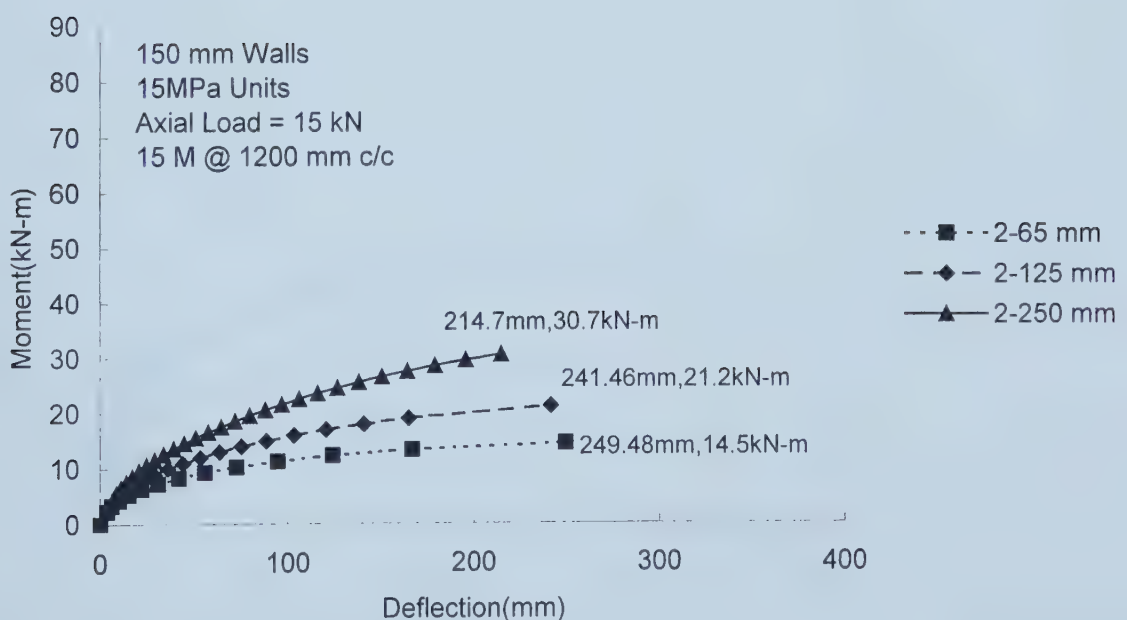
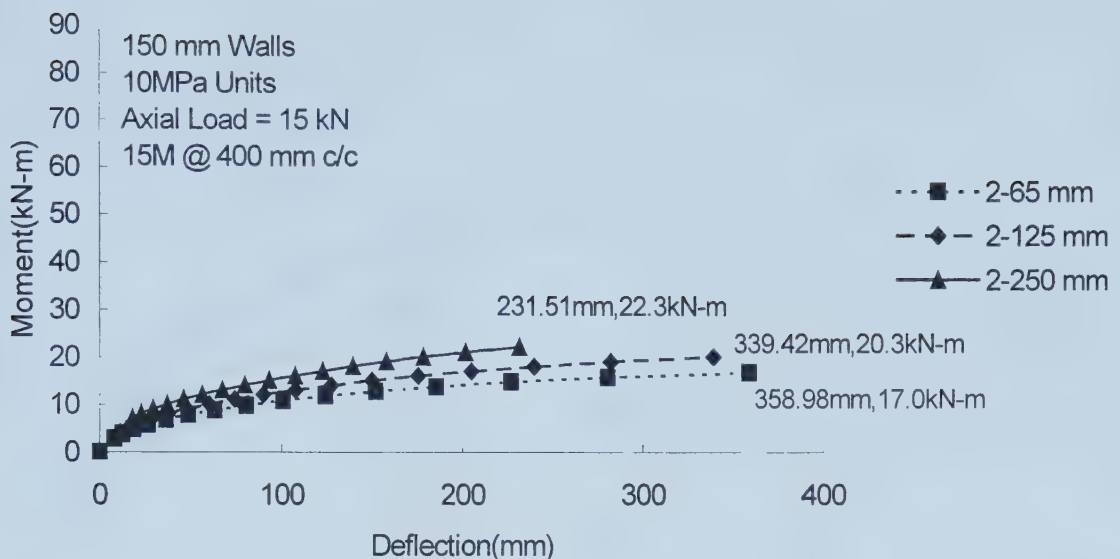


Figure 5.1 Ultimate Moment versus Mid-Span Deflection for a Typical 150mm Wall

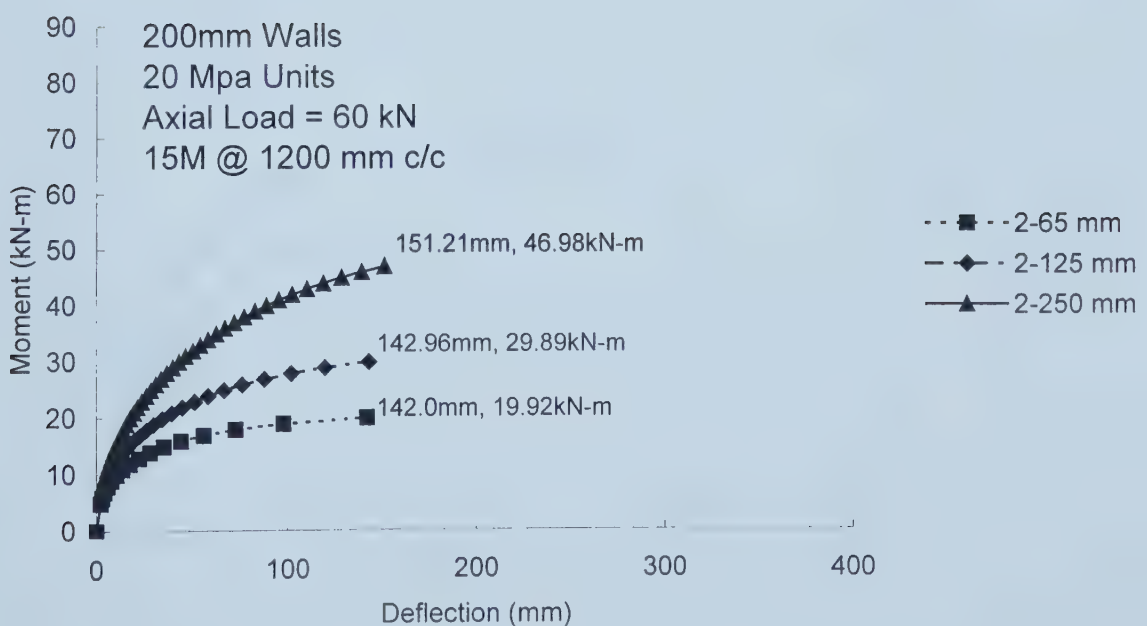
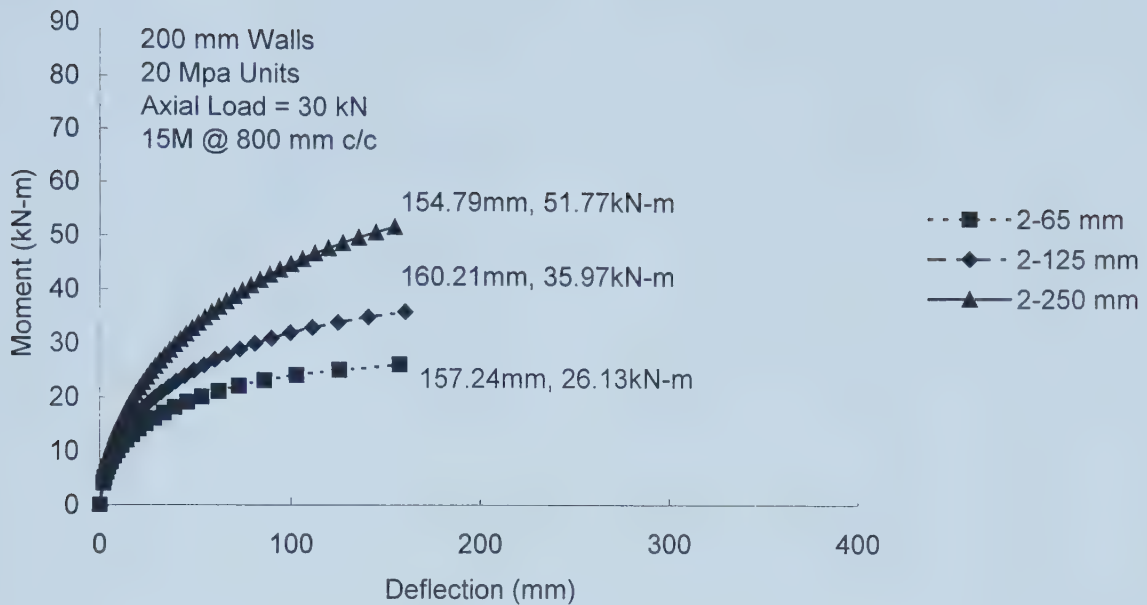


Figure 5.2 Ultimate Moment versus Mid-Span Deflection for a Typical 200mm Wall

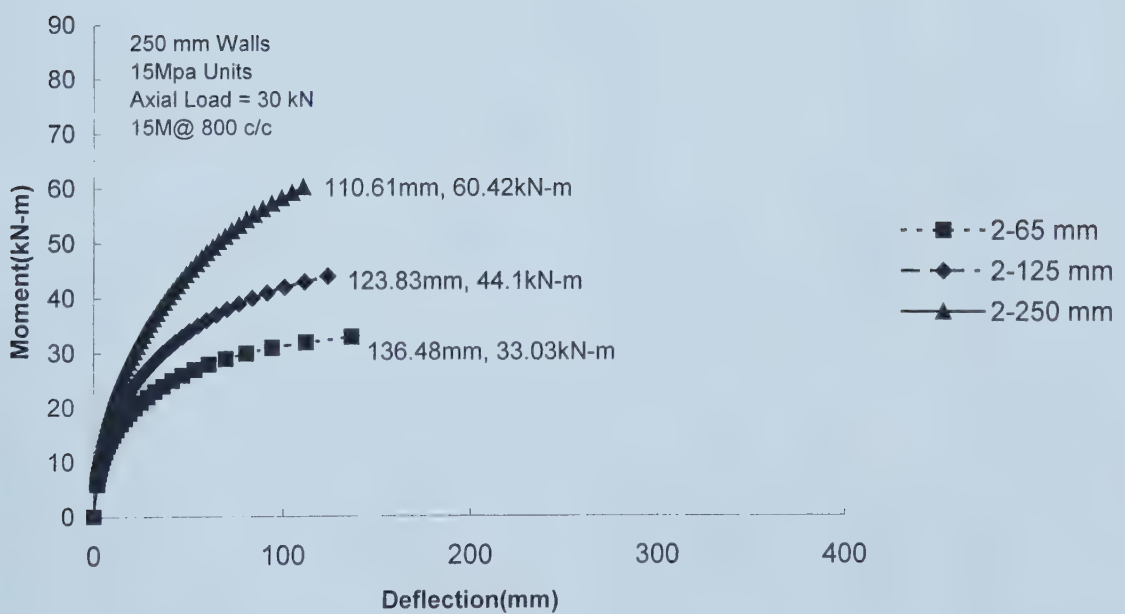
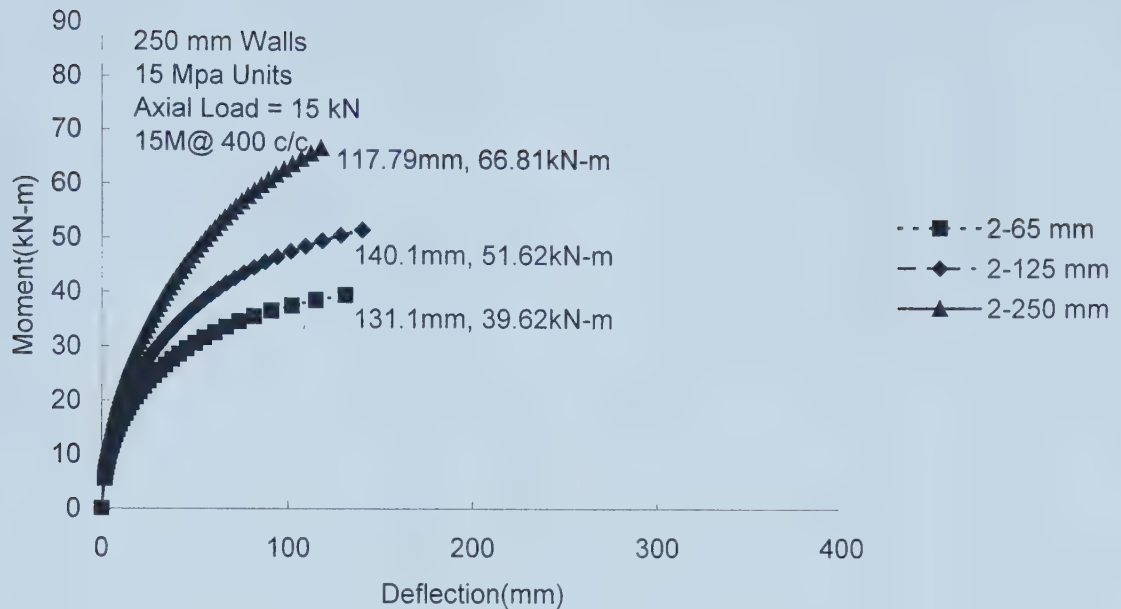


Figure 5.3 Ultimate Moment versus Mid-Span Deflection for a Typical 250mm Wall

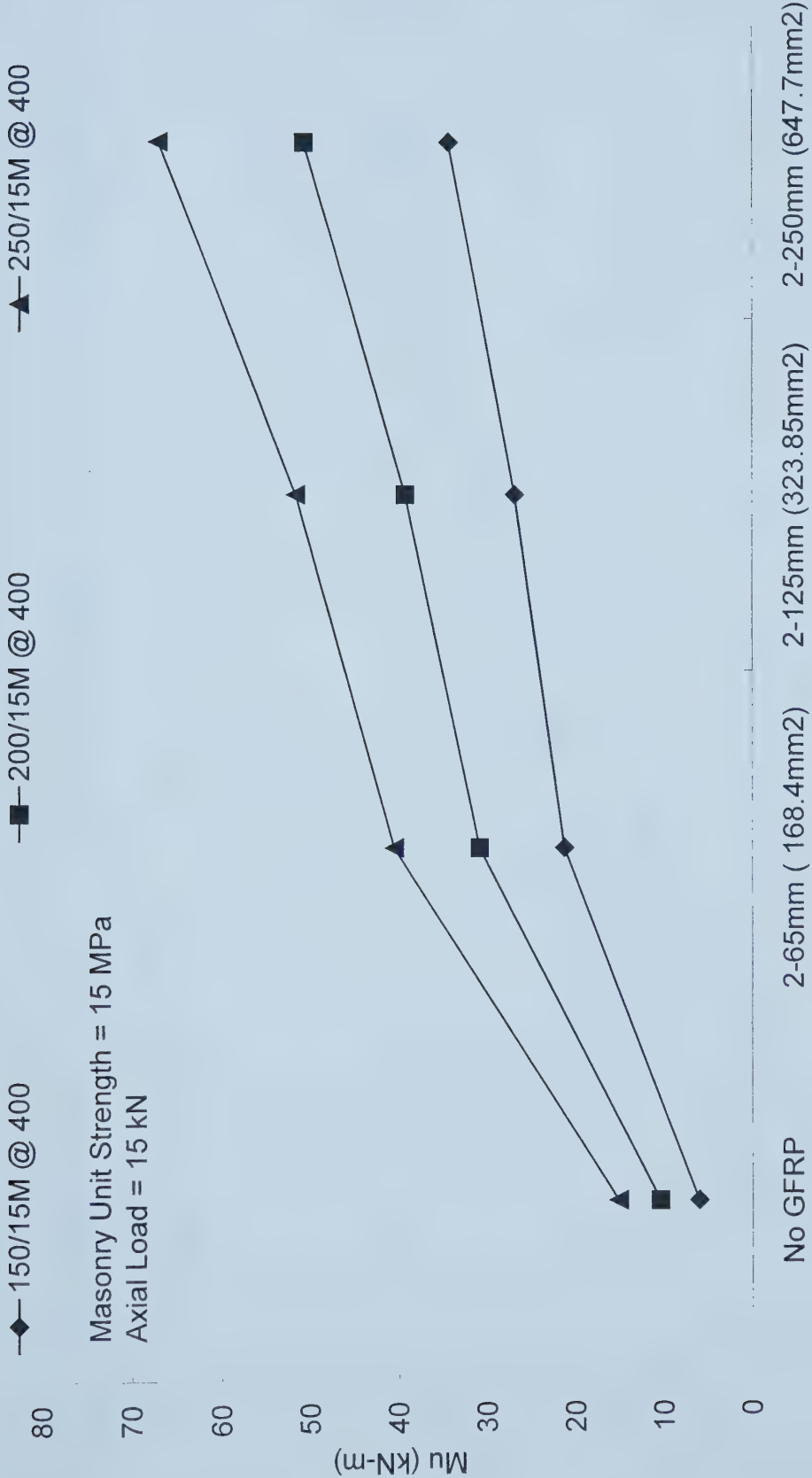


Figure 5.4 GFRP Area versus Ultimate Moment (15MPa Masonry Units, Axial Load = 15kN, 15M@400)

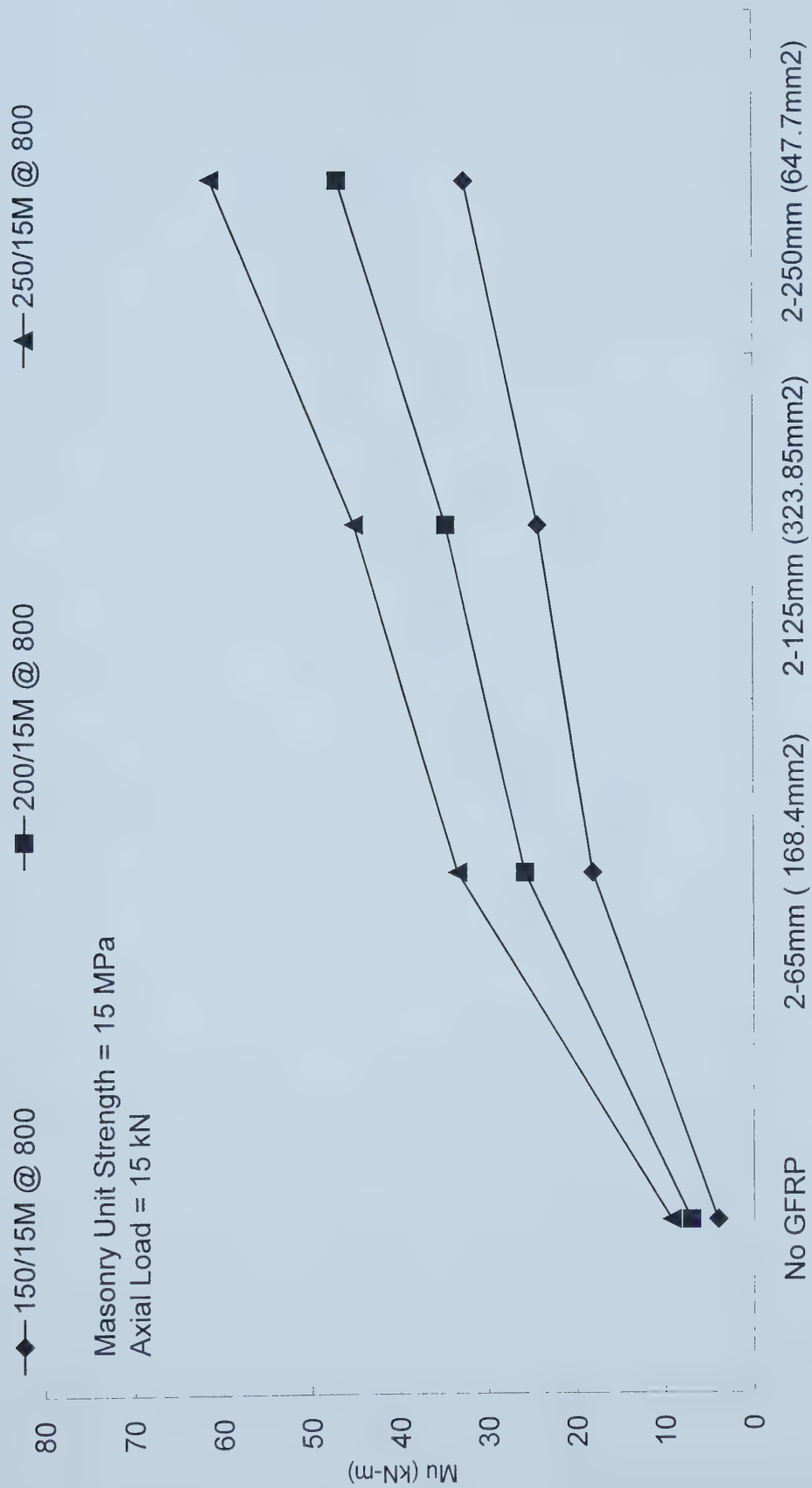


Figure 5.5 GFRP Area versus Ultimate Moment (15 MPa Masonry Units, Axial Load = 15 kN, 15 M@800)

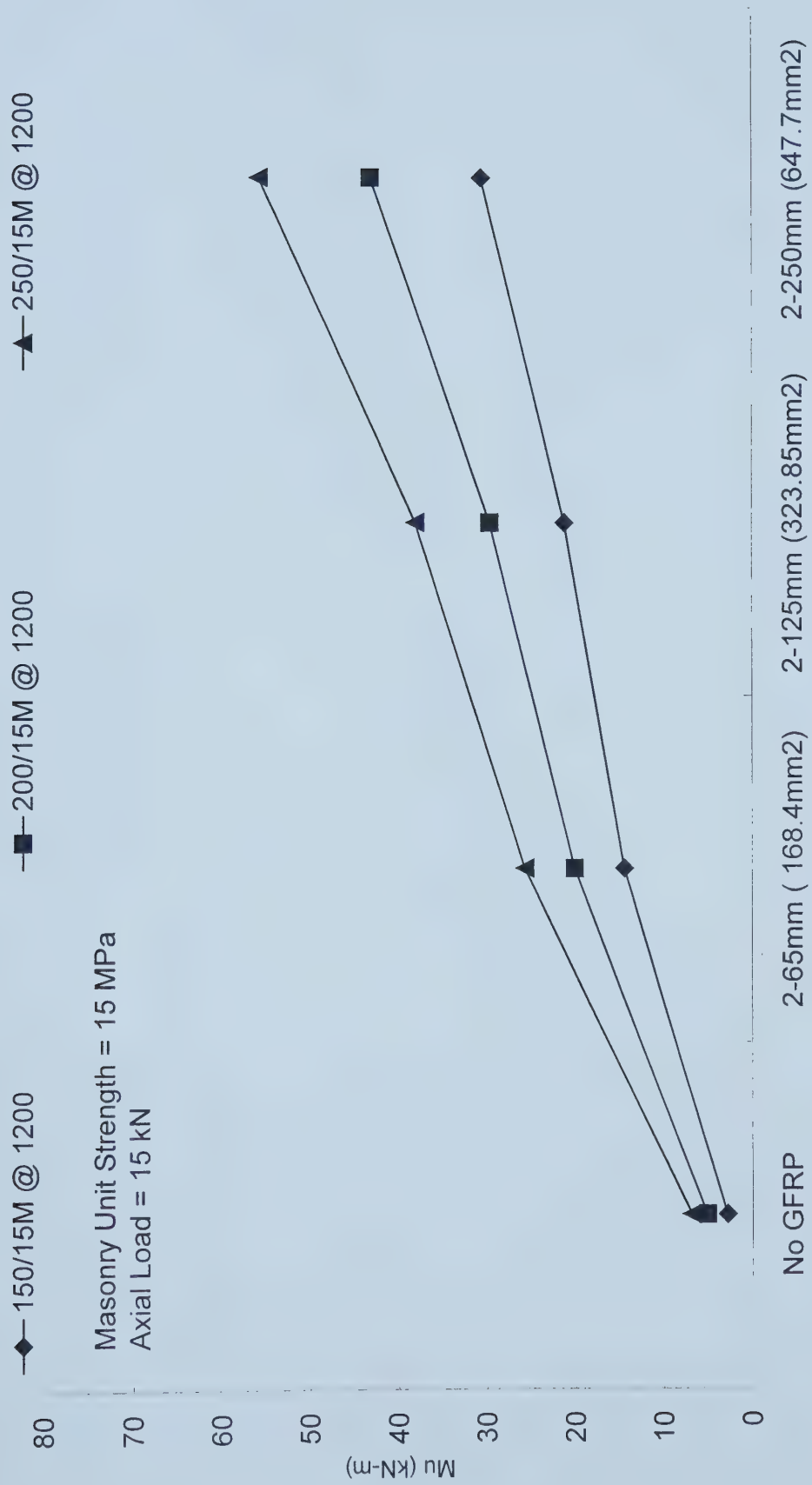


Figure 5.6 GFRP Area versus Ultimate Moment (15 MPa Masonry Units, Axial Load = 15 kN, 15 M@1200)

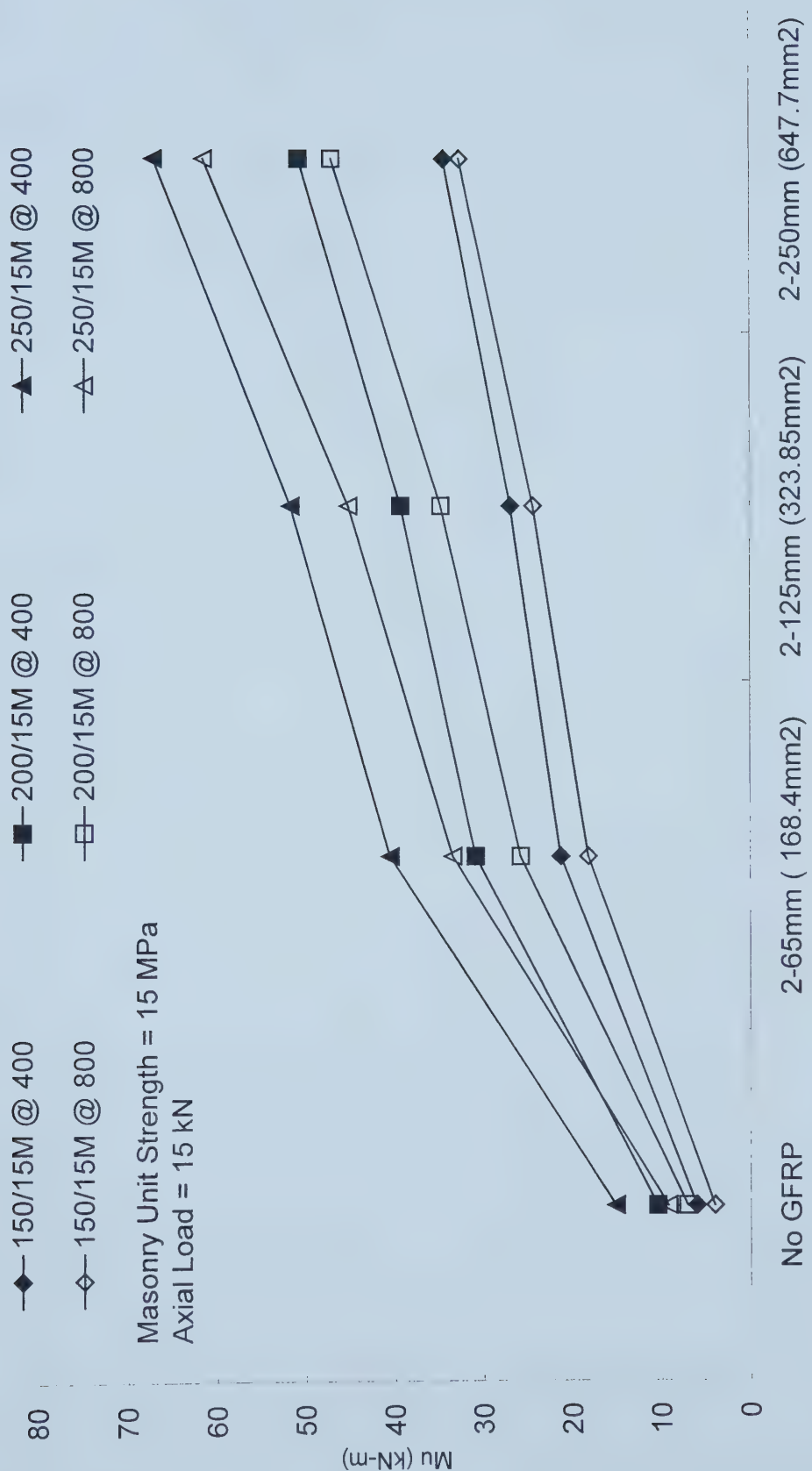


Figure 5.7 GFRP Area versus Ultimate Moment (15MPa Masonry Units, Axial Load = 15kN, 15M@400 and 15M@800)

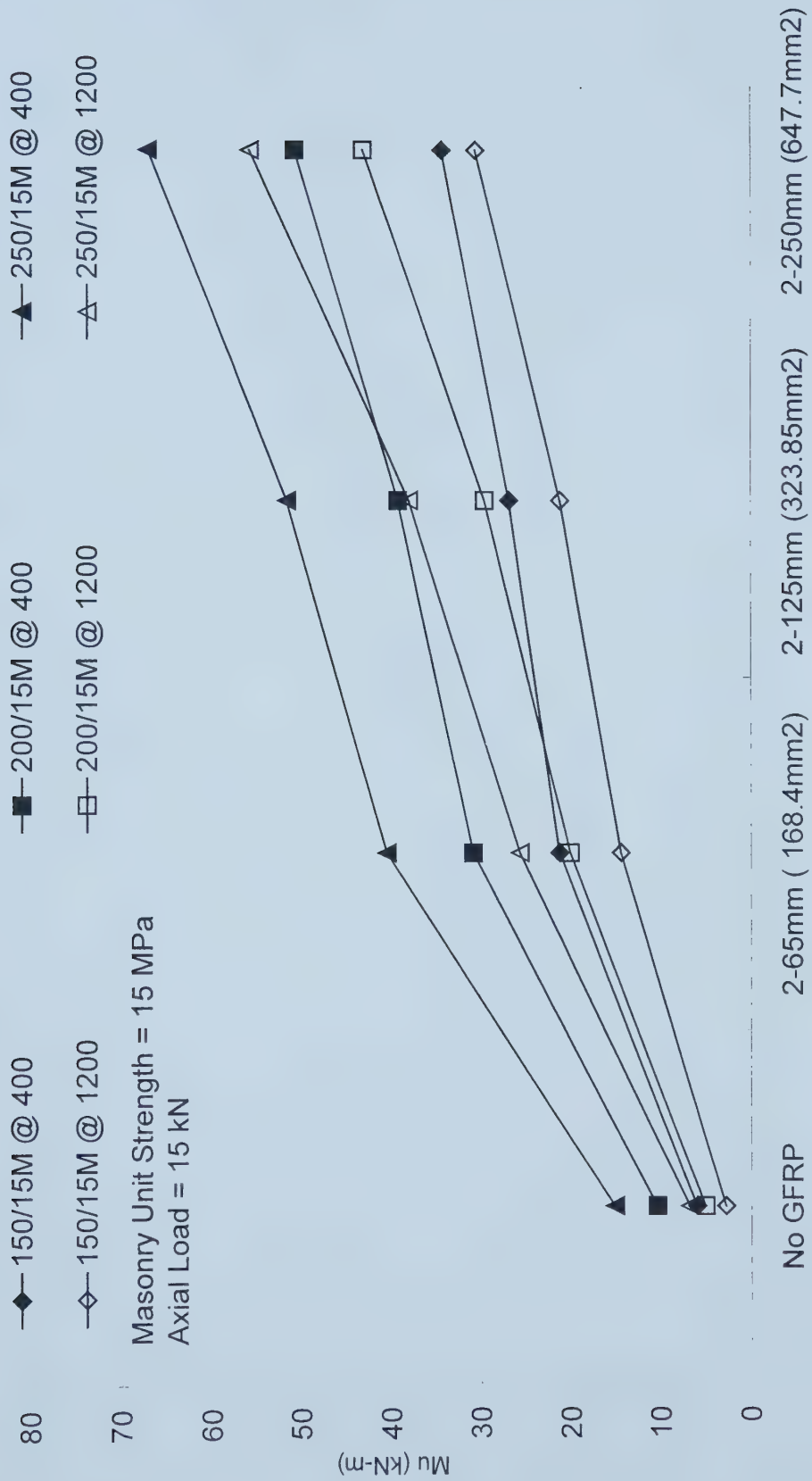


Figure 5.8 GFRP Area versus Ultimate Moment (15MPa Masonry Units, Axial Load = 15kN, 15M@400 and 15M@1200)

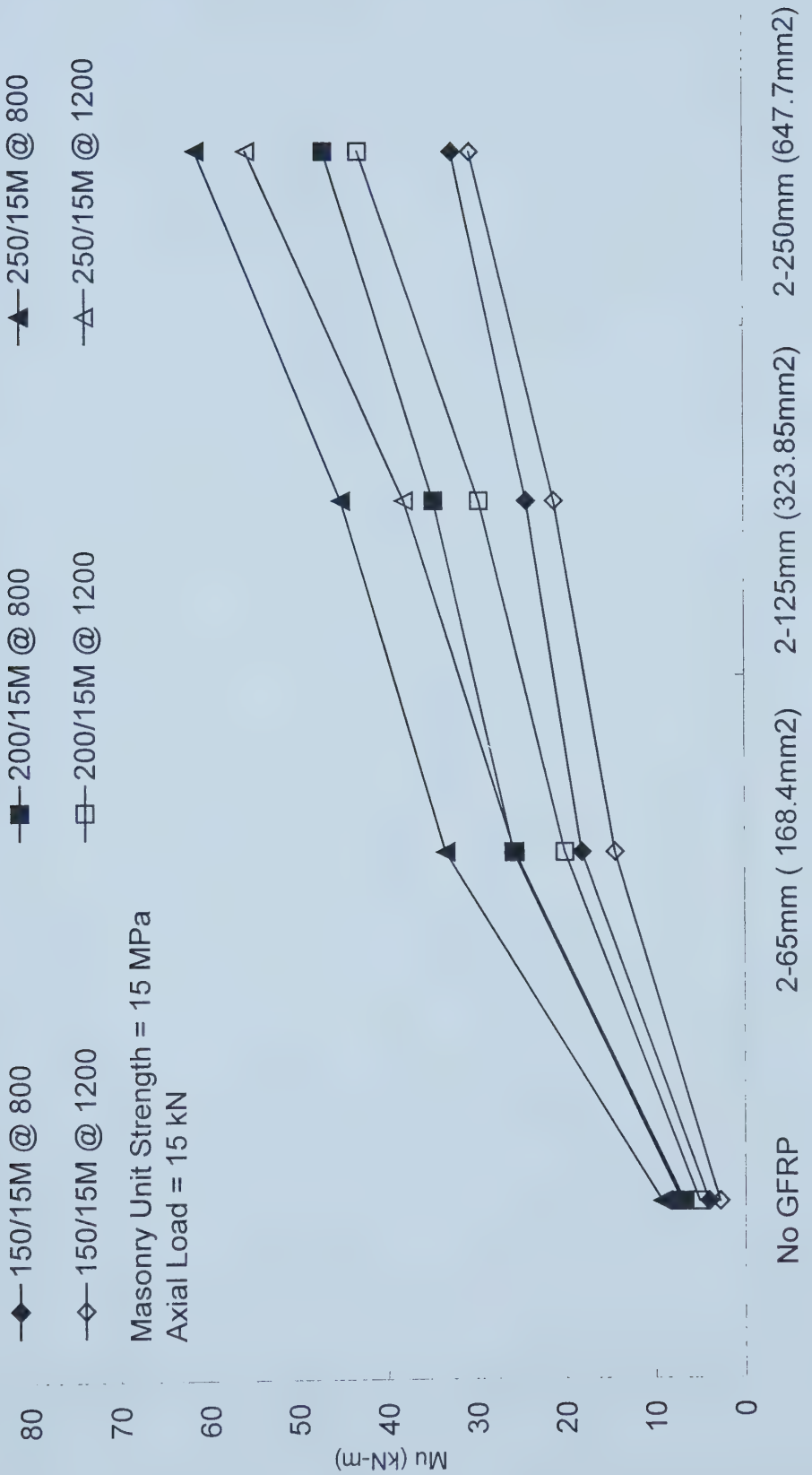


Figure 5.9 GFRP Area versus Ultimate Moment (15MPa Masonry Units, Axial Load = 15kN, 15M@800 and 15M@1200)

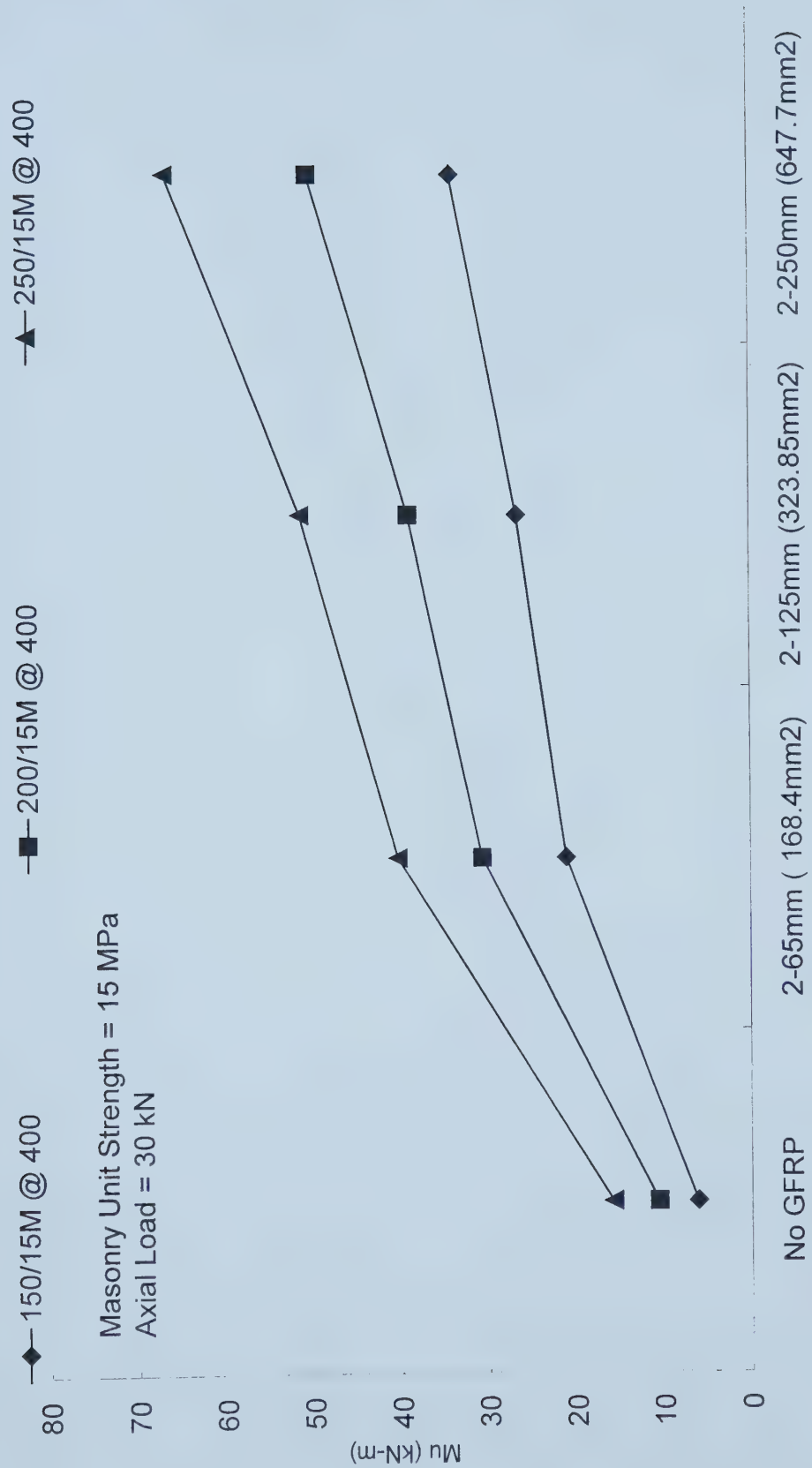


Figure 5.10 GFRP Area versus Ultimate Moment (15MPa Masonry Units, Axial Load = 30kN, 15M@400)

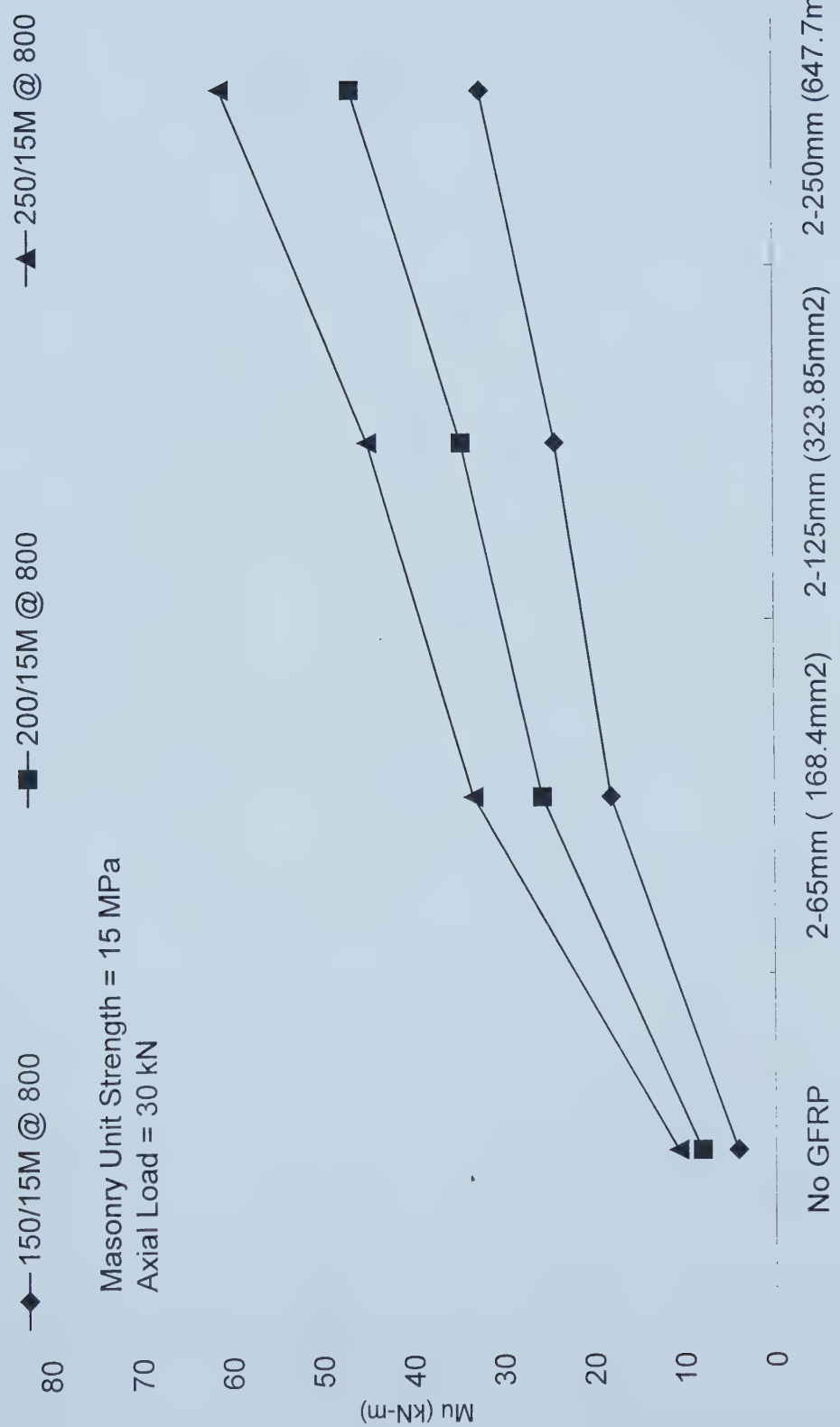


Figure 5.11 GFRP Area versus Ultimate Moment (15MPa Masonry Units, Axial Load = 30kN, 15M@800)

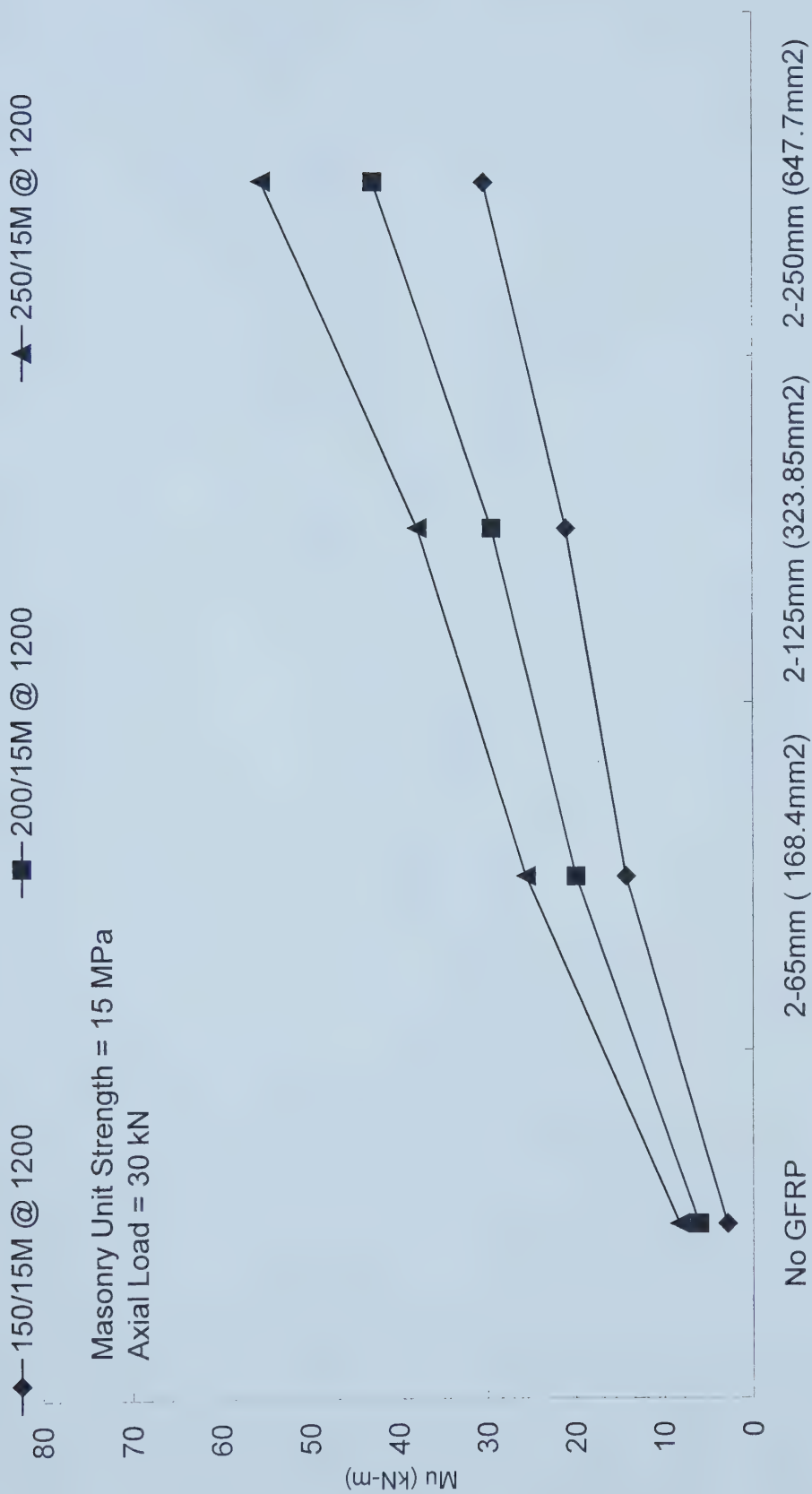


Figure 5.12 GFRP Area versus Ultimate Moment (15MPa Masonry Units, Axial Load = 30kN, 15M@1200)

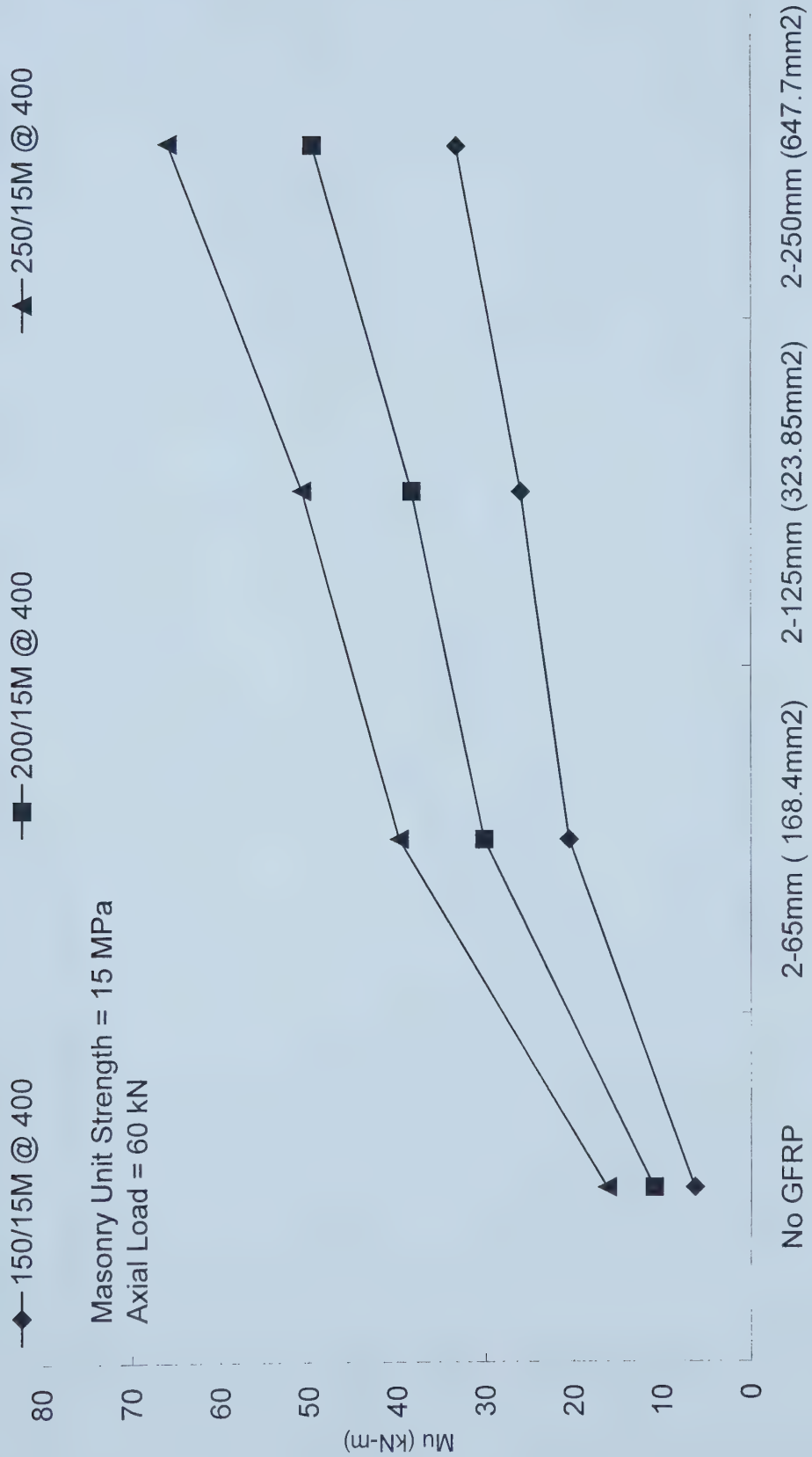


Figure 5.13 GFRP Area versus Ultimate Moment (15MPa Masonry Units, Axial Load = 60kN, 15M@400)

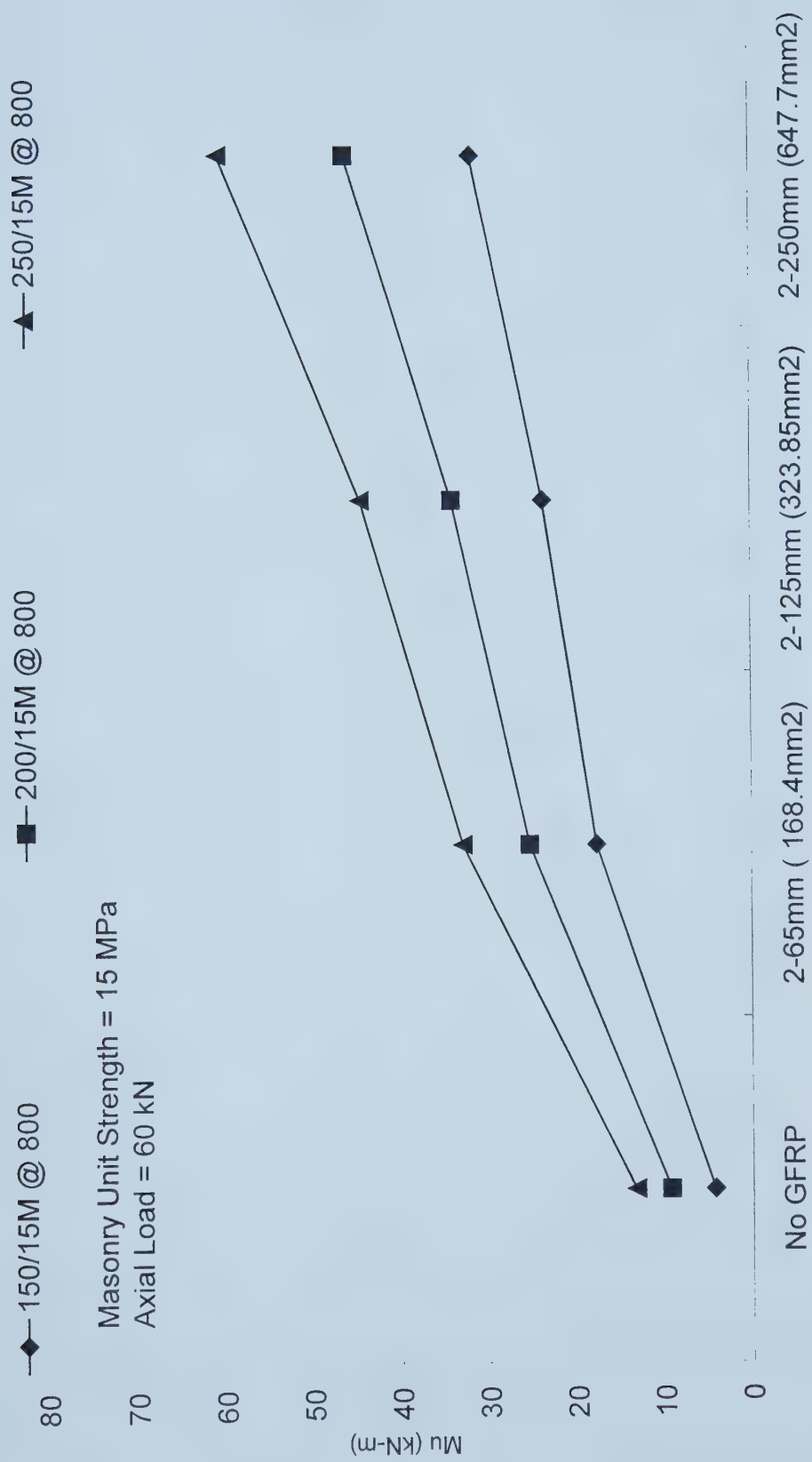


Figure 5.14 GFRP Area versus Ultimate Moment (15MPa Masonry Units, Axial Load = 60kN, 15M@800)

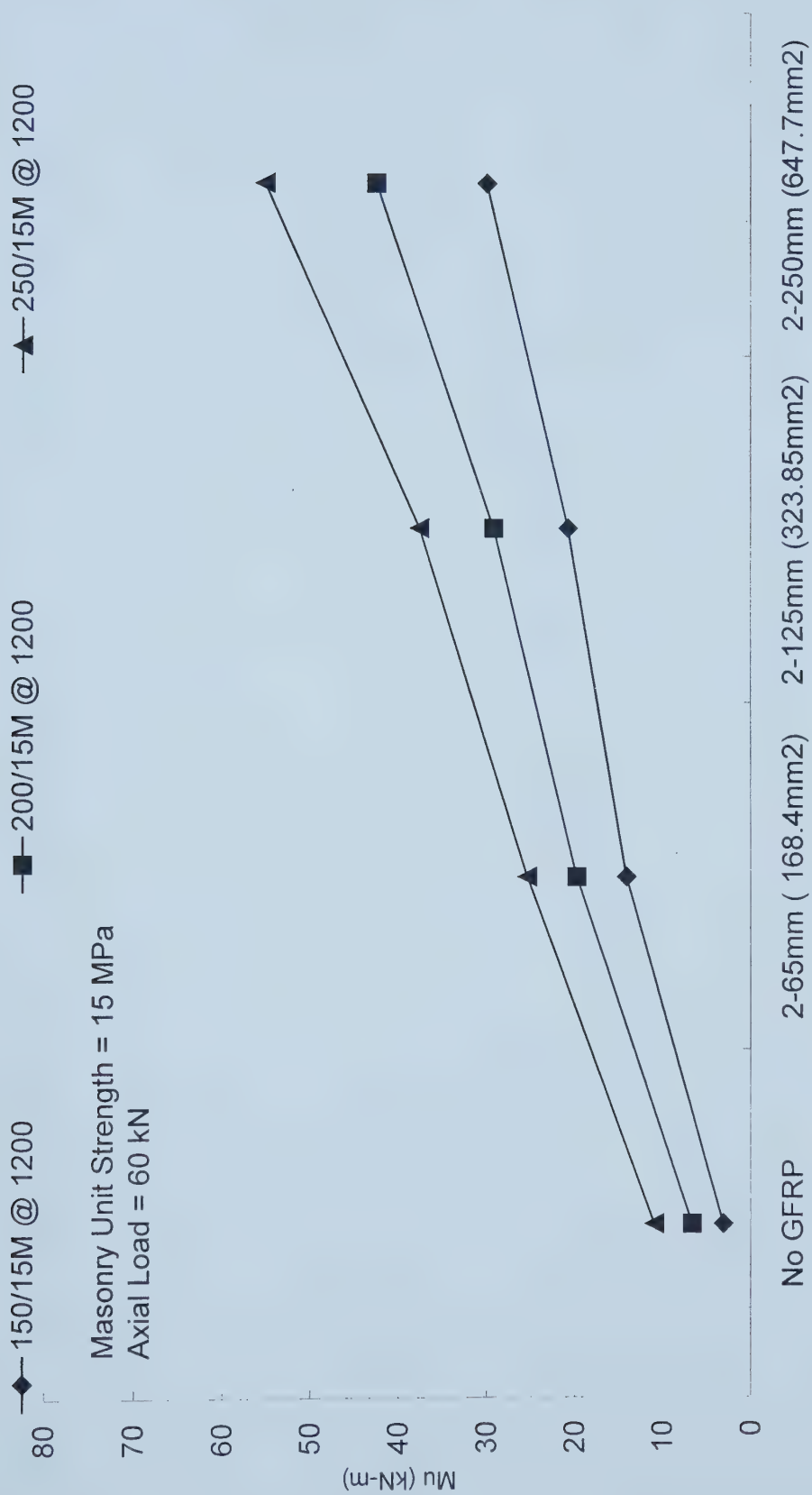


Figure 5.15 GFRP Area versus Ultimate Moment (15MPa Masonry Units, Axial Load = 60kN, 15M@1200)

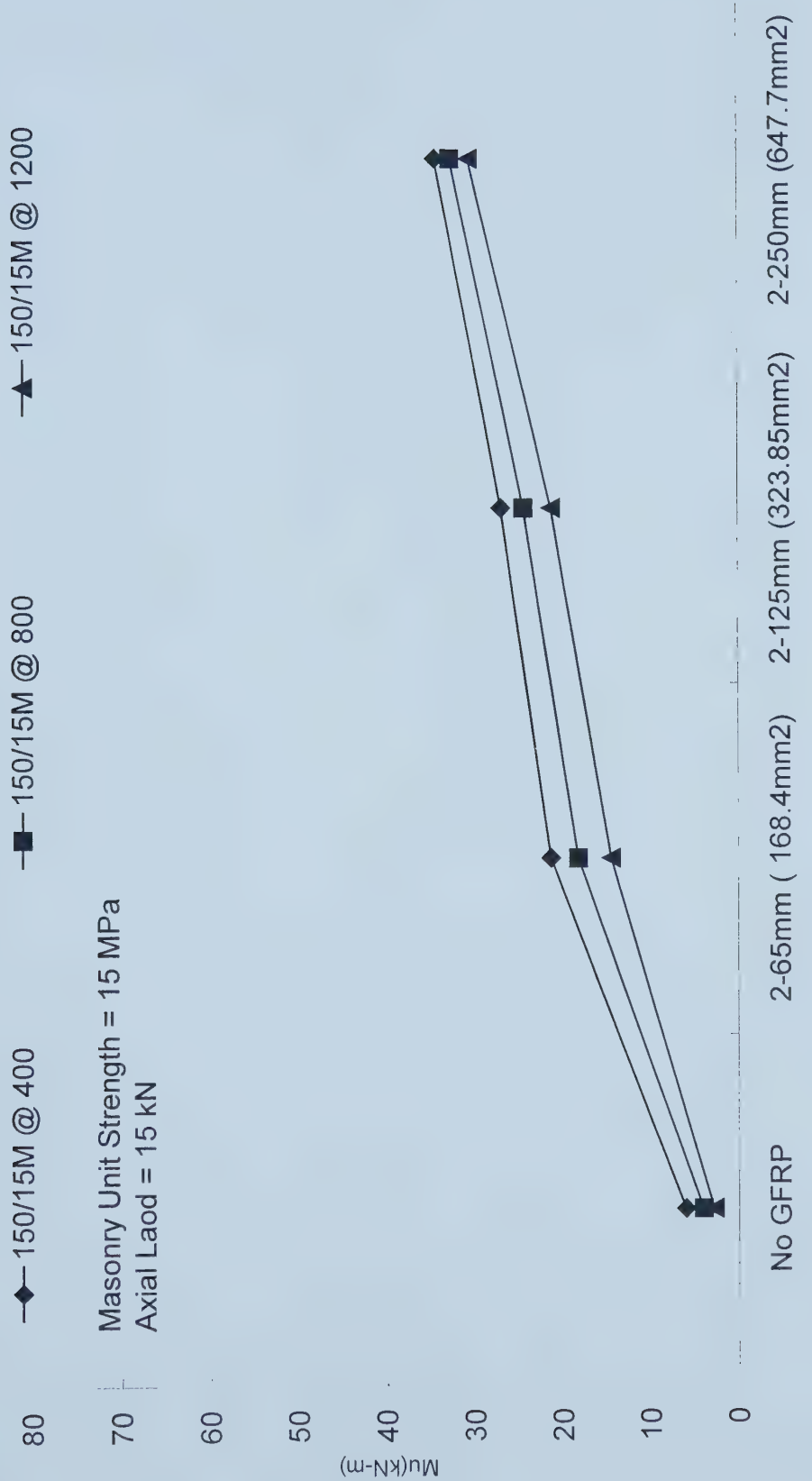


Figure 5.16 GFRP Area versus Ultimate Moment (15MPa, 150mm Masonry Units, Axial Load = 15kN, 15M@400, 15M@800, and 15M@1200)

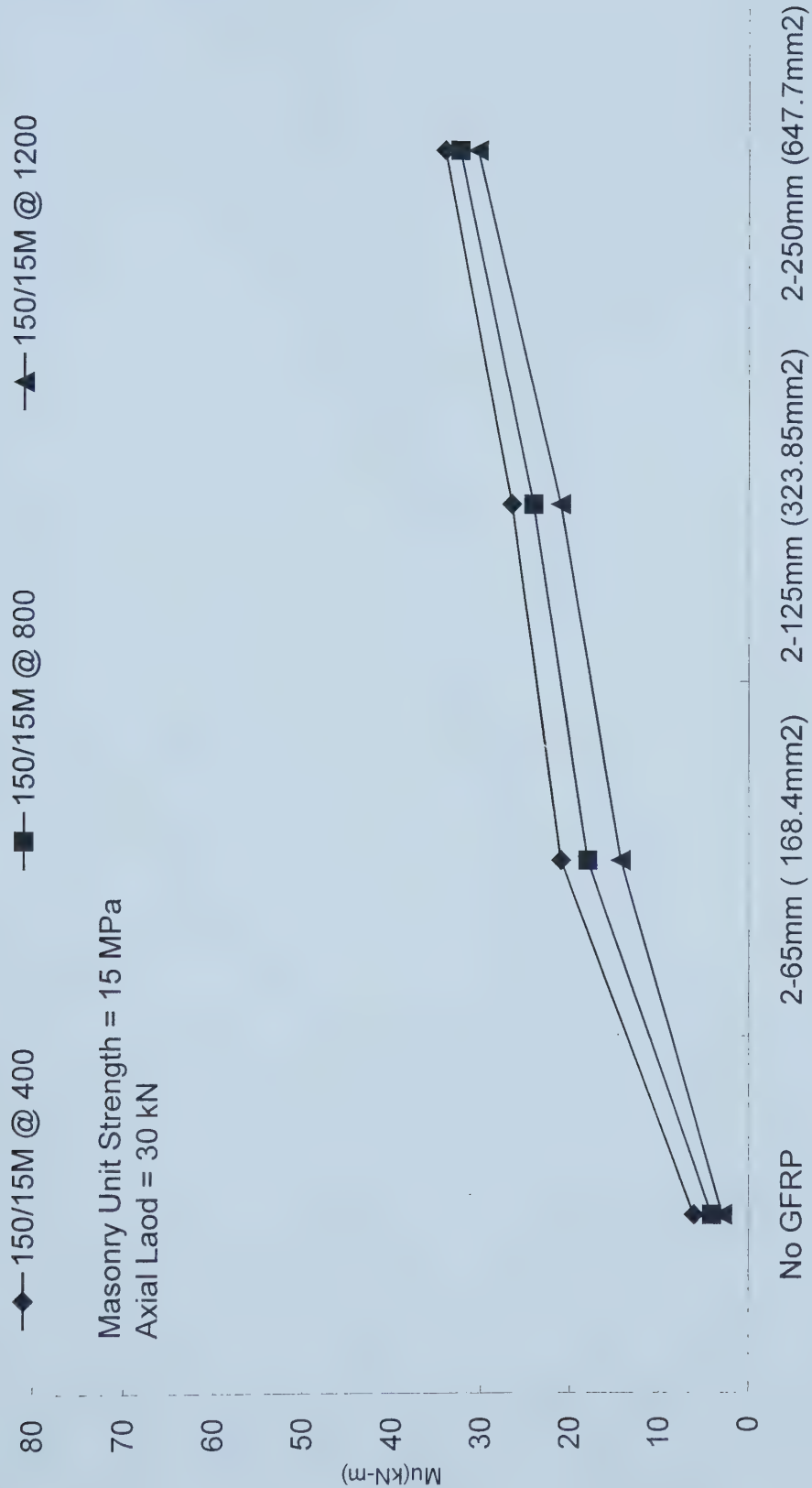


Figure 5.17 GFRP Area versus Ultimate Moment (15MPa, 150mm Masonry Units, Axial Load = 30kN, 15M@400, 15M@800, and 15M@1200)

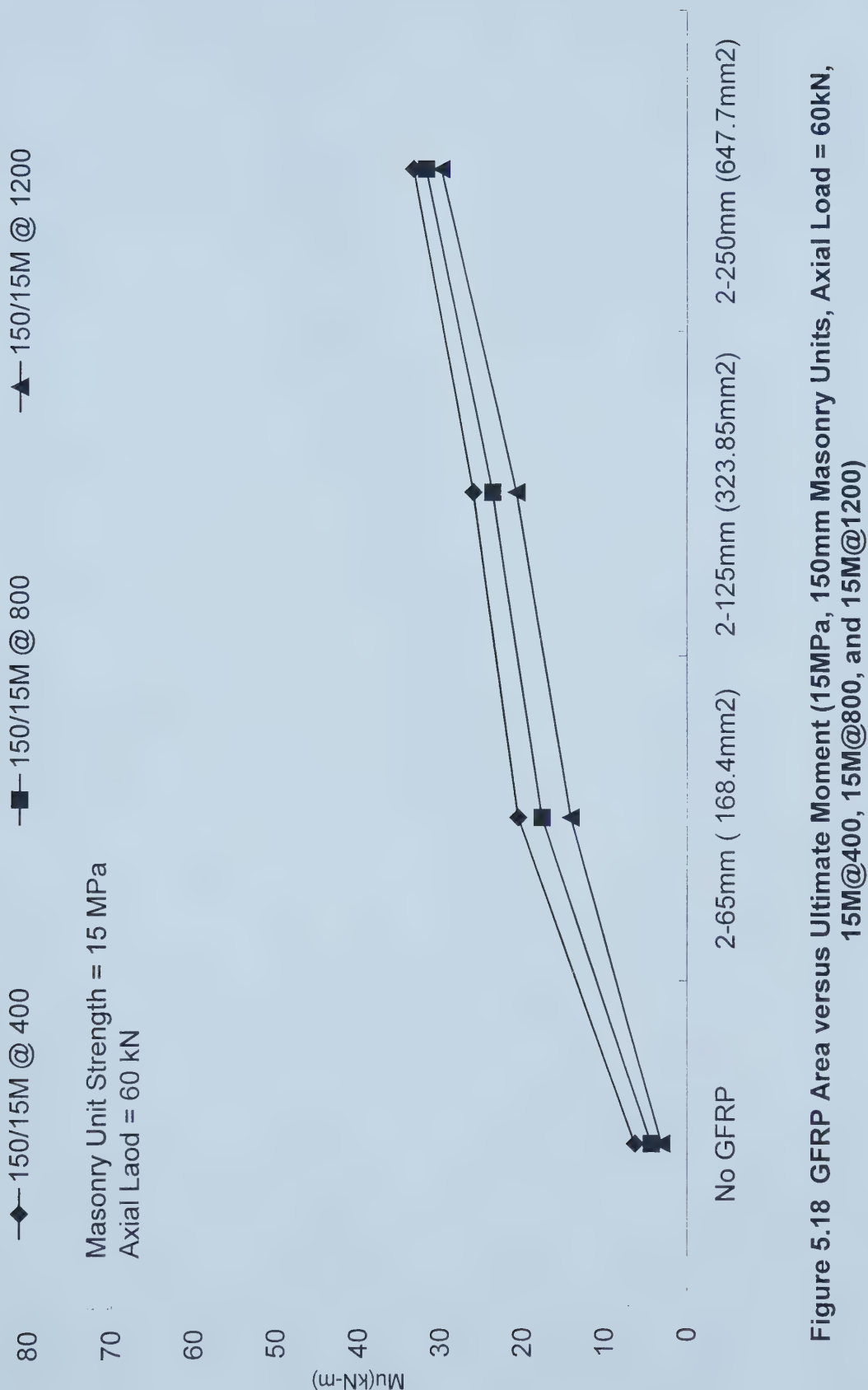


Figure 5.18 GFRP Area versus Ultimate Moment (15MPa, 150mm Masonry Units, Axial Load = 60kN, 15M@400, 15M@800, and 15M@1200)

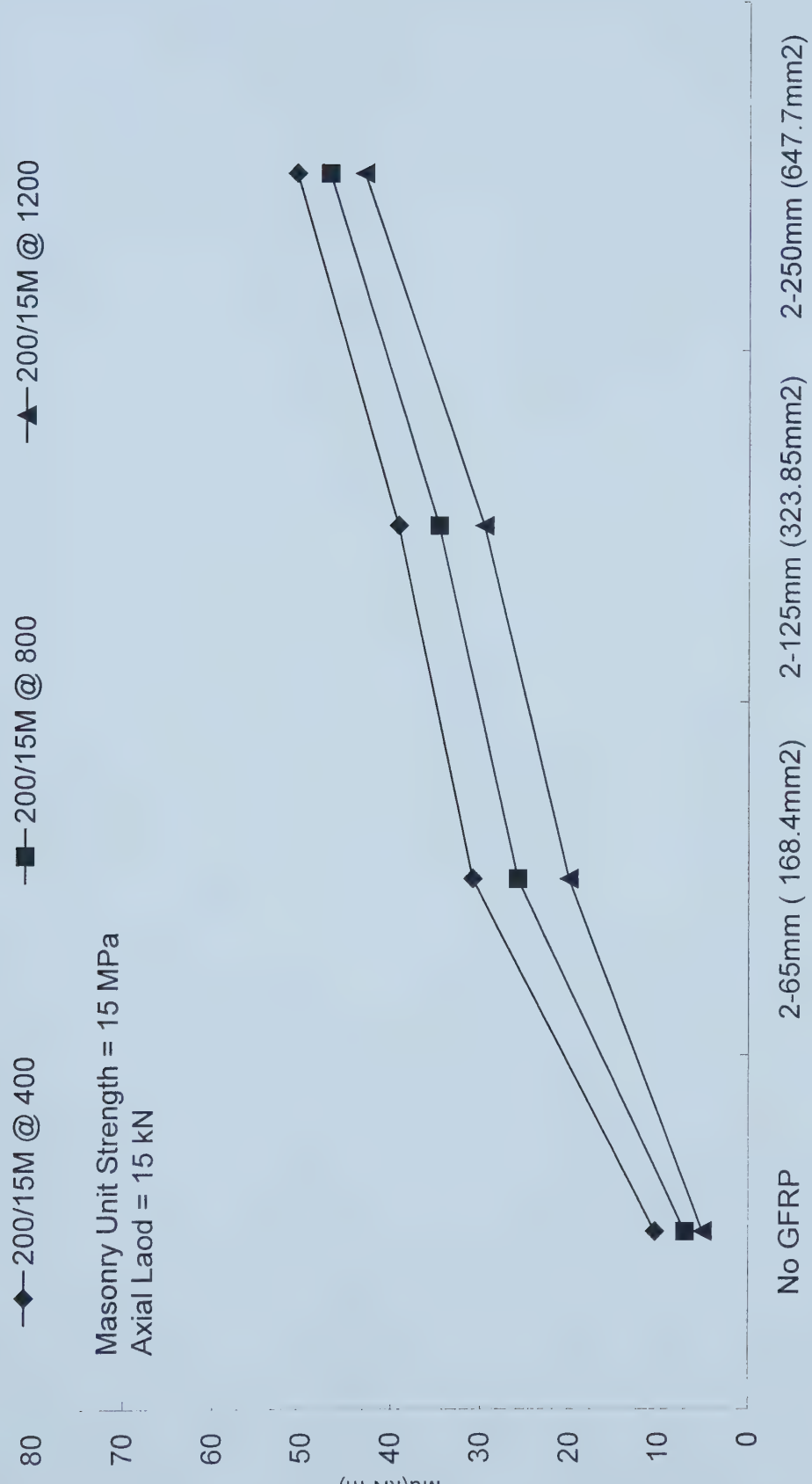


Figure 5.19 GFRP Area versus Ultimate Moment (15MPa, 200mm Masonry Units, Axial Load = 15kN, 15M@400, 15M@800, and 15M@1200)

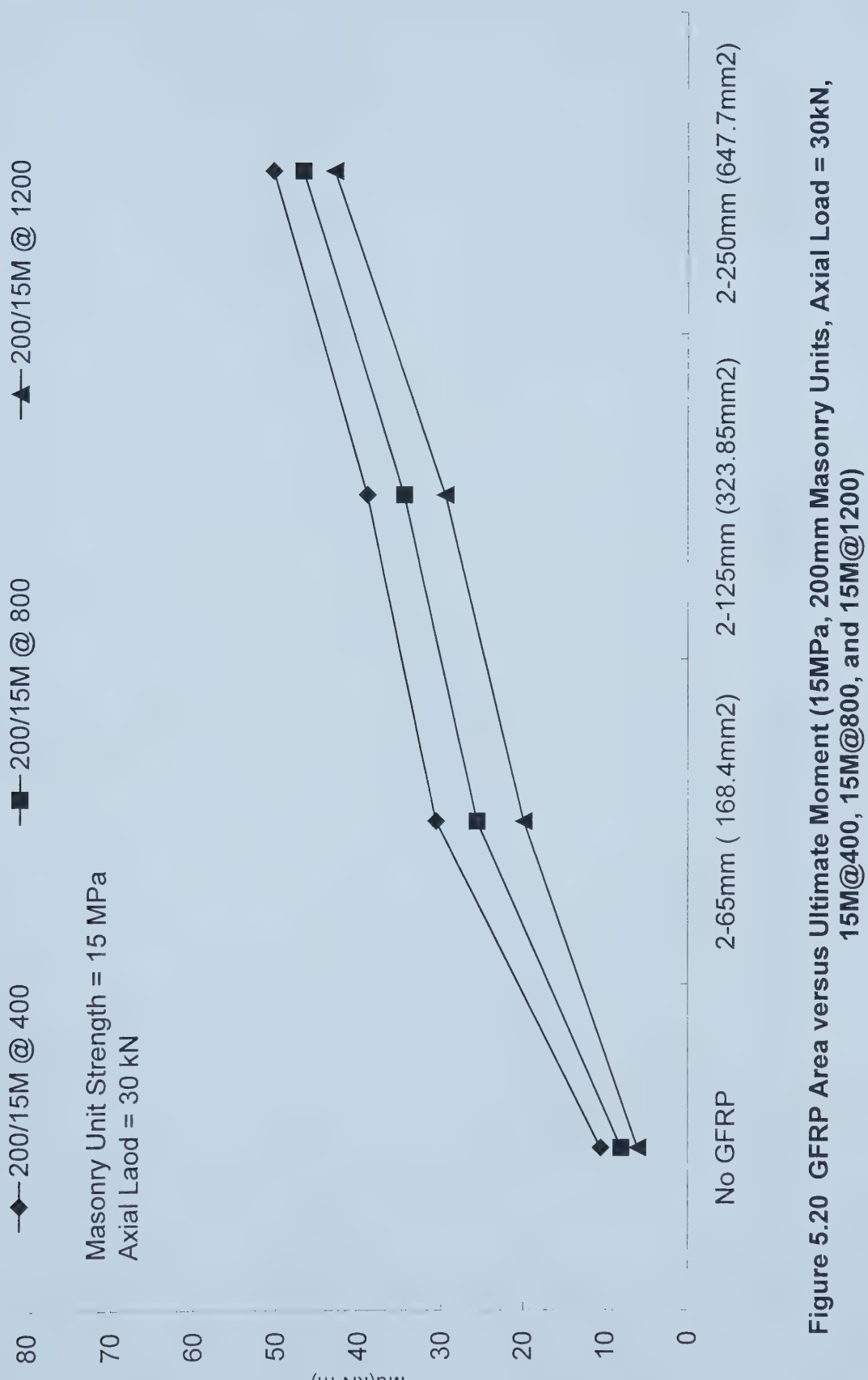


Figure 5.20 GFRP Area versus Ultimate Moment (15MPa, 200mm Masonry Units, Axial Load = 30kN, 15M@400, 15M@800, and 15M@1200)

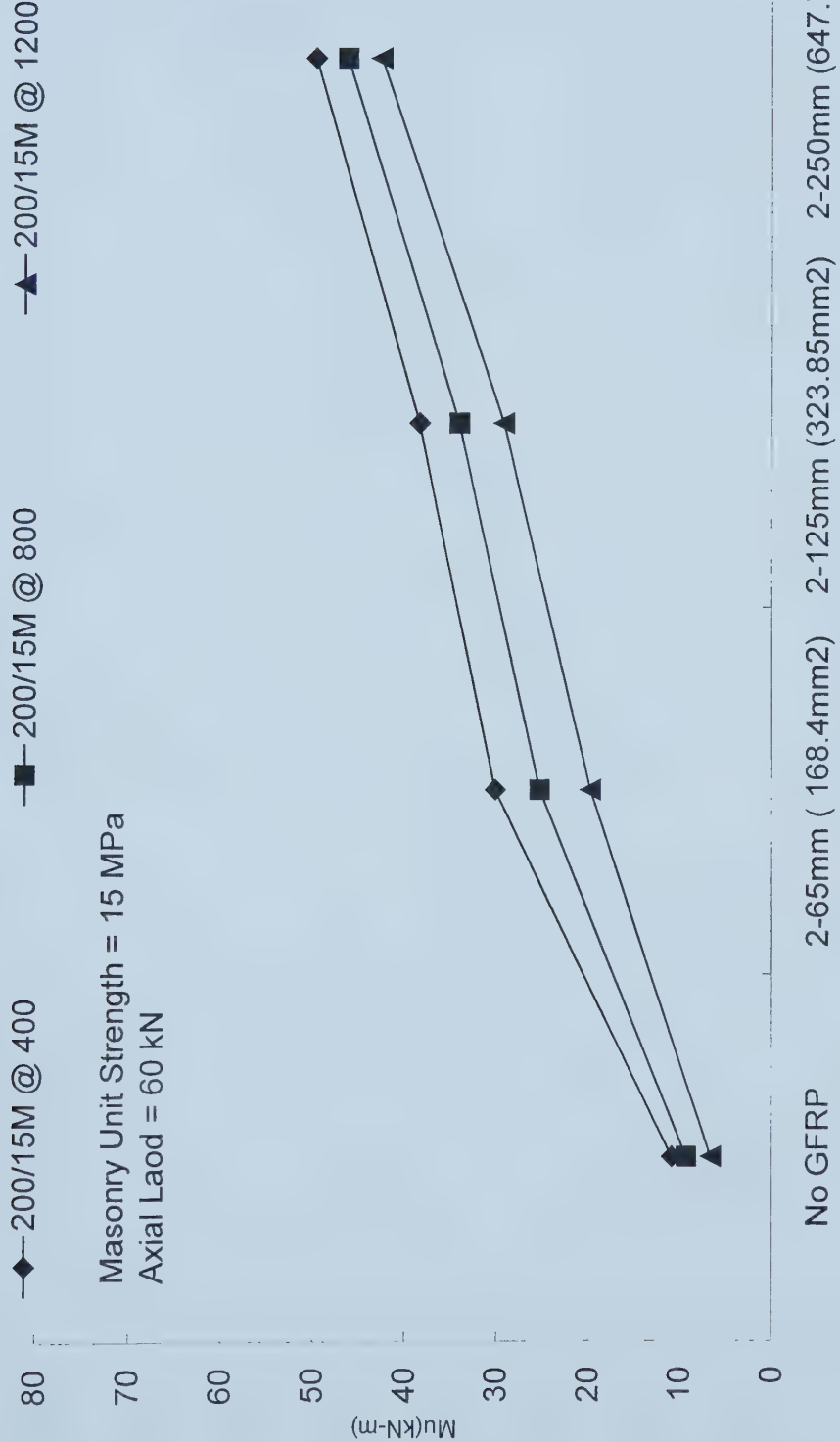


Figure 5.21 GFRP Area versus Ultimate Moment (15MPa, 200mm Masonry Units, Axial Load = 60kN, 15M@400, 15M@800, and 15M@1200)

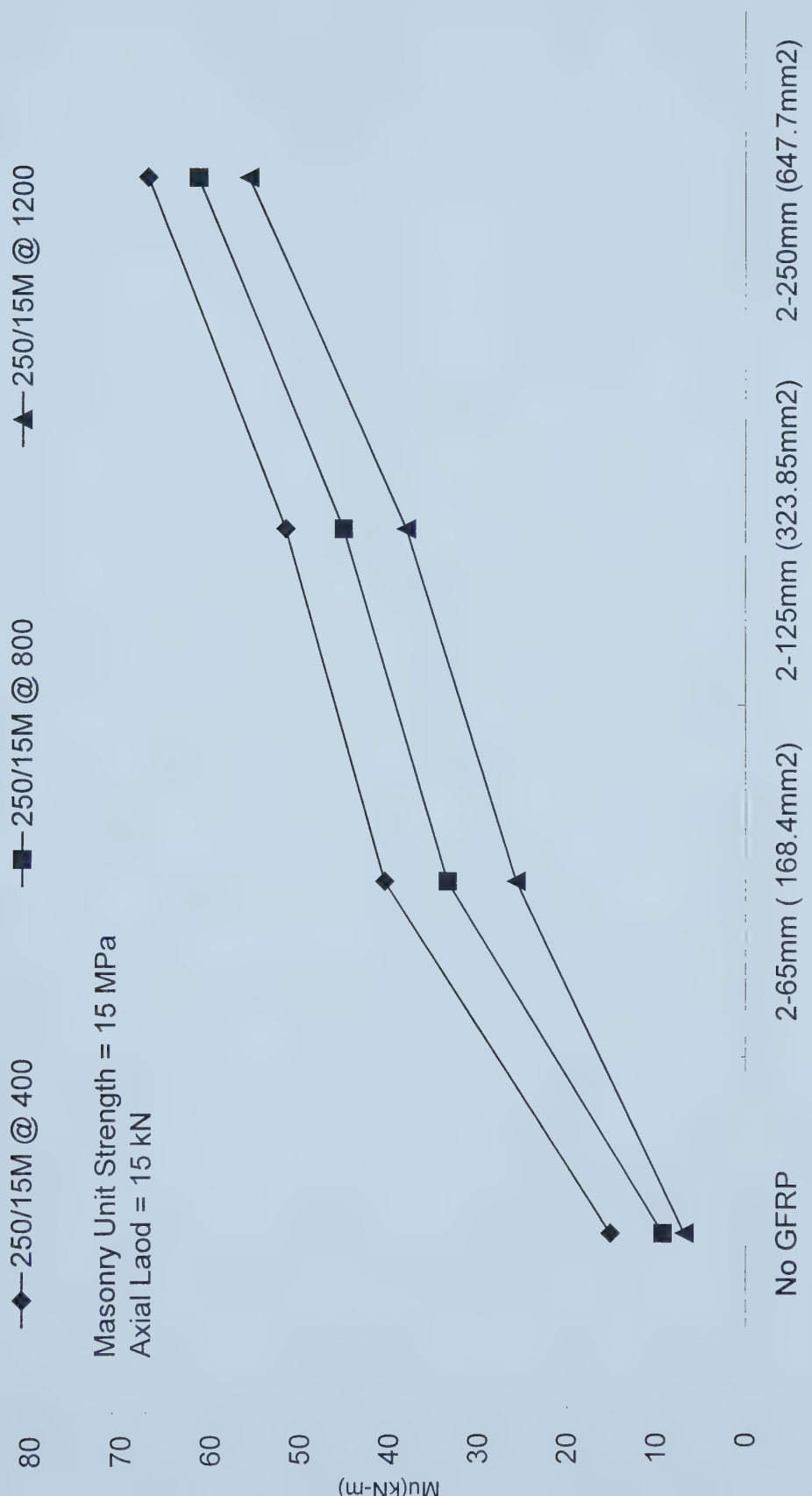


Figure 5.22 GFRP Area versus Ultimate Moment (15MPa, 250mm Masonry Units, Axial Load = 15kN, 15M@400, 15M@800, and 15M@1200)

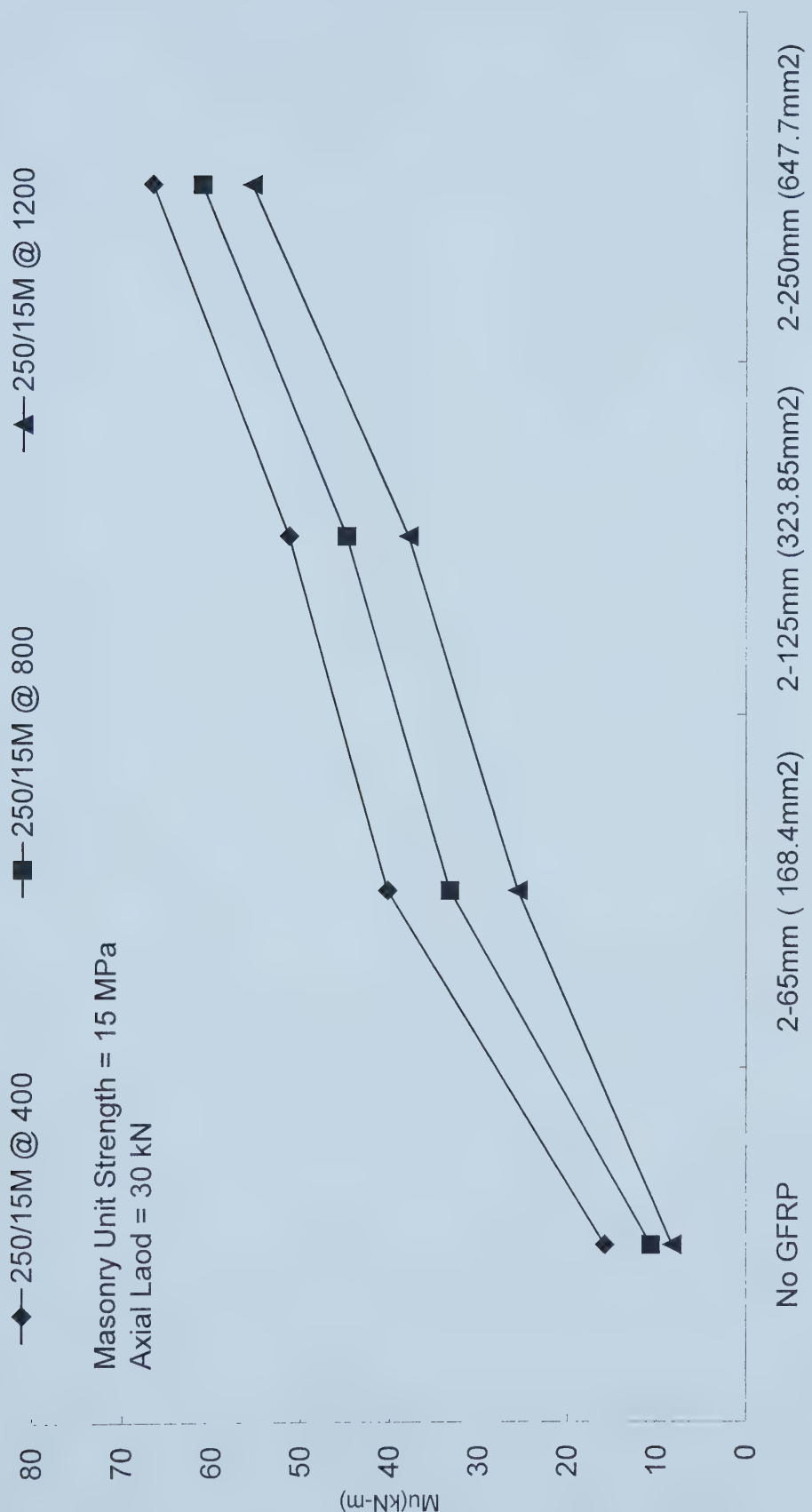


Figure 5.23 GFRP Area versus Ultimate Moment (15MPa, 250mm Masonry Units, Axial Load = 30kN, 15M@400, 15M@800, and 15M@1200)

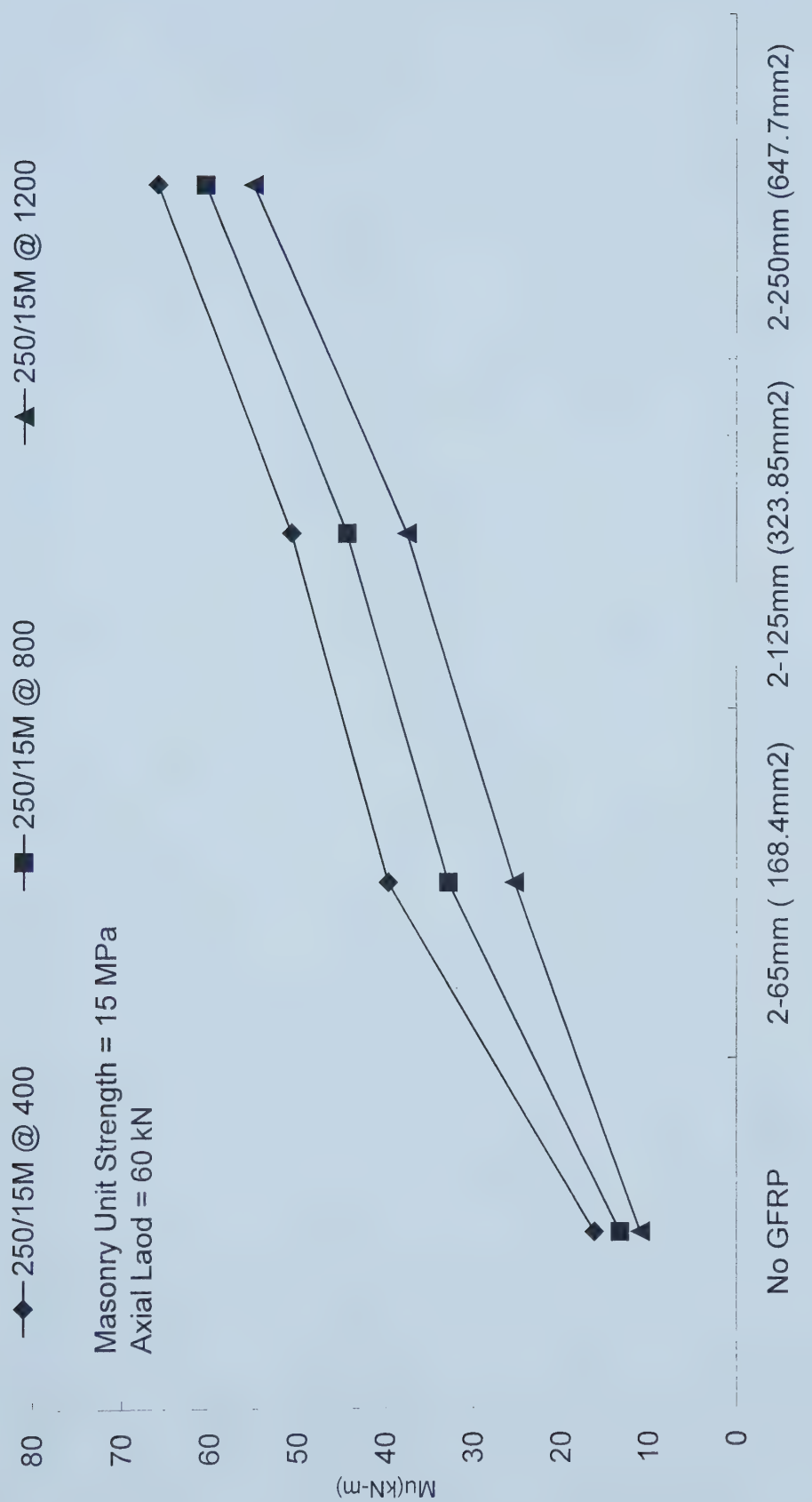


Figure 5.24 GFRP Area versus Ultimate Moment (15 MPa, 250 mm Masonry Units, Axial Load = 60 kN, 15 M@400, 15 M@800, and 15 M@1200)

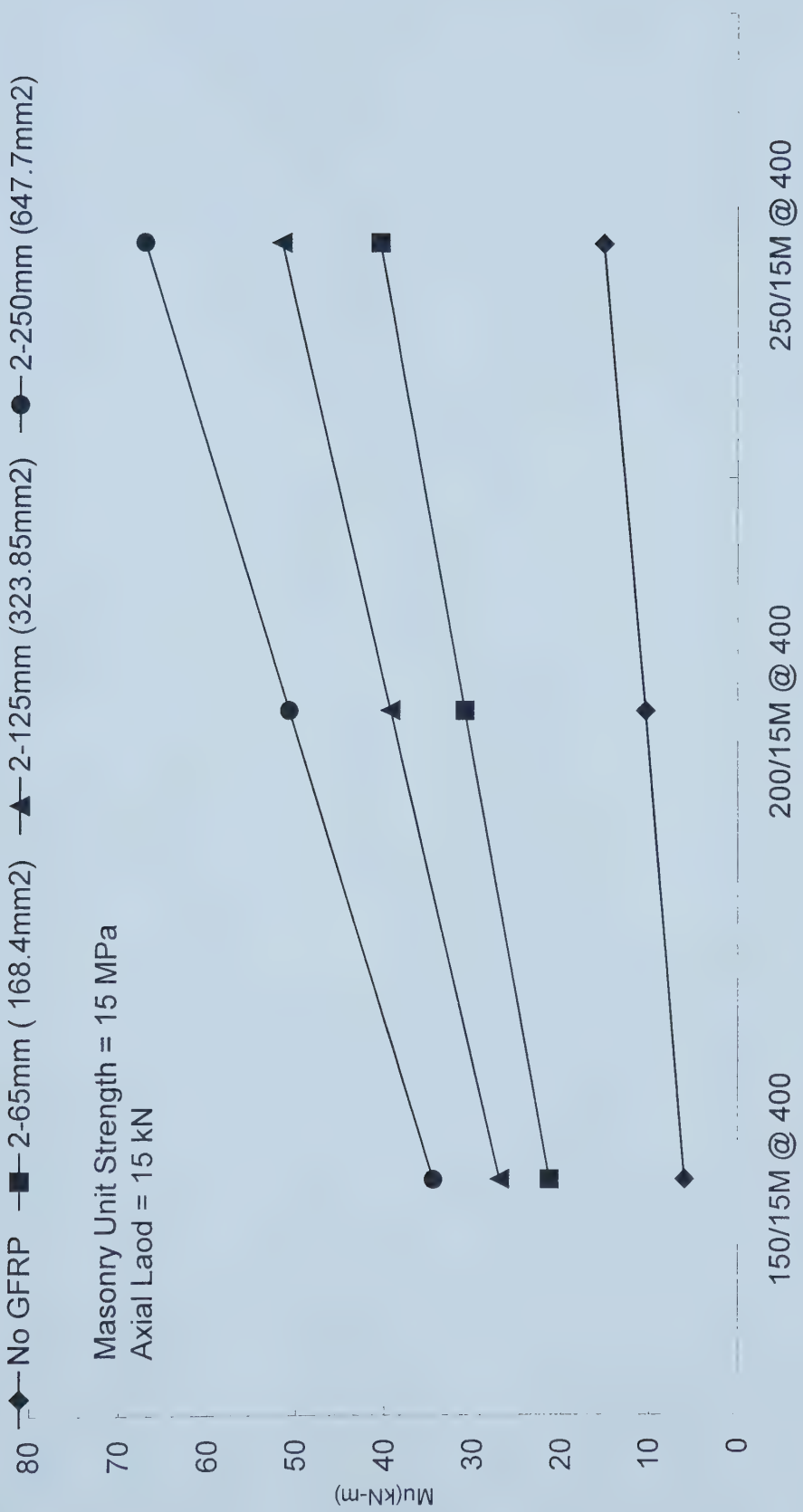


Figure 5.25 Vertical Steel (15M@400) versus Ultimate Moment (15MPa Masonry Strength, Axial Load = 15kN, Various Amounts of GFRP)

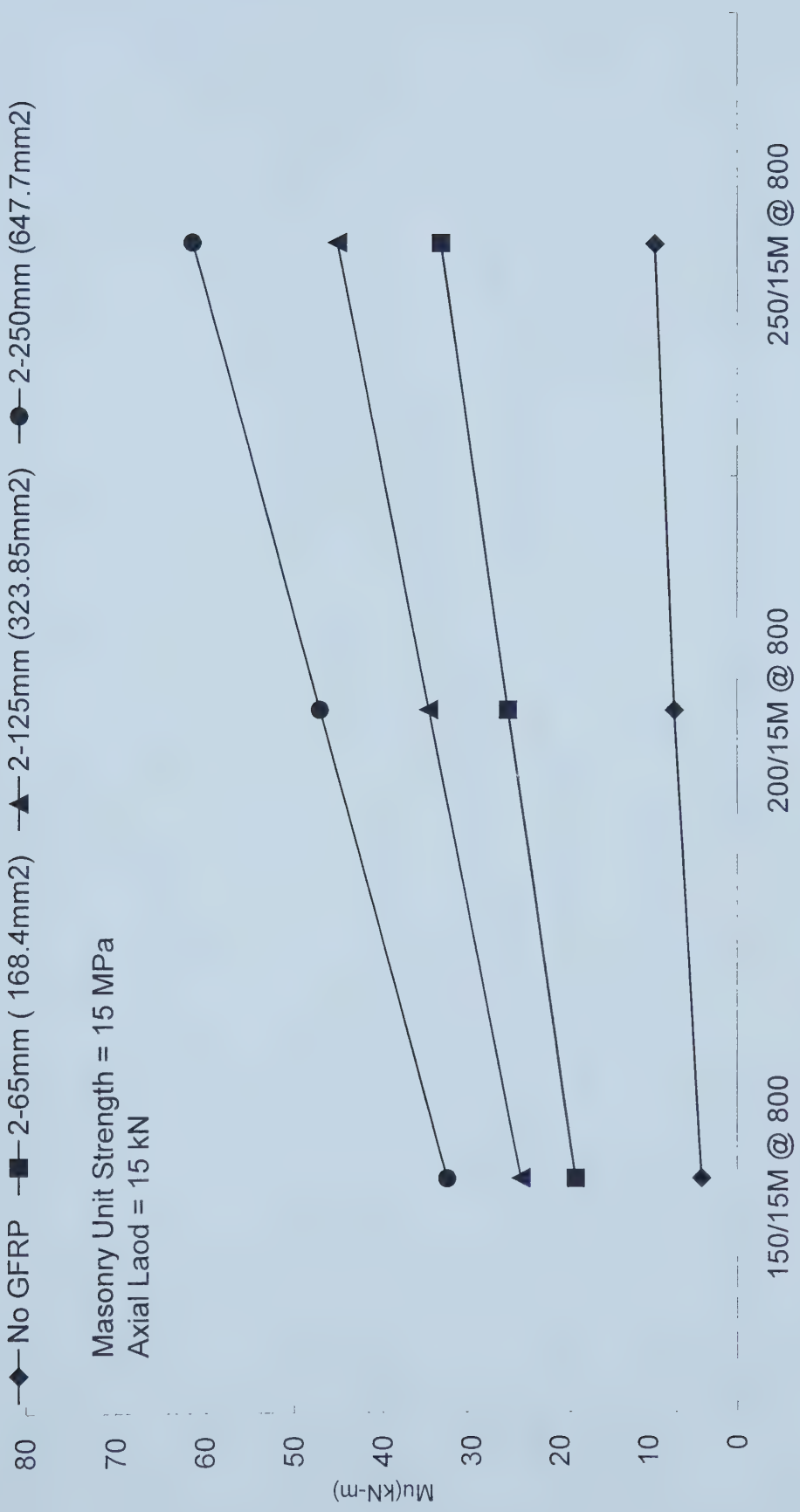


Figure 5.26 Vertical Steel (15M@800) versus Ultimate Moment (15MPa Masonry Strength, Axial Load = 15kN, Various Amounts of GFRP)

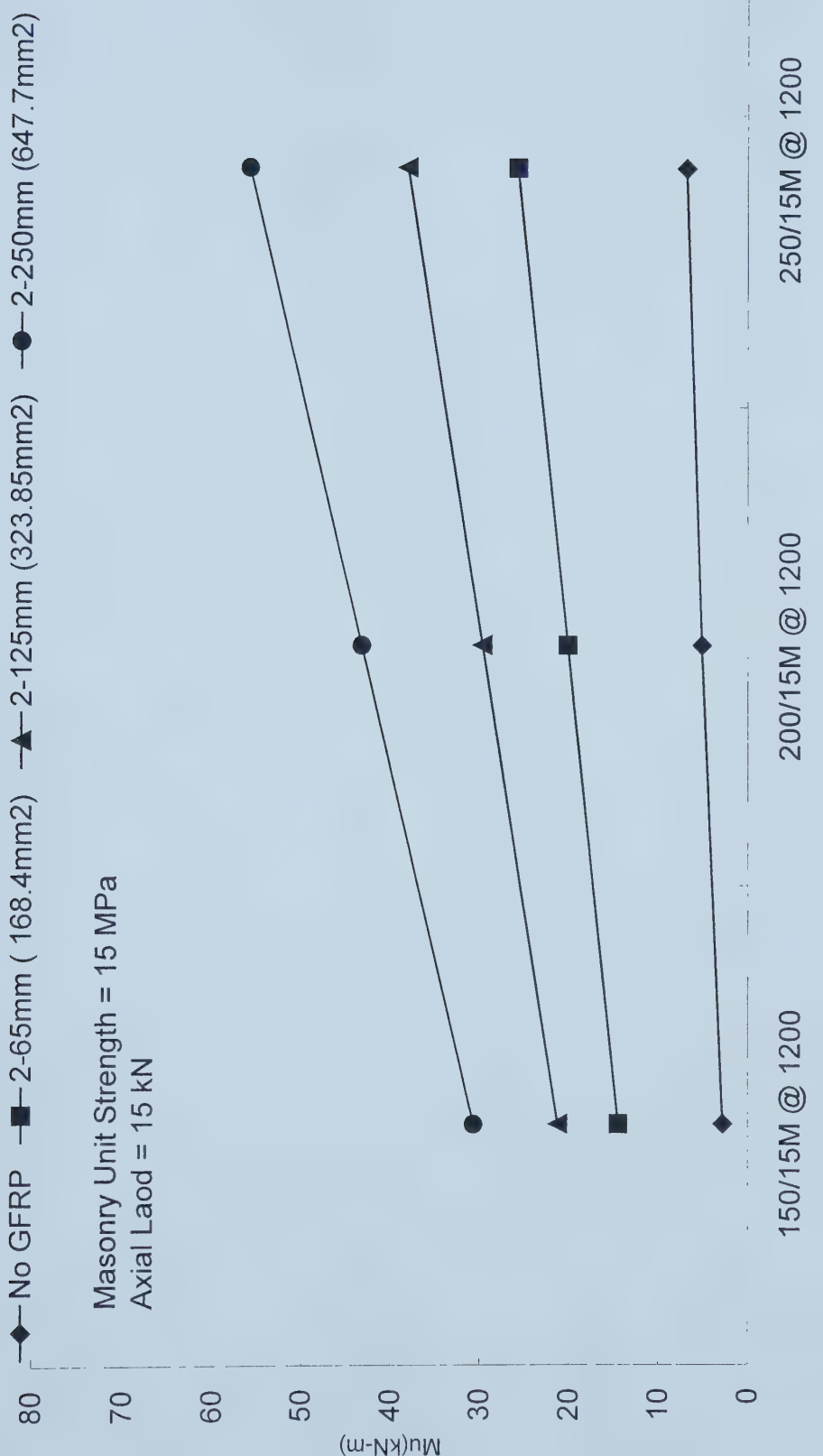


Figure 5.27 Vertical Steel (15M@1200) versus Ultimate Moment (15MPa Masonry Strength, Axial Load = 15kN, Various Amounts of GFRP)

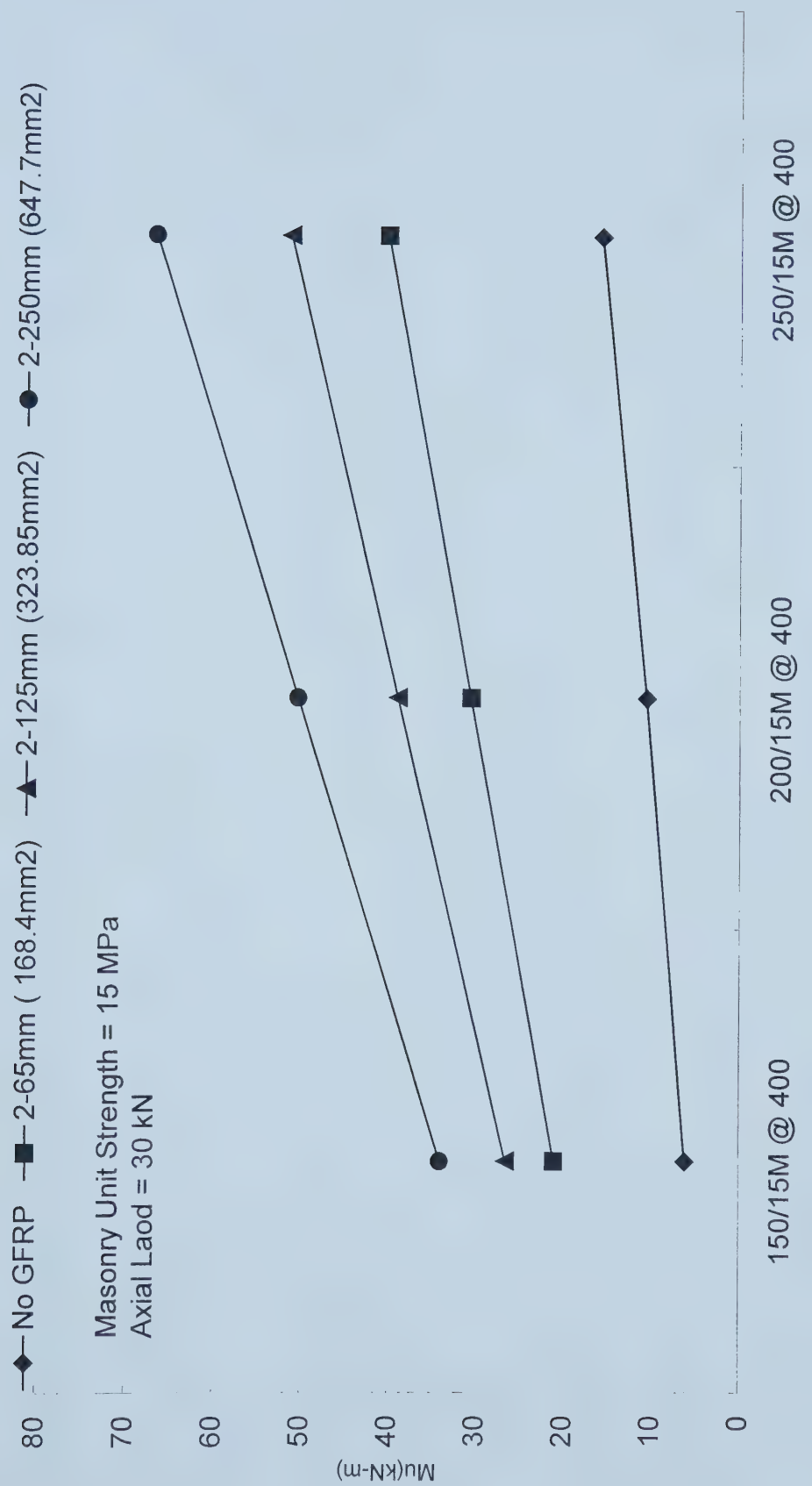


Figure 5.28 Vertical Steel (15M@400) versus Ultimate Moment (15MPa Masonry Strength, Axial Load = 30kN, Various Amounts of GFRP)

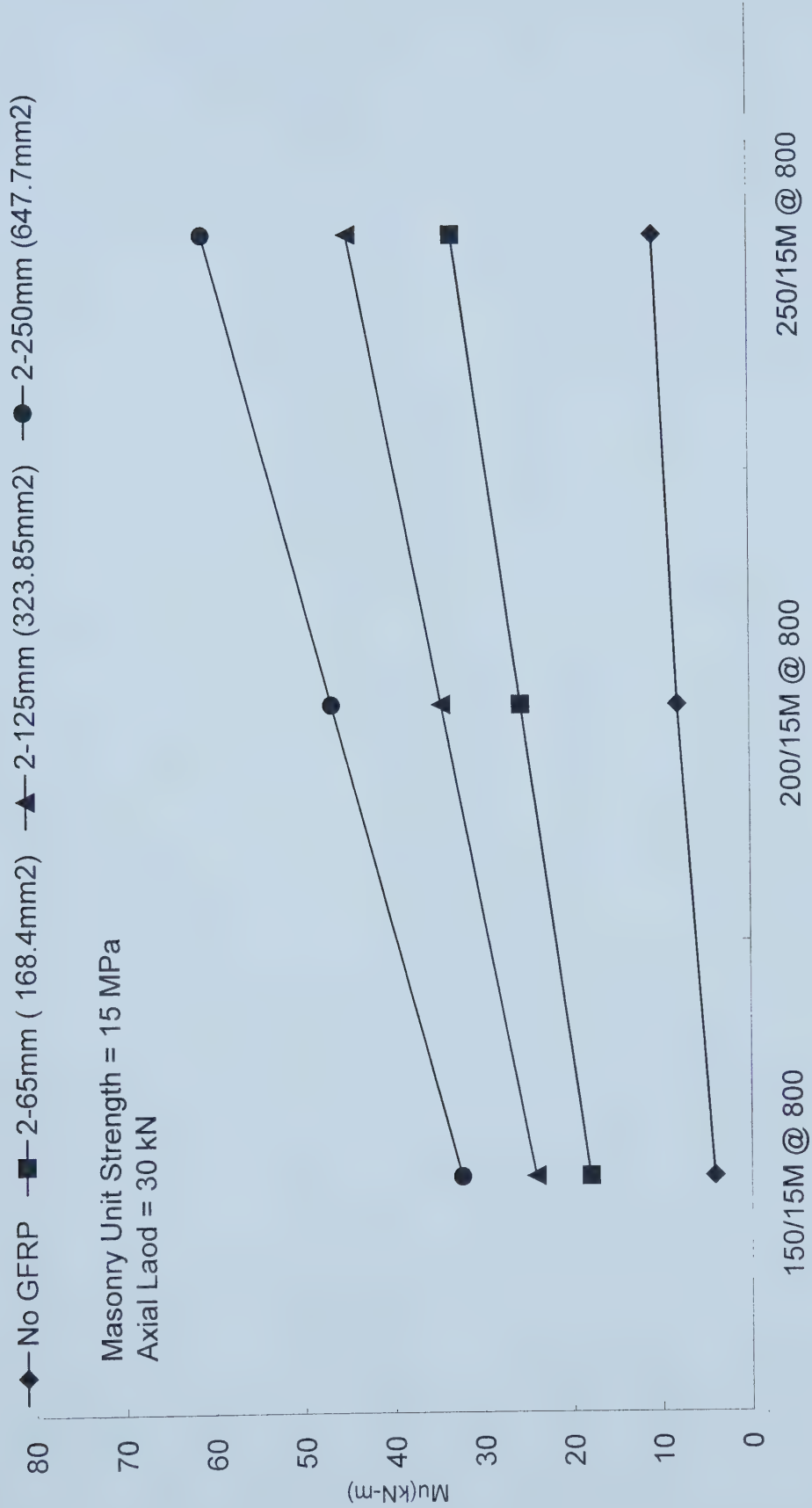


Figure 5.29 Vertical Steel (15M@800) versus Ultimate Moment ($15M@800$) versus Various Amounts of GFRP, Axial Load = 30kN,

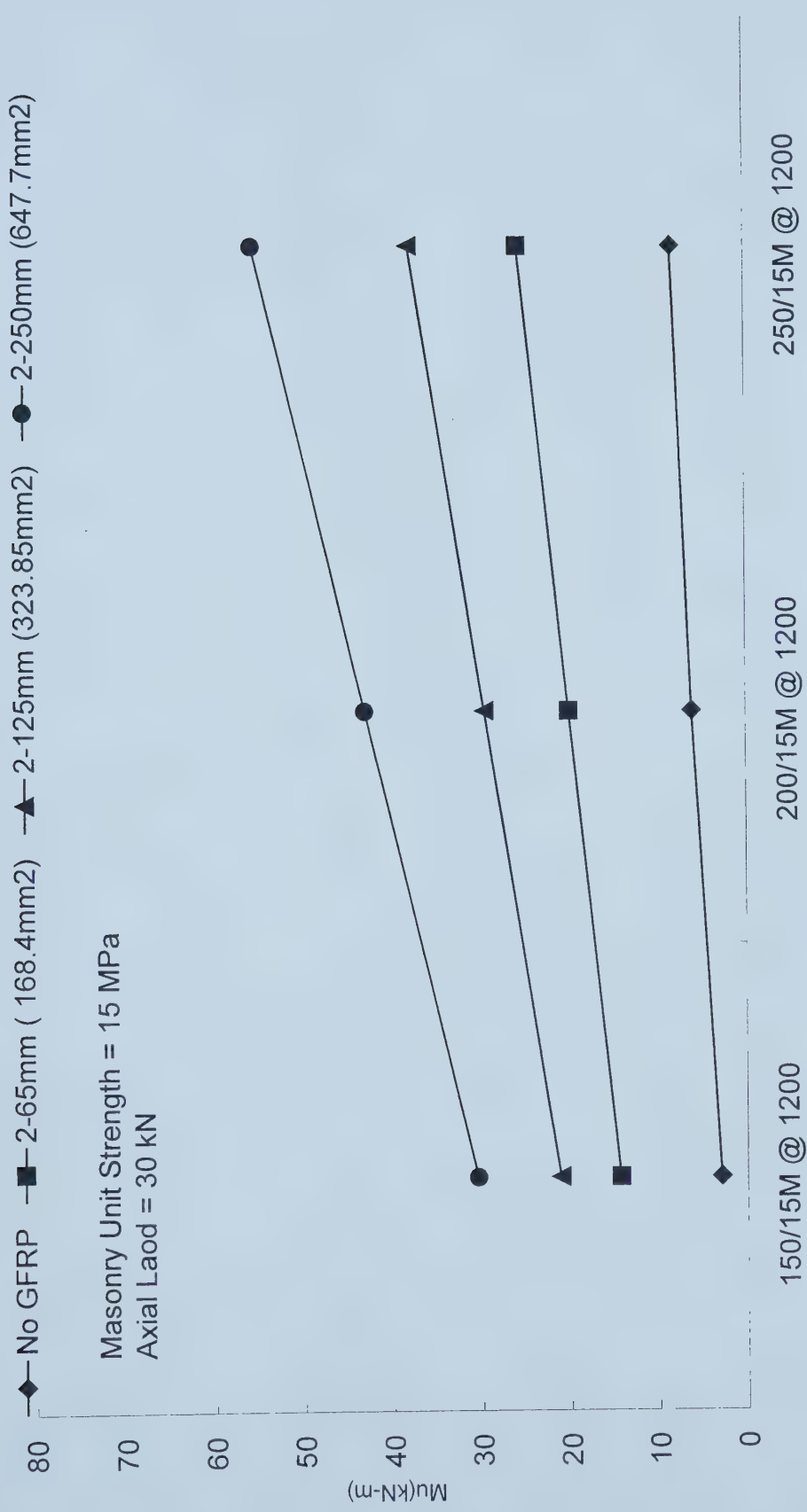


Figure 5.30 Vertical Steel (15M@1200) versus Ultimate Moment (15MPa Masonry Strength, Axial Load = 30kN, Various Amounts of GFRP)

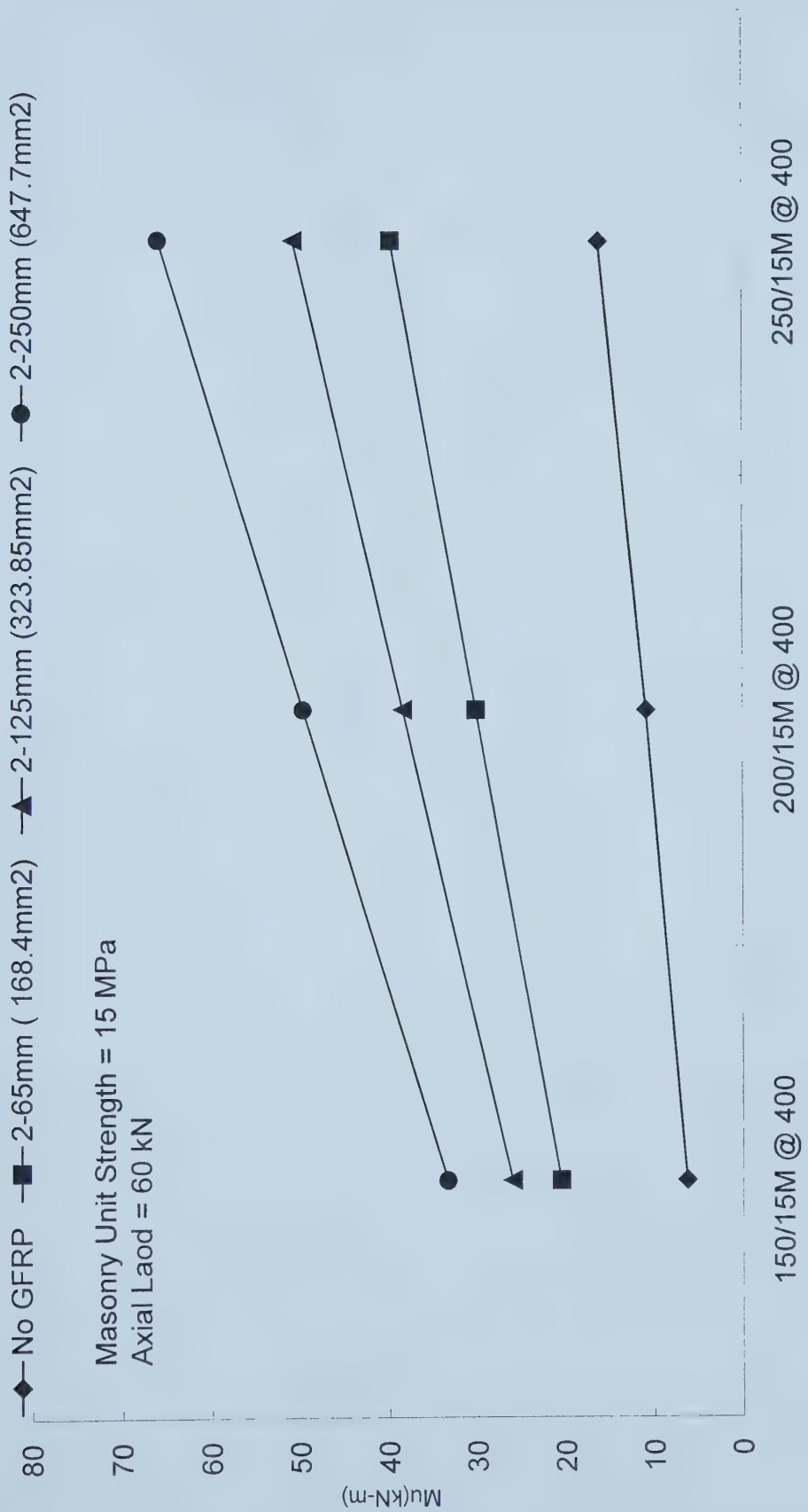


Figure 5.31 Vertical Steel (15M@400) versus Ultimate Moment (15MPa Masonry Strength, Axial Load = 60kN, Various Amounts of GFRP)

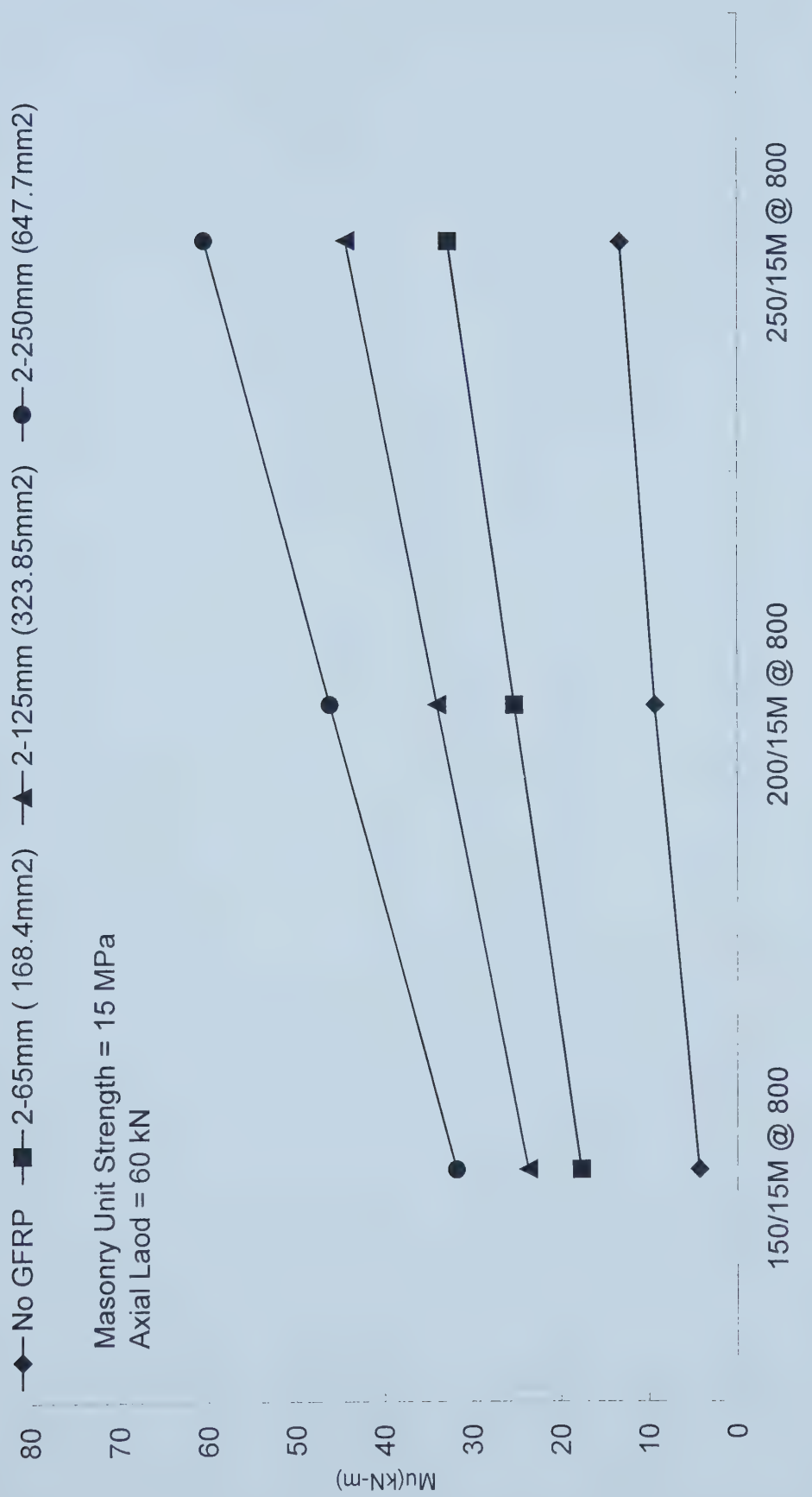


Figure 5.32 Vertical Steel (15M@800) versus Ultimate Moment (15M@800) for various amounts of GFRP

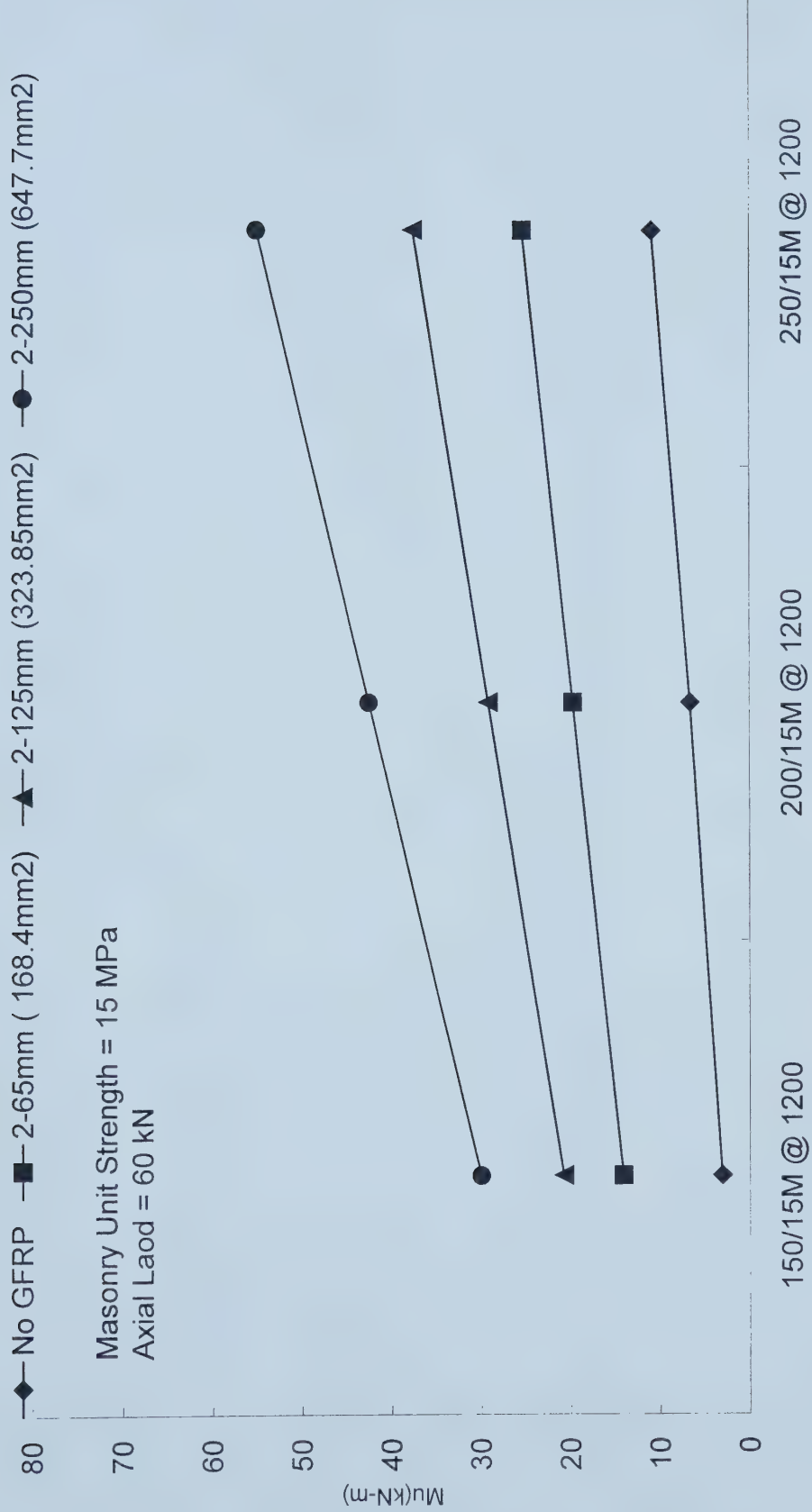


Figure 5.33 Vertical Steel (15M@1200) versus Ultimate Moment (15MPa Masonry Strength, Axial Load = 60kN, Various Amounts of GFRP)

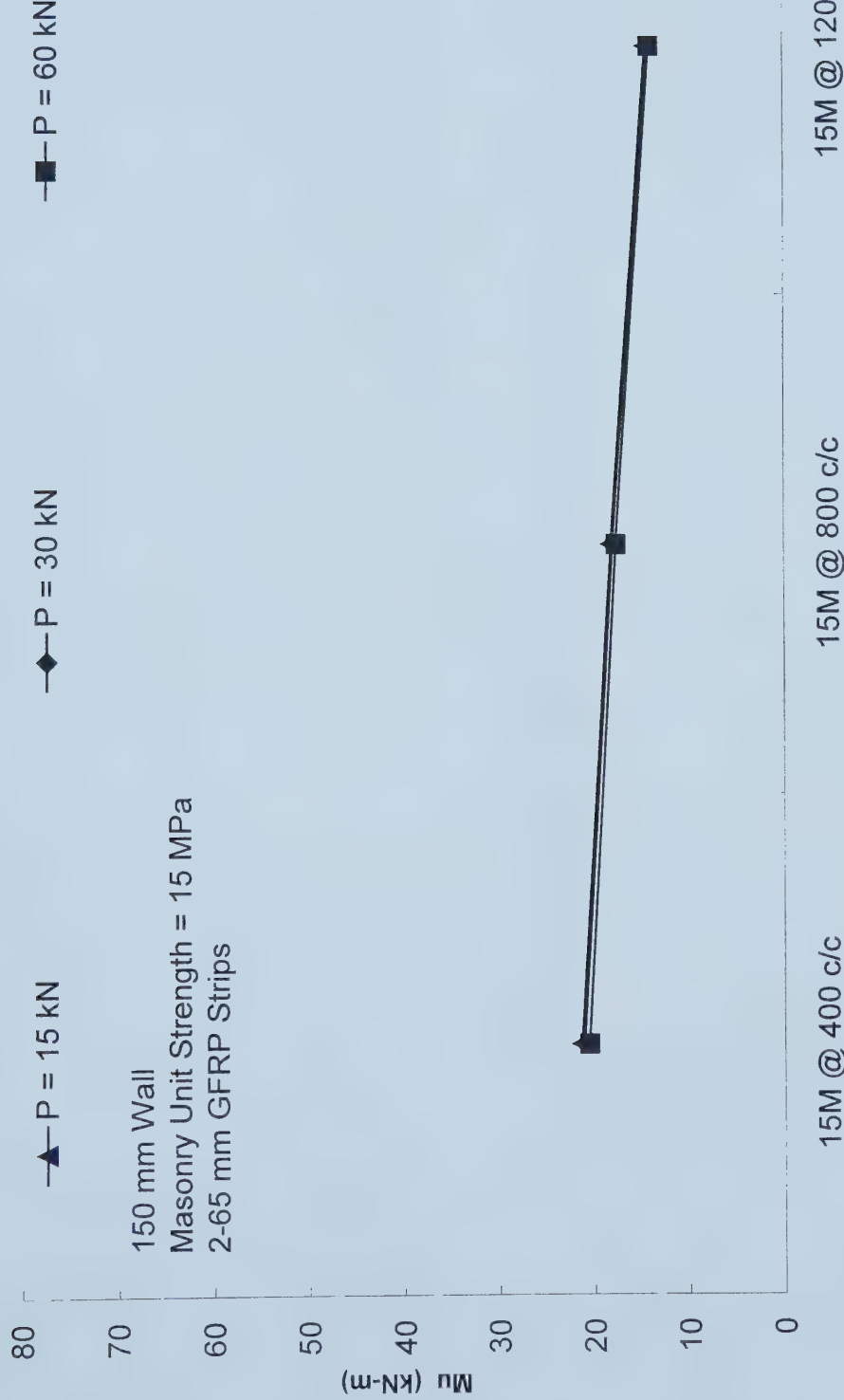


Figure 5.34 Vertical Steel ($15M @ 400, 800, 1200\text{mm}$) versus Ultimate Moment ($15\text{MPa}, 150\text{mm Masonry Units}, 2.65\text{mm GFRP, Various Amounts of Axial Load})$

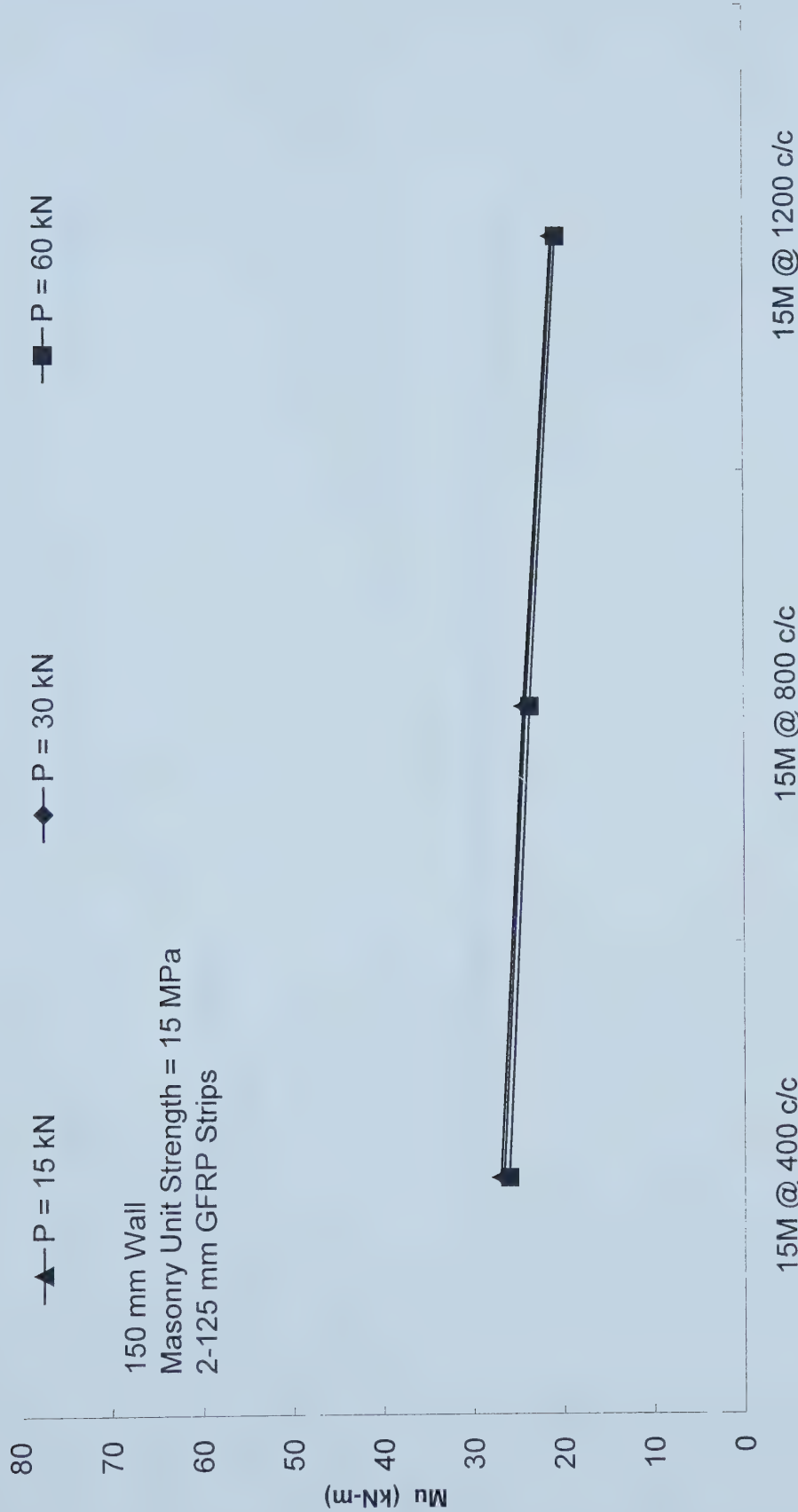


Figure 5.35 Vertical Steel (15M@400, 800, 1200mm) versus Ultimate Moment (15MPa, 150mm Masonry Units, 2-125mm GFRP, Various Amounts of Axial Load)

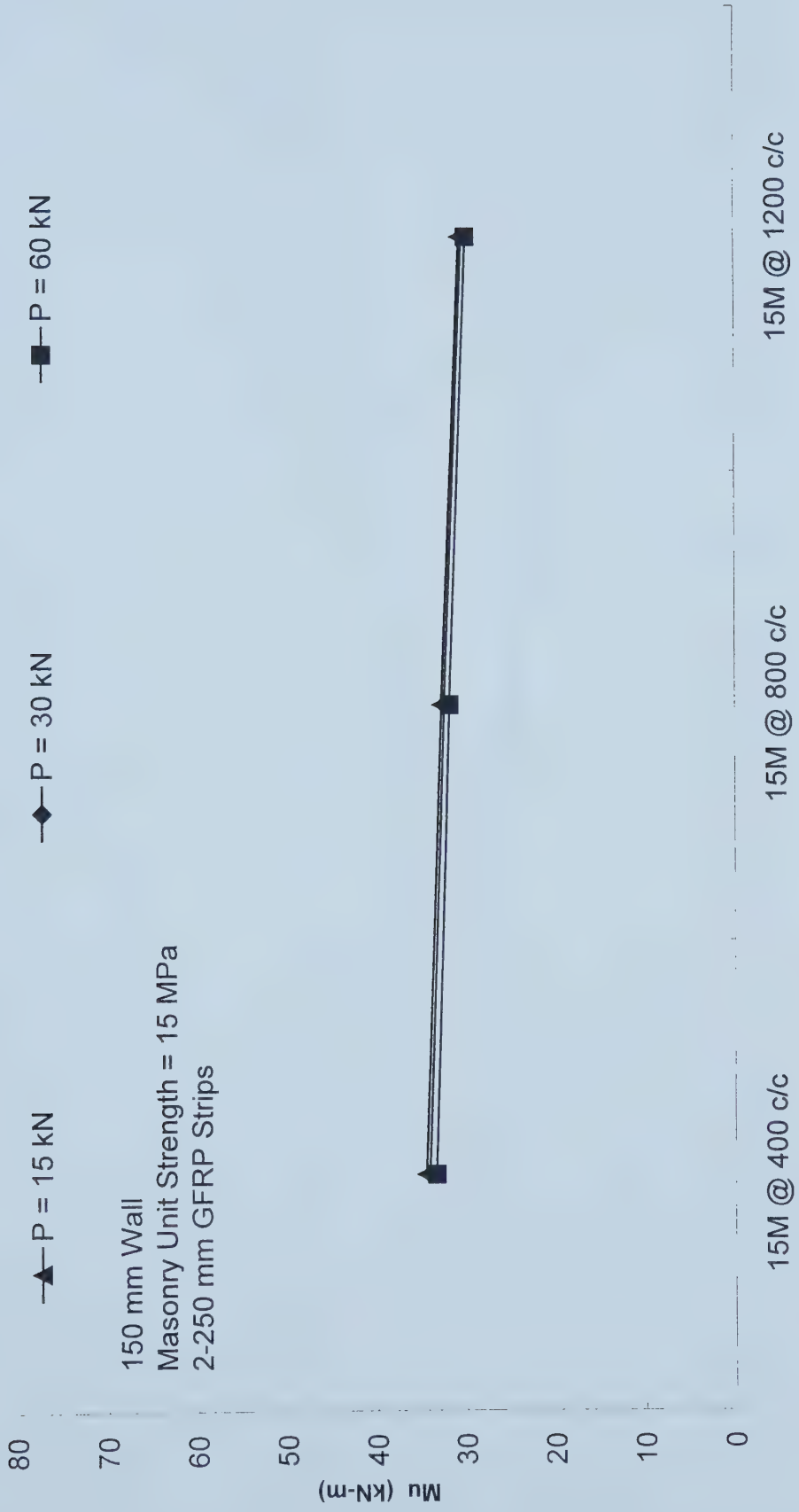


Figure 5.36 Vertical Steel (15M@400, 800, 1200mm) versus Ultimate Moment (15MPa, 150mm Masonry Units, 2-250mm GFRP, Various Amounts of Axial Load)

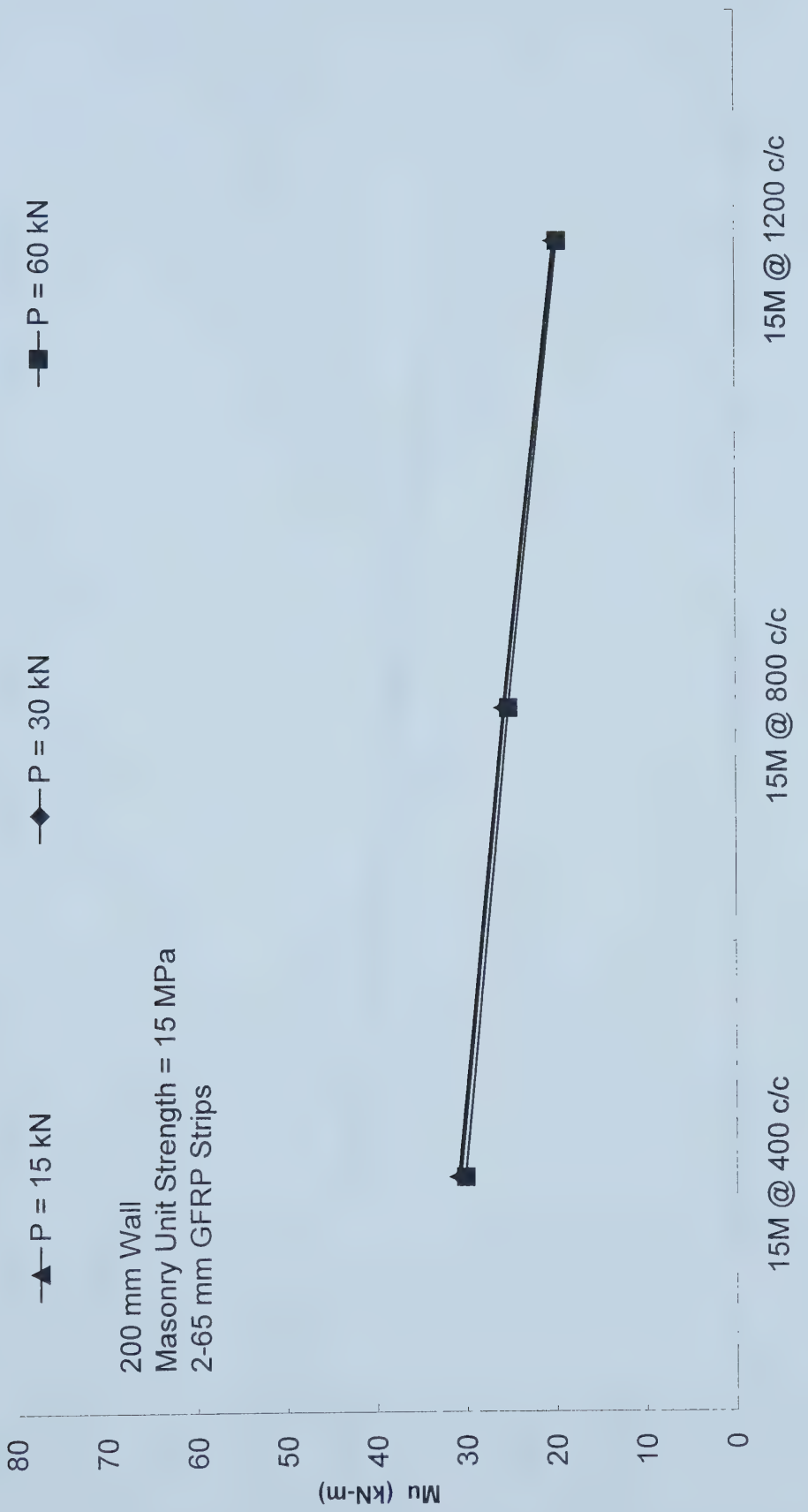


Figure 5.37 Vertical Steel (15M@400, 800, 1200mm) versus Ultimate Moment (15MPa, 200mm Masonry Units, 2-65mm GFRP, Various Amounts of Axial Load)

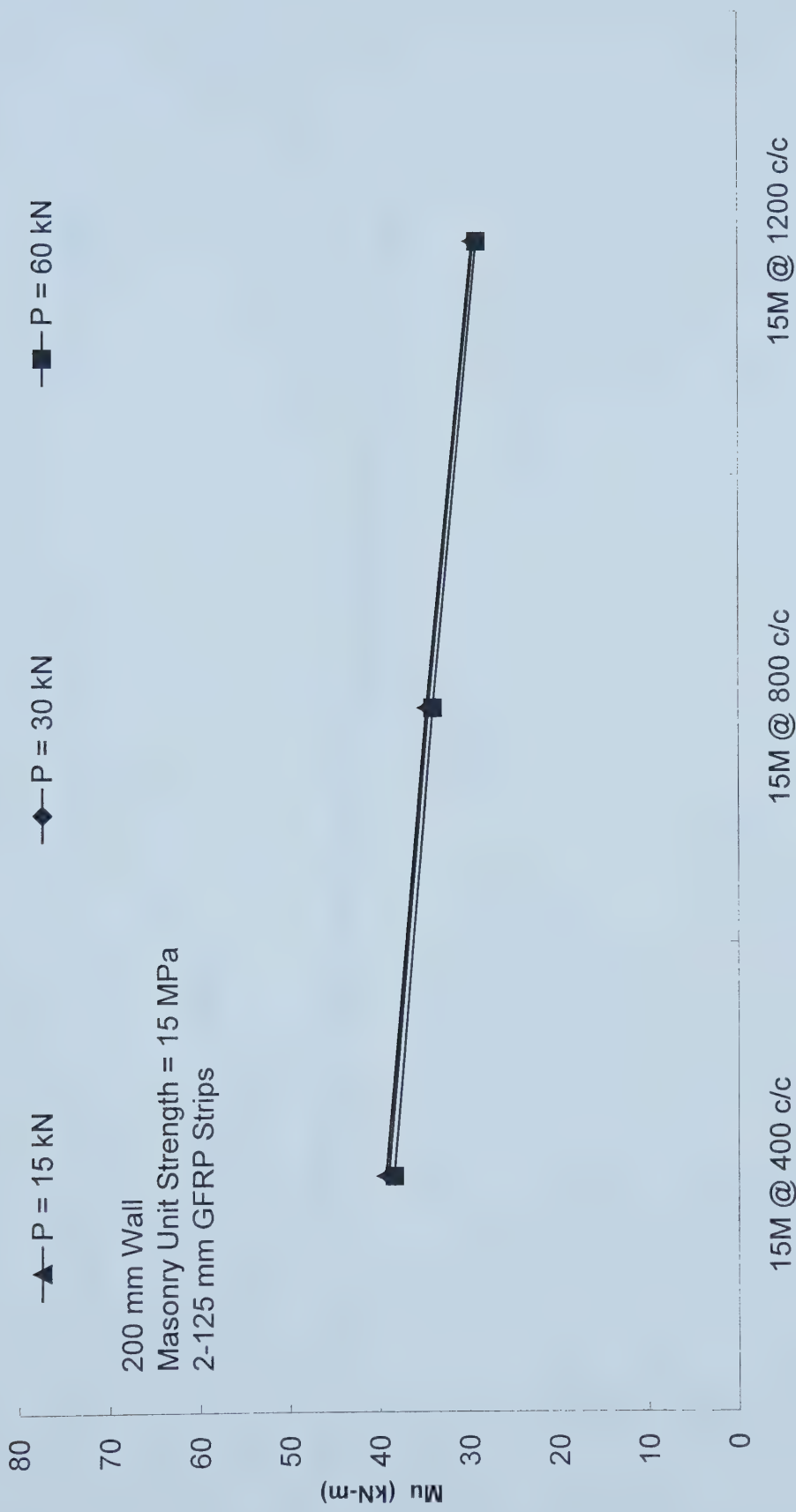


Figure 5.38 Vertical Steel (15M@400, 800, 1200mm) versus Ultimate Moment (15MPa, 200mm Masonry Units, 2-125mm GFRP, Various Amounts of Axial Load)

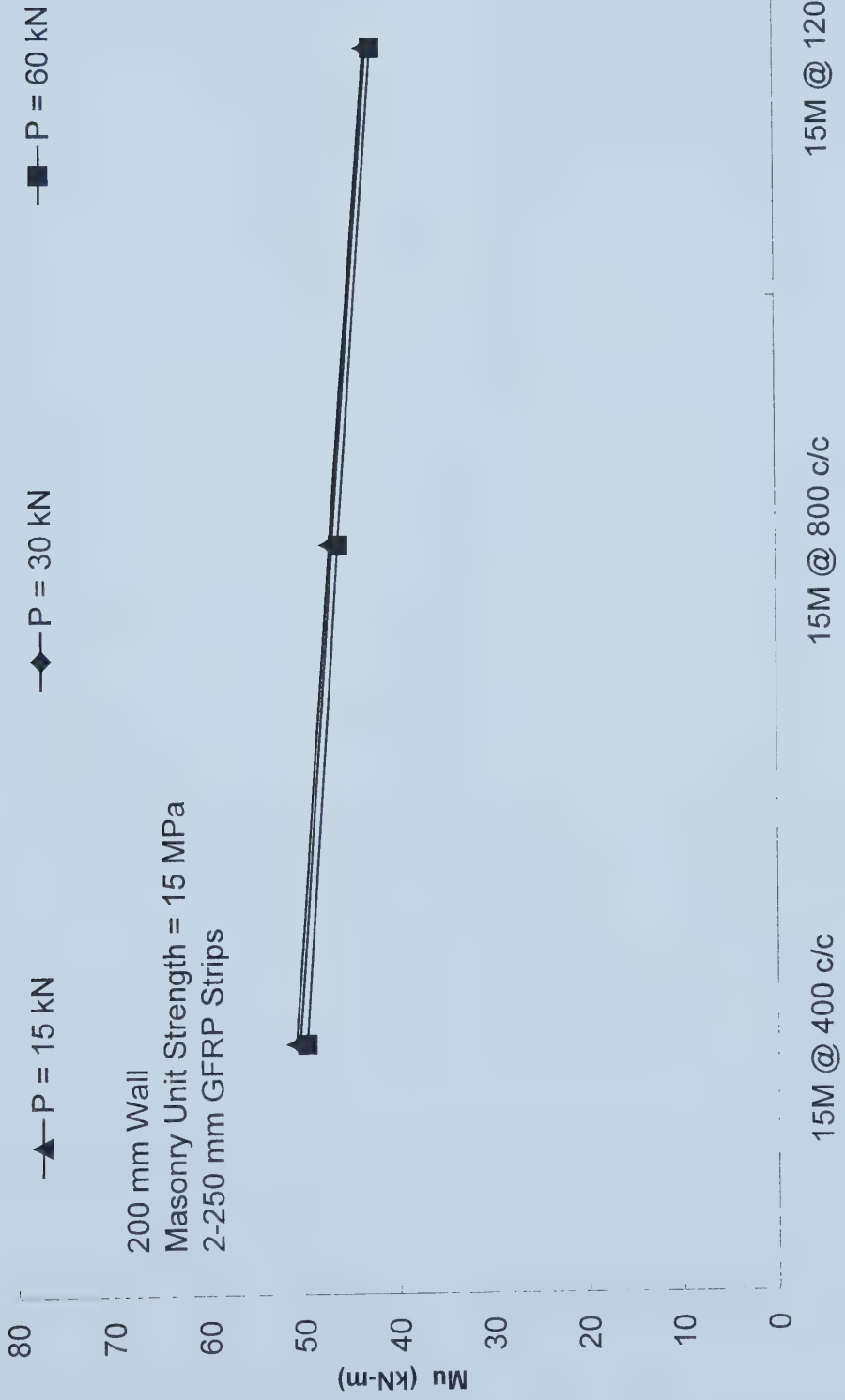


Figure 5.39 Vertical Steel (15M@400, 800, 1200mm) versus Ultimate Moment (15MPa, 200mm Masonry Units, 2-250mm GFRP, Various Amounts of Axial Load)

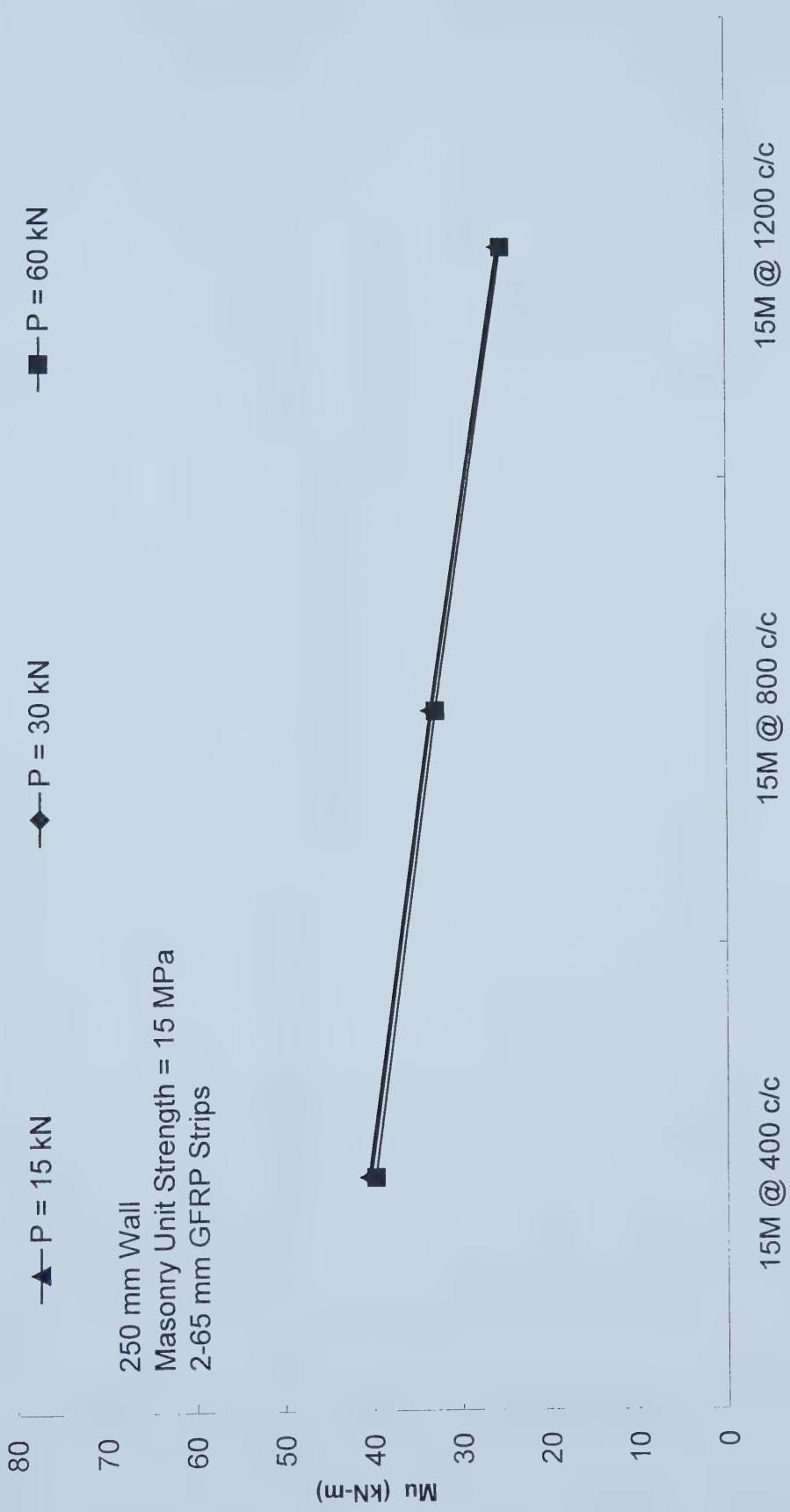


Figure 5.40 Vertical Steel ($15M@400, 800, 1200\text{mm}$) versus Ultimate Moment ($15\text{MPa}, 250\text{mm Masonry Units}, 2\text{-}65\text{mm GFRP, Various Amounts of Axial Load}$)

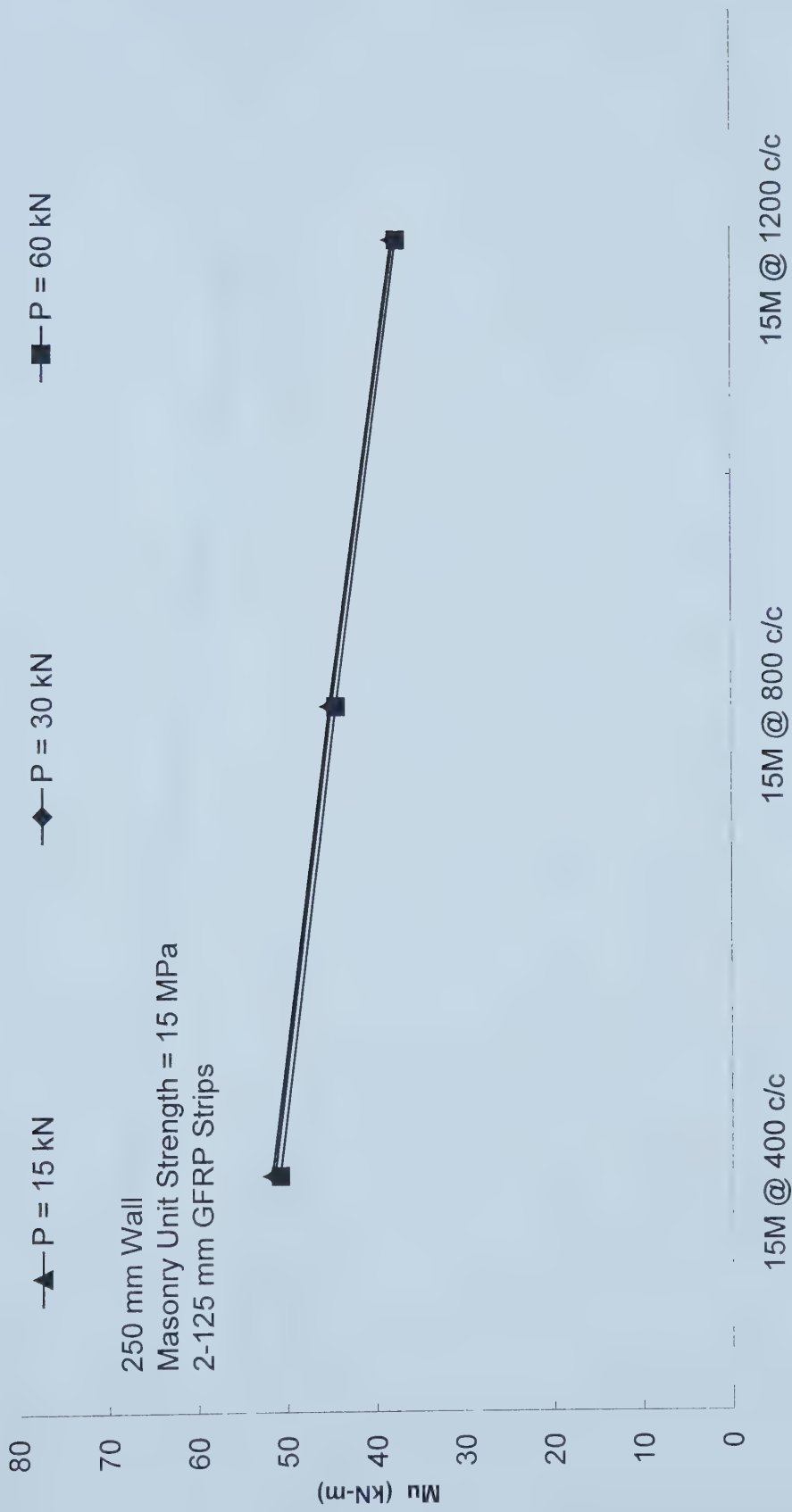


Figure 5.41 Vertical Steel (15M@400, 800, 1200mm) versus Ultimate Moment (15MPa, 250mm Masonry Units, 2-125mm GFRP, Various Amounts of Axial Load)

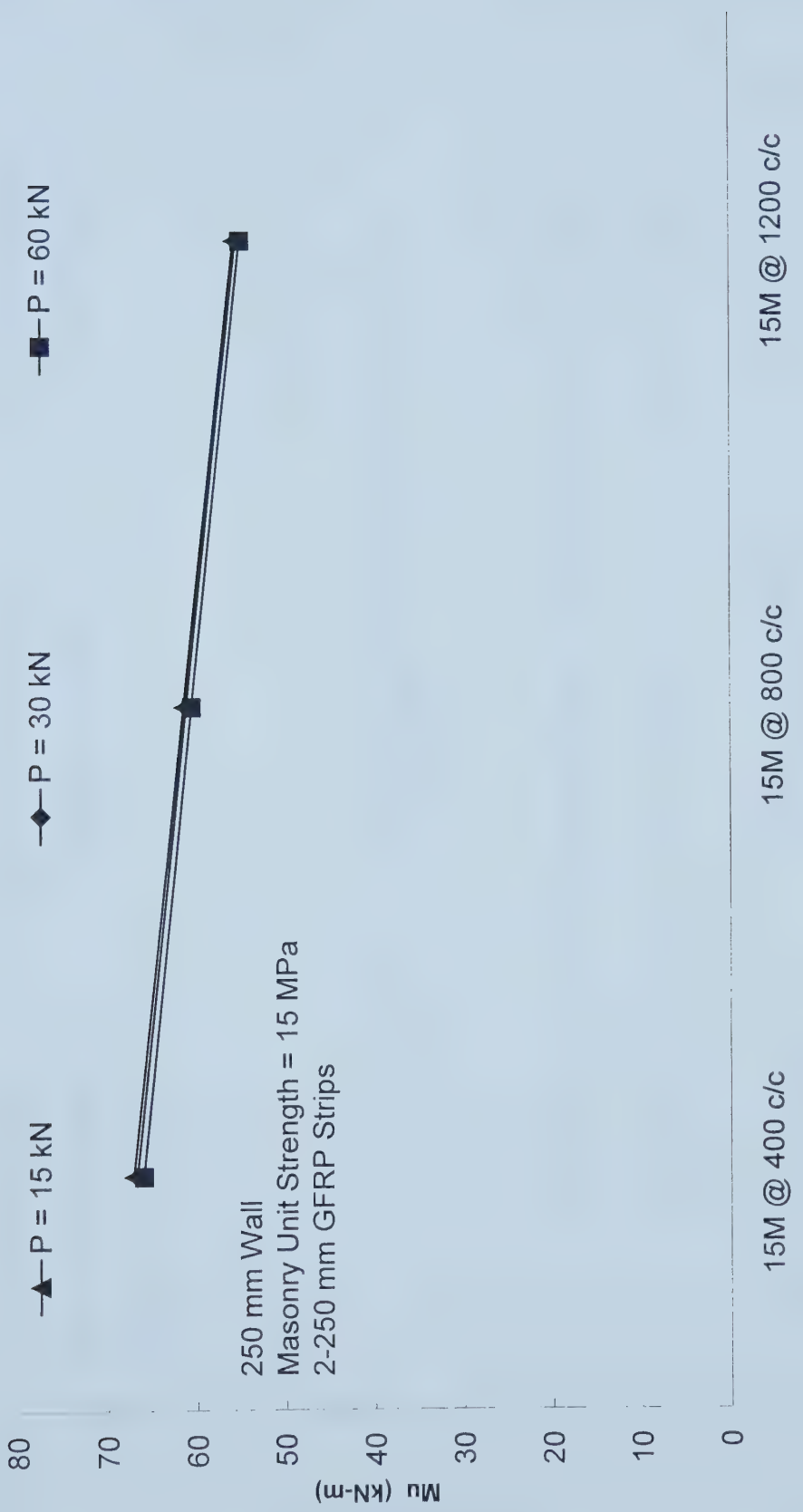


Figure 5.42 Vertical Steel (15M@400, 800, 1200mm) versus Ultimate Moment (15MPa, 250mm Masonry Units, 2-250mm GFRP, Various Amounts of Axial Load)

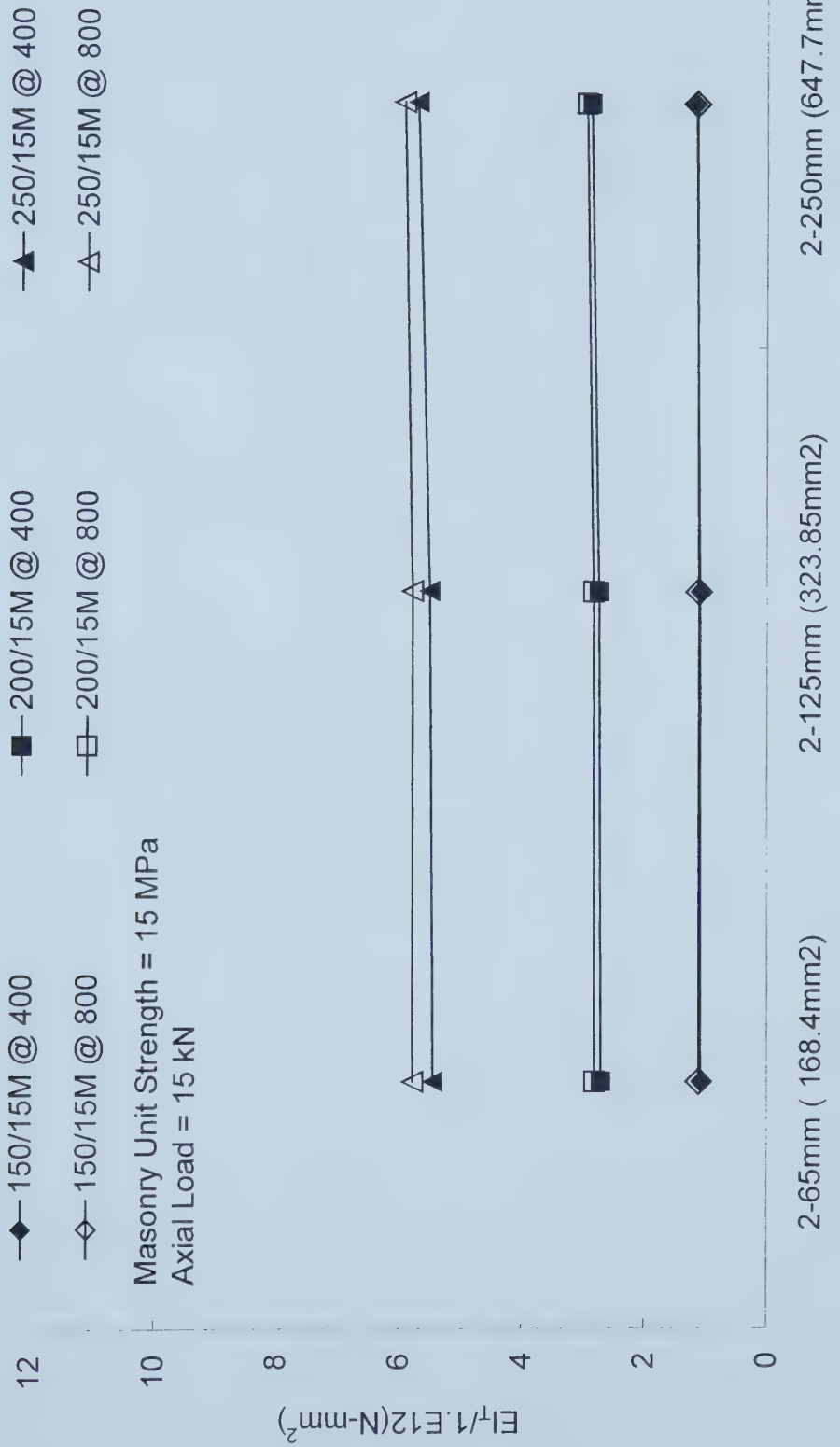


Figure 5.43 Area of GFFRP versus Flexural Rigidity (15 MPa Units, Axial Load = 15kN) Various Unit Thicknesses
Vertical Steel 15M@ 400 and 800 mm c/c

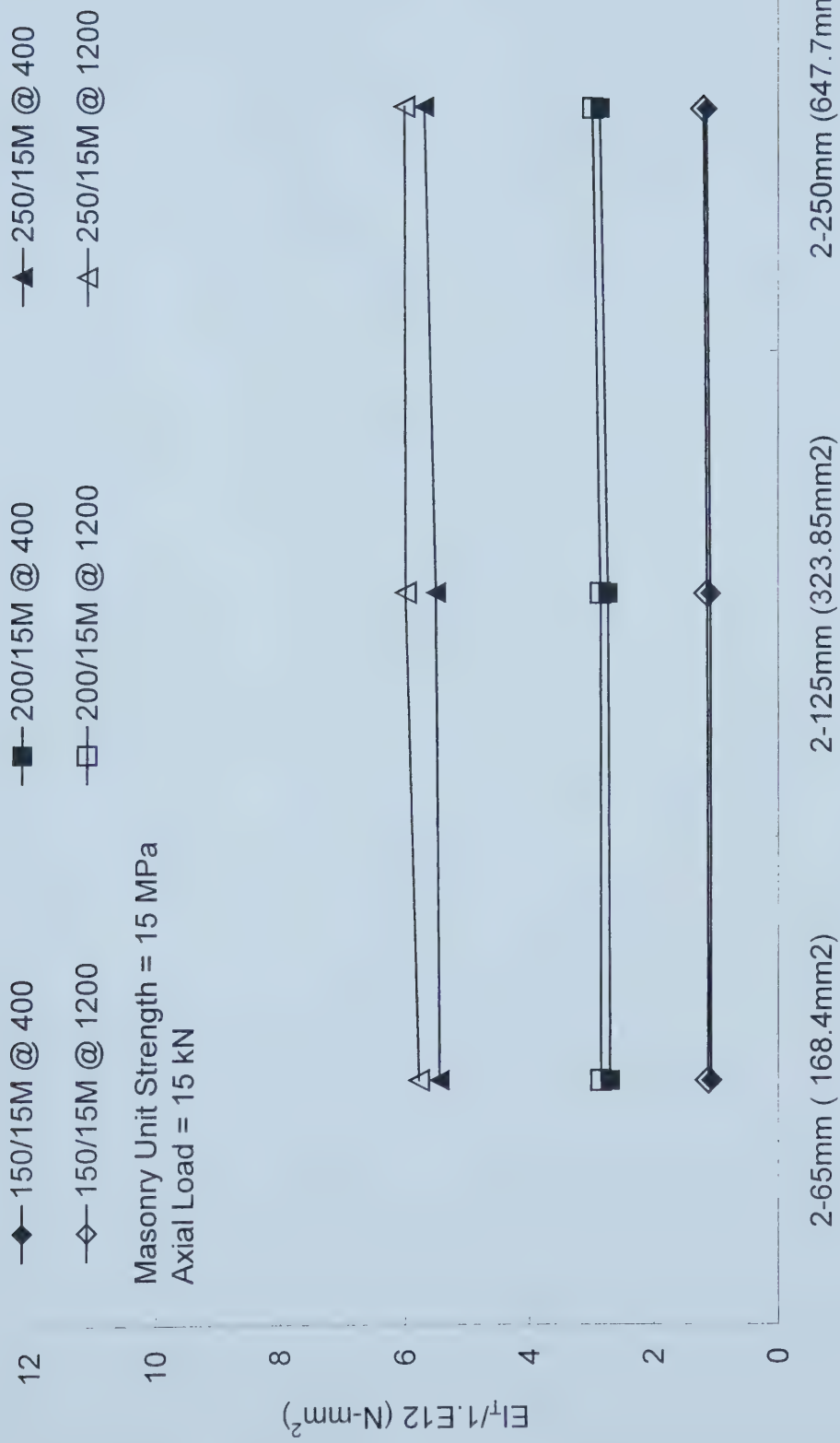
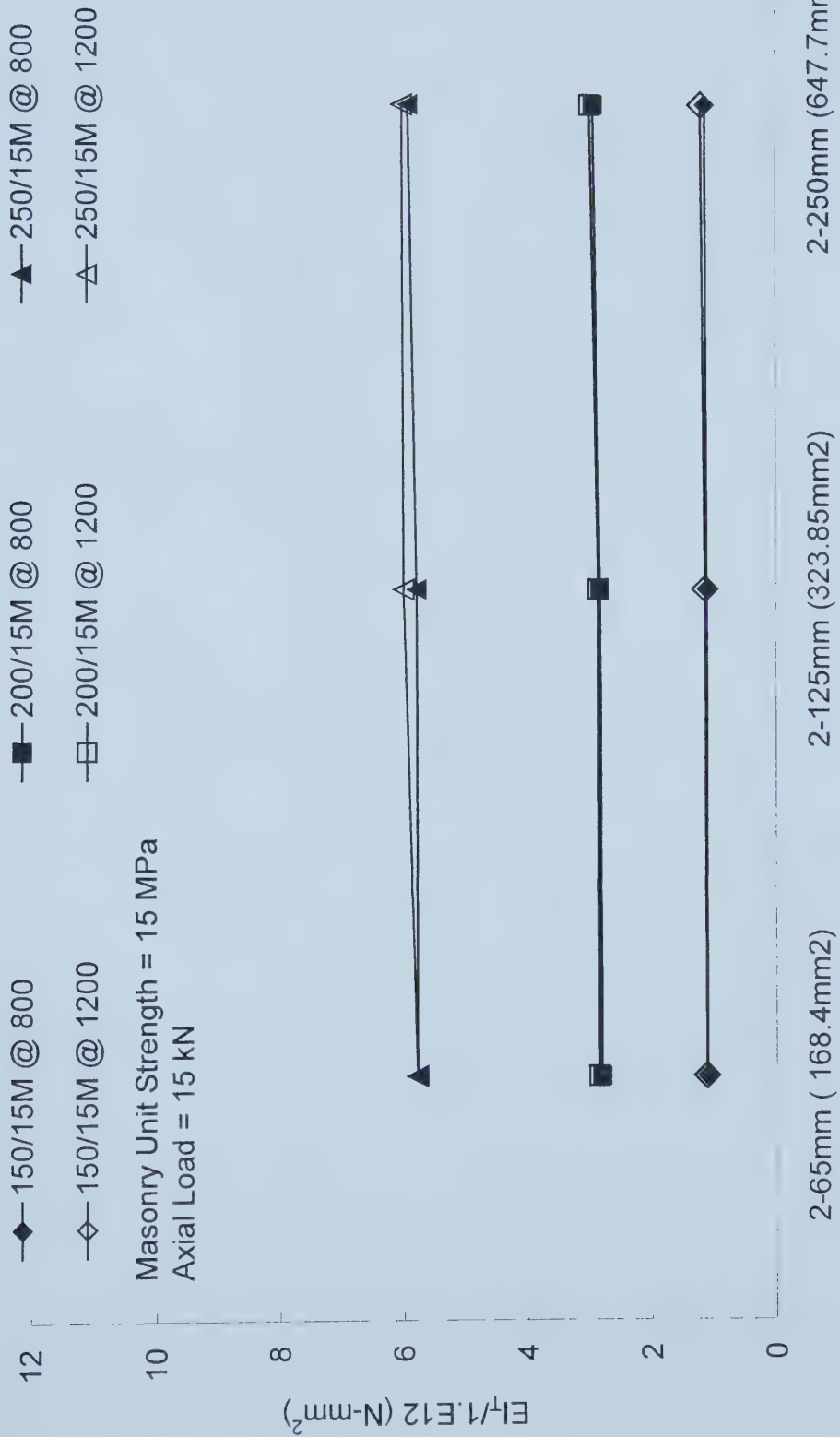


Figure 5.44 Area of GFFRP versus Flexural Rigidity (15 MPa Units, Axial Load = 15kN) Various Unit Thicknesses Vertical Steel 15M@ 400 and 1200 mm c/c



**Figure 5.45 Area of GFFRP versus Flexural Rigidity (15 MPa Units, Axial Load = 15kN) Various Unit Thicknesses
Vertical Steel 15M@ 800 and 1200 mm c/c**

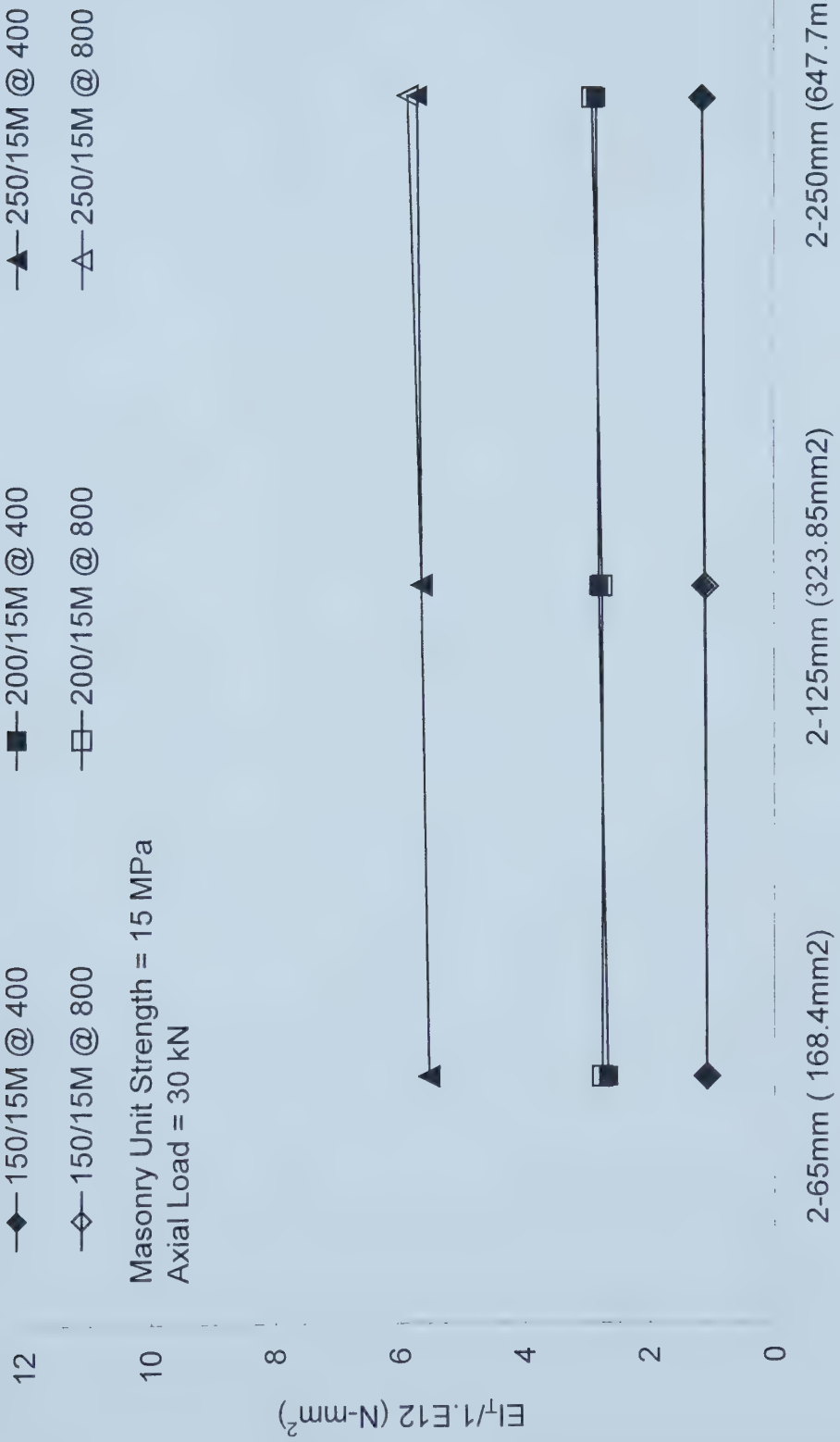


Figure 5.46 Area of GFFRP versus Flexural Rigidity (15 MPa Units, Axial Load = 30kN) Various Unit Thicknesses
Vertical Steel 15M@ 400 and 800 mm c/c

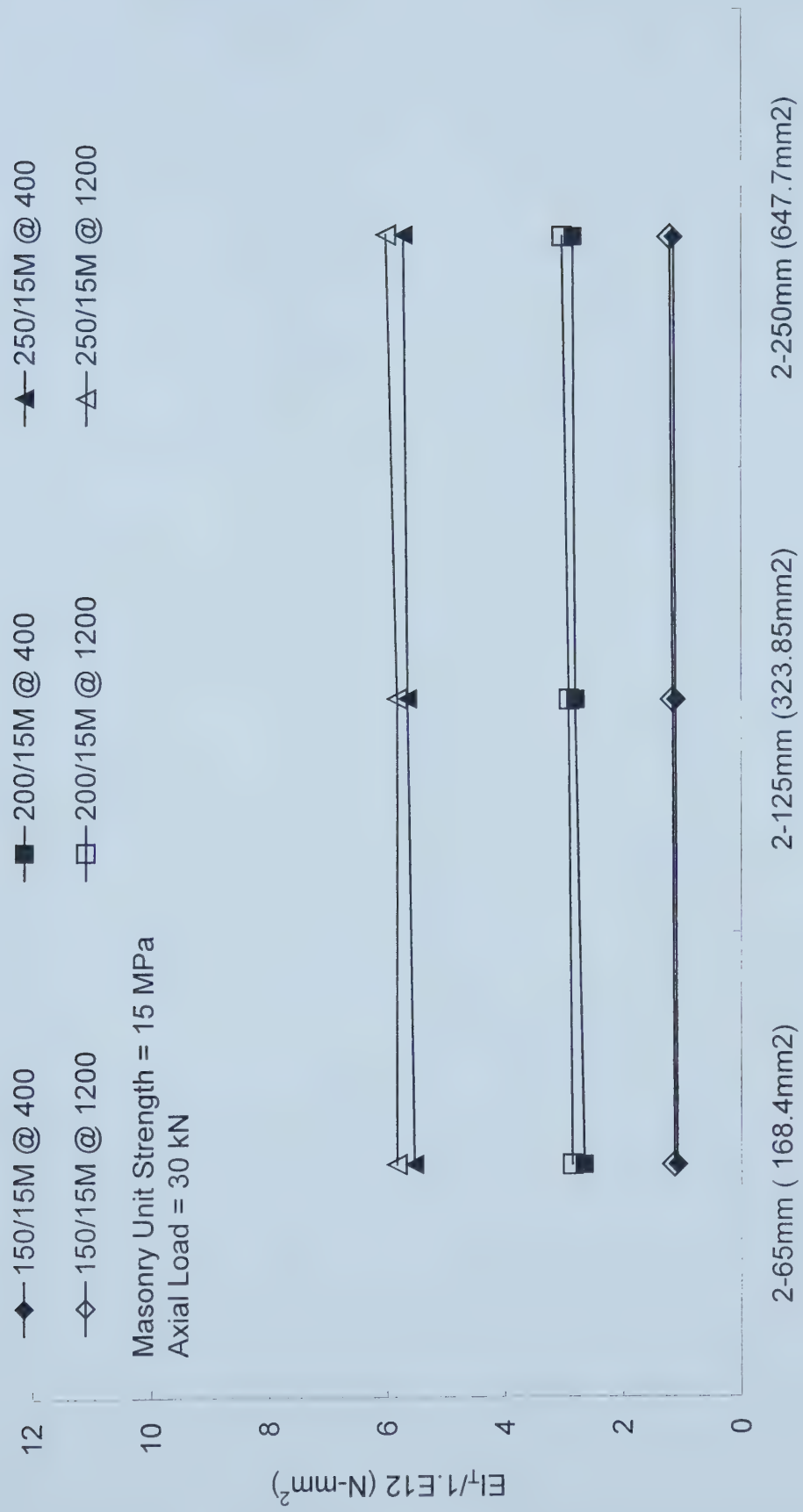


Figure 5.47 Area of GFRP versus Flexural Rigidity (15 MPa Units, Axial Load = 30kN) Various Unit Thicknesses
Vertical Steel 15M@ 400 and 1200 mm c/c

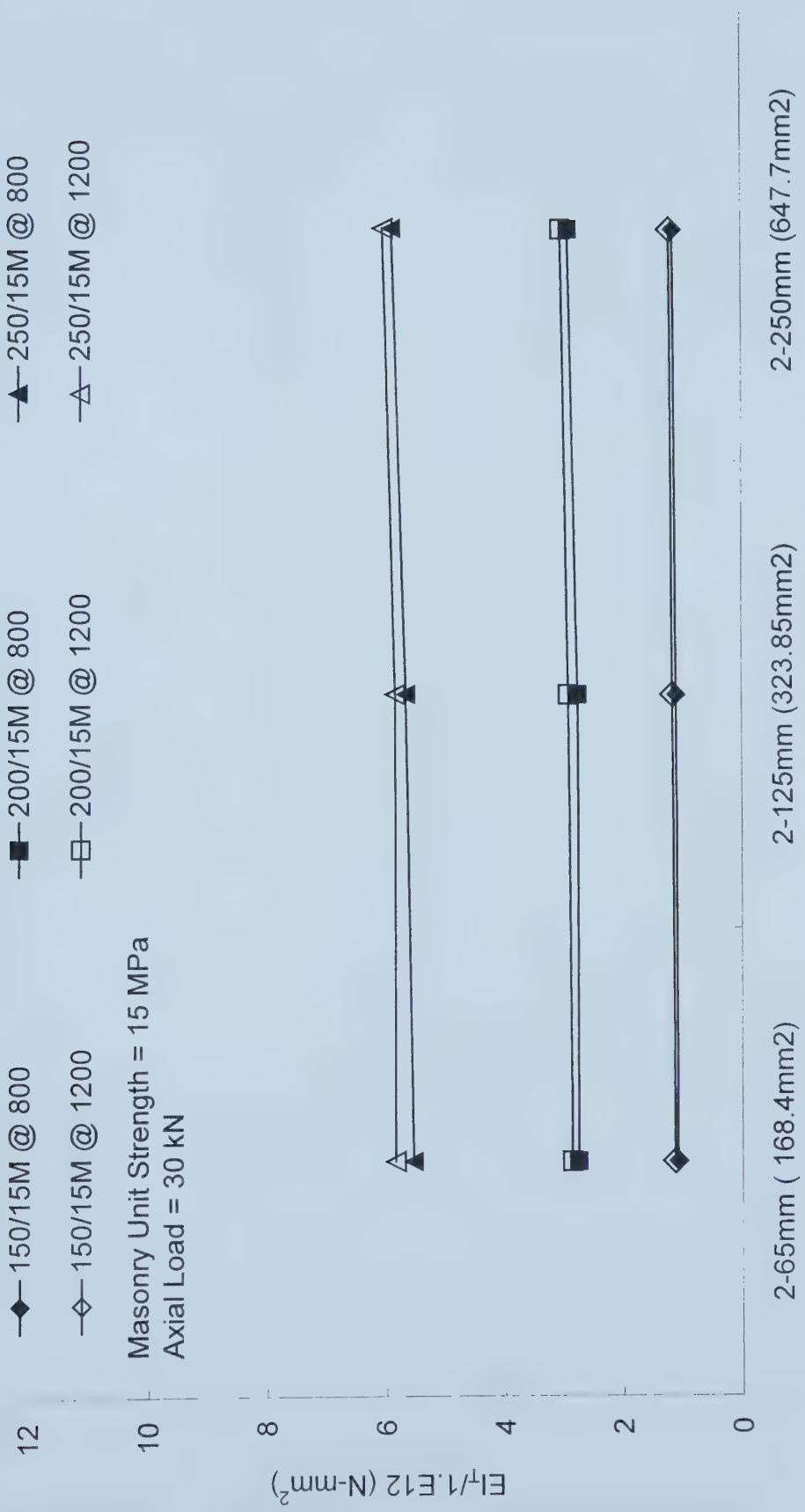


Figure 5.48 Area of GFRP versus Flexural Rigidity (15 MPa Units, Axial Load = 30kN) Various Unit Thicknesses

Vertical Steel 15M@ 800 and 1200 mm c/c

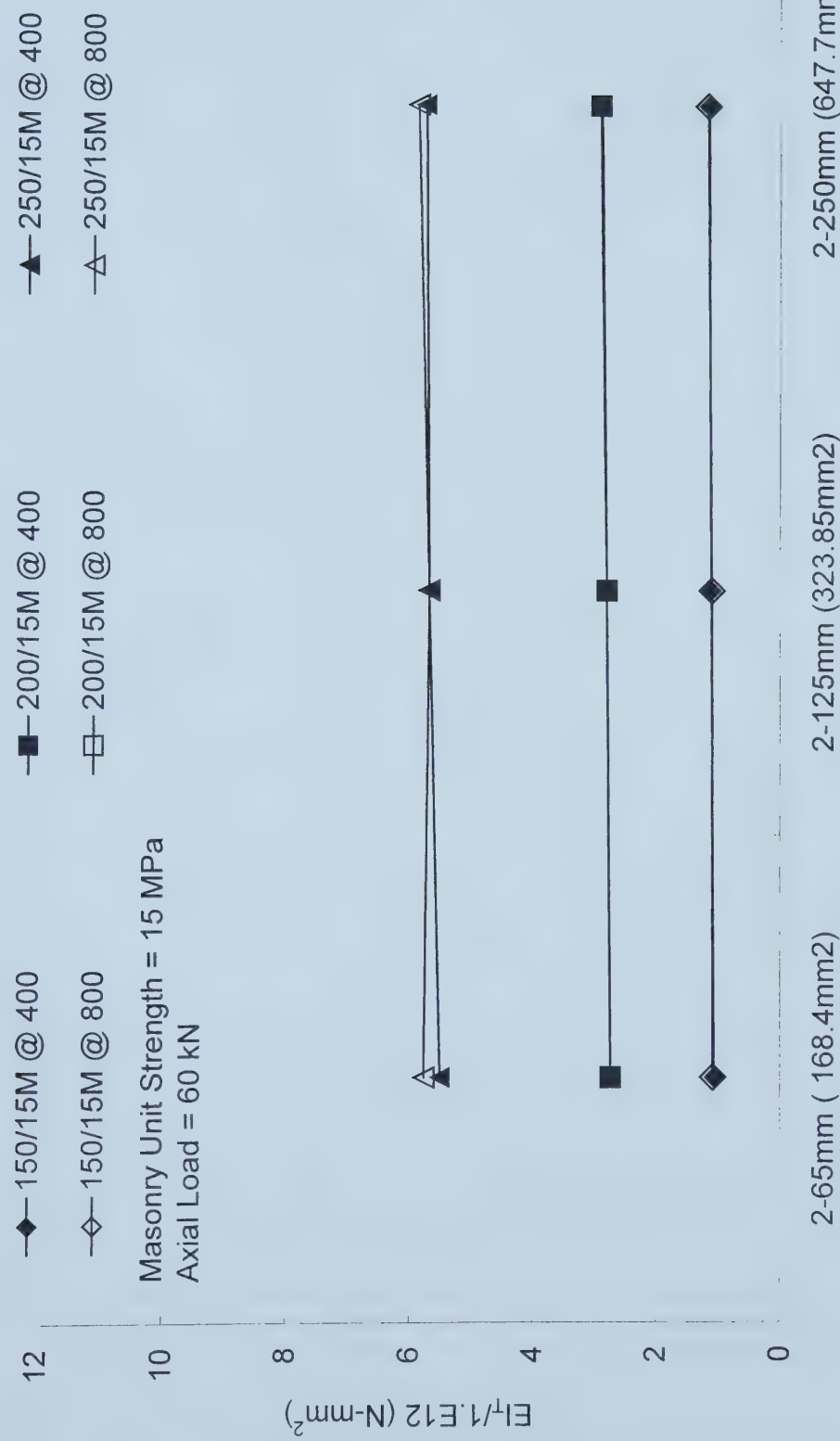


Figure 5.49 Area of GFRP versus Flexural Rigidity (15 MPa Units, Axial Load = 60kN) Various Unit Thicknesses
Vertical Steel 15M@ 400 and 800 mm c/c

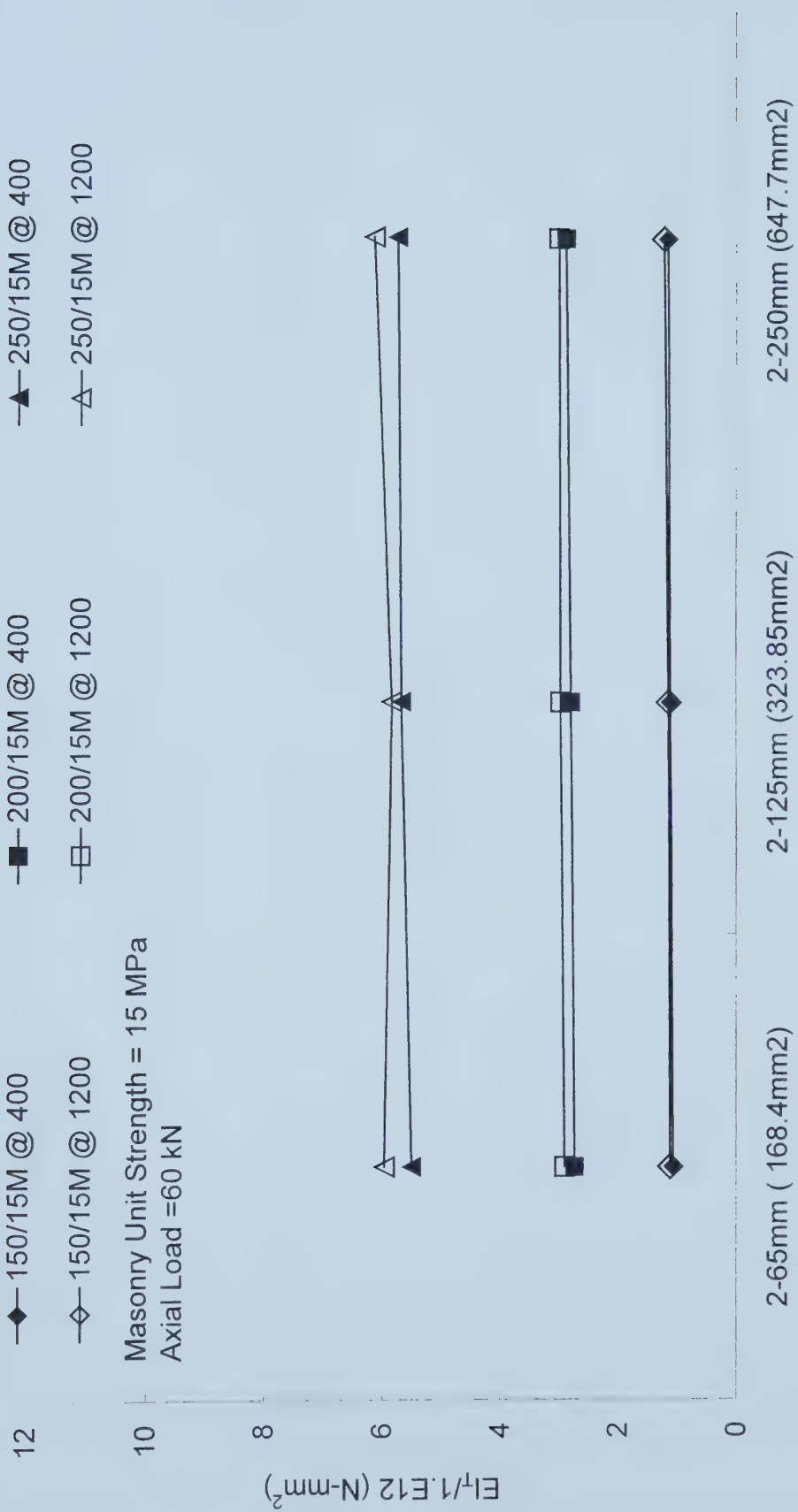


Figure 5.50 Area of GFRP versus Flexural Rigidity (15 MPa Units, Axial Load = 60kN) Various Unit Thicknesses
Vertical Steel 15M@ 400 and 1200 mm c/c

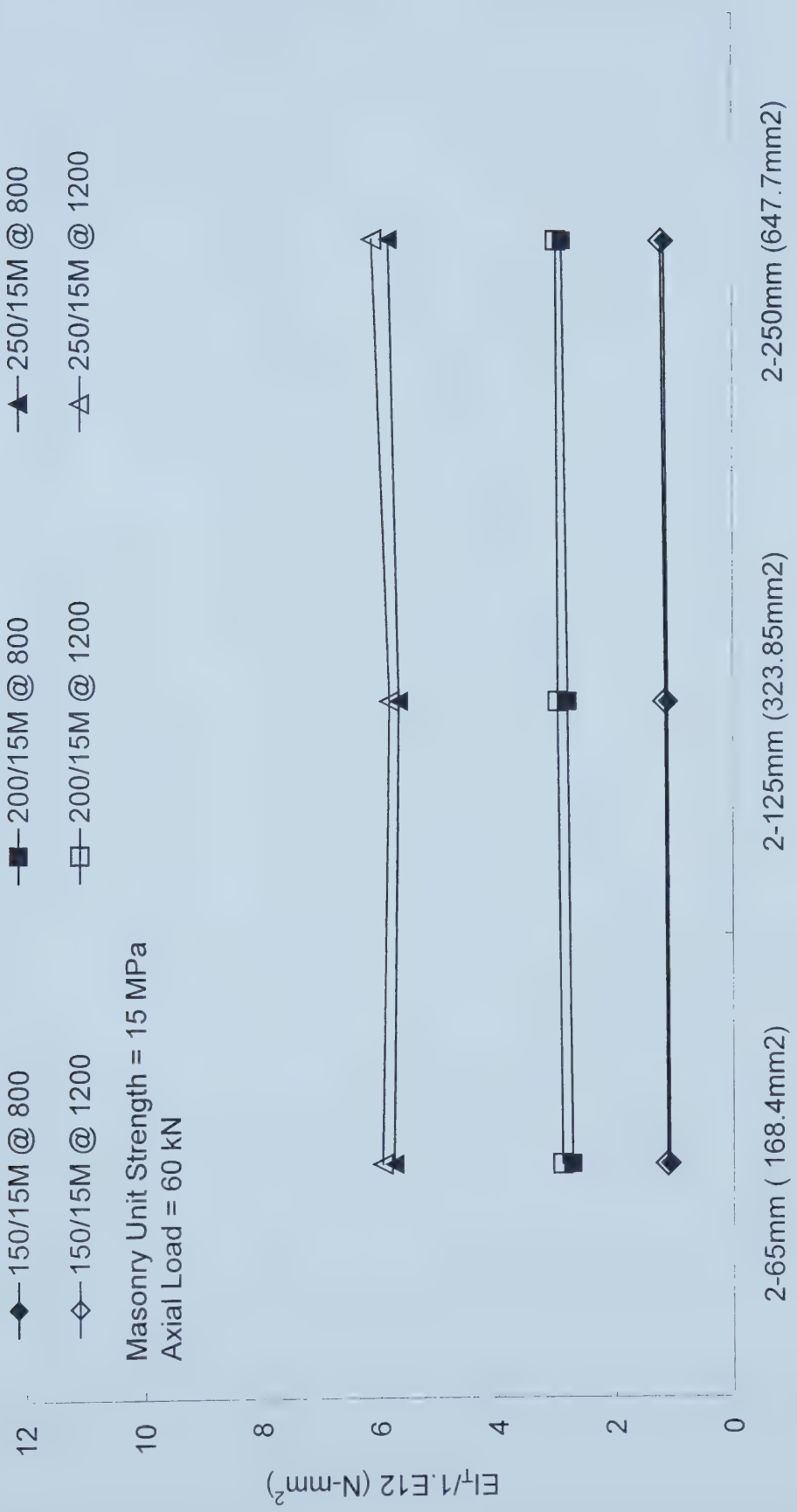


Figure 5.51 Area of GFRP versus Flexural Rigidity (15 MPa Units, Axial Load = 60kN) Various Unit Thicknesses
Vertical Steel 15M@ 800 and 1200 mm c/c

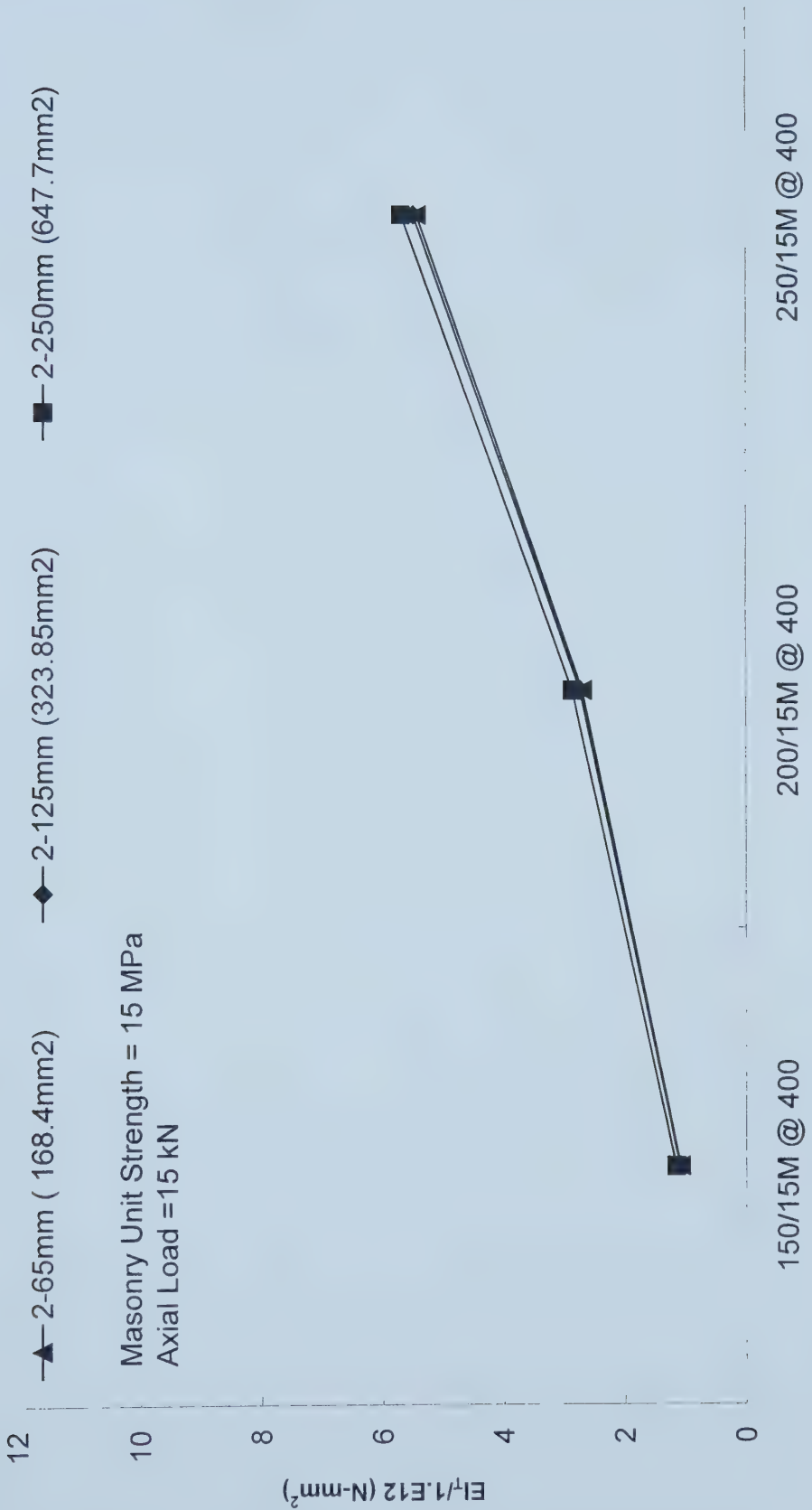


Figure 5.52 Area of Vertical Steel(15M @ 400c/c) versus Flexural Rigidity (15 MPa Units, Axial Load = 15kN)
Various Amounts of GFRP Reinforcement

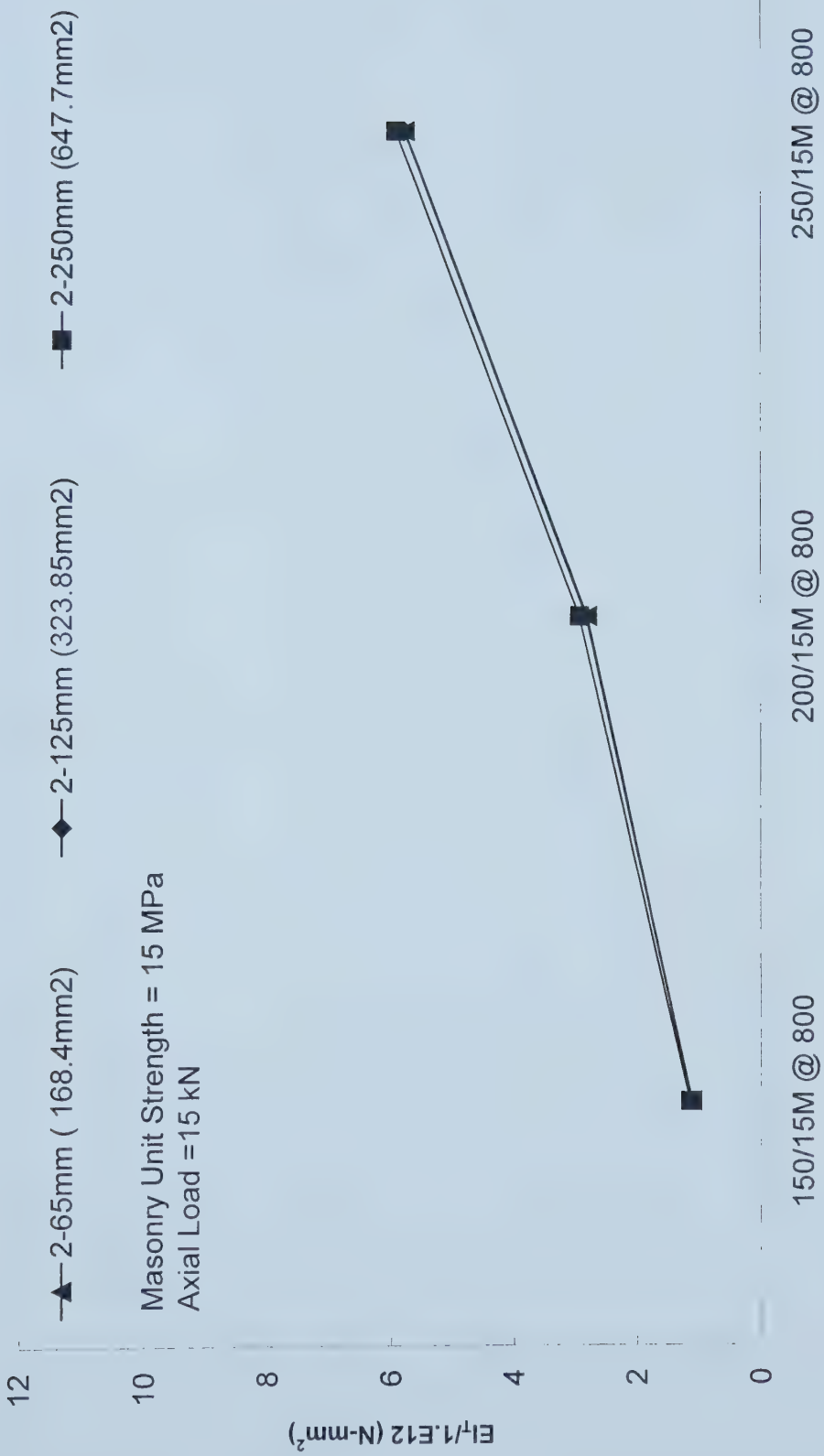


Figure 5.53 Area of Vertical Steel(15M @ 800c/c) versus Flexural Rigidity (15 MPa Units, Axial Load = 15kN)
Various Amounts of GFRP Reinforcement

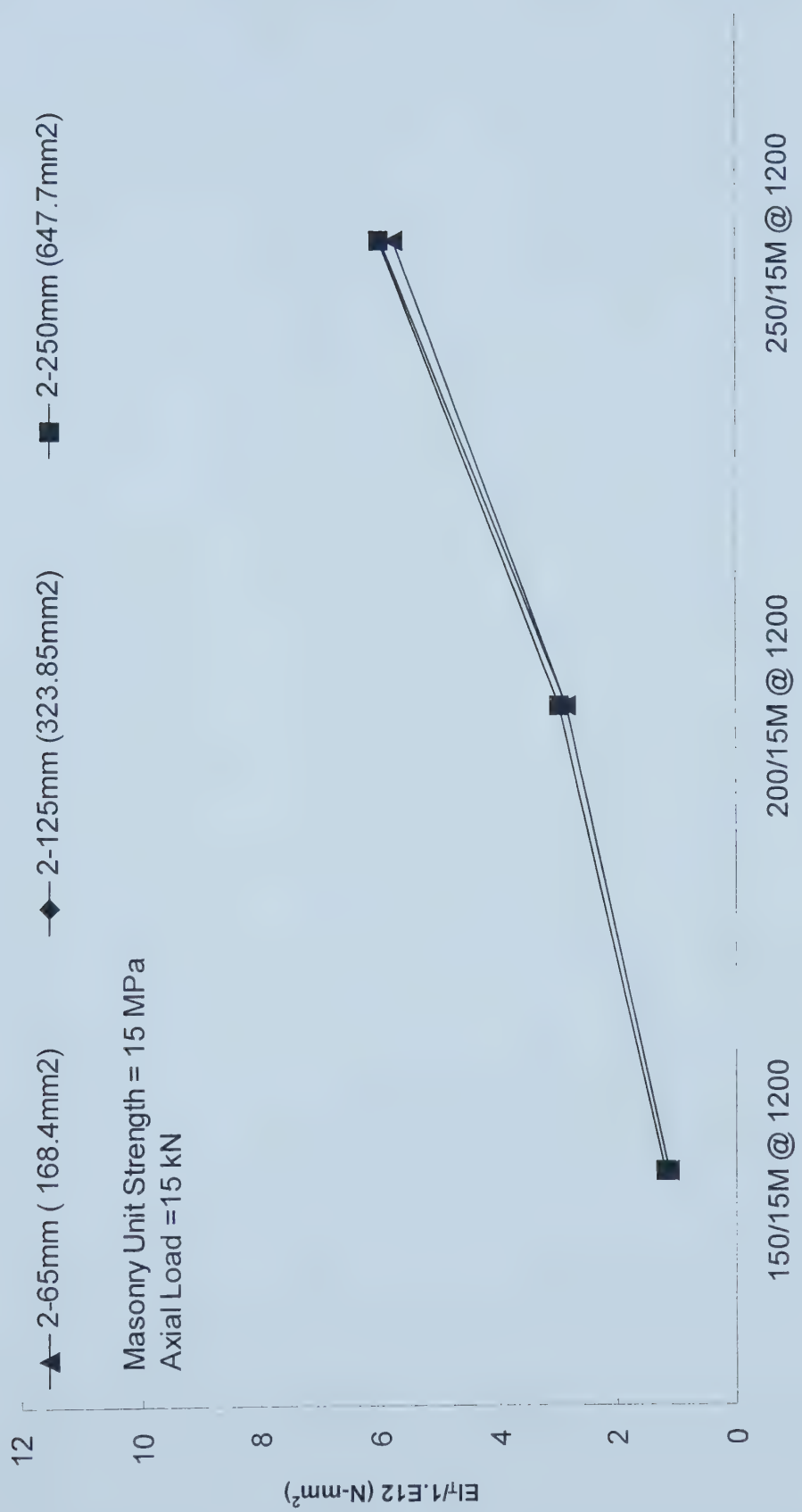


Figure 5.54 Area of Vertical Steel(15M @ 1200c/c) versus Flexural Rigidity (15 MPa Units, Axial Load = 15kN)
Various Amounts of GFRP Reinforcement

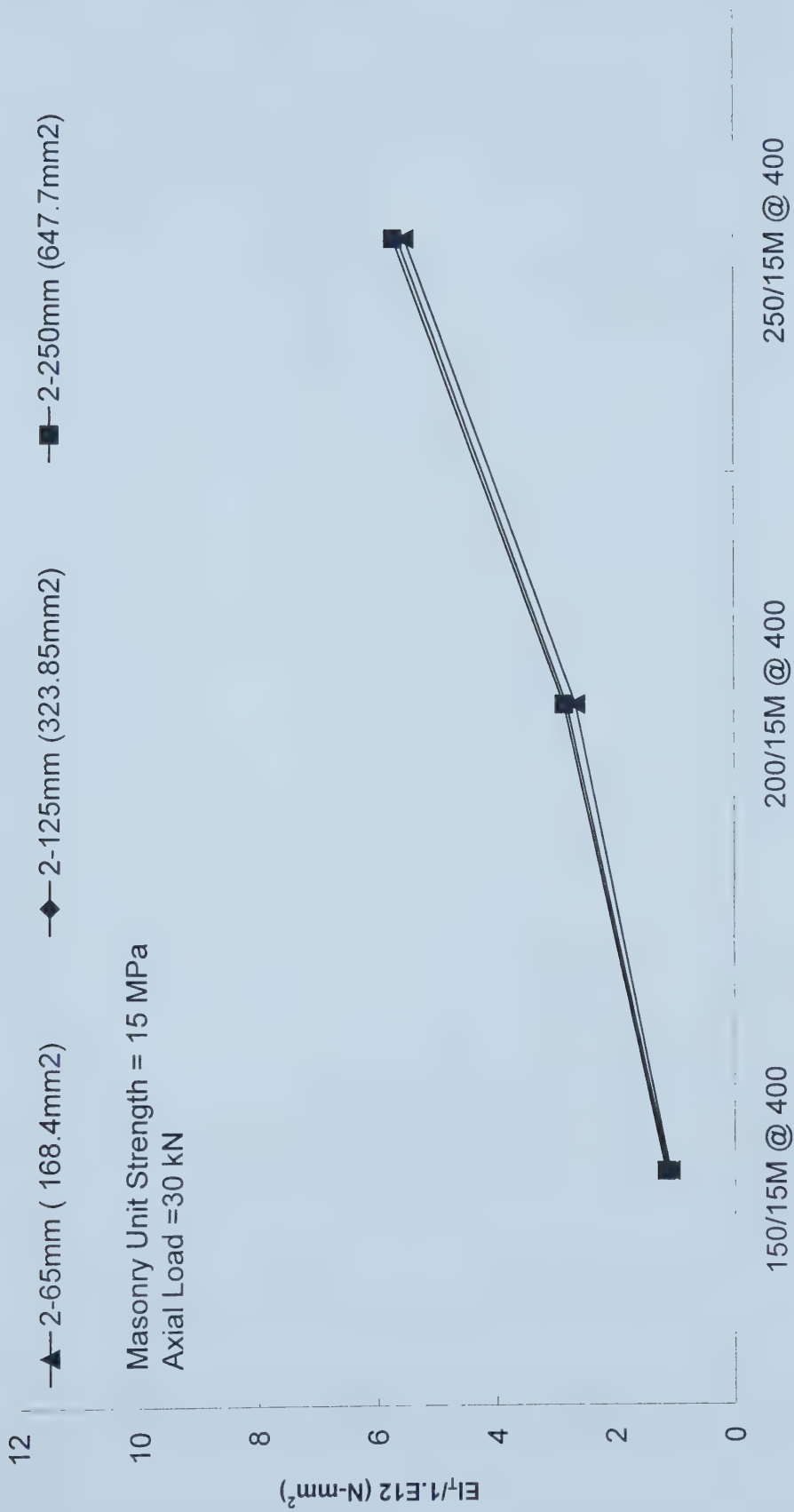


Figure 5.55 Area of Vertical Steel($15M @ 400c/c$) versus Flexural Rigidity (15 MPa Units , Axial Load = 30kN) Various Amounts of GFRP Reinforcement

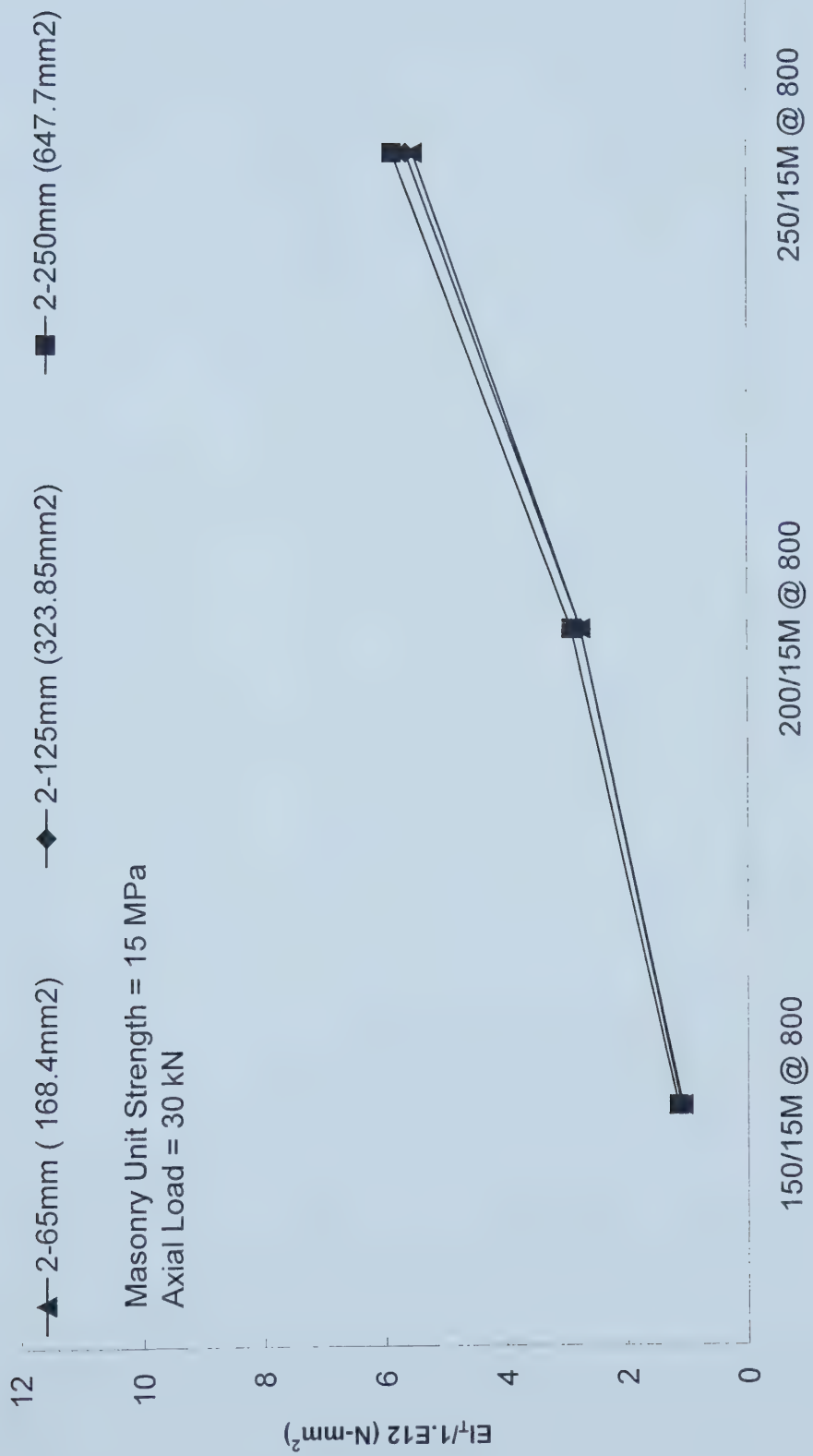


Figure 5.56 Area of Vertical Steel($15M @ 800c/c$) versus Flexural Rigidity (15 MPa Units, Axial Load = 30kN)
Various Amounts of GFRP Reinforcement

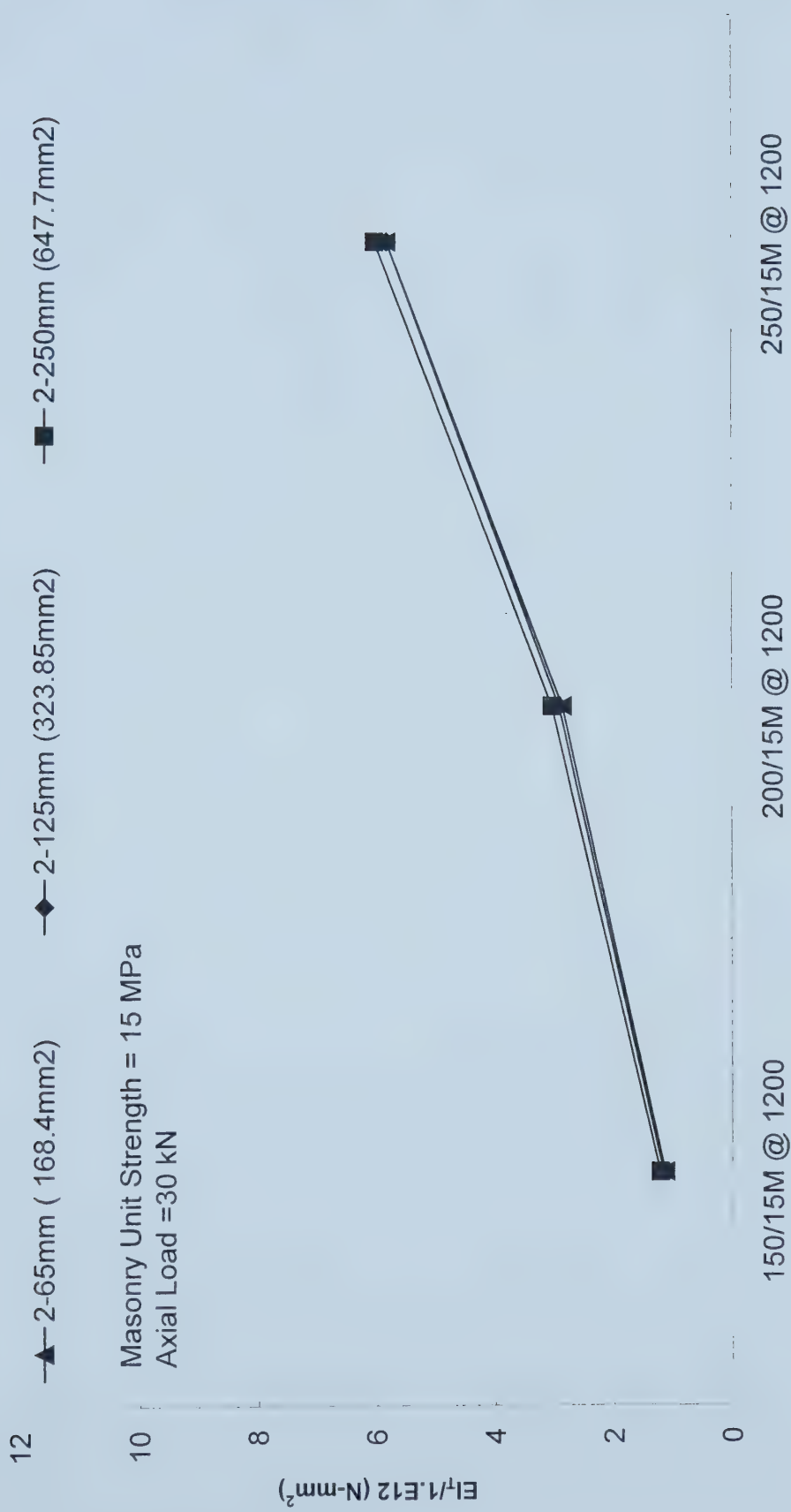


Figure 5.57 Area of Vertical Steel($15\text{M} @ 1200\text{c/c}$) versus Flexural Rigidity ($15 \text{ MPa Units, Axial Load} = 30\text{kN}$) Various Amounts of GFRP Reinforcement

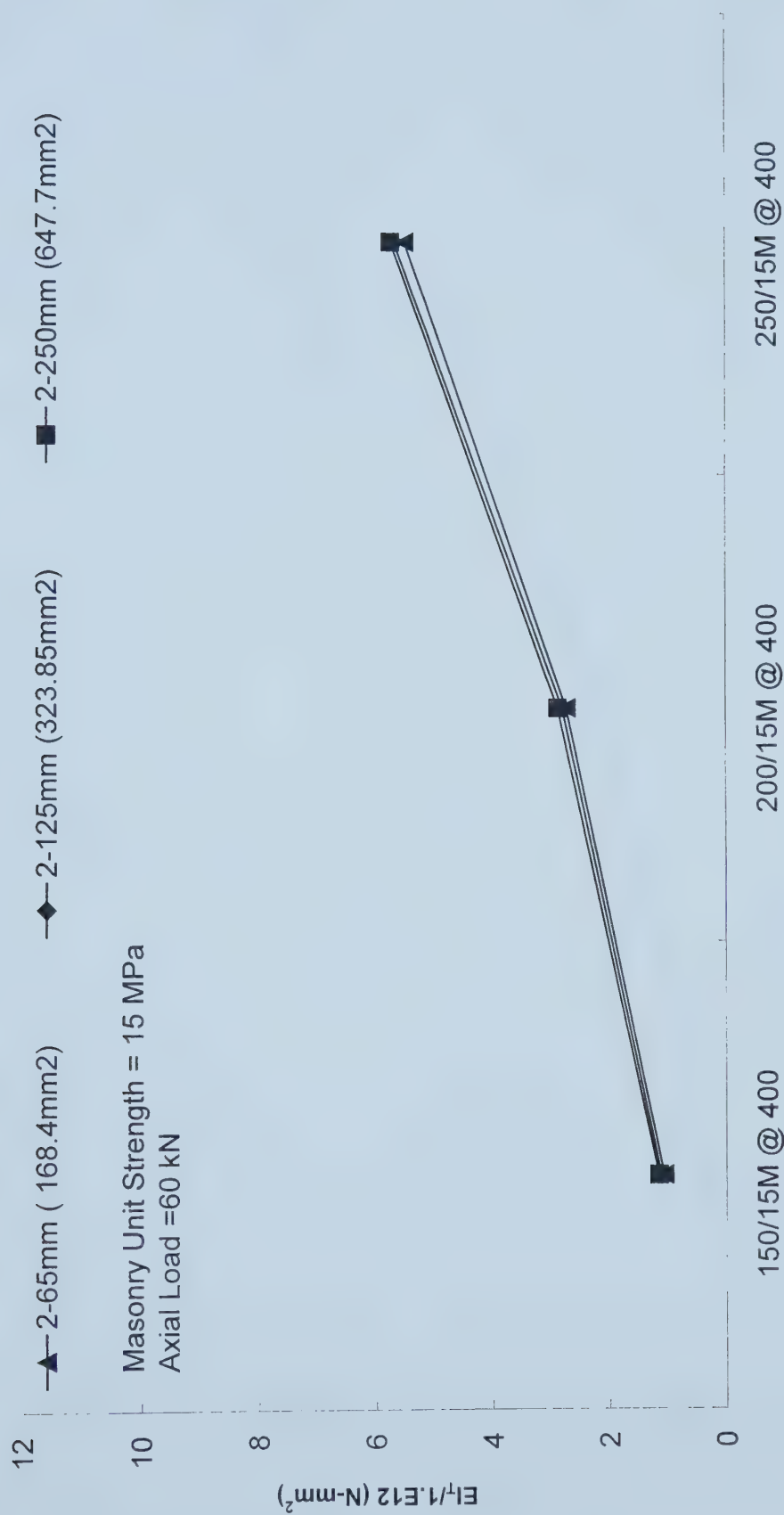


Figure 5.58 Area of Vertical Steel(15M @ 400c/c) versus Flexural Rigidity (15 MPa Units, Axial Load = 60kN) Various Amounts of GFRP Reinforcement

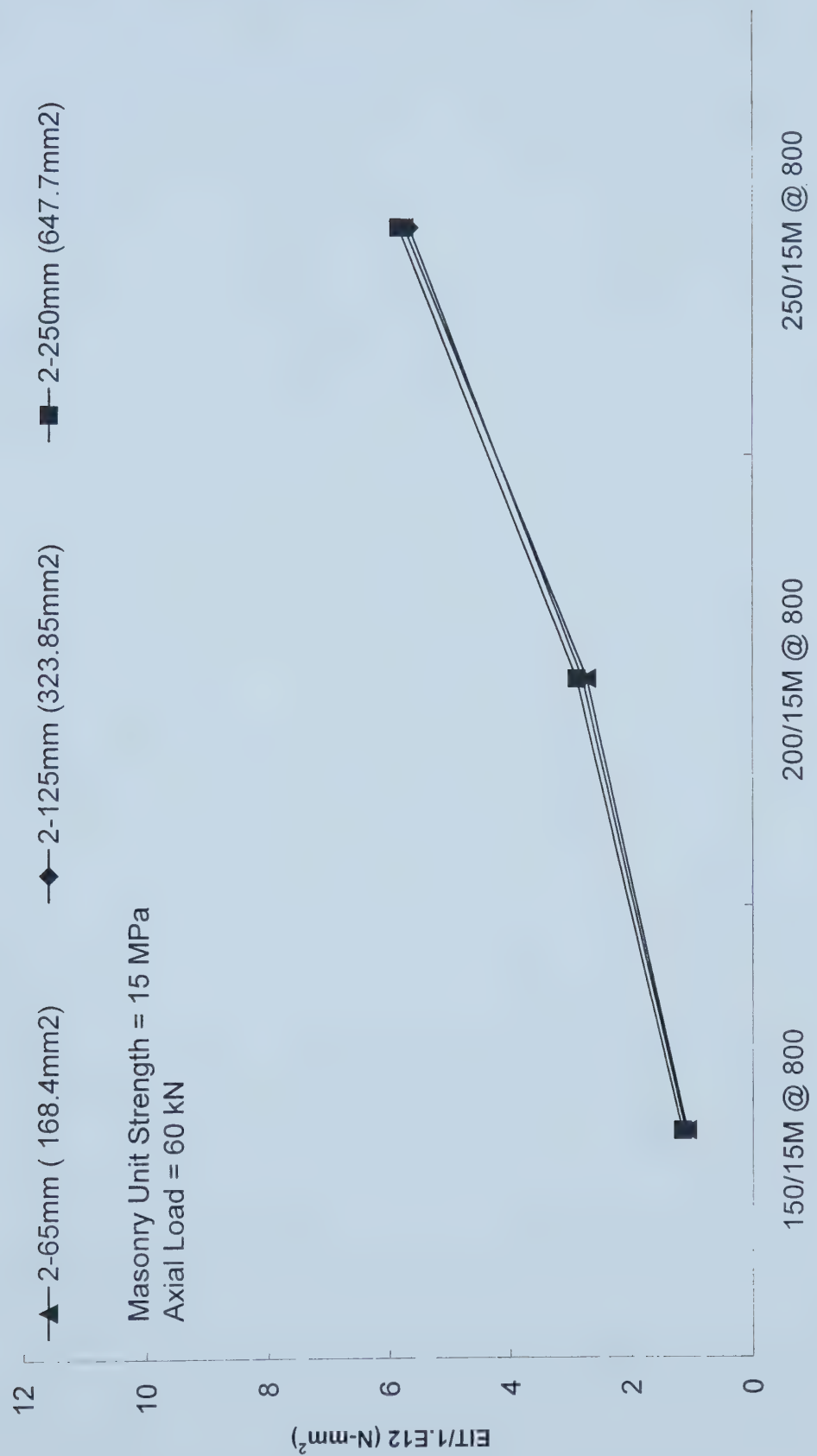


Figure 5.59 Area of Vertical Steel(15M @ 800c/c) versus Flexural Rigidity (15 MPa Units, Axial Load = 60kN)
Various Amounts of GFRP Reinforcement

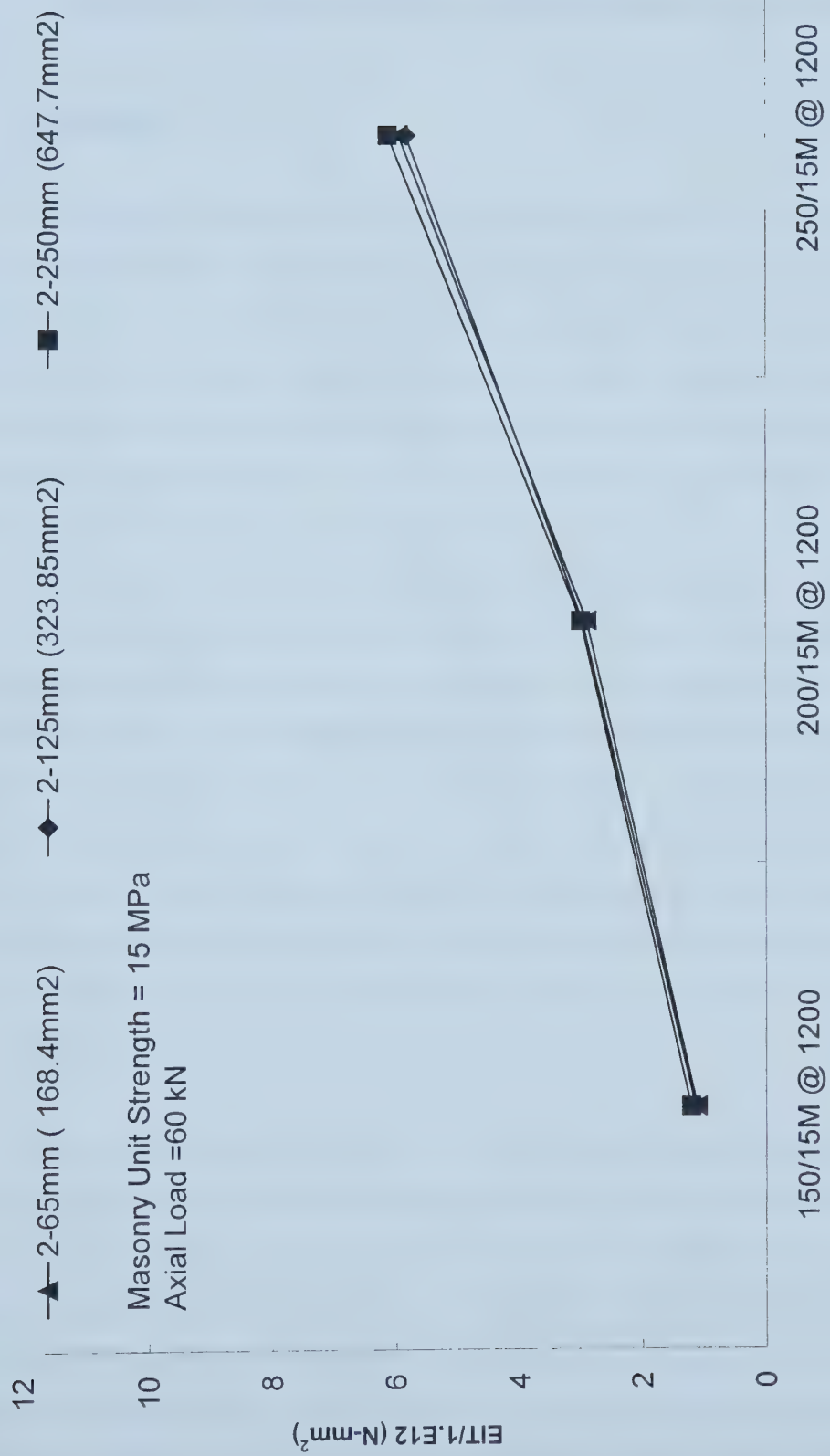


Figure 5.60 Area of Vertical Steel(15M @ 1200c/c) versus Flexural Rigidity (15 MPa Units, Axial Load = 60kN) Various Amounts of GFRP Reinforcement

Chapter 6

SUMMARY, CONCLUSIONS AND RECOMMENDATIONS

6.1 Summary

The objective of this thesis to study the behavior of reinforced masonry walls with externally bonded GFRP strips under monotonic and cyclic loading. The testing program comprised of two series of walls. The first series consisted of four 150 mm walls, out of which two were tested monotonically and two were tested cyclically. The second group consisted of four 200 mm walls, out of which two were tested monotonically and two were tested cyclically. All walls were 1.2 m wide and 4.0 m high, built by professional masons. Lateral out-of-plane load was applied at a distance of 1.2 m from the top and bottom respectively and a constant axial load was maintained. The tests were performed at I. F. Morrison Structural Laboratory at University of Alberta. An existing load frame was modified to allow large deflections and used to perform the full-scale out-of-plane tests described above. The parameters investigated were amount of GFRP, strain transfer, amount of constant axial load, thickness of masonry walls, spacing of vertical steel, and amount of GFRP reinforcement in the form of externally bonded strips. Three different modes of failure were observed during the experimental part of this program. Delamination of GFRP accompanied by severe cracking being the most common. High strains in GFRP were recorded for 150 mm thick walls. This is attributed to high out-of-plane deflections

The model developed by Kuzik *et al.* (1999) to describe the behavior of masonry walls externally reinforced with FRP strips was modified by making use the full database obtained to date. That model was used to conduct a parametric study. From the parameters studied, the axial load at the level applied in the study has an insignificant effect on the ultimate moment capacity of the specimens. The governing parameter is the amount of externally applied GFRP, leading to a maximum increase in capacity of 415%. Increasing the thickness of masonry wall increases the efficiency of the externally applied

GFRP reinforcement. However, the amount of externally applied GFRP reinforcement has little effect on the flexural rigidity of the specimen at transition level. Other parameters investigated have relevant effects as described in Chapter 5.

6.2 Recommendations

The response of masonry walls to out-of-plane seismic excitation is one of the most complex and ill understood areas of seismic analysis. Addition of vertical steel reinforcement and externally applied GFRP strips has made this area more demanding and challenging. This requires more insight into the material behavior of the masonry and composite materials and analytical models to closely predict the behavior of the specimen under out-of-plane loading.

An attempt was made to study the out-of-plane behavior of reinforced masonry walls with externally bonded GFRP. In order to study the strain history adjacent to the bonded GFRP strips, strain gages were applied directly on the masonry surface. However, the technique did not prove to be an effective tool due to congestion of wires from strain gages and porous masonry surface. For any future study, application of strain gages directly on the masonry surface must be avoided. Photo elastic methods of strain analysis are one alternative to perform this type of study.

As mentioned earlier the GFRP material properties used were the same as used by Kuzik *et al.* (1999). Further experimental investigation is required to determine the physical properties of the fiber. The wet lay up procedure used to bond the GFRP strips on the surface is an easy and effective way to apply GFRP as an external reinforcing. However, as reported earlier, some of the failures were caused by the delamination of the GFRP. Better results from the use of GFRP strips bonded on the masonry surface can be obtained by developing an insight to the boundary conditions that actually exist in the field. In other words, the mechanics of bond stress transfer must be studied further at a basic level.

REFERENCES

- American Society of Testing Materials. 1995. D 3039M-95a: Standard Test Method of Tensile Properties of Polymer Matrix Composite Materials. West Conshohocken, Pennsylvania, USA.
- Abboud, B.E., Hamid, A.A., and Harris, H.G (1996). "Flexural Behavior of Reinforced Concrete Masonry Walls under Out-of-Plane Monotonic Loads" ACI Structural Journal, Vol.93, No.3, pp.327-335.
- Abboud, B.E., X., and Becica, I.J. (1995). "Deflection of Reinforced Masonry Walls under Out-of-Plane Loads," Proceedings of the Seventh Canadian Masonry Symposium, McMaster University, Hamilton, Ontario, Vol.2, pp. 895-910.
- Albert, M.L., Cheng, J. J. R., and Elwi, A. E. (1998). Rehabilitation of Unreinforced Masonry Walls with Externally Applied Fiber Reinforced Polymers, Structural Engineering Report No. 226, Department of Civil & Environmental Engineering, University of Alberta, Edmonton, T6G 2G7.
- Bruneau, M. 1994b. State-of-the-art Report on the Seismic Performance of Unreinforced Buildings. Structural Journal of the American Society of Civil Engineers, 120: 230-251.
- Canadian Standard Association. 1984. CAN3-A369.1-M84: Method of Test for Compressive Strength of Masonry Prisms. Rexdale (Toronto) Ontario, Canada.
- Canadian Standard Association. 1985. CAN3-A165 Series-M85: Concrete Masonry Units. Rexdale (Toronto) Ontario, Canada.
- Canadian Standard Association (1994) S304.1-94 Masonry Design for Buildings (Limit States Design), Canadian Standard Association, Rexdale, Ontario.

Ehsani, M.R., Saadatmanesh, H., Al-Saidy, A., (1997). "Shear Behavior of URM Retrofitted with FRP Overlays," Journal of Composites for Sonstruction, v1, no1, February. Pp. 17-25.

Ehsani, M.R., Saadatmanesh, H., I.H., Alkafrawy, W. "Flexural Behavior of Masonry Walls Strengthened with Composite Fabrics", Proceedings, ACI International Symposium on Non-Metallic Continuous Reinforcement. Ancouver, Canada, March 1993. pp.497-507.

Ehsani, M.R., "Strengthening of Earthquake Damaged Masonry Structures with Composite Materials", Non-Metallic Reinforcement for Concrete Structures. E&F Spon, London, 1995. pp.680-687.

Engineered Masonry Design, J. I. Glanville, M.A. Hatzinikolas, H. A. Ben-Omran 1996, Winston House Enterprises, 264 Wildwood Park Winnipeg, Manitoba, Canada.

Kenneth E. R, Strain Transfer Analysis of Masonry Prisms Reinforced with Sheet Bonded Carbon Fiber Reinforced Polymers, 1998.

Out-of-Plane Cyclic Behavior of Masonry Walls Reinforced Externally with GFRP by Marc D. Kuzik, A.E. Elwi, and J.J. Roger Cheng, September 1999.

T. Paulay and M. N. Priestley, Seismic Design of Reinforced Concrete and Masonry Buildings, John Wiley & Sons, Inc., New York, 1992.

University of Alberta Library



0 1620 1492 0621

B45438